Quaternary volcanic signatures in high-resolution stalagmite trace element datasets

ALICE RUBY PAINE

Thesis submitted for the degree of *Master of Science by Research (Volcanology)*

Quaternary volcanic signatures in high-resolution stalagmite trace element datasets

Alice R Paine

Primary Supervisor: James U.L. Baldini

Secondary Supervisor: Richard J. Brown

DEPARTMENT OF EARTH SCIENCES
DURHAM UNIVERSITY

October 2020

CONTENTS

LIST OF FIGURES

LIST OF TABLES

LIST OF ABBREVIATIONS

AMOC = Atlantic Meridional Overturning Circulation

EM = East Mediterranean

GG = Glen Garry

ka BP = thousand years before 1950

LA-ICP-MS = Laser Ablation Inductively-Coupled-Plasma Mass Spectrometry

LaMEVE = Large Magnitude Explosive Volcanic Eruptions (*database*)

LCY = Los Chocoyos

LGM = Last Glacial Maximum

LGP = Last Glacial Period

LIS = Laurentide Ice Sheet

Ma = million years ago

NADW = North Atlantic Deep Water

NH = Northern Hemisphere

PCA = Principal Component Analysis

SH = Southern Hemisphere

SST = Sea Surface Temperature

YTT = Youngest Toba Tuff

ABSTRACT

Identification and analysis of tephra preserved in paleoenvironmental sequences can provide key insights into the characteristics and consequences of explosive volcanism. Notable evidence gaps in the Quaternary eruption record confounds the ability to link volcanism to impacts on climate and terrestrial environments, yet studies suggest that geochemical analysis of high-resolution stalagmite records can address these gaps, through detection of transient enrichments associated with incorporation of volcanogenic trace elements, and perturbation of regional hydroclimate by volcanic forcing. However, the mechanisms controlling deposition and preservation of eruption signals in stalagmites are poorly understood. Here, Principal Component Analysis (PCA) is applied to two stalagmite trace element datasets: the first (NIED08-05 – 0-3 ka BP) from Niedźwiedzia Cave (SW Poland) to detect volcanic ash fall events; and the second (DIM-3 – 70-90 ka BP) from Dim Cave (South Turkey) to assess the climatological impact of super-volcanism during the Last Glacial Period. Results suggest that volcanic eruptions do have the capacity to influence stalagmite geochemistry, however notable limitations are evident. Discrepancies in the NIED05-05 record appear linked to regional climate, karst hydrology, sequence growth rate, depth, and cave ventilation - all impeding direct incorporation of volcanic material into the stalagmite. Conversely, poor chronological control of eruption dates and complexities associated with the pacing, duration, and characteristics of stadial-interstadial transitions in the Eastern Mediterranean restricts interpretation of the DIM-3-A record. Effective use of stalagmites in paleo-volcanology requires further work to constrain the absolute timing of individual eruption events, and better understand the expression of volcanic-induced climate change during the late Pleistocene. By quantifying the environmental processes acting to either enhance or attenuate the preservation of volcanic signals, we can gain a better indication of which karst conditions most effectively preserve the signals generated by explosive volcanism. Ultimately, rioritizing analysis of these stalagmites in paleo-volcanology may consequently provide an interpretive framework for linking the timing of eruption events with other global paleo-environmental archives to construct robust regional tephrochronologies, improve Holocene eruption dating, and constrain regional climate transitions using volcanic events as time-stratigraphic markers.

DECLARATION

I declare that this thesis, submitted for the degree of Master of Science by Research at Durham University, is my own work and does not bear any resemblance to work previously submitted at this or any other university.

Sections 1.0 and ***5.0*** of this thesis were submitted as part of a manuscript to *Chemical Geology* on **4th September 2020** (myself as the lead author). However, this means these sections have been subject to feedback and input from co-authors external to my supervisory team:

Franziska A. Lechleitner[1], Lisa M. Baldini[2], Wolfgang Müller[3], Fabian B. Wadsworth[4], Helena Hercman[5], Michał Gąsiorowski[4], Krzysztof Stefaniak[5], Paweł Socha[5], Artur Sobczyk[7], Marek Kasprzak[8]

[1] Department of Chemistry and Biochemistry and Oeschger Centre for Climate Change Research, University of Bern, Bern, Switzerland

[2] School of Health and Life Sciences, Teesside University, UK

[3] Institut für Geowissenschaften, Goethe Universität, Germany

[4] Department of Earth Sciences, Durham University, UK, DH1 3LE

[5] Institute of Geological Sciences, Polish Academy of Sciences, Poland

[6] Department of Palaeozoology, Zoological Institute, University of Wrocław, Poland

[7] Department of Structural Geology and Geological Mapping, Institute of Geological Sciences, University of Wrocław, Poland

[8] Institute of Geography and Regional Development, University of Wrocław, Poland

ACKNOWLEDGEMENTS

In a year which has brought multiple challenges due to the COVID-19 pandemic, there are so many people I need to thank - for their unremitting support, guidance, and encouragement while I have completed this project.

Firstly, huge thanks go to my primary supervisor James Baldini for his tireless enthusiasm, patience, assistance, and expertise. I wholeheartedly thank my secondary supervisor Richard Brown, and also Fabian Wadsworth. Three exceptional scientists in their own right, it has been a true privilege to work with them this year - in doing so, I have acquired invaluable skills and been challenged to surpass all expectations/limitations I had previously placed upon myself. I also thank Madeleine Humphreys, Alex Iveson, Colin Macpherson, and fellow MScR student Tom Verniers - for taking the time to provide insightful ideas and comments that helped improve respective sections of this thesis. Thank you to all members of the Durham Volcanology group, for creating a friendly space every Wednesday (virtually throughout lockdown!) within which I have learnt a huge deal, broadened my curiosity as a scientist, and made some amazing friends. Thanks also go to Julie Prytulak and Andy Aplin, for their unending support of PGRs during the department shutdown. It has been an honour to be a member of Durham Earth Sciences and to work alongside so many absolutely exceptional people – it is an opportunity I will be forever grateful for.

I am also extremely grateful to my manuscript co-authors, Bob Jamieson, David Pyle, Ezgi Ünal-İmer, and Francesco Pausata - for their insightful comments, feedback, and assistance with respective sections of this thesis.

Finally, I thank my mum (Sue), sister (Scarlett), Dad (Mark) Meg, Becky, Annabelle, Nathan, Holly, Sean, Lauren, and Ariane who, at a distance, never failed to make me smile. Even in the midst of lockdown, not once did I feel isolated.

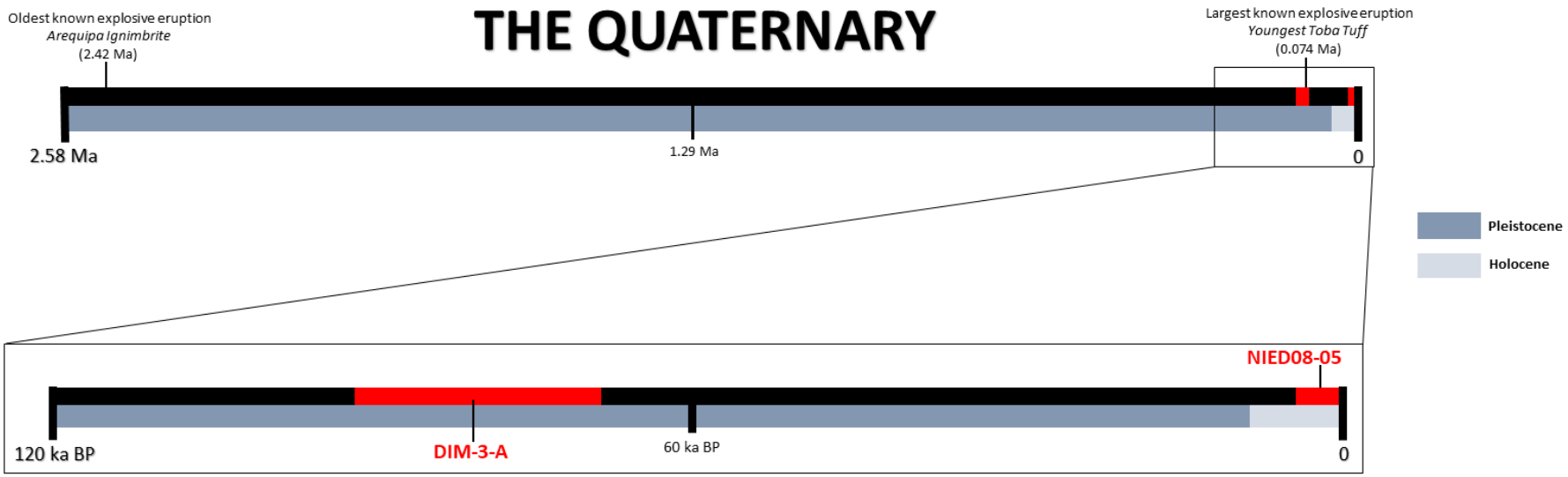

A schematic diagram showing the growth periods of stalagmitesamples utilised in this study (red shading), respectively.

1.0. INTRODUCTION

Volcanic eruptions substantially affect the Earth system, and their effects can be spatially and temporally extensive (Guillet et al. 2020; Kobashi et al. 2017; Sigl et al. 2015; Stoffel et al. 2015). Distal transmission of tephra can cause inter-continental social, political and economic disruption (Birtchnell & Büscher, 2011), and atmospheric injection of volcanic gases can cause global climatological perturbation on annual-to-centennial timescales (e.g. Baldini et al. 2018; Zanchettin et al. 2014, 2013; Miller et al. 2012; Zhong et al. 2011). Therefore, studying the frequency and impact of past volcanism is critically important to prepare for future events.

Historical records of volcanic eruptions are limited in spatial and temporal scope (Rougier et al. 2018), but can be augmented through interrogation of paleo-environmental archives. Ice cores are the primary source of such additional information, through detection of acidity spikes in annual layers at a high degree of precision (Zielinski et al. 1996). Exceptionally large eruptions such as Laacher See (12.9 ± 0.040 ka BP, Germany – Bronk Ramsey et al. 2015), Aniakchak (3.595 ± 0.001 ka BP, Alaska – Blackford et al. 2014), Samalas (1257 CE, Indonesia), and Tambora (1815 CE, Indonesia) are all synchronous with sulfate spikes in ice core records from Greenland and Antarctica. However, in many cases, tracing the volcanic source of such enrichments is more difficult, because the ice sulfate concentration is not always proportional to estimated eruption size (Rasmussen et al. 2014). Part of the complexity here may arise because adequately resolved polar ice cores reflect a preservation bias toward high-latitude eruptions (Hildreth & Fierstein, 2012), and non-polar ice records are limited to high-altitude environments (Frisia et al. 2008), where volcanic aerosols are poorly preserved within the ice (Wantanabe et al. 2004). Delay between the atmospheric injection of sulfur species during the eruption and the subsequent incorporation in ice as well as uncertainties in annual ice-layer counting and absence of tephra deposits (Cole-Dai et al. 2009) can all compound chronological uncertainty of ice cores of volcanism. Consequently, there are apparent gaps in the Holocene volcanic ice core record, which hinders assessment of synchronicity between volcanism and associated environmental impacts. These gaps can be filled by (1) a more complete and more accurate record of pre-historic volcanism globally, and (2) additional paleoclimate records sourced from lower latitudes than the poles that may also contain evidence for volcanism.

The global record of volcanism often relies on direct tephrochronology from well-preserved deposits proximal to a given volcano. However, the preservation potential is not always high (Dugmore et al. 2020), and so this is supplemented by distal tephra records such as ombrotrophic peat, marine and lacustrine sequences (Lowe et al. 2011), within which tephra particles can be preserved as complete layers, or microscopic shards (e.g. cryptotephras; Lane et al. 2014). High-resolution particle analysis

of tephra in such sequences can, in ideal cases, aid characterisation of eruption source, magnitude (M) and magma composition (Ponomareva et al. 2015). Effective characterisation of ash layers consequently relies on a combination of physical, mineralogical, and geochemical observations from laboratory and field studies (Lane et al. 2017). However, ash layers in peatlands can experience particle migration and alteration due to structural (Payne & Gehrels, 2010), hydrological (Watson et al. 2015) and anthropogenic (Swindles et al. 2013) disturbance. These can alter, remove, or obscure tephra records of an eruption, and therefore hinder robust chronological correlations between tephra records in different locations. These disturbances are less prevalent in lacustrine and marine environments (Watson et al. 2016), however a larger depositional catchment, dynamic sedimentation, and secondary transport processes in the water column (Griggs et al. 2014) increase the difficulty of clear tephra detection (Scudder et al. 2016; Schacht et al. 2008). Evidently, novel, high-resolution archives are required.

The application of stalagmite records to climatological (e.g. Cheng et al. 2019; Wong & Breecker, 2015) and hydrological (e.g. Hartmann & Baker, 2017; Denniston & Luetscher, 2017) investigations is well established. Stalagmite growth initiates due to interaction of weakly acidic infiltrating surface water with calcium carbonate ($CaCO_3$) bedrock. This infiltrating water becomes supersaturated with respect to calcite and, once it reaches the cave atmosphere, degasses CO_2 and deposits $CaCO_3$ speleothems (e.g., stalactites and stalagmites). Stalagmite geochemistry reflects atmospheric (e.g. temperature, precipitation, air composition, atmospheric circulation) and environmental conditions (e.g. soil bioproductivity, vegetation dynamics) at the surface at the time the stalagmite was growing (Fairchild & Treble, 2009). Their tendency for continuous growth, and low affinity for diagenetic modification (Frisia & Borsato, 2010) means stalagmites provide geographically ubiquitous, high-resolution isotope and trace element concentration records that can be used to reconstruct a range of external environmental conditions (Baldini, 2010).

Three key mechanisms allow entry of volcanic material (tephra or aerosols) into caves (**Figure 1**). The first (1) is aeolian transport and dry deposition of solid tephra particles (Pashchenko et al. 1993). Fine ash from eruption plumes is dispersed widely by atmospheric circulation (Rose & Durant, 2009), transported into caves by ventilation, deposited on the stalagmite growth surface , and integrated into the stalagmite mineral fabric as it grows (Badertscher et al. 2014). One way periods of increased aeolian transport into the cave are detected is by $\delta^{13}C$ and $\delta^{18}O$ concentrations, which reflect enhanced disequilibrium fractionation due to ventilation (Ünal-İmer et al. 2020). Direct incorporation of volcanic particles into calcite can thus reflect regional ash deposition, and variations in atmospheric composition after major eruptive events (Dredge et al. 2013). The second (2) mechanism is the deposition of solid tephra on the Earth's surface above the cave, and subsequent

groundwater leaching of incompatible elements from the solid tephra into groundwater, which percolates through the rocks comprising the cave roof system and supplies volcanogenic elements to the speleothem growth surface (e.g. Jamieson et al. 2015; Badertscher et al. 2014). The third (3) mechanism is groundwater leaching. Volcanoes emit sulfur dioxide (SO_2), which oxidises into sulfuric acid (H_2SO_4) in the atmosphere where it resides for days to years (Robock, 2000). Sulfate (SO_4) is removed from the atmosphere by either wet deposition via meteoric precipitation (Loosmore & Cederwall, 2004; Mather et al. 2003), or by dry (wind) deposition (Petroff et al. 2008) – for which airborne tephra particles provide a nucleation surface. Sulfate is highly soluble, showing rapid dissolution upon contact with ground and/or rainwater (Jones, 2015; Jones & Gislason, 2008). This results in the release and accumulation of volcanic aerosols and trace elements into soils, as dissolved ions or colloidal particles (Martin et al. 2009), which can consequently enter the aquifer and are transported to the stalagmite through karst fractures and interconnected pore spaces (Wynn et al. 2013; Fairchild & Treble, 2009). Of these three mechanisms, (3) is likely to provide sulfate to the speleothem, whereas (1) and (2) may provide sulfate but also REEs and other trace elements indicative of volcanic eruptions. Herein, we therefore focus on (1) and (2) as mechanisms for REE enrichment.

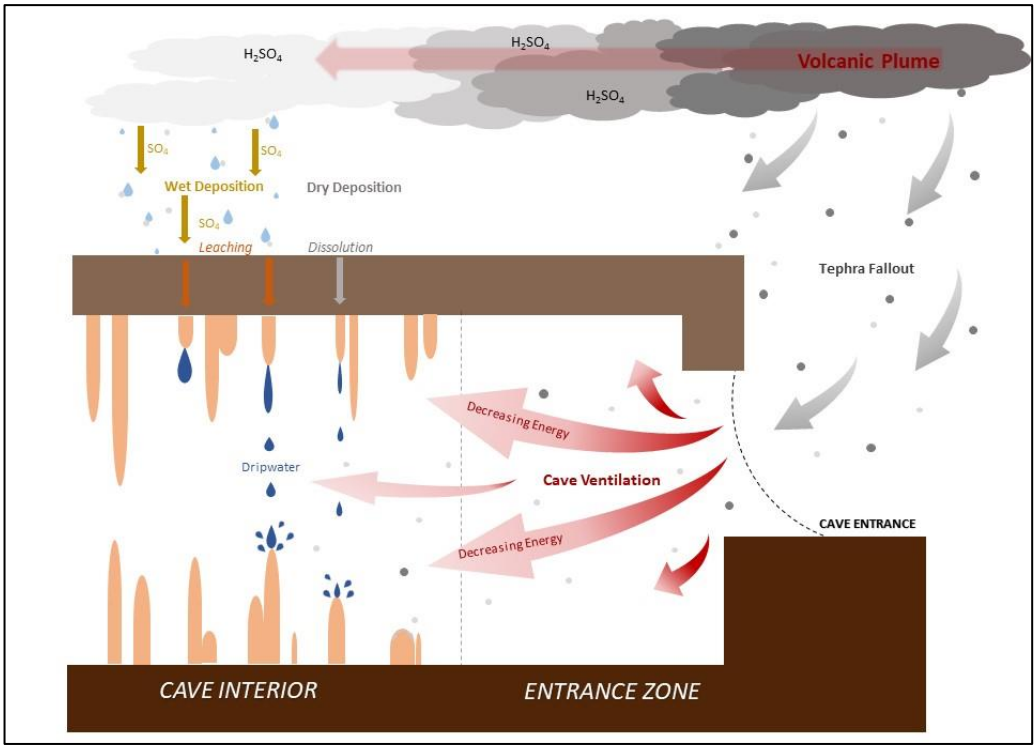

Figure 1: A conceptual diagram illustrating the modes of direct deposition of volcanic tephra into a cave. Shown here are aeolian transport and dry deposition of solid tephra particles, and groundwater leaching of both solid tephra and aerosols deposited above the cave. This is schematic and not drawn to scale.

Intra-cave deposition of tephra is influenced by karst geomorphology, depth, soil/bedrock thickness, surface vegetation (Borsato et al. 2015), and biogeochemical cycling (Wynn et al. 2013). However, the extent to which this varies according to cave location is poorly understood. Analysis of stalagmites sourced from different sites, at different latitudes, will strengthen understanding of how the abovementioned processes affect stalagmite geochemistry, and consequently how regional climatic and environmental change controls volcanic deposition into caves.

2.0. BACKGROUND

2.1. The Holocene

2.1.1. *Volcanic History of the Holocene*

The Holocene volcanic record identifies 832 known high magnitude (>M4.0) explosive volcanic eruptions, from 11.65 ka BP to present. However, very few have been observed directly. Eruption recording probability decreases as a function of time (**Figure 2***:* Brown et al. 2014; Siebert et al. 2010) and environment (Pyle, 2016), so contemporary volcanology strives to develop the temporal resolution and spatial diversity of eruption records (Cooper et al. 2018), using diverse techniques and archives. This section evaluates how geological and historical evidence has been used to uncover the volcanic history of the Holocene, and understand key events attributed to substantial environmental and climatic change.

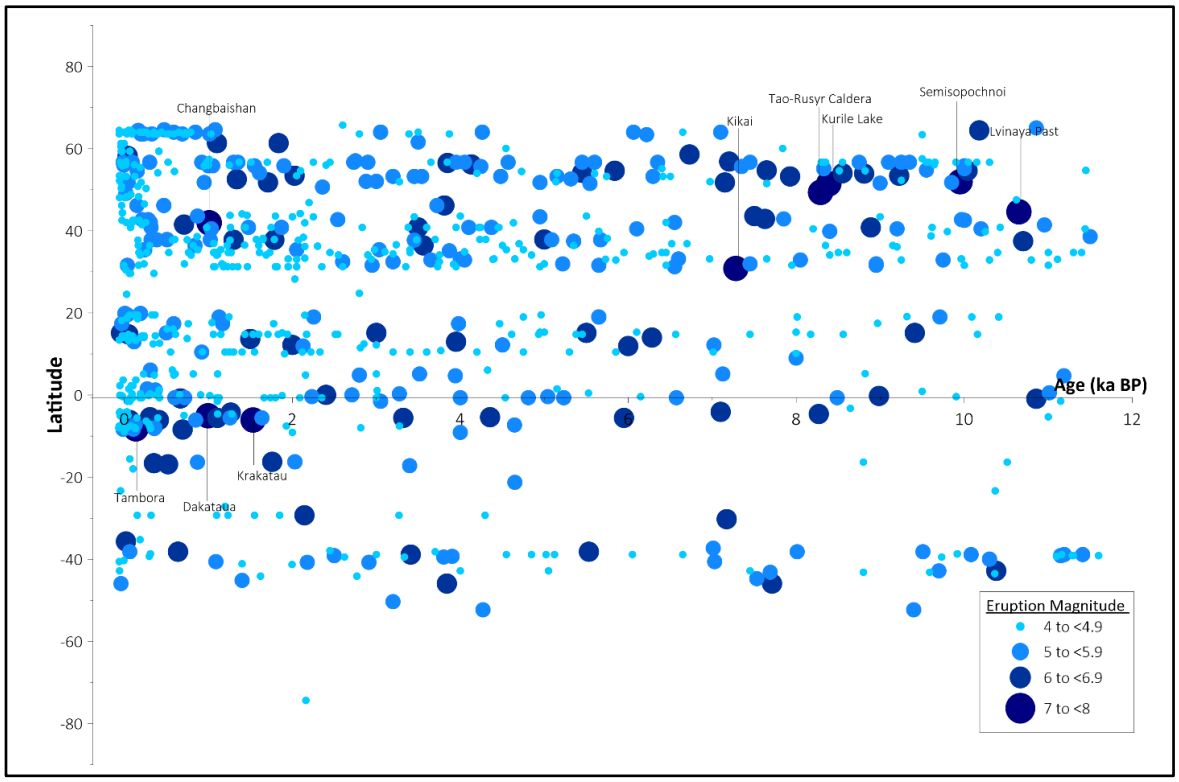

Figure 2: The global occurrence of volcanic eruptions exceeding M4.0 from 11.65ka BP to present, presented as a function of latitude. Marker size is proportional to eruption magnitude. Eruptions ≥7.0 are labelled. Eruption number decreases as a function of time and latitude, with greater scarcity evident in the Southern Hemisphere (data sourced from LaMEVE: Crosweller et al. 2012).

2.1.1.1. Geological Records

The geological record is invaluable in acquisition and global integration of knowledge regarding key locations, driving mechanisms and environmental impacts of prehistoric eruptions (Watt et al. 2013; Rampino, 1991), as only 11% of known Holocene eruptions ≥M6.0 have occurred since 1500 CE. Holocene deposits have not been subject to the erosion and degradation associated with aridity, ice sheet advance, eustatic change, and land modification due to dynamic geomorphological processes occurring in stadial intervals (Lowe & Walker, 1997), and pioneering geochemical techniques have enabled detection of fine-ash (Tomlinson et al. 2015), trace metals (Witt et al. 2008), and ignimbrite deposits in environmental archives and sequences across the world.

Calderas represent the largest visible manifestations of explosive eruptions (de Silva & Lindsay, 2015). 77% of known >M7.0 Holocene eruptions are associated with creation of a caldera, as mass ignimbrite emplacement from a subsurface magma reservoir (Branney & Acocella, 2015) can create a topographic depression often kilometres in diameter (Cole et al. 2005). Calderas forming on land often manifest as lakes such as Kurile (Kamchatka - 8.387 ± 0.023 ka BP), Ilopango (El Salvador - 1.5 ± 0.03 ka BP; Pedrazzi et al. 2019), Mount Mazama (USA - 7.627 ± 0.150 ka BP; Buckland et al. 2020;

Bacon & Lanphere, 2006; Young, 1990), and Dakataua (Papua New Guinea - 0.998 ± 0.063 ka BP; Silver et al. 2009) – all formed since 11 ka BP. The huge volumes of tephra and rock ejected by caldera-forming eruptions subsequently become incorporated into surrounding sediments, which can also provide key indications of eruption features. Marine sediments, in cases whereby calderas are located amongst, or even concealed by ocean, provide the best archives for large Holocene events. For example, the Minoan (3.560 ± 0.014 ka BP: Johnston et al. 2014) eruption chronology was advanced through study of ignimbrite deposits on the Aegean Sea floor surrounding Santorini caldera, Greece (e.g. Nomikou et al. 2016; Sigurdsson et al. 2006). Similarly, study of the submarine Kikai Caldera, Japan (formed at 7.280 ka BP: M7.3), has primarily been conducted by analysis of submarine pyroclastic flow deposits (Maeno & Taniguchi, 2007) and signatures of tsunami propagation across the East China sea (Nanayama & Maeno, 2018; Tatsumi et al. 2018., Geshi et al. 2017). However, observable calderas are not always attributed to a Holocene event. For example, the Taupo eruption of 1.720 ± 0.016 ka BP (New Zealand - Wilson et al. 2009) did not form the present day caldera lake: instead this is attributed to the prior Oruanui super-eruption of 27.1 ± 0.96 ka BP (Vandergoes et al. 2013). Disentangling observable structures from their respective formation events can be difficult, so in such cases, more evidence is required.

Analysis of proximal deposits has facilitated study of smaller eruptions, not associated with caldera-scale geomorphological features (Burden et al. 2013; Fierstein & Nathenson, 1992). Geochemical analysis of deposits from compositionally unique volcanic systems has enabled characterisation of erupted volume, column height, erupted mass, duration and intensity of eruptions occurring in geographical proximity (Sparks et al. 1997). One key example is Somma-Vesuvius, Italy, with 13 eruptions >M4.0 since 10 ka BP (e.g. Santacroce et al. 2008; Cioni et al. 2008; Bertagnini et al. 1998) – all characterised by unique tephra geochemistries (De Vivo et al. 2001).

Similar methods are employed to identify the sources of Icelandic tephra layers, along with understanding the mechanisms of tephra emplacement and distribution (Moles et al. 2019; Carey et al. 2009a). For example, analysis of proximal deposits and PDC sub-units from the Askja 1875 CE eruption (Carey et al. 2009a, 2009b), has improved understanding of ash dispersal associated with different eruptive phases (Stivrins et al. 2016., Watson et al. 2016). Similarly, geochemical characterisation of proximal deposits from Katla (Oladottír et al. 2008; Larsen, 2010) has indicated glacial meltwater availability as a controlling factor in eruption frequency and character (Schmith et al. 2018; Elíasson, 2014), raising concerns regarding the potential impact of increased meltwater flux due to global warming (Swindles et al. 2018; Sparks & Cashman, 2017; Compton et al. 2015). Proximal organic matter engulfed by ash can also aid constraint of ambiguous eruption dates. For example, the Kurile Lake eruption age was calculated through radiocarbon dating of soils overlying

proximal tephra horizons (Ponomareva et al. 2004; Braitseva et al. 1993), and the Changbaishan (China/North Korea - 1.008 ka BP) eruption date was constrained using dendrochronological fragments (Oppenheimer et al. 2017). Furthermore, buried vegetation (Friedrich et al. 2006), grains (Manning et al. 2014), and tree rings (Pearson et al. 2018) helped to constrain ambiguity surrounding the Minoan (3.629 ± 0.014 ka BP) eruption date.

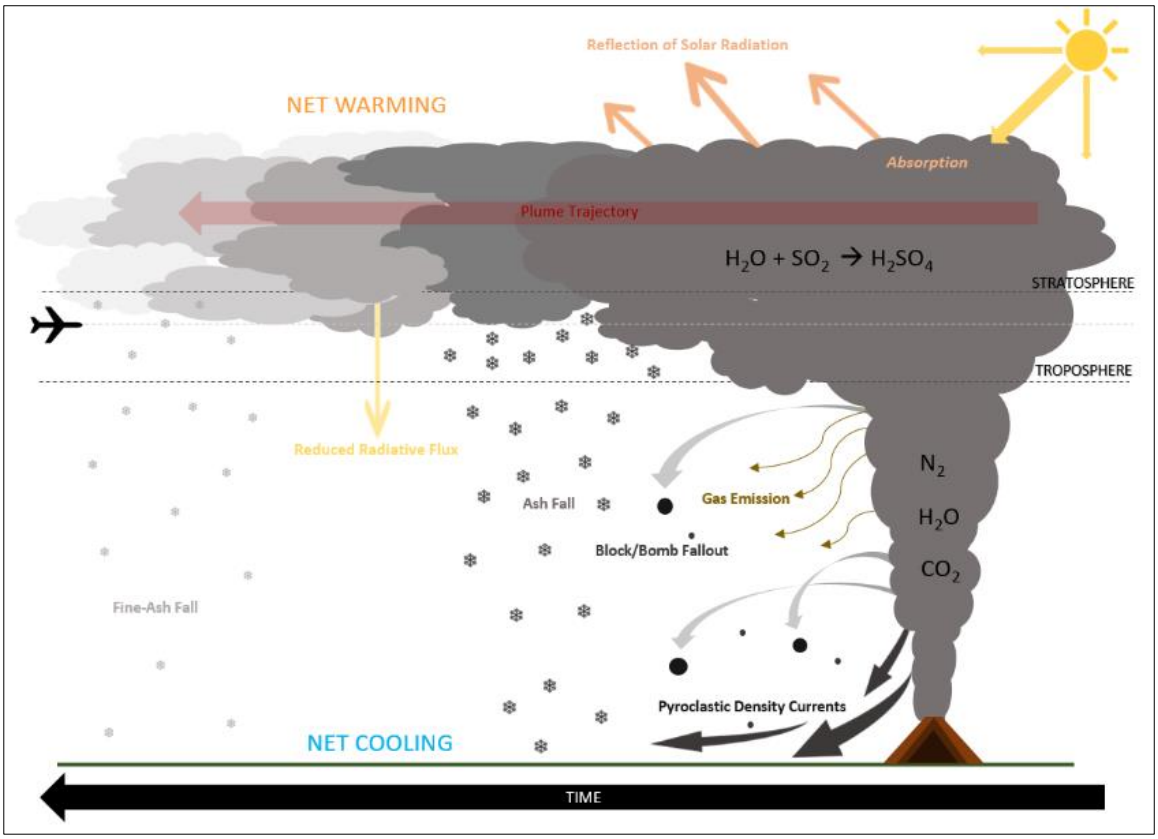

Figure 3: A conceptual diagram showing the proximal & distal impacts of explosive volcanism, most notably the dispersal of solid pyroclastic material and volcanogenic aerosols (adapted from Robock, 2000, not to scale).

Unfortunately, proximal deposits can experience reworking as a product of erosion, sea level change, and/or further eruptions (Lane et al. 2017; Ponomareva et al. 2015; Brown et al. 2015; Rawson et al. 2015). In such cases, cryptotephra layers can provide information of known eruption frequency, intensity (e.g. Plunkett & Pilcher, 2018; Watson et al. 2017; Gale, 2009), plume trajectory (Dugmore et al. 2020; Davies et al. 2010), and environmental impacts (Dugmore et al. 2020), for both documented and undocumented (Martin-Jones et al. 2017) eruptions. Well-dated layers can also become event-stratigraphic markers, synchronous with other sedimentary sequences featuring the same layer (Lowe, 2011; Blockley et al. 2008; Payne et al. 2008) and thus can be applied to define significant environmental changes (e.g. Sun et al. 2017; Chen et al. 2017; McLean et al. 2016; Jensen et al. 2014; Wei et al. 2013; Davies et al. 2012). Certain regions have proved hugely valuable for such work. Kamchatka, Russia, hosts a large number of peatlands, and also 37 large volcanic

centres (Ponomareva et al. 2007) responsible for nine >M6.0 eruptions since 11.65 ka BP (Crosweller et al. 2012). In the absence of regional glacial advance since the late Pleistocene (Barr & Solomina, 2014), peat sequences have preserved distinct tephra layers distinguishable by major and trace-element geochemistry (Kyle et al. 2011). Iceland has also been very volcanically active during the Holocene (Crosweller et al. 2012; Thordarson & Larsen, 2007), and as a result hosts a significantly comprehensive tephrostratigraphic record (Swindles et al. 2013., Larsen, 2000) which has greatly improved empirical understanding of ambient tephra flux (Ponomareva et al. 2015) and the ecological effects of surface ash loading (Cutler et al. 2018, 2016a). Tephrochronology is thus a unique tool showing huge potential for future applications in novel locations for further development of the Holocene volcanic record.

For some Holocene eruptions, signatures of their occurrence are best preserved in paleoclimate archives, such as tree rings, ice cores, sedimentary sequences, and speleothems (e.g. Sigl et al. 2015; Stoffel et al. 2015; Badertscher et al. 2014; Zielinski et al. 1996). For example, transient atmospheric perturbation associated with the Huaynaputina (1600 CE: M6.1) eruption, Peru, due to due to exceptional tephra (Prival et al. 2020; Thouret et al. 2002; Adams et al. 2001) and aerosol (Costa et al. 2003) emission are recorded in dendroclimatological (Briffa et al. 1998) and polar (Budner & Cole-Dai, 2003) records. Further observations of summer cooling of -0.8^{o}C renders the eruption's impact equivocal to other high-magnitude eruptions such as Kuwae (0.520 ka BP, Vanuatu) and Ilopango (1.5 ka BP, El Salvador) (Stoffel et al. 2015). Similarly, the presence of a cataclysmic eruption at 1257CE was initially identified by a sulphur enrichment in Greenland and Antarctica (Oppenheimer, 2003), supported by environmental (Stothers, 2000) and anthropogenic (Connell et al. 2012) evidence for climatic anomalies in 1258 CE (Guillet et al. 2017; Whelley et al. 2015). However, it was not until 2013 that the source of these perturbations was confirmed as Mount Samalas, Indonesia (Lavigne et al. 2013). Since identification, geochemical analysis of deposit major and trace element composition suggests exceptional volatile degassing (Vidal et al. 2016, 2015), resulting in cooling between -0.6^{o}C and -5.6^{o}C for 4-5 years post-eruption and fortifying Samalas as a significant driver of the Little Ice Age cooling interval (Kobashi et al. 2017).

The Holocene-age geological record benefits from minimal reworking due to glaciation, eustatic, and geomorphological change, thus providing excellent archives for contemporary volcanology. Where direct event observation has not been possible, robust integration of proximal, distal, and climatological volcanic records can allow us to define eruptive successions, understand the mechanisms underpinning eruptions of varied magnitudes, and assess the relative environmental impacts of individual events.

2.1.1.2. Human Records

Cultural perceptions of volcanoes and their eruptions have profoundly evolved through historical time. Volcanoes were initially recognized as symbolic entities in religious, philosophical, and artistic works (Chester, 2005) prior to the Scientific Revolution. Mount Vesuvius, Italy (e.g. Macedonio et al. 2008; Scandone et al. 1993) and Changbaishan, China/North Korea (Kwon & Kim, 2019), are two examples of volcanoes rich in symbolic significance – with a profound place in ancient human history. The 1700's first saw the multi-national, quantitative documentation of volcanic activity, global articulation of trade, society, and economy in the *Common Era* has since enabled synchronous use of geological, and historical, archives to unravel the impacts of volcanism on society and environment (Pyle & Barclay, 2020). However, volcanic hazards such as pyroclastic flows, landslides, tsunamis, and lahars initially proved fatal for those close enough to observe eruptions in detail (Brown et al. 2017). Instead, the indirect effects of many eruptions are recorded in historical literature (Chester et al. 2018; Fisher, 1997) as perturbations to geochemical cycles (Jones, 2015), and sources of pollution (Schmidt et al. 2012) and radiative change (Stoffel et al. 2015) - all intrinsically linked to national-scale production of organic product, and consequently society (Oppenheimer & Donovan, 2015). For example, ≤5 months of severe atmospheric pollution due to the sulfur-rich Lakagígar (Iceland – 1783/4) eruption plume (e.g. Sonnek et al. 2017; Schmidt et al. 2012; Oman et al. 2006a; Thordarson et al. 1996; Thordarson & Self, 1993) is detectable in mortality, food price, and weather records (Oman et al. 2006b; Witham & Oppenheimer, 2004).

Records of the Indonesian Mount Tambora (1815 CE: M7.0) and Krakatau (1883 CE: M6.5) eruptions also refer to indirect environmental perturbations (Self & Gertisser, 2015; Self, 1991). For Tambora, information can be sourced from memoirs and writings of Western scholars such as Lord Byron, who describes how "*the icy earth swung blind and blackening in the moonless air*" (McGann & Weller, 1980-92). This is now understood to be a product of atmospheric pollution by tephra and gas (Kandlbauer & Sparks, 2014), and such observations appear simultaneous with global records of widespread crop failures and social conflict (Post, 1977), discernible in record capital prices, disease outbreaks and mass migration (Oppenheimer, 2003a). Conversely, the Royal Society's pioneering study of Krakatau in 1883 (Symons, 1888) represents the first real-time, comprehensive study of volcanic perturbation of local diurnal cycles and global optical effects (Prata et al. 2018; Wohletz, 2000; Symons, 1888), and facilitated the initial discovery of the Polar Jet Stream (Winchester, 2003). However, these eruptions occurred in Western-occupied territories, and prior to the satellite era remote eruptions often went undetected. The Novarupta eruption of 1912 CE is the largest recorded in the 20th Century (Adams et al. 2006; Hildreth, 1987), however its isolated location in

Southwestern Alaska has complicated attempts to constrain the eruption's distal effects using historical records, shifting emphasis onto geological deposits. Similarly, the 1902 eruption of Santa María, Guatemala, appears less commonly in human literature despite an exceptional magnitude (Metzner et al. 2014; Williams & Self, 1983): ambiguity potentially due to socio-economic factors contributing to delayed volcanological research in Guatemala (Rougier et al. 2018). Proximal eruption effects are primarily recorded by survivor accounts (Aragón, 2013), however scientists of Europe had no knowledge that the eruption ever occurred prior to the 21st Century, and often prioritised volcanological study in colonial territories such as Martinique and St. Vincent (Williams & Self, 1983). The Novarupta event of 1912, and Santa María in 1902, therefore, demonstrate the difficulties associated with studying eruptions occurring in remote regions utilising anthropogenic records.

By the late 20th Century, volcanic recording probability reached 100% (Newhall, 2018., Rougier et al. 2016; Furlan, 2010), and research focus shifted to the histories of contemporaneously active volcanoes. The eruption of Mount Pinatubo (1991) in the Phillippines was a pioneering event for synchronous use of land and satellite-based volcano monitoring systems (Tupper, 2005; Guo et al. 2004), and amalgamation of geological and instrumental techniques could further identify an episodic Quaternary eruption pattern (Newhall & Solidum, 2018; Newhall et al. 1996). Satellite-derived data can, alongside seismometers, tiltmeters and the Global Positioning System (GPS) (Ebmeier et al. 2018), can also provide indicators of pre-eruption geodetic deformation and magma emplacement, for example at Merapi, Indonesia, in 2010 CE (Pallister, 2013), Reyjkanes, Iceland, in 2020 CE (Global Volcanism Programme, 2020) and the 1995-1999 eruptive episode at Soufriére Hills, Montserrat (Wadge et al. 1999). Advances in instrumental monitoring have significantly benefitted human society, however eruptions still pose a substantial risk to infrastructure due to increased globalisation, increased infrastructural complexity, and a novel reliance on inter-continental trade (Mattsson & Jenelius, 2015). This risk was highlighted during the eruption of Eyjafjallajökull, Iceland, in 2010 CE, when disruption to 80% of the European aviation network incurred a cost of >£4 billion by halting key supply chains (Oxford Economics, 2010). The extent of damage was not measured by lives lost nor environmental perturbation, but by economic loss (Birtchnell & Büscher, 2011) – denoting a shift in concepts of volcanic hazard in a developing, transnational society (Reinchardt et al. 2017; Lund & Benediktsson, 2011). Modern understanding of high-magnitude volcanism is largely extrapolated from observations of smaller eruptions (Engwell et al. 2014), as most volcanic systems are often characterised by prolonged quiescence (Papale, 2018), and punctuated by rare, ephemeral episodes of activity (Pyle, 2018., Siebert et al. 2015). However, urbanization continues to drive development into volcanic landscapes, so millions now live under the threat of volcanism (Donovan

& Oppenheimer, 2018; Skinner, 2008), which can permeate global political, social and economic infrastructures (Donovan & Oppenheimer, 2019; Reichardt et al. 2018). Evidently, eruption magnitude is becoming less proportional to economic impact, and volcanic risk has exponentially increased in line with the spatial influence of anthropogenic substructure (Fearnley et al. 2018; Birtchnell & Büscher, 2011).

2.1.2. Holocene Climate: Patterns & Events

The Holocene marks the stratigraphic end of the Pleistocene (Gibbard & van Kolfschoten, 2004), and is often considered the more climatologically 'stable' epoch of the Quaternary (Agenbroad & Fairbridge, 2018; Rasmussen et al. 2014), with no prolonged glaciations and a warmer interstadial regime (Roberts, 2014). However, the Holocene has been interspersed by rapid cooling events (Wanner et al. 2011; Mayewski et al. 2004) which appear geographically diverse across meridional temperature gradients, in turn causing variable changes in Earth Surface conditions (Roberts et al. 2011) across different environments (e.g. Rehfeld et al. 2018; Zhang et al. 2015; Laepple et al. 2014., Kobashi et al. 2011). This section discusses the characteristics, and catalysts, of Holocene climate variability, and how, in certain cases, stalagmite records have enhanced their study.

Three, abrupt onset Holocene cooling intervals have been meticulously studied. One of which is the 8.2 ka BP event (herein referred to as the 8.2k event), as the similarity between present boundary conditions (Alley & Ágústsdóttir, 2005), and those prior to the 8.2k event (Renssen et al. 2009) enables study of rapid environmental change under interstadial conditions, and thus calibration of contemporaneous climate models (Weijer et al. 2019; Liu et al. 2017; Ahn et al. 2014). The 8.2k event is defined as a 0.4-0.6kyr interval characterised by rapid global temperature decrease of 3.3^{o}C ± 1.1^{o}C (Harning et al. 2018), and arid conditions across multiple continents (Peckover et al. 2019., Alley et al. 1997), most prominently in the North-Atlantic (Ahn et al. 2014; Wanner et al. 2011) and Europe (e.g. Fohlmeister et al. 2012). Minimum temperatures were reached ~20 years after cooling (Kobashi et al. 2007), and this rapid onset is commonly attributed to a freshwater outburst from Lake Agassiz (fed by the Laurentide Ice Sheet) into the Labrador Sea (Wagner et al. 2013; Kleiven et al. 2008). Such an outburst could have abruptly perturbed the thermohaline circulation of the North Atlantic (Clark et al. 2001) and reduced of Atlantic Meridional Overturning Circulation (AMOC) strength (Hoffman et al. 2012; Carlson et al. 2009), consequently prompting cessation of the North-Atlantic-Deep-Water (NADW) conveyor belt (Teller, 1995). Asian and South American stalagmite $\delta^{18}O$ monsoon records suggest an antiphased response concurrent with North Atlantic meltwater pulses (Cheng et al. 2009; LeGrande & Schmidt, 2008), supported by further identification of 0-8-2.2m eustatic sea level rise in temporal propinquity to the supposed outburst event (Törnqvist and

Hijma, 2012). However, the Agassiz-outburst hypothesis for 8.470 ± 0.3 ka BP as the cause of the 8.2k event is falsifiable, with alternative theories suggesting the mass freshwater flux acted as the 'final push' toward instability in an already unbalanced thermohaline regime in the North Atlantic due to deglaciation (Teller et al. 2002). This would render the Agassiz outburst as one of several compounding factors instigating rapid cooling (Rohling & Pälike, 2005).

The recurrence of high-magnitude volcanic eruptions directly before prior to the 8.2k event, such as Kurile Lake (Kamchatka - 8.387 ± 0.023 ka BP) and Tao-Rusyr Caldera (Kuril Islands - 8.290 ± 0.076 ka BP) (Bazanova et al. 2016) alternatively propose volcanism as a catalyst of the 8.2k event; due to previously-suggested associations between volcanic forcing, and changes in internal modes of ocean-atmosphere variability. The antiphase relationship between Chinese and South Asian (Cheng et al. 2009) speleothem $\delta^{18}O$ records show monsoon perturbations coincident with $\delta^{18}O$ excursions in Greenland dated to ~8.2 ka BP (Vinther et al. 2006) - suggesting atmosphere-ocean circulation weakening potentially caused by Inter-Tropical Convergence Zone (ITCZ) migration. Research suggests this migration can occur following volcanogenic aerosol injection (Pausata et al. 2020; Baldini et al. 2015; Ridley et al. 2015) which, alongside decreased solar receipt due to atmospheric dust-veil propagation (Robock, 2000), may further act to amplify ice sheet growth and instigate cooling. The attribution of equivocally large volcanic eruptions to notable Holocene cooling excursions further support this connection (Kobashi et al. 2017; Sigl et al. 2015; Haywood et al. 2013), and the widespread nature of the 8.2k event signal hints toward a common catalyst capable of affecting oceanic circulation and associated climatic regimes (Porinchu et al. 2019) - to which explosive volcanism adheres. Furthermore, intermediate ice conditions (Baldini et al. 2018; Zhang et al. 2014) at the 8.2ka boundary may have contributed to an amplified impact of sulfur-rich volcanism. However, volcanic forcing as a driver of the 8.2k event lacks robust empirical support as the eruptions in question are sparsely studied. Hence, understanding of the mechanisms driving this global climatological excursion remains ambiguous.

The second of the three best-known Holocene climate excursions is the 4.2 ka event (referred to herein as the 4.2k event). Globally visible in paleoenvironmental archives (Weiss, 2016; Head & Gibbard, 2015) as a prolonged interval of cooler, drier conditions (Berkelhammer et al. 2012; Roland et al. 2012; Drysdale et al. 2006), anthropological studies have attributed the event to the transformation and/or decline of major civilisations in Egypt, Mesopotamia and China (Ran & Chen, 2019; Wang, 2004). However, the event manifests in a non-linear fashion across the world (Railsback et al. 2018), thus it is unclear what caused the transition to cooling (Carter et al. 2018). Mayewski et al. (2004) identify a peak in ^{10}Be records coincident with the event, but not in $\Delta^{14}C$ records - suggesting no orbital influence. Additionally, research in the Mediterranean indicates that

pronounced hydrological changes at ~4.2 ka appear unrelated to the North Atlantic Oscillation (Bini et al. 2019) and no notable change is observed in Northern Europe/Atlantic regions (Roland et al. 2014), providing minimal evidence for oceanic circulation change as a catalyst (Bradley & Bakke, 2019). Arguably, such evidence implies a cause related to direct radiative forcing, for example volcanic or dust aerosols. Low-latitude aridity combined with increased North Atlantic wind strength and advance of North American glaciers would affect the Asian and African monsoon (Liu & Feng, 2012), and evidence for 'wetting' at high-latitudes (Jordan et al. 2017; Menounos et al. 2008) is also consistent with southward ITCZ migration and consequent elongation of the Polar front (Olsen et al. 2012). Interestingly, the eruption date of Mount Veniaminof (4.131 ± 0.654 ka BP), Alaska, corresponds with the onset of the 4.2k event (Waythomas, 2015). Furthermore, Kobashi et al. (2017) propose that ice-core temperature reconstructions may not fully capture sharp climatological transitions such as the 4.2k event, due to smoothing caused by ice sheet diffusion of heat. Thus, the absence of a notable signature in the ice lends support to the theory of a transient catalyst, such as a volcanic eruption. However, confirming a volcanic cause is complicated by complex atmospheric responses following aerosol injection (Hudson, 2012), and some suggest the observed decline in summer insolation at ~4.2 ka BP is simply part of a long-term cooling trend (Weiss, 2017), which increased ENSO activity and declined tropical SST during the mid-Holocene (Liu & Feng, 2012; Wanner et al. 2008).

The Little Ice Age (LIA) is the most recent example of abrupt cooling (Grove, 2004) characterised by advance of continental, high-latitude Arctic, and Alpine glaciers (Matthews & Briffa, 2005), followed by rapid recession at the beginning of the 20th century (Miller et al. 2010; Mann et al. 2009). This interval also witnessed a significant fall in Northern Hemispheric summer temperatures in relation to prior boundary conditions (Briffa et al. 2001), rendering the LIA as the coldest multi-centennial climate interval since the 8.2ka event (Wanner et al. 2011) and identifiable in proxies across the world. Despite its widespread manifestation (Mann et al. 2008), the controls on LIA expression and onset remain perplexing. Some initially hypothesised the event was caused by decreased solar flux associated with the Maunder and Spörer Minima (Crowley, 2000; Eddy, 1976), and modelling studies have indeed identified a prolonged period of diminished solar irradiance within temporal coincidence of the LIA (Schmidt et al. 2011) – proposed to have resulted in perturbations to thermohaline circulation cells (Renssen et al. 2007; Weber et al. 2004), and weakening of the North-Atlantic Oscillation (NAO) (Trouet et al. 2009; Emile-Geay et al. 2007). However, interrogation of GISP2 sulfate records has indicated that high-magnitude, tropical eruptions frequently appear prior to and during the LIA period (Kobashi et al. 2017; Sigl et al. 2015; Kobashi et al. 2013; Mayewski et al. 1997), consequently suggesting that volcanic forcing could both catalyse and sustain widespread

cooling, due to sea-ice and ocean interactions (Miller et al. 2012). Poleward transmission of volcanic aerosols from the tropics is also associated with generation of stronger stratospheric winds, increased activation of halogens and subsequent loss of ozone: further increasing the temperature gradient (Barnes et al. 2016; Muthers et al. 2014). Therefore, the hypothesized link between latitude and climatological impact (Baldini et al. 2015; Timmreck et al. 2012) provides a compelling case for volcanism as a catalyst for the LIA, synchronous with solar insolation minima (Wanner et al. 2011). However, as the extent of atmospheric perturbation by volcanism appears conditional on season (Toohey et al. 2016, 2011), and rate/magnitude of gaseous emission (Oppenheimer et al. 2018), coupled with an inherently dynamic relationship between sulphur yield and associated cooling (Kravitz & Robock, 2011), volcanically induced cooling at the LIA interval is spatially diverse and results in often ambiguous effects across different environmental archives (Guillet et al. 2017; Emile-Geay et al. 2008).

Bond Events (BEs) are an enigmatic, recurring feature of Holocene climate. BEs are named from 0-8 (Bond et al. 1997), defined as instances of increased ocean ice-rafting in temporal coincidence with global cold intervals (Thompson et al. 2009; Debret et al. 2007) at a mean return interval of 1.470 ± 0.5ka. The sporadic nature of these events, similar to Dansgaard-Oeschger (D-O) events, thus do not appear forced by orbital variability. BEs also appear coupled to cold intervals recorded in global stalagmite archives (Wanner & Bütikofer, 2008). $\delta^{18}O$ data from China and Southern Oman indicate an antiphased seasonal response to change in glacial boundary conditions at BEs 0-5 (Wang et al. 2005) and 2-6 (Fleitmann et al. 2003) respectively, and in India $\delta^{18}O$ records show monsoon weakening in antiphase with the South American Monsoon (Strikis et al. 2011), concurrent with 2 of the 8 BEs (Band et al. 2018). In Europe and the Arctic, notable excursions in winter precipitation (stalagmite $\delta^{18}O$) are concurrent with 5 of the 8 BEs and significant hydrological change in the North Atlantic (Mangini et al. 2007), suggesting solar forcing as an influence on North Atlantic climate (Broecker, 2004). BE signatures also appear at low latitudes, with drying coincident with 6 of the 8 BEs observed in the Caribbean (Fensterer et al. 2013). However, no speleothem record has yet clearly recorded all 8 BEs, suggesting a multitude of causal factors (Wanner & Bütikofer, 2008) such as solar variability (Viau et al. 2006; Yu et al. 2003), deep-ocean circulation (Oppo et al. 2003), ITCZ migration (Russell & Johnson, 2005) and cumulative volcanism (Wanner et al. 2008) - all amassing to sustain a feedback loop favouring cooler temperatures. Therefore, it is unlikely that BEs have one sole cause, and they are likely the product of intricate connections between ocean, atmosphere, tectonic regimes and cryospheric change.

Continued observation of increased anthropogenic forcing in the late Holocene (IPCC, 2014., Collins et al. 2013; Osborn & Briffa, 2006) demonstrates a dominant warming trend disparate from the

anticipated cooling paced by cyclic orbital forcing (Tzedakis et al. 2012), and attributed to increased human activity in the post-industrial era (Martin et al. 2019; Miller et al. 2012). Quantifying the relative influences of natural forcings such as ice sheet recession, volcanism, and solar minima, will further aid understanding of the Earth as a system, and consequently how it may change in the future (Liu & Feng, 2012; Eriksson et al. 2012).

2.2. The Last Glacial Period

2.2.1. High-Magnitude Volcanism: Mechanics & Distribution

2.2.1.1. Contemporary Issues & Debates

The Last Glacial Period has witnessed explosive volcanism unrivalled in historical time (Costa & Marti, 2016., Miller & Wark, 2008). 67% of known Pleistocene eruptions >M7.0 are associated with a remnant caldera structure (Crosweller et al. 2012; Geyer & Marti, 2008) created by either stratocone destruction (e.g. Mount Mazama, Santorini, Krakatau) or structural collapse; the latter often linked to large systems such as Toba (Indonesia), Cerro Galán (Argentina), Taupo (New Zealand), and Yellowstone (USA) (Cole et al. 2005). An understanding of eruptive frequencies and characteristics associated with these volcanoes is crucial for future hazard evaluation and management (Cooper & Kent, 2014). For example, Toba shows episodicity similar to other caldera systems across the world (Forni et al. 2018; Barker et al. 2015; Till et al. 2015; Wilcock et al. 2013) alongside geophysical and petrological consanguinity with Sinabung ~40km to the north (Mucek et al. 2017; Jaxybulatov et al. 2014). Sinabung erupted in 2013 CE (M4.0) and has been magmatically active since (Gunawan et al. 2019); prompting re-evaluation of contemporary hazards posed by the Toba magmatic system, and subsequently all 'dormant' large volcanic networks (Andersen et al. 2019; Townsend et al. 2019; Sparks et al. 2008). By seeking to address prevailing uncertainties associated with catalysts, consequences, and frequencies of high-magnitude volcanism, we can study the histories and anticipate the potential futures (Parker, 2015) of Earth's most volcanically active regions. This section discusses the three key uncertainties associated with exceptionally large volcanic eruptions: (1) magmatic system anatomy, (2) eruptive frequency, (3) climatological implications.

The first uncertainty (1) concerns the rheological, petrological, and structural catalysts of eruptive activity. Caldera size and structure links to total erupted magma volume (Kennedy et al. 2018), however understanding of this relationship is constantly evolving (Aspinall & Woo, 2019) and the extent to which the processes driving large eruptions differ from small ones is ambiguous (Andersen et al. 2019; Wotzlaw et al. 2015; de Silva & Gregg, 2014; Gualda et al. 2012; Wilson, 2008). These

differences must be clarified in order to gain a deeper understanding of magma lifetimes, timescales of quiescence, and ultimately eruptive triggers (Myers et al. 2016; Caricchi et al. 2014) for assessment of future risk. However, the paradigm of a petrologically coherent, single-chamber magmatic system below the volcanic edifice (Gualda & Ghiorso, 2013) is now contentious following geophysical studies at large systems such as Yellowstone (USA - Huang et al. 2015) and Altiplano-Puna (Peru/Argentina - Ward et al. 2014) and geochemical analyses of volcanic deposits (Rubin et al. 2017; Szymanowski et al. 2017). The mush reservoir hypothesis (MRH) represents a novel framework for study of large volcanic systems – describing a culmination of heterogenous igneous processes occurring in vertically extensive networks (Jackson et al. 2018; Cashman et al. 2017; Bachmann & Bergantz, 2008) whereby melt co-exists alongside igneous 'mushes' (Sparks et al. 2019) characterised by gradual accumulation (Sparks & Cashman, 2017) and rapid expulsion (Carrasco-Núñez et al. 2017) of magma. Reactive upward flow of buoyant melt (Jackson et al. 2018) prompts systemic instability, as crystalline interactions promote changes in bulk composition and melt fraction (Hepworth et al. 2020; Solano et al. 2014, 2012), giving rise to overpressure (Tramontano et al. 2017; Bachmann & Huber, 2016) and/or mobilization of near-eruptible mush to form eruptible, volatile-rich magma in the upper crust (Cashman et al. 2017). This trans-crustal complexity is supported by observations of crystalline diversity in igneous minerals (e.g. plagioclase - Cashman & Blundy, 2013) and rocks erupted during one event, suggesting assembly at different depths (Pearce et al. 2020; Lucci et al. 2020; Swallow et al. 2019, 2018; Andrews et al. 2008) and suggesting that transient magmatic processes act as primary drivers of eruptive variability.

However, two key components of MRH remain puzzling. Firstly, systemic longevity: *what dictates the timescales and rates of magma production*? Processes of fractional crystallisation and assimilation appear supressed in regions of thick, low density crust whereby ascent of less-viscous magma is inhibited (Bachmann & Bergantz, 2008), however differences in tectonic regimes and magma type are also significant (Karlstrom et al. 2010). Secondly, timescales of shallow accumulation: *what influences the residence time of shallow, melt-dominated magma within the crustal domain before eruption*? This question is particularly elusive as rates of growth and recharge (Townsend et al. 2019) in large magma systems operate diachronously (Tavazzani et al. 2020; Oppenheimer & Donovan, 2015). Shorter timescales are generally associated with magmatic instability, rejuvenation and amalgamation (influenced by viscosity - Costa et al. 2009), yet there is seemingly no correlation between crystal age and emplaced magma volume (Reid, 2008) suggesting large spatio-temporal variability between systems (Rubin et al. 2017; Barboni et al. 2016)**.** Furthermore, the extent to which crustal stress-driven segregation influences shallow melt extraction is unclear. Volcanism and tectonic deformation exist synchronously (Allan et al. 2017; Kohlstedt & Holtzmann, 2009), and

geophysical observations of Pleistocene-active systems (Allan et al. 2013; Hildreth, 2004) together with subduction zones (Schaen et al. 2017) indicate an influence of active deformation on crystal fractions and magma viscosity (Caricchi et al. 2007). However, quantifying timescales of segregation in deforming mushes remain contingent on: (i) extrapolation of experimental/theoretical studies to real-world conditions (Kohlstedt & Holtzmann, 2009), and (ii) disentangling the true impact of external stress, based on available field and experimental evidence, from other geophysical factors (Holness, 2018; Rosenberg & Handy, 2005) – both remain a challenge (Schoene et al. 2012). An improved understanding of melt generation, segregation, and flux in the Earth's crust will undoubtedly provide crucial insights into past drivers of high-magnitude eruptive episodes, transitions from visible 'dormancy' to 'activity', and causes for variability between different volcanic systems (Laumonier et al. 2019; Gelman et al. 2013).

The second (2) uncertainty relates to eruption frequency (Sheldrake & Caricchi, 2017; Deligne et al. 2010), which can be studied on systemic or global scales. System-scale research focusses on mechanisms governing observable episodicity of individual volcanic systems, to understand precursors of imminent or future eruptive activity (Wadsworth et al. 2017). Contemporary instrumental observations suggest no link between eruption size and the magnitude of multi-parametric unrest (Papale, 2018), with unpredictable, ephemeral activity at smaller volcanoes (Aiuppa et al. 2010) reinforcing a capacity for notable variance in pre and syn-eruptive behaviour (Tierz et al. 2019). This is problematic, as the lack of modern analogues for larger events means extrapolation of observational data lacks context (Andersen et al. 2019). Complexity further arises as timescales of true dormancy are poorly defined (Connor et al. 2006) due to unknown precursory indicators for large eruptions, and volcanic records that reflect a distorted and imperfect view of global eruptive frequency (e.g. Siebert et al. 2015; Compton et al. 2015; Mead & Magill, 2014; Brown et al. 2014; Swindles et al. 2011; Deligne et al. 2010). Mathematical assessments have attempted to assimilate these uncertainties for applications to contemporary hazard management (Wang et al. 2019; Rougier et al. 2016; Kiyosugi et al. 2015; Wang & Bebbington, 2012), however gaps in the eruptive histories of volcanoes in Indonesia, Australasia, South America, Kamchatka and the Kurile Islands occur simply due to fewer paleo-volcanic studies being conducted in these regions. This reflects spatial dissimilarity in evidence provision (Kiyosugi et al. 2015), and increases the difficult in separating variations in eruptive frequency due to environmental change (e.g. Cooper et al. 2020., Smith et al. 2019; Swindles et al. 2018; Rawson et al. 2016; Watt et al. 2013) from improvements in evidence acquisition (Watt et al. 2013). The issue of imperfect eruptive recording is therefore one of global significance, with profound implications for knowledge of recurrence, characteristics, and timescales of high-magnitude volcanism.

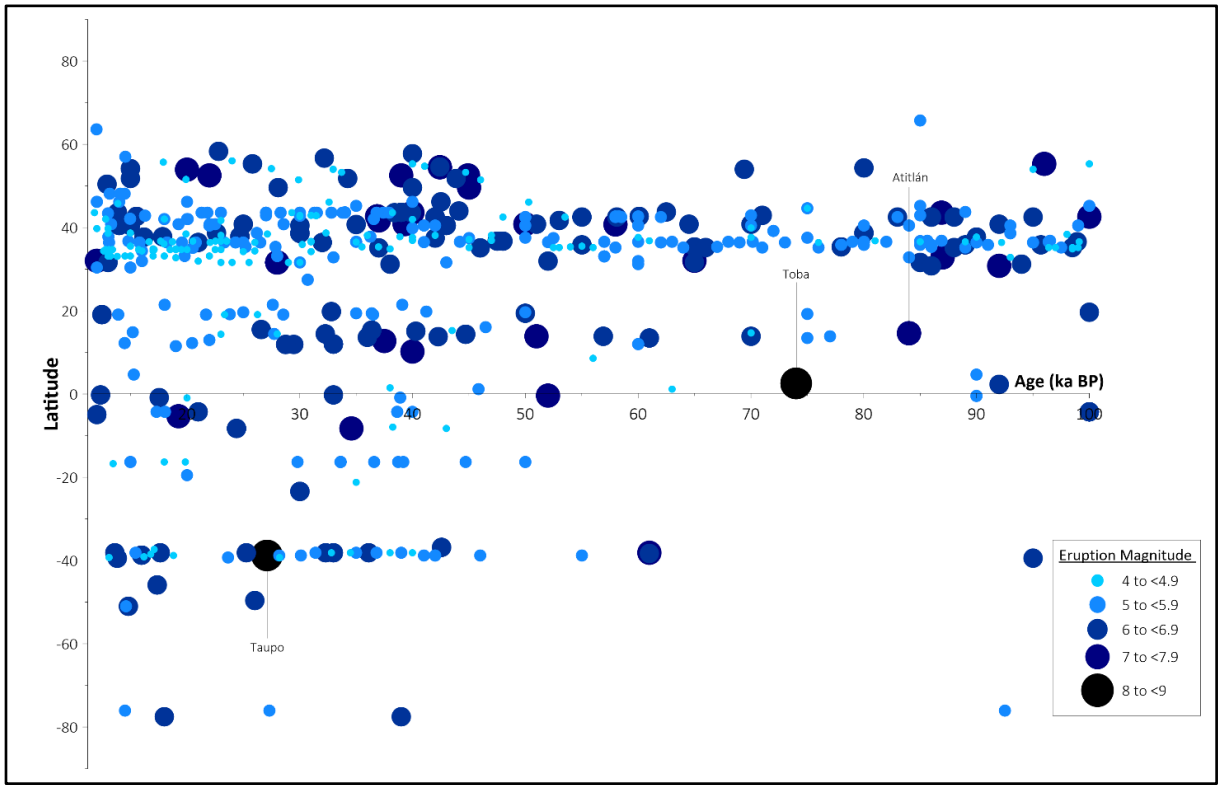

Figure 4: The global occurrence of volcanic eruptions exceeding M4.0 from 11.65-100ka BP (Last Glacial Period), presented as a function of latitude. Marker size is proportional to eruption magnitude. Eruptions discussed later in this section are labelled. Recording probability appears to increase with magnitude, however eruption number decreases as a function of time and latitude; with greater scarcity evident in the Southern Hemisphere

The final uncertainty (3) concerns the impact of explosive volcanism on millennial-scale climate variability. Climate variability is defined as variations in the mean state of the climate system yet results from complex interconnections between components (e.g. atmosphere, hydrosphere, geosphere, cryosphere, and biosphere) (Hernández et al. 2020). Discerning the magnitude to which the Last Glacial Period climate differed from the Holocene is thus a challenge (Rasmussen et al. 2014), and the occurrence of rapid climate oscillations such as Dansgaard-Oeschger (D-O) events (Dansgaard et al. 1993) in Greenland (Andersen et al. 2004) anti-phased with Antarctic Isotopic Maxima (Pedro et al. 2018; EPICA Community Members, 2006) suggest the presence of intricate, inter-hemispheric global teleconnections with large spatio-temporal variability in their modes, interactions and impacts. Quantifying the role of volcanism in these variabilities is confounded by two obstacles: (a) eruption date uncertainty, and (b) poorly constrained eruptive parameters. Beyond the radiocarbon limit, dating of older eruptions is conducted through orbital tuning to polar $\delta^{18}O$ ice core records (Storey et al. 2012), or alternative isotopic dating techniques (e.g. $^{40}Ar/^{39}Ar$ - Mark et al. 2017). However, accurate dating relies on deposit quality which, for many volcanoes/calderas, become increasingly poorer with age due to periglacial processes, eustatic

changes, and active erosion (Baldini et al. 2015; Arnalds, 2013; Watt et al. 2013). These problems also influence (b), as determination of volatile gas ejection is largely contingent on the quality and quantity of residual deposits. Ascertaining sulfur ejection is particularly important when assessing an eruption's climatic impact, as atmospheric oxidation and condensation allow a 'sulphate haze' to encircle the globe and disturb the Earth's radiative budget (Timmreck et al. 2012; Oppenheimer, 2002; Robock, 2000). Other volatile gases and halogens, however, can also contribute to the post-eruptive climatic response (McConnell et al. 2017; Vidal et al. 2016; Cadoux et al. 2015) which can include perturbation of oceanic thermohaline circulation (Pausata et al. 2015), sea ice flux (Zanchettin et al. 2014; Miller et al. 2012), modes of climatic variability (Maher et al. 2015), and ITCZ position (Baldini et al. 2015; Ridley et al. 2015). However, this can vary on several orders of magnitude depending on eruption (e.g. Carn et al. 2016) and plume dynamics for high-magnitude eruptions remain poorly understood (Costa et al. 2018), as current understanding is extrapolated from results of simple integral models – not designed for eruptions with such large ejecta quantities (Costa et al. 2016; Jessop et al. 2016; Engwell et al. 2016). Similarly, models aiming to quantify the extent of volcanically forced climate variability are conducted under Holocene baseline climate conditions (e.g. Brenna et al. 2020; Toohey et al. 2019; Stoffel et al. 2015; Robock et al. 2009; Jones et al. 2005), and recurrently fail to capture the dynamic circulatory responses to volcanic aerosol injection (Driscoll et al. 2012). Evaluating the impact of high-magnitude volcanogenic forcing on climate variability consequently relies on accurate synchronization of high-resolution paleoenvironmental archives, containing both volcanogenic and climatic signals.

Unlike Large-Igneous-Province (LIP) volcanism (Bryan et al. 2010), large explosive eruptions are not defined by distinct, prolonged episodes, thus represent a more geologically imminent threat (Thordarson et al. 2009) and so acquisition of such knowledge has profound societal implications. Contemporary study of high-magnitude volcanism continues to reinforce the complexity associated with generation, and emplacement, of large magma bodies, however the complexities associated with the drivers of high-magnitude volcanism render understanding and identifying their pre and syn-eruptive characteristics (Biggs & Pritchard, 2017), and intra-crustal evolution, a notable challenge. Paucity in eruption records also limit understanding of how high-magnitude eruptions can be differentiated from smaller events, which in turn complicates assessment of how these eruptions can perturb the Earth system.

2.2.1.2. Measuring Eruption Size

Volcanic eruptions are diverse by size and impact. Magnitude scales are used to effectively measure and catalogue these events, enabling effective and clear communication of eruption size across

empirical disciplines and geohazard management (Plag et al. 2015). The Volcanic Explosivity Index (VEI) (Newhall & Self, 1982) is the most frequently employed, yet although this scale allows comparison between modern and ancient eruptive events (Pyle, 2015), the two parameters used in calculation are problematic for study of bigger events. First is plume height, which is effective for moderate smaller eruptions, but ejecta from large eruptions are predominantly ignimbrites associated with laterally spreading pyroclastic flows (Brown & Andrews, 2015), which are difficult to quantitatively constrain and yield large margins for error (Costa et al. 2018; Bursik & Woods, 1996). Second is bulk volume, which does not account for deposit density (Mason et al. 2004) and is notably affected by poor preservation of smaller (Houghton et al. 2013) or older (Ponomareva et al. 2015) eruption deposits. Furthermore, the VEI is ordinal so cannot simultaneously reflect intra-eruptive variation in magnitude *and* intensity (Rougier et al. 2018), thus applications to continuously erupting systems and/or long-lasting discrete events, such as Lakagígar, Iceland, in 1763-64 (Thordarson & Self, 2003) and Kīlauea, Hawai'i, in 2018 (Gansecki et al. 2019) are contentious.

To accurately quantify the geological significance of exceptionally large eruptions, two size measures can be employed: a) Magnitude –the total ejecta volume (***i***) and b) Intensity – the mass eruption rate (***ii***)

i) $M = log_{10}(mass\ of\ erupted\ material,\ kg) - 7$

ii) $I = log_{10}(mass\ eruption\ rate, kg\ per\ second) + 3$

Magnitude and intensity are not independent variables (Pyle, 1995) as both are a product of mass erupted, showing logarithmic increase with overall eruption size. Large errors estimation of mass flux and/or mass eruption rate are also not reflected in large errors as the scales are continuous, accounting for inevitable uncertainties associated with study of eruptions on pre-Holocene timescales (Pyle, 2015). Therefore, using magnitude and intensity autonomously allows for robust comparison of volcanic events across the effusive-explosive spectrum, and on a range of temporal scales where volatility may oscillate throughout an eruptive episode (Houghton et al. 2013).

Defining the magnitude and intensity of past volcanic eruptions requires integration of numerical and field data (Buckland et al. 2020). Proximal deposits facilitate magnitude calculations by quantification of grain-size distributions and bulk ejection, while distal dispersal trajectories provide key insights into eruptive intensity through airborne ash flux and atmospheric transmission. Isopach/dispersal maps based on proximal deposit identification (Bonadonna & Costa, 2012) can quantify primary dispersal axes, and semi-empirical descriptive modelling can be used to derive eruptive volume estimates from such data (Engwell et al. 2015). However, a reliance on quantitative analyses creates unique challenges related to the dynamic nature of volcanic landscapes (Dugmore

et al. 2020; Pyle, 2016; Fontjin et al. 2016; Brown et al. 2015), and topographical accessibility can also limit effective characterisation of proximal volcanic deposits and stratigraphies (Watt et al. 2013). In such cases, distal tephra deposits in conjunction with sophisticated modelling (Costa et al. 2014) can supplement volume estimates. However, as measured deposit thicknesses only represent a minimum estimate (Ponomareva et al. 2015) and where distal records are incomplete, appraisals are based on extrapolation beyond known limits of tephra fallout – which runs the risk of over/under estimation of eruption size. Therefore, incorporating low-concentration tephra layers into ash-distribution models is persistently difficult. The resolution of tephra records will likely improve as a function of time with investigation of novel sites and repeated sampling (Watson et al. 2016), increasing the chance of discovering well-preserved tephra layers in locations whereby degrading processes are less influential (Cook et al. 2018).

2.2.1.3. Super-Volcanism

In volcanology, the term "super-eruption" describes the largest explosive volcanic events on Earth. There are 47 known super-volcanoes (Mason et al. 2004) denoting the most productive magmatic systems on the planet capable of simultaneously emplacing $>10^{15}$ kg magma (equating to $>1000kg^3$ bulk tephra volume; Sparks et al. 2005), huge volumes of volatile gases, and invoking environmental disturbance on inter-continental scales (Self & Blake, 2008). This section describes the two super-eruptions occurring within the DIM-3 interval: *Youngest Toba Tuff* and *Los Chocoyos*. Inclusion and classification of Los Chocoyos as a super-eruption is based on new erupted volume estimates by Kutterolf et al. (2016), which yield a magnitude estimate of 8.0.

2.2.1.3.1. Los Chocoyos (LCY)

Atitlán is the largest volcanic centre in Guatemala. The formation of three overlapping calderas since ~14 Ma (**Figure 5**) has created a southerly track of land subsidence (Rose et al. 1987., Newhall, 1987), with Lake Atitlán marking the third and most recent stage of caldera-forming activity ~84ka BP. The lake measures 18 km × 8 km (11.2 mi × 5.0 mi) in area and houses ~20 km^3 of water, with an average depth of 220m. The caldera system is situated at the northern tip of the Central American Volcanic Arc (CAVA), which extends 1400km from the Mexico-Guatemala border to Central Costa Rica near parallel to (150-200km to the West of) the Middle America deep-sea trench (Carr et al., 2007). Formed during the Late Cretaceous (Elming, 1998) volcanic activity commenced during the Tertiary (Donnelly et al. 1990) with the formation of large stratovolcanoes both at, and behind, the volcanic front. At present, the CAVA is one of the most volcanically active arcs on Earth, and explosive volcanism accounts for 65% of total magma output (Kutterolf et al. 2008).

Prior to ~158 ka BP, activity at Atitlán was largely mafic (Rose et al. 1987). A period of silicic volcanism during the Mid-Pleistocene is initially marked by the emplacement of the widespread W-Pumice Fall (158 ± 3 ka BP), attributed to a M7.1 eruption with an estimated volume of ~23.3 km^3 (Kutterolf et al. 2016). A transition back to mafic volcanism is observed following the Los Chocoyos eruption (~84 ka BP), with the resurgent formation of basaltic/andesitic stratovolcanoes Atitlán, Tolimán and San Pedro (Rose et al. 1987; Newhall, 1987; Williams, 1960). An unusually prolonged, bimodal eruptive lifetime (Newhall, 1987) in concurrence with periods of intensified CAVA volcanism (Schindlbeck et al. 2018; McBirney, 1976) suggests the eruptive regime of Atitlán is a function of large-scale subsurface magma differentiation and storage conditions, which in turn paces eruptive frequency in the northern CAVA region (Rose et al. 1999). However, the major/minor element geochemistry of CAVA magmas reflect non-linear conditions of subduction (e.g. Freundt et al. 2014; Bolge et al. 2009; Hoernle et al. 2008; Syracuse & Abers, 2006; Vogel et al. 2006; Feigenson et al., 2004; Abers et al. 2003; Barckhausen et al. 2001; Patino et al. 2000; Carr, 1984) and variable degrees of magma differentiation (Heydolph et al. 2012; Kutterolf et al. 2008), crystallization and extraction (Vogel et al. 2006), influenced by state of hydration, slab angle, crustal thickness, sediment cover composition and upper-plate characteristics of the Cocos plate. This results in significant along-arc variation in erupted tephra geochemistry (Carr et al. 2007, 2003; Feigenson et al. 2004; Hoernle et al. 2002; Patino et al. 2000), which has facilitated accurate geochemical fingerprinting of detected tephras and construction of a robust offshore tephrostratigraphy for Central America (e.g. Schindlbeck et al. 2018; Kutterolf et al. 2008a, b). Stratigraphies for calderas Ilopango, Coatepeque, Ayarza, Amatitlán, and Atitlán are all relatively well defined (**Table 1**), and have been used for kyr-scale analyses of global eruption frequency (Kutterolf et al. 2018, 2013), study of Central American Mayan civilisation (Lohse et al. 2018; Anselmetti et al. 2007), and characterization of stadial-interstadial transitions in the Neotropics (Kutterolf et al. 2016; Hodell et al. 2008).

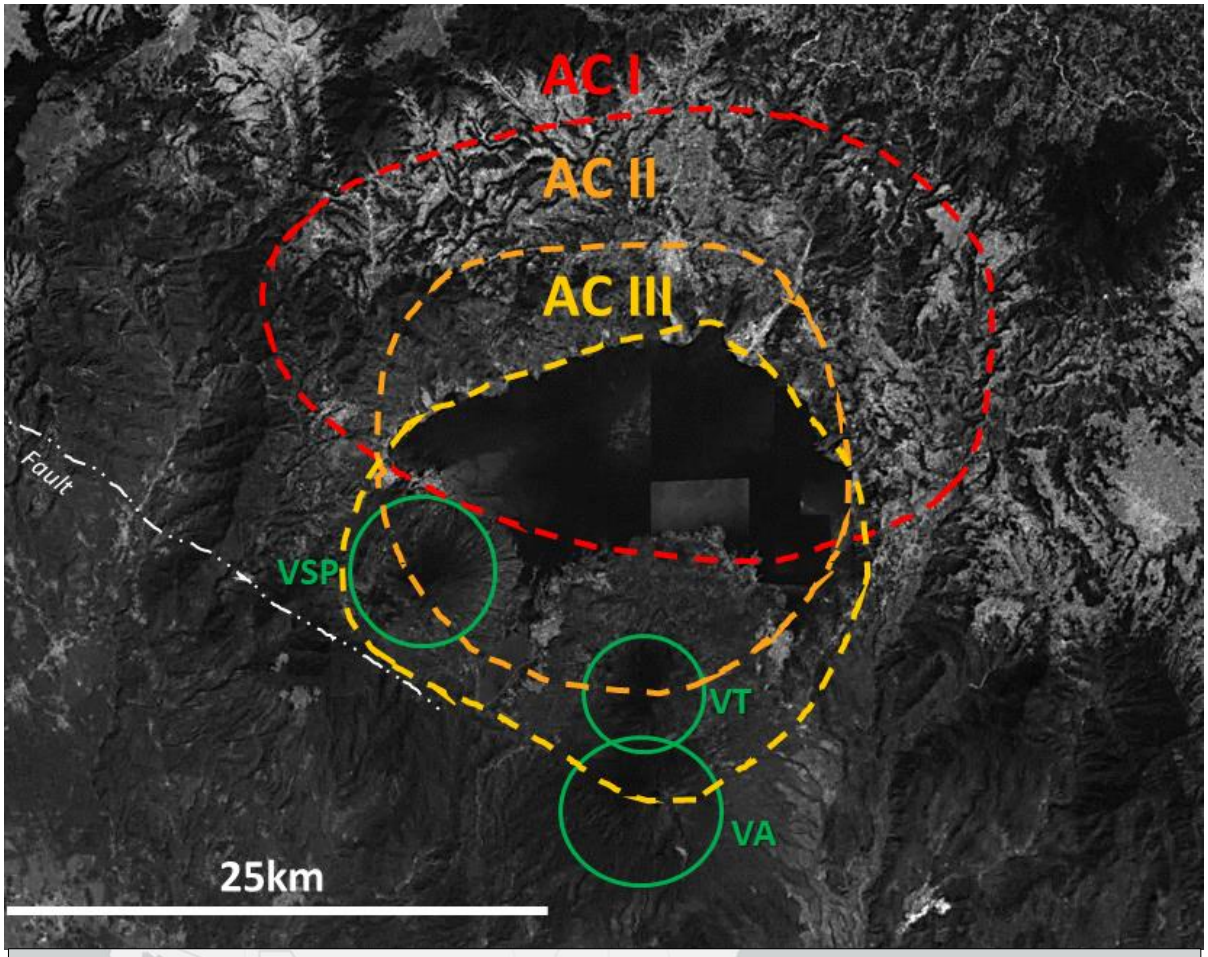
AC I
AC II
AC III
Fault
VSP
VT
VA
25km

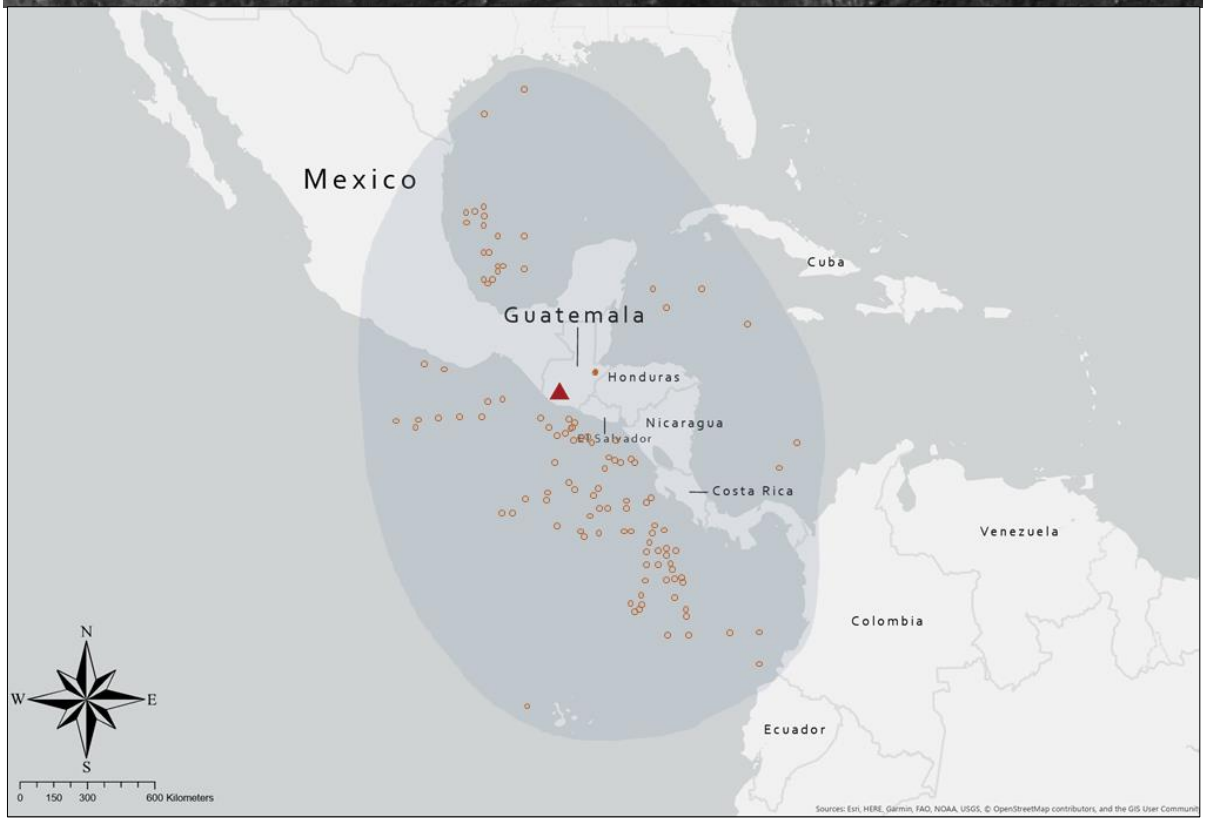
Mexico
Cuba
Guatemala
Honduras
Nicaragua
El Salvador
Costa Rica
Venezuela
Colombia
Ecuador
N
W
E
S
0 150 300 600 Kilometers

Figure 5: (TOP) Map of Atitlán caldera, with caldera boundaries (stages I-III) marked as red, orange, and yellow circles respectively, and proximal volcanoes marked by green circles. VSP – Volcan San Pedro, VT – Volcan Tolimán; VA – Volcan Atitlán. Adapted from Rose et al. (1987). Base image sourced from Google™ Earth Pro.
(BOTTOM) Map of sites with identified LCY tephra and/or tephra (featuring data from Bowles et al. 1973; Drexler et al. 1980; Ledbetter, 1985; Kutterolf et al. 2008, 2016; Schindlbeck et al. 2016, 2018), with Atitlán caldera marked as a red triangle. Non-filled circles depict marine core sites, filled circles indicate terrestrial sites. Created in ArcGIS Pro (v2.5)

The Los Chocoyos (LCY) eruption (84 ± 0.5 ka BP) is the third largest known Quaternary eruption (Crosweller et al. 2012) and largest of the CAVA by magnitude and ejecta volume (Rose et al. 1999), yet the characteristics and impacts of the event are relatively ambiguous/understudied (Brenna et al. 2020). Analysis of proximal deposits suggest LCY released 420 km^3 (280 km^3 DRE) of rhyolitic tephra (Rose et al. 1987), and ash covered a minimum ~6 x 10^6 km^2 area from the Pacific to the Gulf of Mexico and Florida (Kutterolf et al. 2008; Drexler et al. 1980; Rose et al. 1999, 1987). These proximal deposits can be divided into three stratigraphic categories: fall, flow and surge (Rose et al. 1987). Flow units are characterised by ~200m thick ignimbrites spread across western Guatemala (Koch & McLean, 1975), and the H-fall unit is the largest known Plinian fall deposit in Central America erupted during the Quaternary (**Table 1**), with a distinctly high K_2O and SiO_2 content. H-fall ash was primarily transmitted to the South West over the Pacific Ocean due to easterly stratospheric winds, however a multi-directional dispersion lobe is also implied by marine evidence – potentially indicating a prolonged and/or phased eruptive episode due to seasonally variable winds over Central America (Sáenz & Durán-Quesada, 2015). The LCY isochron is documented in >100 submarine stratigraphies from the East Pacific and Caribbean (e.g. Marcantonio et al. 2020; Kutterolf et al. 2016; Mueller et al. 2010; Hodell et al. 2008; Kutterolf et al. 2008; Rose et al. 1999; Ledbetter, 1985; Drexler et al. 1980), and provides a robust time-stratigraphic marker during Greenland Interstadial 21 (Correa-Metrio et al. 2012; Dubois et al. 2011). Since the 1970's, layers attributable to LCY have been found to extend to off-shore Florida and Ecuador (Schindlbeck et al. 2018; Kutterolf et al. 2008), and stratigraphic correlations improved by analysis of LCY whole-rock composition (e.g. Vogel et al. 2006; Rose et al. 1999, 1987; Newhall, 1987).

Table 1: Major Quaternary tephrostratigraphic markers for each CAVA region, ordered by Proximal Fallout Volume (km^3) (based on data from Kutterolf et al. 2016, 2008a, b; Schindlbeck et al. 2016). Ages sourced from LaMEVE (Crosweller et al. 2012), those highlighted in grey represent 'best-estimates' based on stratigraphic placement. The LCY isochron is highlighted in yellow.

Unit Name	Volcano	Source Region	Age (ka BP)	Proximal Fallout Volume (km^3)
Los Chocoyos	Atitlán	Guatemala	84 ± 5	266.2

W-fall	Atitlán	Guatemala	158 ± 3	41.5
Tierra Blanca Joven	Ilopango	El Salvador	1.5 ± 0.03	32
Terra Blanca 4	Ilopango	El Salvador	*~36*	25.9
L-fall	Amatitlán	Guatemala	*~191*	19.6
Arce	Coatepeque	El Salvador	70 ± 2	11.6
Upper Apoyo	Apoyo	Nicaragua	29468 ± 126	7.2
Congo	Coatepeque	El Salvador	56.9 ± 2.8	6.3
E-fall	Amatitlán	Guatemala	*~51*	5.0
Masaya Tuff	Masaya	Nicaragua	*~1.8*	4.8
Chiltepe	Chiltepe	Nicaragua	2 ± 0.1	3.9
Lower Apoyo	Apoyo	Nicaragua	28762 ± 338	3
Mixta	Ayarza	Guatemala	32.255 ± 1.763	2.9
Upper Ometepe	Concepción	Nicaragua	*~19*	2.9
Upper Apoyeque	Chiltepe	Nicaragua	14.462 ± 0.317	2.2
Blanca Rosa	Berlin-Chinameca	El Salvador	75 ± 10	1.9
Mafic Cosigüina Tephras	Cosigüina	Nicaragua	~ 21-23 (*multiple layers*)	1.5
Fontana	Masaya	Nicaragua	*~60*	1.3
Twins/A-Fall	Berlin-Chinameca	El Salvador	61 ± 7.32	1
Masaya Triple Layer	Masaya	Nicaragua	2.129 ± 0.178	0.8
Lower Apoyeque	Chiltepe	Nicaragua	20.455 ± 2.467	0.8
San Antonio	Masaya	Nicaragua	6 ± 0.1	0.5
Concaste	Coatepeque	El Salvador	*~51*	N/A
Pinos Altos	Ayarza	Guatemala	*~23*	N/A
Older Pumice	Ilopango	El Salvador	*~75-84*	N/A

The terrestrial prevalence of LCY tephra, however, remains sparse. Lake Petén Itzá in north-east Guatemala currently represents the only distal onshore record containing an LCY layer (Kutterolf et al. 2016), and marine studies have primarily focussed on visible ash beds. Dominantly silicic, vesicular shards (Kutterolf et al. 2016; Rose et al. 1987) and plume height of ~45 km (Metzner et al. 2014) suggests that LCY fine ash was incorporated into global stratospheric flow, and detection of Central American tephra in Northern European sediments >8000 km away (Plunkett & Pilcher, 2018; Wulf et al. 2016) suggests such distal dispersal is possible. Therefore, it is likely terrestrial factors hinder more frequent detection of LCY fine ash. An eruption age of ~84 ka BP limits effective preservation to sites characterised by high sedimentation, and low bioturbation/reworking. Research suggests high-altitude regions in Central America were glaciated during the LGM (Palacios et al. 2020), so the advance and retreat of mountain/valley glaciers would have perturbed, and potentially increased, the rigour of hydrological and geomorphological processes in the Sierra Madre mountains. Evidence also suggests the eruption plume exhibited a multi-directional dispersal axis,

potentially enhancing particle diffusion and reducing LCY deposit concentrations below the detection threshold, potentially exacerbated as Guatemala is surrounded by ocean, so primary fallout would have occurred over water whereby the preservation, transport, and deposition of ash could be further affected by bathymetric currents or gravitational flows (Engwell et al. 2014; Cassidy et al. 2014; Scudder et al. 2014). Nonetheless, it is hard to disentangle poor preservation from research paucity to explain sparse terrestrial occurrences of LCY tephra. High-resolution analysis of distal tephras from onshore sediments has thus far focussed on regions such as Northern Europe, North America, Kamchatka, Patagonia, New Zealand, Alaska, the Mediterranean and Japan (Lane et al. 2017), so many potentially viable Central America sites remain unstudied. Work is underway to develop a similar tephrostratigraphic lattice for this region (e.g. Schindlbeck et al. 2018; Kutterolf et al. 2016), as Central America hosts several densely populated countries and cities (e.g. Mexico City, Bogotá, Guadalajara). Atitlán volcano alone has 6 cities with >1 million inhabitants within the estimated LCY fallout zone (Kutterolf et al. 2016), which is concerning for the future given tendencies for long-lived, composite super-volcanic systems to display eruptive activity following the caldera-forming event (e.g. Barker et al. 2019). Studies in Central/South America have thus far yielded promising results (Smith et al. 2019; Del Carlo et al. 2018; Watson et al. 2015), so the terrestrial prevalence of the LCY isochron is likely to increase as the number of Central American sites studied increases, and geochemical techniques for identifying distal ashes become more refined.

2.2.1.3.2. Youngest Toba Tuff (YTT)

Toba is the largest Quaternary caldera on Earth. Located on Sumatra, Indonesia, the caldera is 100 x 30 km in area, housing Lake Toba and a central resurgent dome (Samosir Island) which formed within ~1,500 years of the Youngest Toba Tuff (YTT) super-eruption (Mucek et al. 2017; de Silva et al. 2015; Chesner, 2012). The volcano lies 300 km NE of the Sunda subduction trench (Barber et al. 2005): a region known for intense seismic activity, including the devastating 2004 Indian Ocean earthquake (Lay et al. 2005). The Toba system produced three >M7.0 eruptions prior to ~74 ka BP: Haranggoal Dacite Tuff (~1200 ± 160 ka BP), Oldest Toba Tuff (~850 ± 2.2 ka BP), Middle Toba Tuff (~501 ± 5 ka BP) (Chesner, 2012), yet the YTT represents the largest both within the Toba system, and the entire Quaternary period (Oppenheimer, 2011; Chesner et al., 1991) with a magnitude of 8.8 (Crosweller et al. 2012). The eruption ejected ~5300 km^3 DRE of magma and 800 km^3 of tephra over multiple days (Costa et al. 2014), for which geochemical characterisation has identified five distinct compositions (Pearce et al. 2020) - suggesting complex (Reid & Vasquez, 2017), trans-crustal magma petrogenesis comparable to other known supervolcanic systems (Gualda et al. 2019; Swallow et al. 2018). Alongside thick ignimbrite deposits across Sumatra (Rose & Chesner, 1987), an easterly jet

stream (Bühring & Sarnthein, 2000) facilitated coignimbrite plume entrainment to the west, lending to discovery of distal YTT ash in the Indian Ocean (Ninkovich, 1979). Tephrochronological methods have also permitted identification of ~5 cm YTT ash layers in mainland India (Pearce et al. 2014., Matthews et al. 2012) and the South China Sea (Liang et al. 2001) and cryptotephra deposits in East Africa (Smith et al. 2018., Lane et al. 2013) and Malaysia (Smith et al. 2011), rendering the YTT one of 9 inter-continental key Quaternary stratigraphic markers (Lane et al. 2017). Bipolar sulphate enrichments in Greenland and Antarctic ice have tentatively been correlated to the eruption, however an absence of YTT tephra within the ice prevents designation of the eruption to any given sulphate signal (Svensson et al. 2013; Zielinski et al. 1996).

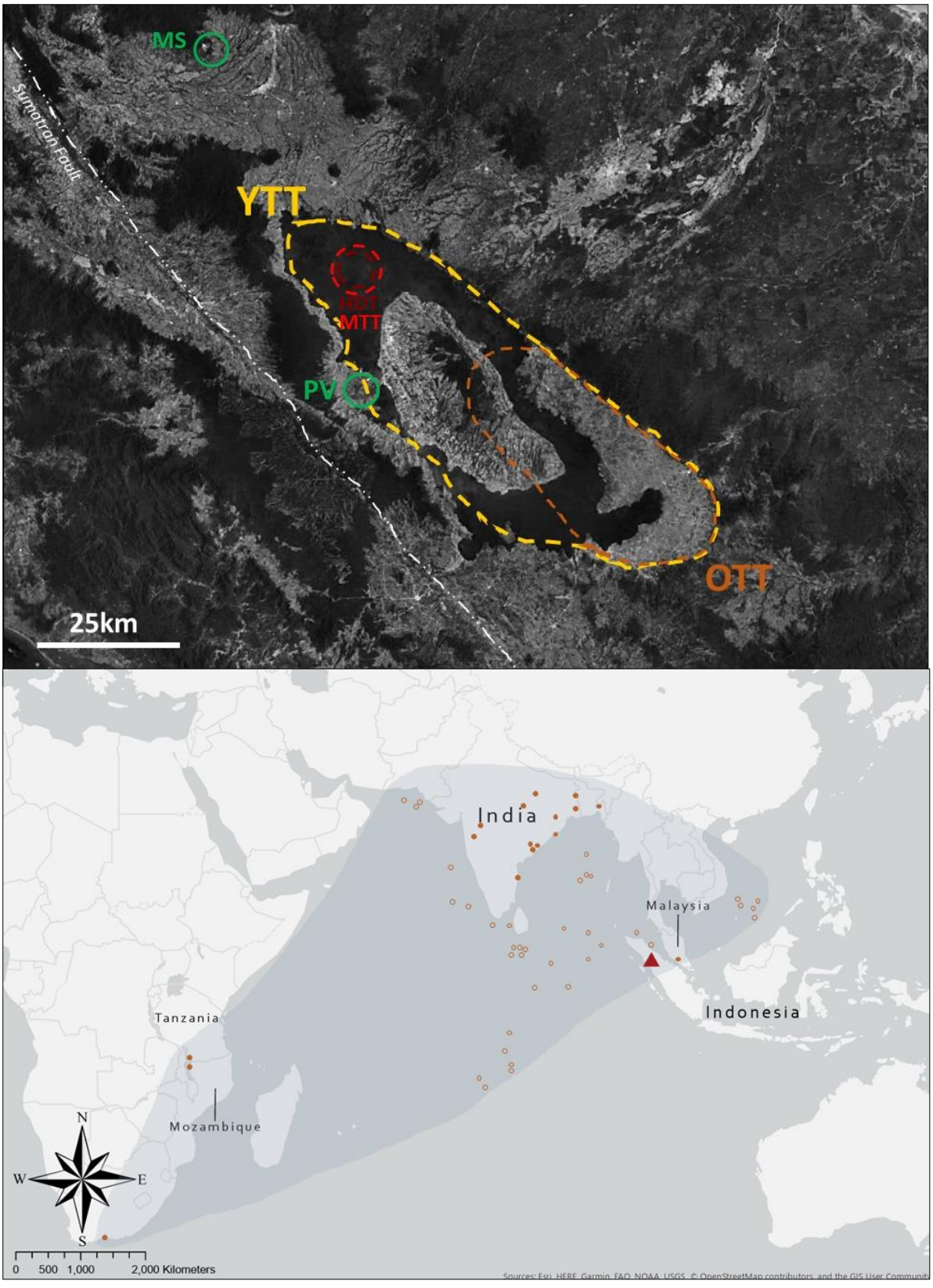
MS
Sumatran Fault
YTT
HDT
MTT
PV
OTT
25km
India
Malaysia
Indonesia
Tanzania
Mozambique
N
W
E
S
0 500 1,000 2,000 Kilometers

Figure 6: (TOP) Map of Toba caldera, with caldera boundaries marked as red, orange, and yellow circles respectively, and proximal volcanoes marked by green circles. YTT - Youngest Toba Tuff; OTT - Oldest Toba Tuff; HDT – Haranggoal Dacite Tuff; MTT – Middle Toba Tuff; MS- Mount Sinabung, PV - Pusikbukit Volcano. Adapted from Chesner (2012) and Oppenheimer (2002). Base image sourced from Google™ Earth Pro.
(BOTTOM) Map of sites with identified YTT tephra and/or tephra (adapted from Lane et al. 2013., Matthews et al. 2012., Liu et al. 2006), with Toba caldera marked as a red triangle. Non-filled circles depict marine core sites, filled circles indicate terrestrial sites. Created in ArcGIS Pro (v2.5)

The YTT is central to ongoing debate concerning its environmental and anthropogenic repercussions. These range from catastrophic (Williams et al. 2009; Rampino & Ambrose, 2000; Ambrose, 1998; Rampino & Self, 1993) to negligible (Yost et al. 2018; Smith et al. 2018; Jackson et al. 2015; Lane et al. 2013; Petraglia et al. 2007), and have been extensively studied across a range of academic disciplines. Through extrapolation of instrumental data from Pinatubo (1991) and Tambora (1815), in conjunction with pioneering computer models, early hypotheses suggested that drastic reductions in global temperatures following a YTT-induced dust-veil event was capable of causing a 'volcanic winter' with catastrophic effects on the biosphere (Rampino & Self, 1993, 1992) and early human population diversity (Ambrose, 1998). However, many now reject this '*catastrophe theory*'. From an archaeological perspective, it is difficult to establish YTT as cause for near extinction of early humans due to the recurrence of other environmental stressors throughout the Pleistocene (Oppenheimer, 2002), and difficulty establishing true population numbers solely based on archaeological evidence. Environmental impacts would have also likely been heterogeneous due to geographically variable ash-fall concentrations, and variable atmospheric circulation (Costa et al. 2014). Evidence from Africa (Smith et al. 2018; Jackson et al., 2015; Lane et al., 2013) and continental India (Petraglia et al. 2007) suggests *Homo* populations prevailed in the absence of extreme climatic change; resilience supported by the fact the *Homo* lineage survived following 20 other high-magnitude eruptions (Oppenheimer, 2002). Evidently, more evidence is needed (Williams et al. 2012) to provide robust support for the YTT as a catalyst of notable anthropogenic disturbance, and the assumption that eruption magnitude is directly proportional to anthropogenic impact is notably deterministic.

Quantifying the climatological effect of the YTT is complex. Computational modelling of radiative forcing in the eruption aftermath (e.g. Timmreck et al. 2012; Robock et al. 2009; Jones et al. 2005., Oppenheimer, 2002) largely relies on parameter estimation, due to ambiguity surrounding the eruption's plume height, eruption intensity and sulfur yield. Values for YTT aerosol flux are often derived from notably smaller historical eruptions (e.g. Pinatubo, 1991 - Timmreck et al. 2012) which, when extrapolated as a function of magnitude, increase the risk of overestimation for the YTT. Sulphur flux is fundamental in the climatic impact of volcanism but can notably differ between eruptions of the same magnitude (Carn et al. 2016; Sun et al. 2014; Oppenheimer et al. 2003). The

YTT is described as an explosive coignimbrite eruption (Costa et al. 2018) characterised by substantial ejection of fine-ash and potent gases (Woods & Wohletz, 1991). However, intra-atmospheric processes may have spatio-temporally attenuated the magnitude of radiative forcing (English et al. 2013; Timmreck et al. 2010). Enhanced volatile interactions and increased net particle size could result in shorter aerosol residence times in the atmosphere, and the radiative effect of SO_2 (GHG) comparable to sulphate aerosol may have reduced the magnitude of climatological perturbation by inhibiting ozone photolysis, offsetting the effects of sulphate aerosols (Osipov et al. 2020; Bindeman et al. 2007). Furthermore, partial (~25%) syn-eruption exsolution (Chesner & Luhr, 2010) of SO_2 suggests greater petrological comparability to Tambora (1815 CE: M7.0) – one order of magnitude smaller with a relatively modest climatic effect. A growing number of studies suggest no ubiquitous long-term cooling effect consistent with a prolonged 'global winter' (Haslam & Petraglia, 2010), however climatic perturbation following the YTT could have instead manifested in a hemispherically-asymmetrical manner (Baldini et al. 2015) by means of an antipodal teleconnection between both hemispheres (Svensson et al. 2013; Stocker & Johnsen, 2003) – meaning reorganisation of major atmospheric systems (e.g. the ITCZ – Colose et al. 2016; Ridley et al. 2015) could ensue following volcanic-derived aerosol injection and resultant cooling in the NH. This hypothesis supported by proxy evidence suggesting cooling in the Northern Hemisphere (Polyak et al. 2017; Baldini et al. 2015; Carolin et al. 2013) and warming/no change in the Southern Hemisphere (Yost et al. 2018; Smith et al. 2018; Cheng et al. 2013; Lane et al. 2013). Climatological disequilibrium resulting from intermediate NH ice volume may have further exacerbated this asymmetrical effect (Baldini et al. 2018; Bintanja and van de Wal, 2008), however the initial state of the tropical Pacific largely influences global distribution of temperature anomalies and is principally unknown at ~74 ka BP (Timmreck et al. 2012). Further quantification of baseline climate sensitivity during the Pleistocene is required to constrain climatological states preceding and following the YTT eruption, yet current evidence suggests the stratospheric loading effects of the YTT were surpassed by feedback-driven responses over several centuries (Robock et al. 2009; Zielinski et al. 1996), consequently sustaining millennial-scale atmospheric reorganisation, and manifesting as climate change contingent on hemisphere.

Despite a growing body of evidence suggesting heterogenous global impacts of the YTT, a more comprehensive understanding of mechanisms and timescales behind accumulation/ejection of the Toba magmatic system is required. Evidence is intermittent and often of low quality, so the existing Toba stratigraphy requires further mapping (Mark et al. 2017) to better characterise the YTT eruption chronology, sulphur yield, intensity, and plume dynamics for applications in climatological and anthropogenic research fields. However, the Middle East and Asia remains one of the most

volcanologically under-studied regions in the world (Brown et al. 2014), meaning many sites containing YTT deposits and evidence of impact are yet to be examined.

2.2.2. Climate Variability

The most recent glaciation on Earth is referred to as the Last Glacial Period (LGP: since ~120 ka BP). This period saw the progressive advance of ice sheets in North America/Canada, Antarctica, Fennoscandia, and Greenland (Mix et al. 2001) to their most southward extent between 26.5 and 19 ka BP (Clark et al. 2009), and the climate was characterised by dynamic and abrupt transitions between stadial and interstadial conditions, characterised by global-scale reorganizations of the Earth's atmosphere-ocean circulation known as: (i) Dansgaard-Oeschger (Dansgaard et al. 1982) events, and (ii) Heinrich (Heinrich, 1988) events. However, their respective causes are equally as complex as their expression. This section discusses contemporary understanding of the mechanisms underpinning Dansgaard-Oeschger and Heinrich events and, specifically, how these events manifest within the paleoenvironmental record.

2.2.2.1. Dansgaard-Oeschger Events

During the LGP, 25 distinct climate cycles are detected in the North Greenland Ice Core Project (NGRIP) record (Rasmussen et al. 2014). These are referred to as *Dansgaard-Oeschger* (D-O) events (Dansgaard et al. 1982): characterised by an initial, rapid transition to warming (up to 16^{o}C rise: Kindler et al. 2014) in mere decades (Erhardt et al. 2019), followed by prolonged, gradual cooling in the NH. D-O events show bipolar synchrony (Gottschalk et al. 2015), although changes to the Antarctic Circumpolar Current and subsequently air temperature in the South (Pedro et al. 2018) lag ~200 ± 100 years behind Greenland (Buizert et al. 2015) – suggesting these climatic signals propagate in a north-south manner (Cheng et al. 2020). D-O events embody the strongest form of climate variability by instigating major changes in global temperature, hydroclimate, and atmospheric circulation (Thomas et al. 2009; Steffensen et al. 2008), measurable in $\delta^{18}O$, Ca^{2+}, and CH_4 ice core records from Greenland (Rasmussen et al. 2014; Blockley et al. 2012., Lowe et al. 2008., Alley, 2000) and Antarctica (Markle et al. 2016; EPICA Project Members, 2007; Wantanabe et al. 2003). These polar archives have been synchronized with each other (Svensson et al. 2020) and also other marine, and terrestrial, sediment sequences using age-transfer methods such as tephrochronology (e.g. Berben et al. 2020; Timms et al. 2019; Abbott et al. 2018; Bourne et al. 2015., Davies. 2015; Blockley et al. 2012) in order to better constrain regional differences in D-O event amplitude, and how these correlate with leads, lags, and teleconnections in the Earth system.

Speleothems are valuable records for study of D-O event signals at the mid/low-latitudes (**Figure 7**) (Corrick et al. 2020). $\delta^{18}O$ ratios derive directly from dripwater and thus meteoric precipitation, so speleothem isotope geochemistry can reflect external hydroclimatic conditions (Baldini, 2010). For example, Asian speleothem $\delta^{18}O$ demonstrate reductions in monsoon convective intensity in concurrence with North Atlantic cooling (e.g. Pausata et al. 2011; Wang et al. 2008; Zhou et al. 2008) associated with D-O events (Wang et al. 2001) – suggesting a teleconnection between North Atlantic temperature and atmosphere-ocean interactions in Asia (Cheng et al. 2019; Du et al. 2019; Cheng et al. 2016). The high chronological resolution provided by speleothem records (Cheng et al. 2013) also permits study of regional variabilities in D-O expression, with links to sea-surface temperature (SST) and precipitation sources (Dumitru et al. 2018; Ünal-İmer et al. 2015). For example, precipitation regimes interpreted from Mediterranean (Budsky et al. 2019), Iberian (Denniston et al. 2018), North African (Hoffman et al. 2016), and West European (Genty et al. 2010) stalagmite $\delta^{18}O$ records are matched by European model outputs (Merz et al. 2015), lake sediment archives (Brauer et al. 2007) and pollen records (Camuera et al. 2019; Sánchez Goñi et al. 2013) – which predominantly suggest that SST change during D-O intervals caused prolonged oscillations in the ocean energy budget, evaporation rates, atmospheric water vapour (Budsky et al. 2019), dominant air masses (Ünal-İmer et al. 2015), and precipitation composition/quantity (Bosmans et al. 2015).

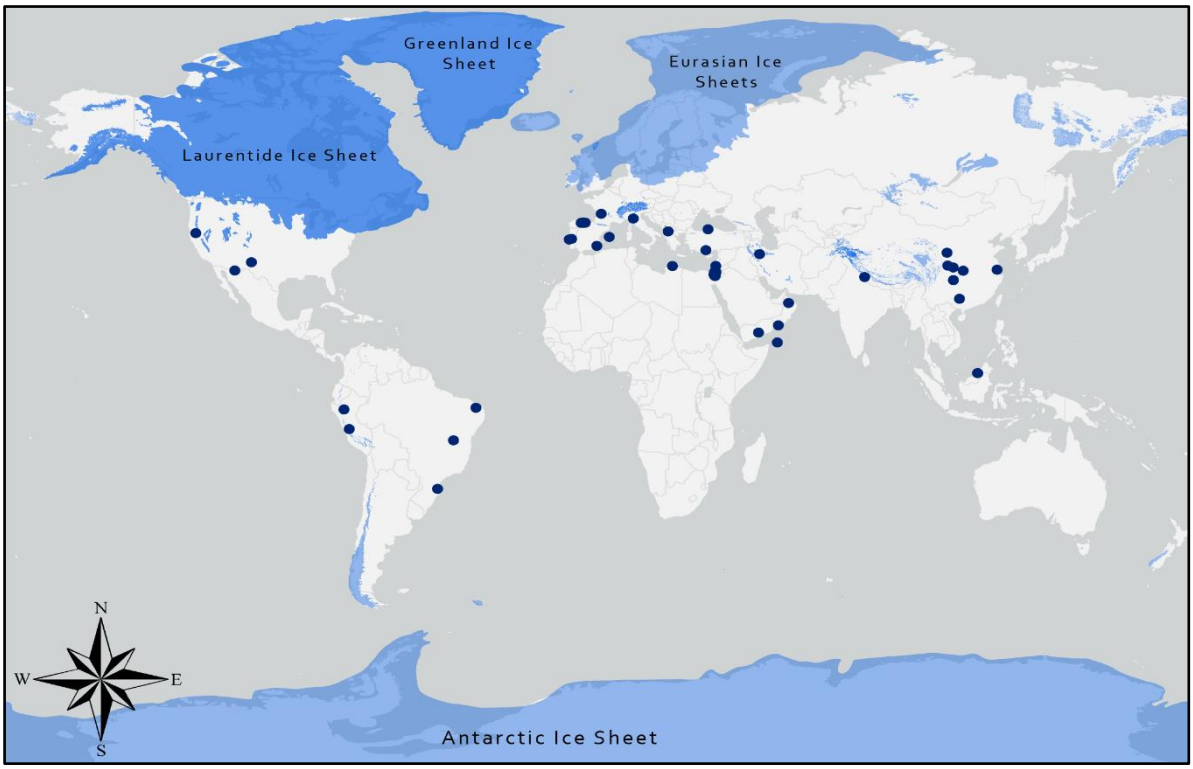

Figure 7: Map showing the locations of stalagmites preserving evidence of millennial-scale climate variability associated with single or multiple D-O oscillations*, marked as blue circles. Ice extent of the Last Glacial Maximum (LGM) 27-21ka BP is also marked in light blue (Ehlers et al. 2011). '**Eurasian Ice Sheets'** denotes the collective name for the Svalbard–Barents–Kara Ice Sheet, Scandinavian Ice Sheet, and British–Irish Ice Sheet respectively (Hughes et al. 2016).

* Oster et al. (2020); Du et al. (2019); Cheng et al. (2019, 2016, 2009); Budsky et al. (2019); Dumitru et al. (2018); Denniston et al. (2018); Regatteri et al. (2018); Mehterian et al. (2017); Kathayat et al. (2016); Ünal-İmer et al. (2016, 2015); Hoffman et al. (2016); Martin-Puertas et al. (2014); Stoll et al. (2013); Kanner et al. (2012); Rowe et al. (2012); Stríkis et al. (2011); Fleitmann et al. (2011, 2009); Pausata et al. (2011); Moreno et al. (2010); Asmerom et al. (2010); Wagner et al. (2010); Vaks et al. (2010); Genty et al. (2010, 2003); Allen et al. (2009); Cruz et al. (2009, 2006); Wang et al. (2008, 2006, 2001); Zhou et al. (2008); van Breukelen et al. (2008); Partin et al. (2007); Shakun et al. (2007); Sinha et al. (2005); Burns et al. (2003); Bar-Matthews et al. (2003); Kaufman et al. (1998).

Perturbation to the atmosphere-ocean system is widely accepted as the driving force behind D-O event initiation (Lynch-Stieglitz, 2017; Henry et al. 2016; Ganopolski & Rahmstorf, 2001), however the causes of perturbation are poorly constrained. D-O events appear concurrent with variability in the Atlantic Meridional Overturning Circulation (AMOC) (e.g. Pedro et al. 2018; Henry et al. 2016; Gottschalk et al. 2015; Piotrowski et al. 2005; Rahmstorf, 2002; Clark et al. 2002; Broecker et al. 1990) – the mechanism regulating oceanic heat transfer between the NH and SH (Pedro et al. 2018). In principle, a weakened AMOC would reduce the northward advection of heat resulting in a southward shift of the ITCZ (Kageyama et al. 2013), consequently weakening the equatorial south easterlies and deepening the equatorial and subtropical thermocline (Pedro et al. 2018); a process amplified by ice-albedo feedbacks in the NH. However, the question prevails: what would initially cause the AMOC to weaken? The influx of large 'freshwater' volumes, originating from proglacial lakes (Broecker et al. 2010), and/or continental ice rafts (during periods of enhanced ice calving from ocean-terminating glaciers - Menviel et al. 2014), into the Atlantic is a widely-cited source of this deterioration (Klockmann et al. 2018), yet fails to satisfy existing proxy evidence. One crucial instance is that not all D-O events are consistent with mass calving events (Lynch-Stieglitz, 2017), suggesting D-O variabilities are forced by factor of differing magnitudes and scales. Furthermore, hypothesis attributing freshwater pulses to pro-glacial outbursts have become contentious due to dubious geomorphological evidence (e.g. Baldini et al. 2018; Leydet et al. 2018). Modelling studies have also suggested changes in ice sheet topography (Zhang et al. 2014), atmospheric CO_2, meteoric moisture transfer (Zhang et al. 2017), and ocean convection (Sadatzki et al. 2019; Petersen et al. 2013; Li et al. 2005) as catalysts for AMOC deterioration, yet these often disproportionately represent the contemporary atmosphere-ocean state (Ortega et al. 2017), and thus their applicability to D-O events is questionable. It is possible that D-O event initiation instead results from multiple catalysts (Lohnmann & Ditlevsen, 2019; Kleppin et al. 2015) – cumulatively acting to send the climate system over an instability threshold (Ganopolski & Rahmstorf, 2001) or 'tipping point' (Lenton et al. 2008). This hypothesis could justify the inconsistency in D-O event frequency as thresholds may be reached faster than others, however quantifying and deconvoluting the

respective influence of different forcing mechanisms is a challenge, due to often poor record resolution and inherent complexities in the climate system not yet fully understood.

Explosive volcanism represents another potential catalyst for D-O events (Baldini et al. 2015). Findings from composite paleoenvironmental records (e.g. Kobashi et al. 2017; Sigl et al. 2015), historical archives (McConnell et al. 2020; Büntgen et al. 2016), and modelling studies (Pausata et al. 2020, 2016; Miller et al. 2012) spanning the past 2.5 kyr suggest volcanic eruptions are linked to large-scale reorganisations of the atmosphere (Ridley et al. 2015; Zanchettin et al. 2014., Haywood et al. 2013), perturbation to ocean circulation, and instigation of self-sustaining positive feedbacks - the magnitude of such influenced by eruption location and stratospheric circulation differences associated with the Brewer-Dobson effect (Butchart, 2014; Toohey et al. 2011; Holton et al. 1995). Theoretically, the same effect could have ensued on a greater scale during the Pleistocene - as 40 known eruptions exceeded the magnitude of the largest Holocene event (Changbaishan: 1.008 ± 0.004 ka BP, M7.4). Using a multi-proxy approach, Baldini et al. (2015) identify how all five known, radiometrically-dated Southern Hemispheric eruptions (>M6.0) occur within chronological uncertainty of a D-O event. This proposed link between explosive volcanism and abrupt climate variability is supported by further proxy (Baldini et al. 2018; Polyak et al. 2017; Carolin et al. 2013) and modelling (Brenna et al. 2020; Metzner et al. 2014; Timmreck et al. 2012) studies conducted for the same geological period. The strength of this correlation appears greater for periods of intermediate global ice volume (Baldini et al. 2018) during which the climate system shows increased sensitivity to perturbation (Zhang et al. 2017), which also justifies why not all known high-magnitude eruptions appear coincident with abrupt climate change (Baldini et al. 2015). Nonetheless, eruption record paucity in the Southern Hemisphere (Rougier et al. 2018; Brown et al. 2014) hampers the ability to quantify the impact of volcanic forcing on D-O event initiation and propagation. The validity of experimental modelling is substantially influenced by the quality of input data, which is inherently poorer and scarcer for pre-Holocene eruptions whereby parameters such as aerosol/volatile/particle flux, SO_2 yield, eruption type and plume height are often unknown (Timmreck, 2012). Tephra layers in annually resolved paleoenvironmental sequences present an alternative proxy for assessing eruption timing relative to observed environmental changes (Berben et al. 2020; Abbott et al. 2018; Bourne et al. 2015). However, this is contingent on whether tephra layers appear unanimously across multiple archives (Davies et al. 2015), and whether the stratigraphic placement of tephra layers accurately represent the time of deposition. For pre-Holocene deposits, there is greater potential for particle dissemination due to sedimentary reworking associated with periglacial processes (Davies et al. 2007; Ballantyne, 2002) and problems can arise if tephra quantities fall below the detection threshold, or the layer lacks a unique geochemical signature (Davies et al. 2015.,

Bourne et al. 2013; Lane et al. 2012). In such cases, a discrete eruption event may be misinterpreted as secondary reworked material (Lowe, 2011). Dating uncertainties associated with Last Glacial Period paleoclimate (Lane et al. 2013) and volcanic (Brown et al. 2014) events are often multi-centennial in scale, and so establishing robust correlations between climate change and volcanism are challenging. Evidently, improvements in the spatial and temporal resolution of eruption records are needed to confidently establish a link between volcanism, and initiation of D-O events.

There is still much to learn about the initiation and drivers of D-O oscillations. Variabilities between high-latitude and tropical climate systems add further complexity to an already intricate network of systems and feedbacks (Cvijanovic & Chiang, 2013). For example, a D-O signal recorded at a tropical site may be the product of either i) fast teleconnections from the high latitudes (annual timescales); or ii) secondary teleconnections due to slowly-evolving change (decadal to centennial timescales) (Rasmussen et al. 2014). Hence, D-O signals can appear different yet be related to the same large-scale atmospheric reorganisation. Establishing causality remains a challenge (Barker et al. 2015; Álvarez-Solas et al. 2013, 2011), further exacerbated by spatial gaps in available records which disproportionately favour the NH, and consequently limit comparison of natural proxies and global atmospheric circulation models (Wong & Breecker, 2015). The AMOC hypothesis appears strong for longer-lasting events, yet difficulties in identifying direct evidence for AMOC disturbance during shorter events suggests other driving mechanisms may have influenced their initiation (Lynch-Stieglitz, 2017). Proposed causal mechanisms must account for the rapidity and hemispheric-scale of D-O events (Baldini et al. 2015), and evidence from the NH (high latitudes) suggests that D-O initiation involved coupled ocean-climate systemic feedbacks (Sadatzki et al. 2019). Until evidence emerges that all D-O events can be attributed to changes in the AMOC, it is questionable whether these changes are the initial forcing underlying D-O events, or just a response/feedback to another driver. Equally, evidence for hemispherically distinct responses to climate change suggests that evidence from the opposing hemisphere must also be considered, if we are to better understand millennial-scale variabilities in the global climate system.

2.2.2.2. Heinrich Events

Of >20 D-O events during the Last Glacial Period, 6 correspond with Heinrich Events (HEs). HEs are defined as the discharge and deposition of ice-rafted debris (IRD) into the North Atlantic Ocean, are synchronous with hemisphere-wide climate variability (Broecker, 1994), and also appear concurrent with ice sheet and mountain glacier maxima in North America, Europe, and South America (Hulbe et al. 2004). IRD layers in marine sediments appear to have originated mainly from (although not limited to) the Laurentide Ice Sheet (LIS) via the Hudson Strait (Stokes et al. 2005; Hemming et al.

2004; Henirich, 1988). However, the driving mechanisms behind HEs are enigmatic due to their occurrence during periods of climatic cooling. Several mechanisms have been proposed to explain their occurrence; however, none have been confirmed nor widely accepted. Current working hypotheses for HE initiation can be grouped into 2 broad categories: internal and external.

One key hypothesis is the Binge-Purge model, which suggests HEs are triggered internally. First developed in the early 1990's (MacAyeal, 1993), the model suggests that ice sheets would grow to maximum extent (binge), then release (purge) large numbers of icebergs due to basal destabilization. In contemporary marine-terminating glaciers, basal destabilization occurs due to melting (e.g. Lemos et al. 2018; Armstrong et al. 2016; Bartholomaus et al. 2008) and is associated with solar insolation and seasonality (Cavanagh et al. 2017; Joughin et al. 2008), as warmer temperatures facilitate the formation and drainage of supra-glacial lakes (Zwally et al. 2002) through hydrologically assisted fractures in the ice (Catania et al. 2008). Basal melt occurs due to friction, entrapment of geothermal heat, and gravitational force – all of which reduce the pressure melting point of ice (Verbitsky & Saltzman, 1995), increase pore water pressure within unconsolidated basal sediments (Boulton et al. 2001), lubricate the bedrock and ultimately reduce the contact between glacier and bed (Clarke, 2005). For ice sheets, accelerated ice flux primarily occurs due to subsole deformation of multiple outlet glaciers (King et al. 2020), and evidence suggests this process was also influential for large ice sheets (**Figure 7**) such as the LIS (Roberts et al. 2016). However, flux and calving rates are not a direct function of basal meltwater volume, and contemporary analogues (e.g. Greenland: Stevens et al. 2015; Van de Wal et al. 2008) have highlighted how contesting effects of sliding, variations in meltwater input, and evolution of the subglacial drainage system can all cause variations in ice speed (Chu et al. 2016). The binge purge model opposes this, by suggesting climate exerted only a peripheral role on ice-sheet calving. Furthermore, the robustness of the binge-purge hypothesis depends on inclusion of HEs 3 and 6 (Bigg et al. 2010; Hemming et al. 2004; Sarnthein et al. 2001) which, if omitted, weakens the argument that common glaciological processes can solely provide an explanation for HE occurrence. Repetitive glacial outburst flooding (jökulhlaups) from lakes in the Hudson Strait have also been suggested as an internal HE catalyst (Hemming, 2004; Johnson & Lauritzen, 1995). Jökulhlaups are large floods that occur when the water contained in a pro-glacial lake exceeds the height of the dam, due to rising lake levels or reduced flow of glacial ice. This theory currently lacks robust evidence which would support the presence of an ice-dammed lake in Hudson Bay throughout the last Glacial Period, yet some argue this scarcity is a function of research bias (Andrews & Voelker, 2018). This is hard to confirm until further evidence is gained.

The size and varying growth conditions of ice sheets responsible for HEs have prompted generation of other theories which suggest an external influence on HE instigation. Hulbe (1997) proposed that

IRD transmission and deposition resulted from rapid disintegrations of ice shelves, as a product of climatic warming. Ice sheet expansion would occur during the cold intervals of D-O oscillations, as cooler air and sea surface temperature would promote increased grounding line ice volume (Hulbe et al. 2004). Conversely, sheet disintegration would occur when surface meltwater directly propagated through ice fractures, saturating basal sediments and causing rapid disintegration of fringing ice shelves. This would reduce the amount of ice stream buttressing – causing ice stream instability, acceleration, and increased calving (Gudmundsson, 2013). Debris would be protected by basal underplating by marine ice which, alongside small, capsized icebergs (debris on top) would be transported East across the North Atlantic and deposit IRD once the iceberg melted entirely (Meyer et al. 2019). This also suggests HEs are predominantly modulated by solar insolation variability (Heinrich, 1988; Bond et al. 1993), however, proxy evidence highlights multiple problems with this hypothesis. For example, evidence for open, mild oceans during the LGM alludes that a vast ice shelves may not have existed (de Vernal et al. 2000, 2005). Equally, HEs seemingly correlate more strongly with changes to ocean circulatory systems rather than solar insolation (e.g. Barker et al. 2015; Álvarez-Solas et al. 2013, 2011; Marcott et al. 2011). Subsequent hypotheses propose this process links to isostasy: by generating a cycle of ice sheet retreat due to warm subsurface waters, sill elevation due to isostatic rebound, and consequent regrowth of the ice sheet when these warm waters became blocked by the sill (Bassis et al. 2017). In this cycle, enhanced calving would occur during the period of rapid retreat. The extent to which these modern analogues can be used to study ice sheet variability is contentious, as these structures were much larger (Batchelor et al. 2019) and timescales upon which HEs operated far surpass timescales of instrumental observation of modern-day ice sheets. However, contemporary work suggests the mechanisms responsible for ice sheet calving during the Last Glacial Period may be more similar to modern-day marine-terminating glaciers than previously believed.

Not one theory fully accounts for why HEs appear inconsistently during D-O events, with the complete absence of IRD deposition during some (Ziemen et al. 2019; Alley et al. 2005). This is notably due to ambiguous causality: it is unclear whether HEs caused ocean circulation changes, or whether they are a product of prolonged change to the ocean-climate system in response to another forcing agent. Research suggests that HEs are temporally coincident with perturbations to the Atlantic Meridional Overturning Circulation (AMOC) (Clark et al. 2007), defined as "*the zonally and vertically integrated northward volume transport*" of the ocean (Buckley & Marshall, 2016: p. 9) which drives the equator-ward transport of cool, dense water formed in the North Atlantic – a system which disproportionately affects NH climate due to its role in heat and carbon transport from the surface to the deep ocean. Research has suggested the AMOC is sensitive to changes in deep

ocean convection (Medhaug et al. 2012) and thus could be weakened by large freshwater flux into the ocean (Clement & Peterson, 2008). On one hand, some suggest that HEs could have provided adequate quantities of freshwater to perturb North Atlantic Deep Water (NADW) formation (He et al. 2020; Rahmstorf, 2002), and thus HEs represent the driving mechanism underpinning AMOC disturbance. Conversely, others argue that HEs are the result of AMOC perturbation, as there is evidence that a weaker AMOC may trigger ice-sheet instability and input of glacier melt to the North Atlantic, rather than be caused by it (Lynch-Stieglitz, 2017; Álvarez-Solas et al. 2013, 2011; Marcott et al. 2011; Gutjahr & Lippold, 2011). Instead, the melting of icebergs into the Atlantic may have provided a positive feedback favouring persistently cool conditions (Barker et al. 2015; Álvarez-Solas et al. 2013), causing a hemispherically asymmetrical response by suppressing the AMOC and allowing large amounts of heat to build up in the Southern Ocean (Buizert et al. 2015). This implies the existence of a threshold beyond which, after a period of gradual cooling, the transition to a stadial state becomes inevitable – as interstadial duration is a function of interstadial cooling rate (Schulz, 2002).

HE signatures do appear global in propagation and impact (Kageyama et al. 2013), however more evidence is needed to fully capture and constrain the nature, scale and drivers of these events. Certain HEs appear strongly correlated to changes in oceanic circulation and temperature, however in this case cause and effect remain notoriously challenging to quantify. For example, many high-resolution benthic carbon isotope records have been generated looking for signatures of deep water change associated with the HEs, yet findings are inconsistent among locations, and hampered by poor time resolution and noisy data (Lynch-Stieglitz, 2017). Furthermore, research of Southern Hemispheric records of HE propagation (Clement & Peterson, 2008; Voelker, 2002) are scarce, and currently lack sufficient resolution to robustly establish cause and effect between ocean-atmosphere perturbations and the occurrence of HEs, and how these link to ice sheet dynamics.

3.0. RATIONALE

The study of Earth's volcanic history relies on geological evidence; however, the current eruption record is incomplete, and uncertainty increases as a function of time (Rougier et al. 2018; Brown et al. 2014). Ice core sequences provide annually resolved, chronologically robust archives of past climate (Rasmussen et al. 2014) and volcanic activity (Svensson et al. 2020; Zielinski et al. 1996), yet show significant geographical bias. For example, as signal clarity decreases as a function of distance, tropical eruption signatures are more likely to experience attenuation before reaching the polar regions, disproportionately favouring higher latitude eruptions (Svensson et al. 2020). This paucity

has profound implications for quantifying the frequency (Papale, 2018) and relative influence of volcanic activity on the pacing and timescales of abrupt environmental change (Davies, 2015). Unlike ice-core, lacustrine, peat, and marine sequences, stalagmites are found across a large latitudinal gradient and can provide similarly precise records of changes to temperature, local precipitation, atmospheric circulation, and composition (Wong & Breecker, 2015). Moreover, they are diverse paleo-volcanic records with potential for preservation and detection of volcanic-derived ash fall (Ünal-İmer et al. 2020; Jamieson et al. 2015; Badertscher et al. 2014; Frisia et al. 2008) alongside millennial-scale perturbation to climate by volcanic forcing – the latter through use of stable isotopes (e.g. $\delta^{13}C$ and $\delta^{18}O$) and climate-responsive trace elements (e.g. Mg, U) (Ünal-İmer et al. 2020; Du et al. 2019; Polyak et al. 2017; Baldini et al. 2015; Carolin et al. 2013). If stalagmite chronologies and eruption dates are well constrained, post-volcanic climate change can be detected in the absence of a tephra horizon. There are likely many volcanic signals preserved in stalagmite sequences, however the number of studies searching for these signals are limited, and the spatio-temporal distribution of stalagmites used in a volcanological context is inconsistent - limiting knowledge of how volcanic signals may manifest within these records.

This thesis studies two new trace element datasets from two separate stalagmites. **Chapter I** presents the analysis of NIED08-05, a stalagmite grown between 0 – 3 ka BP (Lechleitner et al. 2016) and sourced from Niedźwiedzia Cave, south-west Poland. Previous application of PCA to a tropical stalagmite dataset successfully detected ash fall associated with explosive volcanism, through identification of transient trace element enrichments concurrent with ash transport over Actun Tunichil Muknal cave, Belize, between 1979-2001 (Jamieson et al. 2015). By replicating this technique on a temperate Polish stalagmite, the suitability of PCA for detection of volcanic-derived geochemical deposition in a non-tropical, prehistoric archive is tested. **Chapter II** presents the analysis of DIM-3-A (south Turkey) – a sample extracted from the base of stalagmite DIM-3 (Ünal-İmer et al. 2015), which grew between 70 and 90 ka BP (Ünal-İmer et al. 2015) and is sourced from Dim Cave, southern Turkey. Stalagmite dripwater composition is heavily influenced by regional climate and dominated by seasonal flow, meaning colluvial throughput could cause entrainment and deposition of tephra onto the stalagmite. Over centennial-to-millennial timescales, cumulative changes to the Dim Cave dripwater supply and composition also reflect changes in both East Mediterranean moisture availability (Rowe et al. 2020; Ünal-İmer et al. 2016; Baykara, 2014) and storm track displacement (Ünal-İmer et al. 2015). Thus, this sample shows potential for detection of both short (e.g. ash fall) and long (e.g. climate) term volcanic impacts.

Continuing development of global speleochronologies can address key questions regarding the link between volcanism, environmental change, and long-term climate variability. The primary aim of

this thesis is, therefore, to evaluate the suitability of stalagmite trace element sequences as records of explosive volcanism. The outcomes of this work will not only quantify the mechanisms controlling incorporation of volcanic-derived material into stalagmites, but also advocate which karst systems produce records most valuable for future research integrating speleology and paleo-volcanology.

4.0. METHODOLOGIES

4.1. LA-ICP-MS

Laser-Ablation Inductively-Coupled-Plasma Mass Spectrometry (LA-ICP-MS) is a modern analytical technique for in-situ TE and isotope analysis (Ubide et al. 2015; Lin et al. 2013), widely used due to the high analytical resolution achievable per sample, in conjunction with reduced sample preparation, increased speed of analysis, and low cost (Limbeck et al. 2015; Günther & Hattendorf, 2005; Eggins, 2003). The technique involves use of a laser to generate and extract (ablate) fine particles from a solid sample, which is transported to a secondary ionisation source. Ions are extracted by a quadrupole and introduced to a mass spectrometer, to extract isotope and trace-elemental data. The relative abundance of each element within a sample is determined through separation of ions based on their mass-to-charge ratio, and the signal detected by the ICP-MS is directly proportional to this concentration. The researcher can maintain a high level of control throughout the process, as parameters such as beam diameter, laser repetition rate, and raster speed, can be changed in accordance with the sample being analysed (Petrelli et al. 2016; Sigmarsson et al. 2011; Pearce et al. 2011).

LA-ICP-MS is used within two primary areas of paleoenvironmental research: Geochemistry and Chronology (Müller & Fietzke, 2016). Since the late 1990's (Jeffries et al. 1998; Sinclair et al. 1998), advances in mass spectrometry have facilitated the extraction of geochemical data from heterogeneous archives, in order to study Earth-system interactions and changes throughout geological time (Gothmann et al. 2015). For naturally occurring archives, the magnitude of post-depositional alteration is proportional to time, so vigorous rates of erosion associated with climatic, tectonic, and weathering processes (Ganti et al. 2016) can obscure key geochemical signatures. However, further improvements in precision of the laser and mass spectrometer (Russo et al. 2002) means LA-ICP-MS can accurately deconvolute important geochemical changes across a sequence (Müller & Fietzke, 2016), from signals of degradation. This information can consequently be used to reconstruct climatic and environmental conditions at the time of sequence growth/accretion. For example, measurement of isotope and trace element ratios preserved in benthic archives such as corals (Deng et al. 2010), and molluscs (Elliot et al. 2009) can derive ocean composition (Mertz-Kraus

et al. 2009) and temperature (Evans et al. 2015; Griffiths et al. 2013), while analysis of other stable isotopes (e.g. lithium) can measure ocean dissolved-organic-carbon and pH (Vigier et al. 2015). Atmospheric temperature, composition, and precipitation can be derived from terrestrial, land-based archives such ice cores (Sneed et al. 2015), speleothems (Orland et al. 2014; Jochum et al. 2012; Fairchild & Treble, 2009; Desmarchelier et al. 2006), and tree rings (Monticelli et al. 2008). High instrumental sensitivity and low detection limits have also permitted the discovery of transient natural events, which can manifest as discrete enrichments of trace elements, which have become integrated into the archive sequence. These events include dust storms (Sneed et al. 2015), volcanism (Jamieson et al. 2015), and seasonal variations in effective precipitation (Hartland et al. 2012). If the occurrence date is well constrained, geochemical data obtained through LA-ICP-MS can help to characterise the former two events as chronological markers - allowing synchronisation of geographically diverse records featuring the same, distinct isochron (Lowe et al. 2017).

Accurate dating of paleoenvironmental archives requires a robust chronological framework. For this purpose, isotopic analyses by LA-ICP-MS can be hugely beneficial. LA-ICP-MS was initially used to assign zircon ages using U-Pb isotopes (Jackson et al. 1996), however since then, LA-ICP-MS has been used in development and application of Uranium (U)-series and strontium isotope stratigraphy (SIS) techniques. More recently, ^{14}C dating of paleoenvironmental archives has become possible with coupling of gas-source accelerator mass spectrometers to laser ablation instruments (Rosenheim et al. 2008). However, this dating technique is limited by the radiocarbon limit, and thus samples $<10^4$ years in age. U-series dating by LA-ICP-MS is commonly used to date continuously growing, carbonate-based samples, such as speleothems and corals (Eggins et al. 2005), whereby high U-Pb/Th regions are often sub-mm in scale. U-Th disequilibrium dating can date samples up to 10^5 years old, while U-Pb dating can acquire dates for carbonate samples $>10^7$ years in age with remarkable precision (Macdonald et al. 2019; Li et al. 2014).

LA-ICP-MS has played a significant role in creation of robust paleoenvironmental archive networks, for study of paleoclimate and environmental change. However, certain issues remain to be addressed (**Figure 8**), as the effectiveness of conducted analyses largely rely on the stability of the laser system, effective calibration of reference materials, and the homogeneity/size of the reference material (Limbeck et al. 2015). Future work will inevitably focus on the expansion of LA-ICP-MS applications to a wider range of geological samples, while striving for a better understanding of common analytical issues, and development of matrix-matched reference materials (Müller & Fietzke, 2016). Furthermore, the establishment of robust protocols for data processing, uncertainty assessment, reference material selection, and fractionation correction (if a sample has been ablated for a prolonged period) will allow for data sets obtained from different laboratories to be easily

compared (Sylvester & Jackson, 2016). This will broaden the scope of LA-ICP-MS applications across paleoenvironmental archives, and differing fields of expertise.

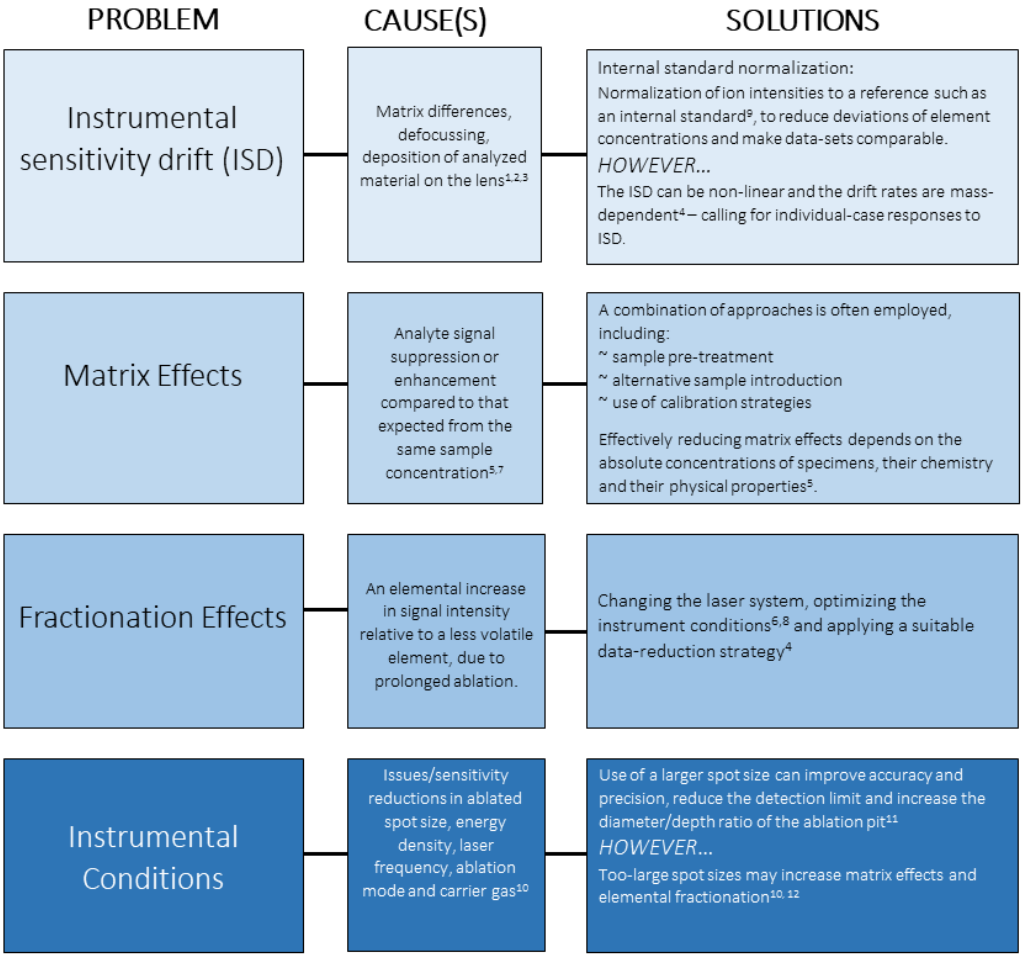

Figure 8: A series of flow diagrams, illustrating the common problems associated with use of LA-ICP-MS in trace-element analyses of geological samples.

[1] Lin et al. (2016); [2] Chew et al. (2014); [3] El Hadri et al. (2016); [4] Liu et al. (2013); [5] Agatemor & Beauchemin (2011); [6] Günther & Hattendorf (2005); [7] Hare et al. (2012); [8] Limbeck et al. (2015); [9] Uerlings et al. (2016); [10] Zhu et al. (2013); [11] Hu et al. (2011); [12] Kroslakova & Günther, D. (2007)

4.2. Principal Component Analysis

Principal Component Analysis (PCA) is a dimension-reduction method of data analysis and exploration, used to examine relatedness between variables. It combines the intra-variable association (covariance matrix), the data dispersion direction (eigenvectors), and the relative importance of these directions (eigenvalues) to assess which Principal Component (PC) explains the largest sum of variability in a sizable multivariate dataset. Put simply, it transforms the data based on a new coordinate system, whereby the largest variance is projected onto the first coordinate, known as PC1, the second largest onto the PC2 coordinate, and so forth (Abdi & Williams, 2010). This technique is particularly well suited for applications in geochemistry. Modern analytical

instruments have such precision that tens of variables (e.g. trace elements) can be measured on one sample, however this can create extremely large, multi-variate datasets. PCA not only improves the ability to visualise and interpret these datasets, but can also detect the sources and characteristics of transient changes in measured components through time. Applications of PCA are temporally extensive. In recent decades it has been used to characterise the modes and timescales of anthropogenic particulate concentrations in urban areas (Đuričić-Milanković et al. 2018), however applications are also valuable for analysis of paleoenvironmental data. For example, Mayewski et al. (1994) used PCA to identify transient changes in atmospheric composition, resulting from sea ice aerosols and atmospheric dust measured in ice cores from the Last Glacial Period.

In volcanology, use of PCA has primarily been within igneous petrology (Unglert et al. 2016) and tephrochronology (e.g. van der Bilt et al. 2017; Pouget et al. 2014), thus applications to assess volcanic frequency through time, through detection of volcanic trace element signals, is novel. Jamieson et al. (2015) identified short-lived trace element enrichments temporally coincident with dispersal of volcanic ash, raising the possibility for stalagmite chemistry to reflect periods of explosive volcanism. This study builds upon the work conducted by Jamieson et al. (2015), by using PCA as a tool for detection of volcanic eruptions in two stalagmites, each grown in different locations and during different periods of the Quaternary. Undertaking this study aims to aid understanding of which karst conditions favour effective preservation of volcanic signals, and in turn quantify the mechanisms controlling deposition, and preservation, of volcanic material in stalagmite sequences.

5.0. NIEDŹWIEDZIA CAVE – *Results Chapter I*

5.1. *Site Description*

5.1.1. Regional Climate

Wrocław Global Historical Climatology Network (GHCN) station is located 100km to the north of the study site (Jaskinia Niedźwiedzia or Bear Cave, near Kletno, SW Poland). Wrocław holds the longest continuous records of precipitation and air temperature in Poland, beginning in 1791 (Bryś & Bryś, 2010). For the period 1981-2010, annual mean temperature in Wrocław averaged 6.4°C (± 3.0°C). Based on a 30-year Industrial Era dataset from Wrocław (1980 – 2010) the climate in SW Poland is highly seasonal, with precipitation ranging from 27.2 mm (in February) to 84.4 mm (in July) and temperature ranging from -1.4°C (in January) to 18.7°C (in July) (**Figure 5B**). Precipitation in SW Poland typically results from the interaction of cold, continental air masses from Eastern Europe and warm, maritime air masses from the Atlantic (Piotrowski & Jędruszkiewicz, 2013). The climatic conditions of the Kleśnica valley in the Eastern Sudetes, where the Niedźwiedzia Cave is located, are harsh with a mean annual air temperature of 5.5 °C for 1992–2003 (Piasecki & Sawiński, 2009). The modern cave entrance is located ~670 m higher than Wrocław meteorological station, and the area is characterized by the absence of a climatic summer. The local air circulation in the valley and common air temperature inversions throughout the year are associated with foehn phenomena (Piasecki & Szymanowski 1995).

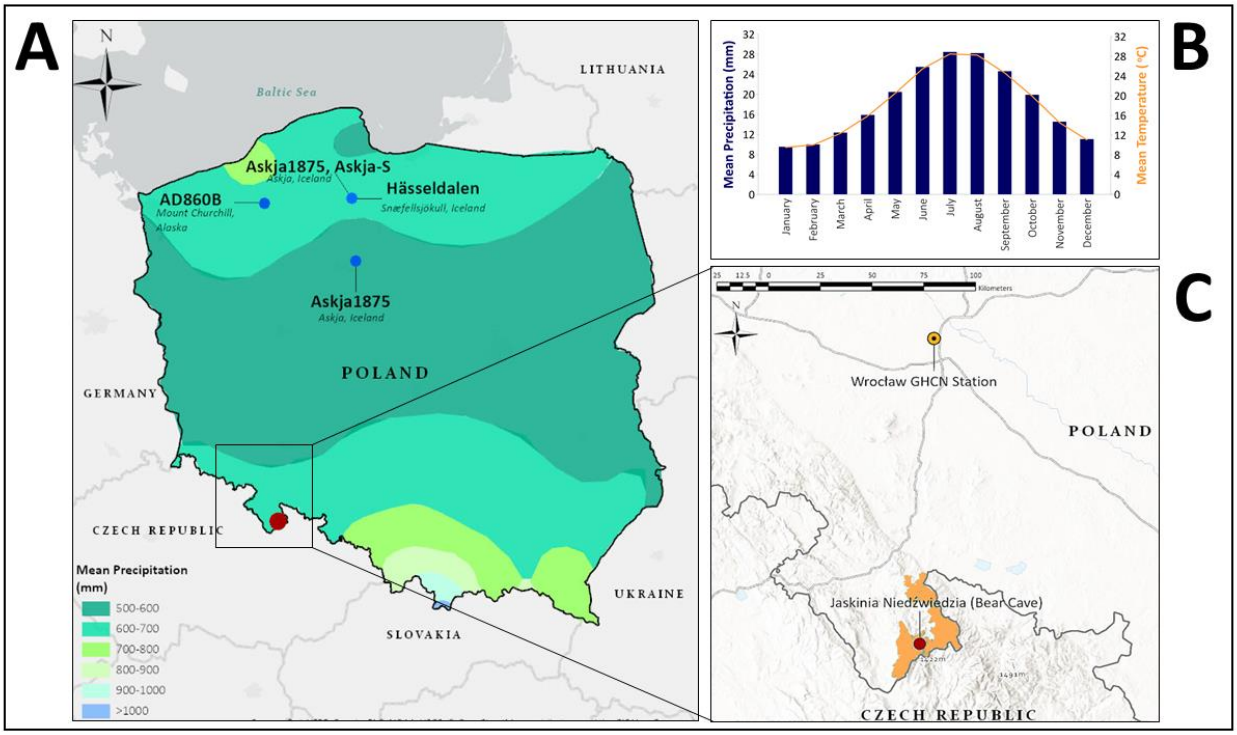

Figure 9: A - Map of Poland showing the location of the Niedźwiedzia Cave site (red circle). Blue circles denote sites with previously identified tephra deposits (Watson et al. 2017; Wulf et al. 2016). Map created in ArcGISPro v. 2.4.2. with precipitation data sourced from Szwed (2019); **B** - Wrocław mean monthly temperature (red line) and precipitation amount (blue bars) for the period 1980-2010 (GHCN Wrocław data). At this central European site, precipitation covaries with temperature with a minimum in winter (between December and March) and maximum in summer (between June and August). Data were obtained from the National Oceanographic and Atmospheric Administration (NOAA)'s Global Historical Climatology Network (GHCN); **C -** Topographic map of the Niedźwiedzia Cave site within Śnieżnik Landscape Park (orange shading) and location of Wrocław WGHCN station (orange circle). Map created in ArcGIS Pro (v. 2.4.2.)

5.1.2. Cave Monitoring

This study utilises stalagmite NIED08-05, extracted in 2008 from the upper cave level of Jaskinia Niedźwiedzia (50°14,068'N, 16°50,558'E; 790 m a.s.l. elevation), 10m below the surface. Jaskinia Niedźwiedzia is one of the largest cave systems in the Sudetes Mountains (Gąsiorowski et al. 2015), with a depth of >100 m, and a known passage length exceeding 4000 m (Kostka, 2014). Formed primarily within metamorphic carbonate rocks, the karst network is comprised of three chamber levels connected by fissures (Kasprzak & Sobczyk, 2017; Sobczyk et al. 2016). The cave is overlain by a mixture of soils and organic debris, weathered rock, and beech-spruce forest punctuated by exposed marble outcrops (Piasecki & Sawinski, 2009). The cave environment is stable with a mean cave air temperature (6°C) that reflects the multi-annual mean external temperature and a relative humidity of 96-98% (Piasecki & Sawiński, 2009).

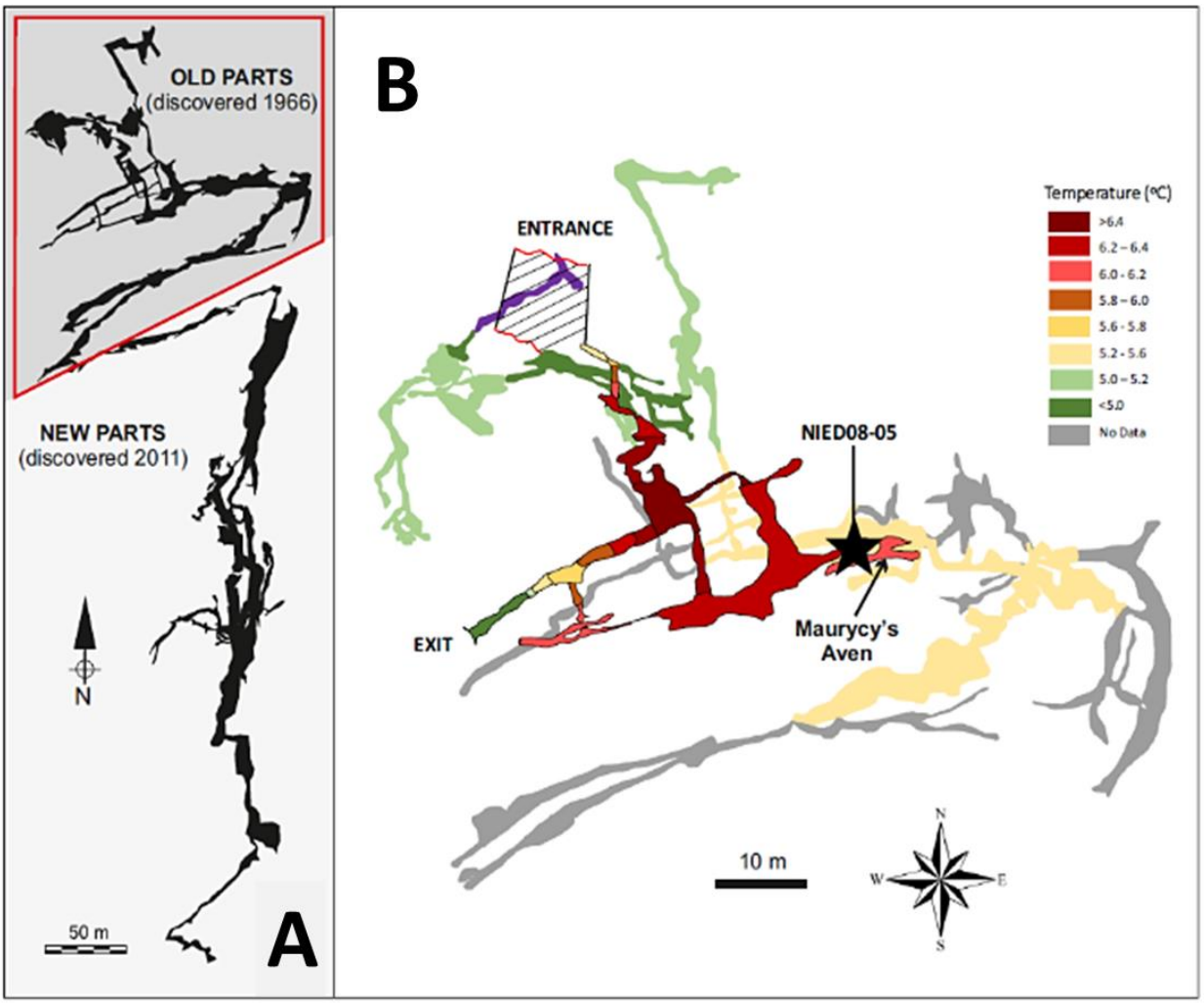

Figure 10: **A** – Plan view diagram of the Niedźwiedzia Cave including "old" and "new" parts and position of analysed area (modified after Kostka 2014); **B** - Plan-view diagram of the Niedźwiedzia Cave old parts and Maurycy's Aven (closest to the surface), depicting mean annual air temperature and the relative location of the NIED08-05 stalagmite. Black outline marks the upper/middle level of the cave (adapted from Lechleitner et al. 2016., Temperature data after Piasecki & Sawiński, 2009).

Modern-day monitoring of the stalagmite feeder drip hydrology and hydrochemistry provides important constraints on the transmission of surface conditions through the karst, and subsequent climate signal preservation in the stalagmite. Prior to stalagmite collection, the NIED08-05 feeder drip and contemporaneous surface precipitation was monitored between April and June 2008 - to determine the stalagmite's sensitivity to seasonal rather than multi-annual surface conditions. Monitoring data revealed a rapid response of drip rate to surface rainfall (within 48 hours) followed by an asymptotic decline in drip rate over several days (**Figure 12A**); a pattern characteristic of seasonal drip sites (Baldini et al., in review). Closer inspection of the data reveals that not all rain events invoke a drip rate response at this fracture fed drip site (e.g. 2nd June) (**Figure 12A**). For example, the largest increase in drip rate occurred on the 19th of May after a 31.3 mm increase in

cumulative rainfall (**Figure 12A**) whereas, a 2.9 mm increase in cumulative rainfall on 2 June 2008, was insufficient to elicit a drip rate response. Thus, a minimum accumulation of rainfall at the surface is required before meteoric water will infiltrate down through the soil and through the fracture feeding NIED08-05.

Whilst drip rate monitoring can be used to classify the drip site (Baldini et al., in review), oxygen isotope ($\delta^{18}O$) monitoring of drip water and contemporaneous surface rainfall provides constraints on climate signal transmission through, and buffering by, the karst and soil overburden (Baldini et al., 2019; Baldini et al., 2015). Between May 2009 and June 2010, monthly-integrated NIED08-05 feeder dripwater and contemporaneous surface rainwater were collected and analysed for $\delta^{18}O$. Surface precipitation $\delta^{18}O$ over this period ranged from -3.71 and -11.06 ‰ VSMOW (mean = -8.42 ‰ VSMOW). Drip water $\delta^{18}O$ monitored at two sites along the same fracture (the NIED08-05 feeder drip and adjacent 'drip site 4': **Figure 11**) exhibited muted variability, ranging from -10.45 to -11.04 ‰ VSMOW with a mean of -10.98 ‰ VSMOW; the lower end of the rainwater isotope range (**Figure 12B**). Therefore, based on available data, the NIED08-05 feeder drip preserves a low $\delta^{18}O$ autumn/winter precipitation signal. In SW Poland, the temperature effect on precipitation $\delta^{18}O$ is dominant - so summer rainfall is characterised by higher $\delta^{18}O$ values, whereas winter $\delta^{18}O$ values are lower (**Appendix Figure S1**). The winter $\delta^{18}O$ bias of NIED08-05 drip water, despite the bulk of precipitation falling during summer (**Figure 12B, Appendix Figure S1**), reflects the role of evapotranspiration from the overlying deciduous forest that significantly limits summer rainfall infiltration. In contrast, winter precipitation is able to infiltrate unimpeded (either immediately or as spring meltwater) leading to a strong winter bias of drip water $\delta^{18}O$.

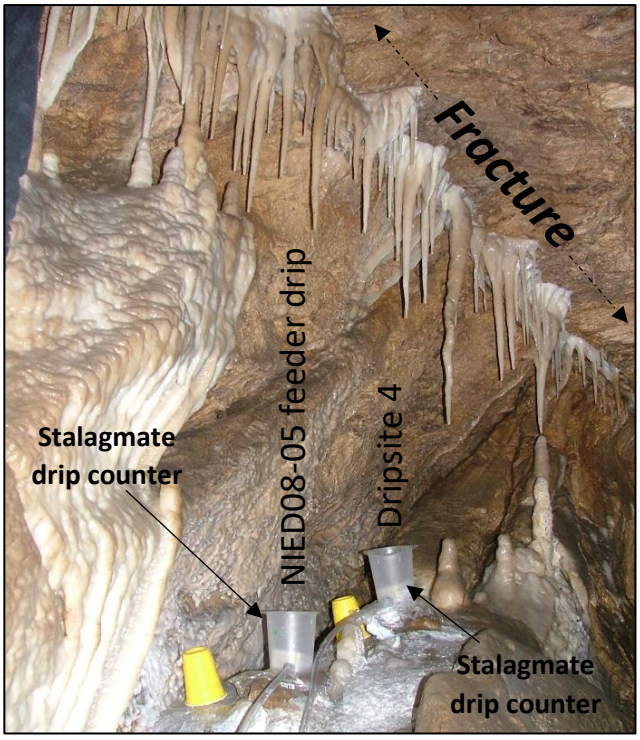

Figure 11: Two drip sites: the NIED08-05 feeder drip and Dripsite 4 (located ~1 m apart along the same fracture) were monitored in Jaskinia Niedźwiedzia, using a Stalagmate drip counter (Collister & Mattey, 2008) between May 2009 and June 2010. Note the well-developed fracture on the ceiling and clear lineation in stalactite and stalagmite deposition.

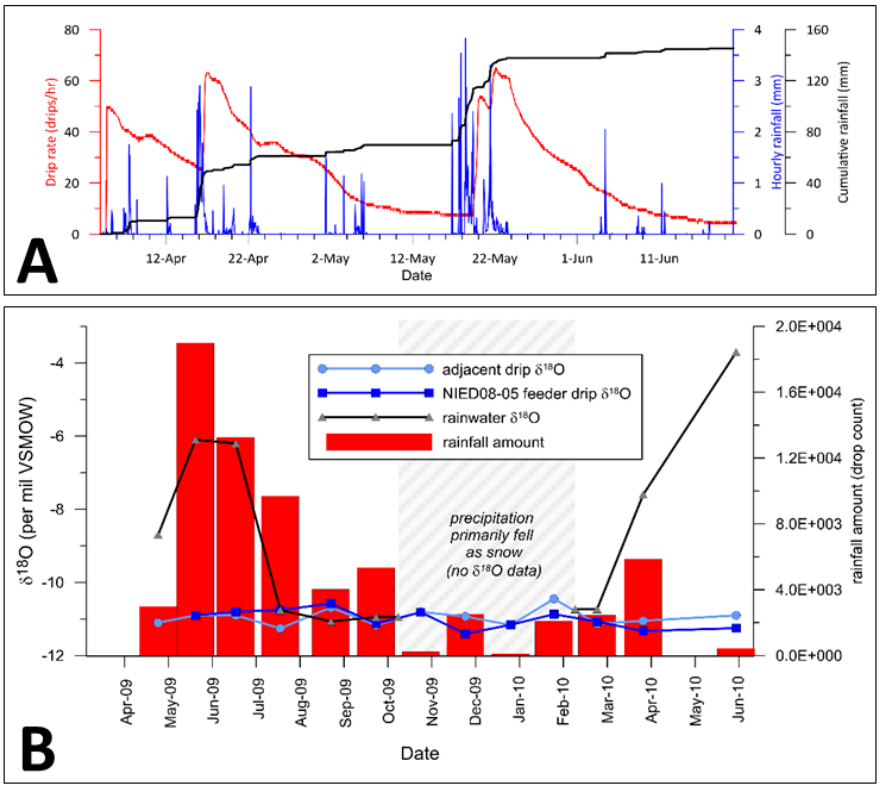

Figure 12 - A: High resolution drip rate (red) data for the stalagmite NIED08-05 feeder drip monitored between April and June 2008. Contemporaneous hourly (blue) rainfall monitored at the surface above the cave is also shown for comparison. Cumulative rainfall is shown in black. **B**: Monthly-integrated dripwater (blue lines), rainwater (black line) oxygen isotopes ($\delta^{18}O$), and surface

precipitation (red bars) monitored at Niedźwiedzia cave between May 2009 and June 2010. No precipitation $\delta^{18}O$ data are available between November 2009 and February 2010 when precipitation primarily fell as snow.

5.1.3. Volcanic Signal Emplacement

Based on 1 year of monthly drip water sampling, the NIED08-05 feeder drip never ceases completely (**Figure 12B**), yet groundwater at the site primarily reflects a winter signal. During summer (when evaporation rates are high), and between November and March (when temperatures are typically below freezing and precipitation falls in the form of snow; **Figure 12B**), colloidal material accumulates at the surface – which could include volcanic ash and sulfate. Tephra deposits traceable to Holocene eruptions of Askja, Churchill, Snæfellsjökull (all Iceland), and Furnas (Azores) have been documented in Polish peat and lake sediments (Kinder et al. 2020; Watson et al. 2017; Wulf et al. 2016; Housley et al. 2014). Thus, Niedźwiedzia cave, and stalagmite NIED08-05, have considerable potential for preserving a long-term record of volcanic activity.

Infiltrating surface water and subsequent leaching is not the only way that volcanic ash could have reached stalagmite NIED08-05 - airborne ash may have infiltrated via natural entrances. Geomorphological evidence suggests alternative points of entry may have existed during the Holocene (Sobczyk et al. 2016) through Maurycy's Aven (**Figure 10B**), and the small Miniaturka Cave just above the Niedźwiedzia exit. Radio wave measurements (Kasprzak & Sobczyk, 2017) suggest these cave sections possessed open voids which allowed further access into the cave, reinforced by paleontological identification of Pleistocene mammal remains (Sobczyk et al. 2016; Stefaniak, 2015; Baca et al. 2014) on the level from which NIED08-05 was extracted. Therefore, tephra may have been directly deposited onto the stalagmite tip.

5.2. *Methods*

5.2.1. NIED08-05

Despite the cave's proximity to economically viable Uranium deposits that prompted Russian mining operations, and the cave's discovery in 1966, stalagmite NIED08-05 is characterised by very low uranium concentrations (Lechleitner et al. 2016). As a result, large uncertainties were associated with the uranium-thorium chronology and an alternative ^{14}C chronological dating technique was established for the stalagmite (full detail in Lechleitner et al. 2016). The NIED08-05 ^{14}C chronology is in stratigraphic order and suggests a near-consistent calcite accretion rate, with one significant growth hiatus present at 51.2 mm from the top (**Figure 13**). Dating uncertainty systematically increases with calcite age, with larger uncertainties in the pre-hiatus interval. To reduce

uncertainties and allow for more precise correlations, only the interval 0-3 ka BP positioned above the hiatus, was utilised in this study. We follow Lechleitner et al. (2016) and fit an age-depth trend based on the corrections and model therein (**Figure 13**).

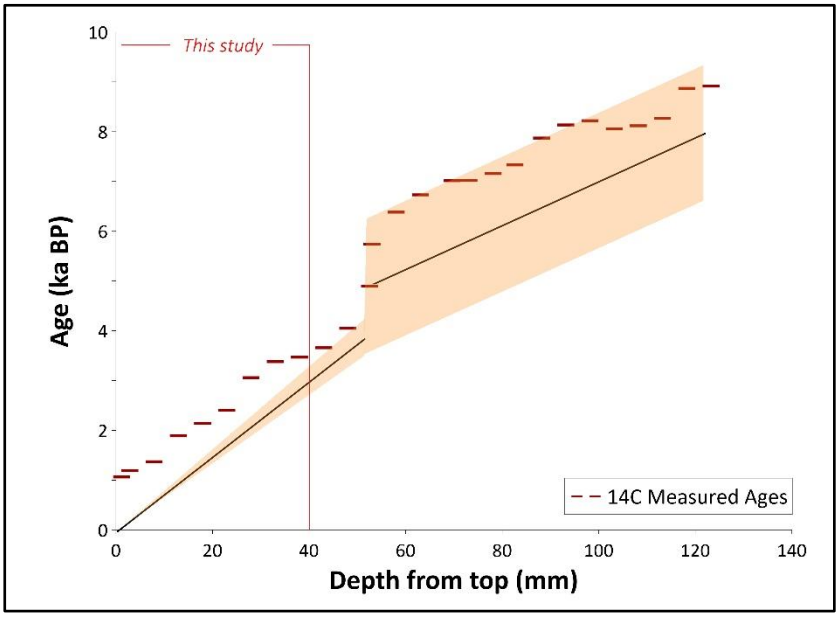

Figure 13: Age-depth ^{14}C-derived chronology for NIED08-05 accounting for Dead Carbon Fraction (DCF), adapted from Lechleitner et al. (2016). Red bars show the measured ^{14}C ages with an anchor point given at the 2008 year of sample collection. The black curve shows the best-fit age-depth trend based on the corrections and model provided in Lechleitner et al. (2016; details therein). The orange shaded region shows the 95% confidence intervals for the model age-depth trend. Based on the large errors after the growth hiatus observed, we restrict our analysis to the quantitative portion of the speleothem at <40 mm from the top, equivalent to calculated ages from 0 to 3 ka BP.

Laser-Ablation Inductively-Coupled-Plasma Mass Spectrometry (LA-ICP-MS) is an analytical technique for *in-situ* trace element and isotope analysis (Petrelli et al. 2016; Ubide et al. 2015). The trace element profile for NIED08-05 was produced at Royal Holloway University, utilising a prototype RESO-lution M-50 excimer laser-ablation system (193nm), in conjunction with a two-volume laser-ablation cell. This cell was coupled to an Agilent 7500ce/cs quadrupole ICP-MS, and measurement of the speleothem profile was measured using a 140 x 10µm laser slit, a 10µm/s^{-1} scan speed and a 15 Hz repetition rate (90 mJ laser spot). The full analytical set-up is described by Müller et al. (2009). Calcium-43 was measured throughout all runs as an internal standard. The Iolite software package was used for data reduction, using NIST 612, 619 and MACS3 standards of quantification (Paton et al. 2011). One issue associated with LA-ICP-MS is instrumental drift (Lin et al. 2016), which can cause matrix differences and thus difficulty in disentangling environmental signals from analytical noise (El Hadri et al. 2016). Stable isotopes ^{24}Mg and ^{25}Mg were both measured in NIED08-05, however anomalous values (> 100ppm difference) were eliminated, as this would suggest such instrumental

error. The LA-ICP-MS results were collected at a higher spatial resolution than the ^{14}C data (**Figure 13**). As such, we use the model constant deposition rate model from Lechleitner et al. (2016) in order to continuously convert geochemical data profiles into time-series data.

5.2.2. Principal Component Analysis

Principal Component Analysis (PCA) is a dimension-reduction data analysis method which combines the intra-variable association, data dispersion direction and relative importance of these directions in order to assess which Principal Component (PC) explains the largest sum of variability in a multivariate dataset: PC1 and PC2 being the greatest (Abdi & Williams, 2010). Prior use of PCA in volcanology is mostly limited to igneous petrology (Unglert et al. 2016), and geochemical characterisation of tephra extracted from sedimentary sequences (e.g. van der Bilt et al. 2017; Pouget et al. 2014). Therefore, use of PCA to detect volcanic trace element signals in speleothems is novel. Jamieson et al. (2015) plotted PC1 scores as a time series, and found short-lived trace element enrichments temporally coincident with dispersal of volcanic ash over the cave site, suggesting stalagmite chemistry reflected periods of explosive volcanism. To test whether the technique could be used to detect volcanic eruptions whose ash affected Poland, PCA was applied to the NIED08-05 trace element data, obtained by LA-ICP-MS. Z-scores were calculated prior to analysis to lessen analysis sensitivity to individual variables. The MATLAB *pca* function (MathWorks, 2019) was used to extract coefficients, t-squared values, percentage-variance and PC scores from the dataset. Scores were then plotted as a time-series, to identify discrete trace element enrichments.

5.2.3. Volcanic Eruptions

Data coinciding with the time window for which the LA-ICP-MS traverse of NIED08-05 was downloaded from the Large Magnitude Explosive Volcanic Eruptions (LaMEVE: Crosweller et al. 2012) database, and the Smithsonian Institution's open-access record of Holocene volcanism (Global Volcanism Programme (GVP): Venzke, 2013).

To assess the presence of volcanic signals within the NIED08-05 chronology, exclusion criteria were applied to eliminate unsuitable eruptions, and allow objective comparison. Niedźwiedzia Cave is not within 100km of an active (since 3 ka BP) volcanic system, so it is reasonable to assume deposition of volcanic material at the cave site would be limited to fine-grained, airborne material (Cashman & Rust, 2020). Eruption magnitude is directly proportional to pyroclastic ejecta volume (Pyle, 2015), and trans-continental identification of tephra linked to high-magnitude eruptions is becoming more common (e.g. Pyne O'Donnell & Jensen, 2020; Timms et al. 2019; Lane et al. 2017; Jensen et al. 2014). Therefore, it is unnecessary to eliminate non-European ≥M6.0 eruptions, so long as they

satisfied all other inclusion criteria. Conversely, lower magnitude eruptions are less likely to produce enough material for ultra-distal transport, reducing the chances of a clear signature in the NIED08-05 speleothem sequence. Consequently, only >M4.5 European explosive eruptions were included in the analysis. Another step in the elimination process relates to dating uncertainty, as large uncertainties associated with eruptions would negatively affect any conclusions drawn, and render them inaccurate (Baldini et al. 2015). Therefore, only eruptions with robust dates (uncertainties <100 years) of a '*high*' or '*medium*' quality (as stated by LaMEVE) were included.

The NOAA Air Resources Laboratory HYSPLIT Ash Dispersion Model (Stein et al. 2015; Draxler & Rolph, 2013) was also used to assess the potential for ash dispersion over Poland from different volcanically active regions. Using a GDAS 1-degree meteorology, one simulation per month (12 in total, per region) was run for the year 2018 to account for annual wind variabilities and events where eruption season is unknown. Simulations were run assuming a 24-hour ash injection period, and plume altitude of 18 km (tropopause). This represents a 'minimum' injection height for all eruptions and was chosen to avoid overestimating outputs for smaller eruptions (<M6.0). We acknowledge that dispersion of volcanic ash is a highly stochastic process and that individual eruptions exhibit a unique combination of parameters (including variable plume heights), however use of a single source term here allows for inter-comparative simplicity regarding ash dispersal directions.

5.3. Results & Discussion

Qualitative analysis of PCA outputs for the NIED08-05 trace element data suggest that, although volcanic signals are potentially present, there are significant uncertainties. As a result, robust links are difficult to define. This section outlines the primary findings of the analysis, potential correlations, and the main challenges facing use of temperate speleothems as archives of explosive volcanism.

5.3.1. Initial PCA Results

Principal Component Analysis revealed that the greatest (16%) trace element variability in NIED08-05 is represented by PC1. Within the PC1 time-series, the background variability is high when compared with short-lived spikes, making it only possible to hand-select with confidence the largest spikes in the series. By contrast, PC2 represents 11% of total dataset variation, but the short-lived, high-amplitude signal spikes are visually clear compared with low background variability in the series (**Figure 14**). Given that the deposition of volcanic material is impulsive on the timescale of this time-

series, we posit that PC2 potentially reflects the signals associated with short-lived events such as storms and volcanism, rather than sustained variability in climate and stochastic low-frequency processes in the cave and karst system. This is supported by the observation that PC2 incorporates the REEs (Y, Nd, La), which are atypically included in calcite during standard background speleothem growth. Prior studies of REE enrichment in speleothems have focused on terrestrial groundwater input tracing (Noack et al. 2014) and characterisation of prolonged climate events (Drysdale et al. 2019; Zhou et al. 2008b) such as the Bølling-Allerød and Younger Dryas (Drugat et al. 2019), as REEs are commonly found in soils (Ramos et al. 2016). Increased weathering of surficial sediments, combined with vigorous hydrological regimes associated with increased humidity appear to expedite REE mobilization in particulate phase (Zhou et al. 2012, 2008a), entering the cave through leaching of groundwater from surface to karst (Fernandez-Cortes et al. 2011; Richter et al. 2004). REEs are also present in volcanic products (Rogers, 2015), and eruptions result in their ejection and distal dispersal. Therefore, observed PC2 spikes and REE enrichments could be a product of volcanic material incorporation into NIED08-05, through processes of (1) tephra particle dissolution into groundwater supplied to the speleothem growth surface, and/or (2) aeolian transport of ash directly into the cave and to the stalagmite.

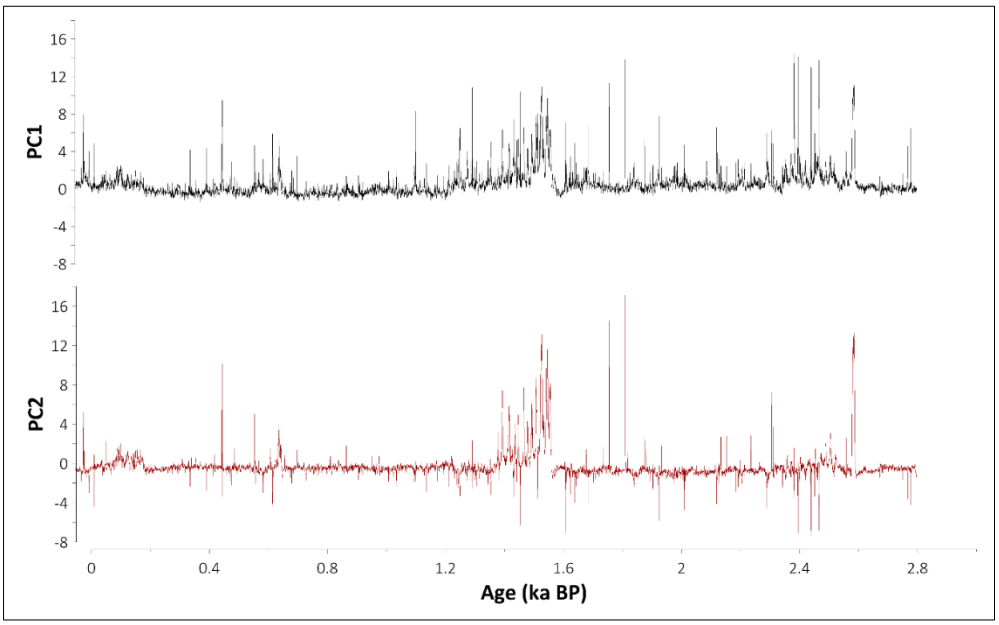

Figure 14: A comparison of PC1 (black, upper panel) and PC2 (red, lower panel) outputs for NIED08-05 since 3ka BP.

PCA results also show weak correlations between Mg and Sr (-0.406), and Mg and Ba (-0.335). Lechleitner et al. (2016) find similarly weak correlations, with a low-amplitude Mg/Ca vs. $\delta^{13}C$ signal suggesting slow degassing of CO_2 from dripwater and subsequently low amounts of prior calcite precipitation (PCP) in NIED08-05. PCP involves prior scavenging of calcite from dripwater prior to deposition, and simultaneous elevation of Mg/Ca, Sr/Ca, and Ba/Ca due to the preferential exclusion

of Mg/Sr, and Ba from the calcite lattice (Fairchild et al. 2000). PCP is enhanced when descending waters can degas more thoroughly, and this is often achieved when there is less recharge (Jamieson et al. 2016., Fairchild & Treble, 2009., Karmann et al. 2007). Low PCP influence on the NIED08-05 geochemistry is likely to reflect the combination of a relatively direct (fracture-fed) and short (< 10 m) water flow path consistent with the findings of Sherwin & Baldini (2011), and a drip regime that is both responsive and continuous (**Figure 12**).

Table 2: Table of descriptive statistics for 7574 measurements of 20 trace elements taken from NIED08-05, and Principal Component 2 coefficients. Elements with positive coefficients are highlighted in grey.

Element	PC2	Max. (ppm)	Min. (ppm)	Median (ppm)	Standard Deviation (ppm)	Mean (ppm)	%RSD
Magnesium (Mg)	0.00	2355	293.93	776.1118	216.40	809.08	26.74
Strontium (Sr)	0.00	98.46	8.29	16.47	3.26	16.79	19.40
Cerium (Ce)	0.032	20.87	0.00	0.02	0.44	0.06	781.54
Aluminium (Al)	0.00	3689.79	0.00	14.08	109.12	31.55	345.78
Phosphorus (P)	0.045	1368.55	0.00	9.04	24.73	11.99	206.27
Vanadium (V)	0.00	32.70	0.00	0.04	0.63	0.12	501.95
Manganese (Mn)	0.00	121.20	0.00	0.72	3.09	1.20	257.18
Iron (Fe)	0.00	42025.89	89.51	158.03	526.81	178.28	295.47
Cobalt (Co)	0.00	11.70	0.00	0.10	0.24	0.12	205.11
Copper (Cu)	0.00	4316.57	0.14	3.31	74.76	7.26	1029.27
Zinc (Zn)	0.00	420.21	1.41	7.57	9.92	9.31	106.60
Rubidium (Rb)	0.00	14.66	0.00	0.03	0.29	0.05	546.07
Yttrium (Y)	0.47	11.29	0.00	0.02	0.98	0.29	339.58
Iodine (I)	0.00	70680.09	0.00	4047.31	2555.66	4050.24	63.09
Barium (Ba)	0.00	73.11	1.14	3.92	1.91	4.16	45.91
Lanthanum (La)	0.42	6.74	0.00	0.02	0.20	0.06	336.52
Neodymium (Nd)	0.46	3.43	0.00	0.002	0.21	0.07	285.63
Lead (Pb)	0.00	336.18	0.014	0.55	6.76	1.17	575.51
Thorium (Th)	0.10	5.23	0.00	0.00	0.10	0.01	1447.39
Uranium (U)	0.045	6.15	0.00	0.01	0.08	0.01	727.62

5.3.2. Volcanic eruptions

From 458 recorded Holocene explosive eruptions between 0 and 3 ka BP, 26 satisfied the inclusion requirements of this study (**Table 3**). Eruptions of Askja (1875 CE, Iceland) and Churchill (1.103 ± 0.001 ka BP, Alaska) both satisfied all criteria and represent the two key eruptions with confirmed identification in Polish sediments (Kinder et al. 2020; Watson et al. 2017). Eruptions from Vesuvius,

Italy adhered most frequently to the selection criteria, as recurrent Holocene activity (Santacroce et al. 2008) and significant socio-cultural importance (Chester et al. 2018) has promoted extensive study. Eruptions from Hekla and Katla volcanoes, Iceland, also feature multiple times - both demonstrating high eruptive frequency (Thordarson & Höskuldsson, 2008).

Table 3: Table displaying global eruptions ≥M6.0 and European eruptions ≥M4.5 (highlighted in grey) utilised in this study. Dates and uncertainty are sourced from LaMEVE and appropriate literature: eruptions in bold have been dated utilising historical records. Icelandic Volcanic Zones are abbreviated: EVZ: Eastern Volcanic Zone, NVZ: Northern Volcanic Zone, ÖVB: Öræfi Volcanic Belt.

VOLCANO	COUNTRY	ERUPTION AGE (ka BP)	ERUPTION MAGNITUDE	PLUME HEIGHT (km)	DOMINANT BULK MAGMA COMPOSITION	REFERENCE(S)
Agua de Pau	**Azores**	**0.387**	**5.0**	**<19**	**Trachyte**	[1]
Askja*	**Iceland (NVZ)**	**0.075**	**4.9**	**<26**	**Rhyolite**	[2]
*Changbaishan***	North Korea/China	1.008	7.4	> 25	Rhyolite-Trachyte	[3, 4]
Churchill	Alaska	1.837 ± 0.08	6.2	-	Dacite	[5]
	Alaska	1.103 ± 0.001	6.1	<45	Rhyolite	[6]
Furnas	**Azores**	**0.32**	**5.0**	**<13**	**Trachyte**	[7]
Grímsvötn	**Iceland (EVZ)**	**0.167**	**5.0**	**<12**	**-**	[8]
(Lakagígar)						
Huaynaputina	**Peru**	**0.350**	**6.1**	**<40**	**Dacite**	[9]
Ilopango	El Salvador	1.5 ± 0.03	6.7	>29	Rhyolite	[10]
Katla	**Iceland (EVZ)**	**0.229**	**5.0**	**-**	**Rhyolite**	[7]
	Iceland (EVZ)	**0.325**	**5.0**	**-**	**Rhyolite**	[7]
Krakatau	**Indonesia**	**0.067**	**6.5**	**<50**	**Dacite**	[7]
Ksudach	Russia	1.71 ± 0.1	6.2	<30	Andesite	[11]
Novarupta	**Alaska**	**0.038**	**6.5**	**< 26**	**Dacite-Rhyolite**	[12]
Okataina	New Zealand	0.640 ± 0.012	6.3	<28	Rhyolite	[13]
Okmok	Alaska	2.026 ± 0.079	6.7	-	Andesite-Dacite	[14]
Opala	Russia	1.340 ± 0.05	6.0	<20	Rhyolite	[15]
Öræfajökull	**Iceland (ÖVB)**	**0.588**	**5.7**	**<30**	**Rhyolite**	[16,17]
Pinatubo	**The Philippines**	**-0.041**	**6.1**	**44.8**	**Dacite**	[1]
Rabaul	New Britain	1.267 ± 0.003	6.0	-	Dacite	[18]
*Rinjani***	Indonesia	0.693	6.4	<43	-	[19, 20]
Santa María	**Guatemala**	**0.048**	**6.3**	**23.7**	**Dacite**	[7]
Tambora	**Indonesia**	**0.138**	**7.0**	**<43**	**Dacite**	[21]
	Italy	**1.871**	**5.8**	**<32**	**Phonotephrite**	[21]
Vesuvius	**Italy**	**0.319**	**5.1**	**<28**	**Phonotephrite**	[22]
	Italy	**1.478**	**5.1**	**<25**	**Phonotephrite**	[23]

Comparison of well-dated volcanic eruptions and the NIED08-05 PC2/REE time series suggests that volcanic-derived material may have been incorporated into the sequence, but if so, the signal is not strong (**Figure 15**). In certain cases, enhanced REE concentrations are coincident with periods of recurrent volcanism. For example, between 0 and 0.2ka BP, increased REE enrichment in the stalagmite appears coincident with seven explosive eruptions, and between 0.5 and 0.7 ka BP, three transient enrichments occurring in conjunction with three volcanic eruptions. Individual eruptions also show concurrence with transient REE spikes, such as Öræfajökull (1362CE), Vesuvius (472CE), Ksudach (1.71 ± 0.1 ka BP), Churchill (1.837 ± 0.08 ka BP), and Okmok (2.026 ± 0.079 ka BP). However, there are multiple REE enrichments which do not coincide with an eruption, and vice versa.

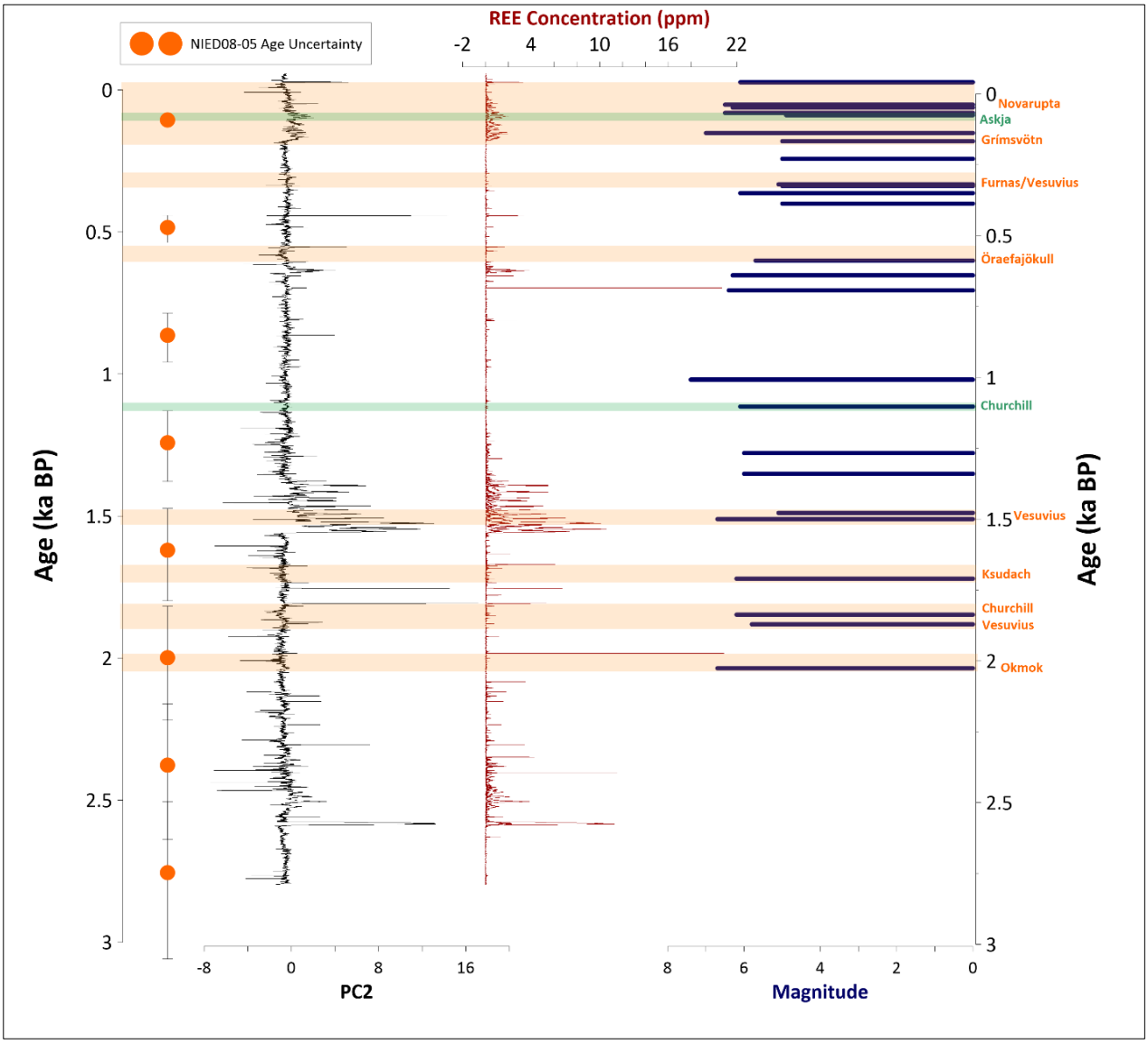

Figure 15: A comparison of REE and PC2 scores for NIED08-05, and Global >M6.0 and European M4.5 eruptions (LaMEVE database). Green highlight indicates eruption events with confirmed tephra dispersal in Poland. Orange highlight indicates other potential Northern Hemisphere eruption signals (discussed below).

In total, 68% of eruptions coinciding with REE enrichments in NIED08-05 can be qualitatively linked to Northern Hemispheric volcanoes (**Figure 15**), and results of HYSPLIT modelling suggests ash from Campania, Southern Iceland, and the Azores could have been deposited over Niedźwiedzia Cave, following an explosive eruption, at multiple points in the year under favourable atmospheric conditions (**Figure 16**). Ash clouds from SE Alaska reach their 72-hour maximum extent only so far as France, and this trajectory appears limited to autumn and winter. However, outputs do not account for fine-ash and aerosol transmission on >72-hour timescales, a phenomenon observed in the aftermath of Pinatubo in 1991 (Holasek et al. 1996). So, it is possible that ash from trans-Atlantic eruptions could be deposited in Central Europe >72 hours after ejection. Indeed, confirmed identification of Alaskan ash in Poland (Watson et al. 2017), and potentially Ireland (Pyne O'Donnell et al. 2012; Plunkett, 1999) suggest deposition in traceable quantities could occur much further East, >3 days following eruption.

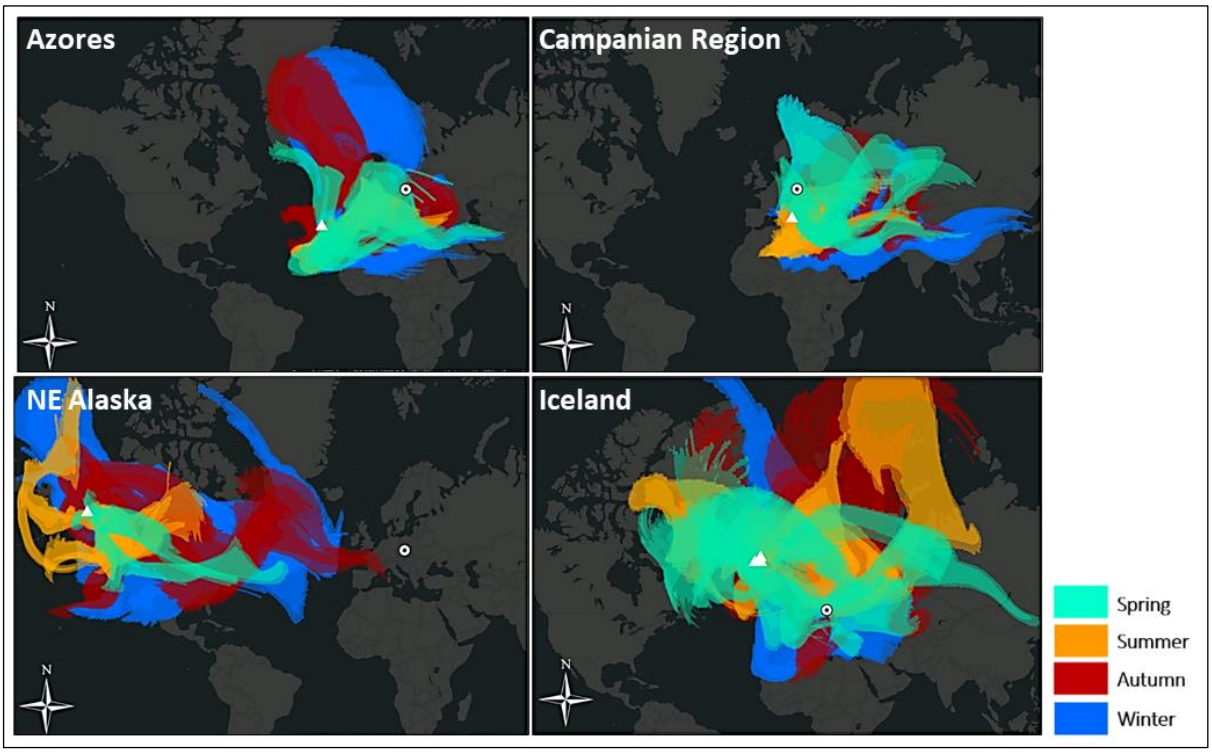

Figure 16: Maps showing ash dispersion for 72 hours post-eruption, for volcanoes with potential links to REE enrichments in NIED08-05. Niedźwiedzia Cave is marked as a white circle. Hekla, Katla and Öræfajökull are grouped under **Iceland**; Campi Flegrei and Vesuvius under **Campanian Region**; Agua de Pau and Furnas under **Azores**; Novarupta and Churchill under **NE Alaska**.
(calculated using the HYSPLIT Dispersion Model for volcanic ash (Stein et al. 2015; Draxler & Rolph, 2013) with GDAS 1-degree 2018 meteorology)

5.3.2.1 Potential eruption signals in NIED08-05

Geographical proximity, and frequent occurrence of explosive (events whereby >95% of magma is tephra - Thordarson & Larsen, 2007), has caused recurrent deposition of Icelandic ash over Europe since 3 ka BP (Swindles et al. 2017). In Poland, tephra from Askja volcano is most common, and has been detected at two of three tephrochronological sites (Watson et al. 2017., Wulf et al. 2016) as two distinct isochrons: Askja1875 (1875 CE - Carey et al. 2010) and Askja-S (10.83 ± 0.057 ka BP - Lilja et al. 2013). The 1875 CE event ejected of 0.3 km^3 (DRE) rhyolitic ash (Carey et al. 2009; Sparks et al. 1981) along an extended south-eastern dispersal axis (Watson et al. 2016; Davies et al. 2007), resulting in widespread transmission of ash into mainland Europe and Fennoscandia (Kalliokoski et al. 2020). Concurrence between the 1875 CE event, and a REE enrichment in NIED08-05, may reflect ash deposition over Niedźwiedzia Cave and preservation in the stalagmite. If this eruption impacted Niedźwiedzia Cave, there is potential that larger Icelandic events could have also deposited ash over this site. The Lakagígar (Lakí: 1783 CE) eruption occurs at the onset of REE enrichment at ~0.2ka BP – an event characterised by prolonged and distal dispersal of volcanogenic aerosol and tephra (Thordarson & Self, 1993), detected in mainland Europe (Thordarson & Larsen 2007; Thordarson & Self, 2003), and Svalbard (Kekonen et al. 2005). Tephra attributed to Öræfajökull (1392 CE) appears comparably widespread, with extended, multi-directional dispersal axes (Sharma et al. 2008) which deposited fine-ash over Greenland (Coulter et al. 2012; Palais et al. 1991), Ireland (Hall & Pilcher, 2002) and Norway (Pilcher et al. 2005).

The 79CE Vesuvius (M5.8: 79 CE) eruption represents one of three Mediterranean events concurrent with an REE spike (also Pollena and 1631 CE - Zanchetta et al. 2011). Geochemically distinct tephra (Tomlinson et al. 2015) and aerosols (Barbante et al. 2013) produced by the Plinian eruption plume were widely dispersed over Europe (Rolandi, 1998). However, like Öræfajökull and Lakí, tephra deposits produced by this eruption remain as yet unidentified in Poland, despite meteorological evidence and HYSPLIT modelling (**Figure 16**) suggesting south-easterly winds may facilitate deposition of Vesuvian tephra over Central/Eastern Europe (Rolandi et al. 2008), and similarly that dominant westerly winds increase the probability of Icelandic ash deposition in this region. Therefore, the absence of these tephras could be an artefact of spatial gaps in the European

tephrochronological record (Timms et al. 2019; Plunkett & Pilcher, 2018). Nonetheless, the small magnitude of concurrent REE enrichments, and lack of recurring links between these and large eruptions in Campania, the Azores, Iceland, place greater value on tephrochronological evidence. At present, this evidence is unavailable in Poland.

5.3.2.2. Missing/ambiguous eruptions

The link between NIED08-05 REE and PC2 spikes, and the well-dated eruption record, is largely inconsistent, with many large geochemical excursions not concurrent with an eruption event. This could be due to attenuation of eruption signals by environmental factors, uncertainties in the stalagmite chronology (Lechleitner et al. 2016), and/or spatial and temporal variations in atmospheric and eruptive dynamics, affecting how ash is transported, deposited, and preserved in the Niedźwiedzia Cave system.

Tephra geochemistry could explain the apparent distribution of Icelandic tephra in Europe, and absence of certain eruption signatures in NIED08-05. The composition of tephra varies according to source volcano and eruptive episode (Pearce et al. 2020) and can directly affect atmospheric suspension time (Schindlbeck et al. 2018; Wolff-Boernish et al. 2004), alongside dispersal distance. Within the NIED08-05 study interval, two explosive eruptions of Katla (1625 CE and 1721 CE) are noted, however neither correspond to a stalagmite REE enrichment. Both associated tephra units remain unidentified outside Iceland (Óladóttir et al. 2008), which is surprising as Katla is located <30 km from Hekla, with well-documented tephra dispersion across Europe (Kalliokoski et al. 2020; Janebo et al. 2016). The scarcity of Katla tephra layers in NIED08-05, and furthermore the European tephrochronological record, may be due to its mafic composition (Schmith et al. 2018; Thordarson & Larsen, 2007). Mafic magmas generally result in less powerful eruptions that inject tephra to lower altitudes (Lowe et al. 2017) and may deposit more rapidly due to greater particle density (Stevenson et al. 2015; Thorarinsdottír & Arnalds, 2012), which can cause low surface tephra concentrations – particularly at sites distal from the erupting volcano. Moreover, studies of peat and lacustrine sediments indicate that mafic particles are subject to post-depositional geochemical alteration (Blockley et al. 2005); resulting in progressive degradation of particles with time, and consequently a scarcity of mafic layers within the European tephrochronological record (Cooper et al. 2019). The chemical stability of tephra in the karstic environment remains poorly studied, so the extent that tephra chemistry could have influenced and/or negated their preservation in NIED08-05 remains unclear.

For ultra-distal eruptions, atmospheric circulation also exerts a significant control on ash distribution. Pyroclasts and gases within an eruption plume separate as a function of height in the

atmosphere (Prata et al. 2017), and advection allows incorporation of tephra particles into stratospheric flow once equal density is reached (Carey & Bursik, 2015). From this point, plume transport and ash distribution are strongly influenced by dominant modes of circulation (Schumann et al. 2011., Holton et al. 1995), producing unique dispersion trajectories for individual eruptions. Such ultra-distal dispersal could be possible if eruption plumes exhibit linear fallout axes associated with strong, unidirectional winds, such as Atlantic westerlies in the Northern Hemisphere (NH). Concentrated dispersal axes from high-latitude eruptions may be further facilitated by jet streams (Bursik et al. 2009), and this mechanism has previously been attributed to deposition of Alaskan tephra in Central Europe (Jensen et al. 2014), including Poland (Watson et al. 2017). However, this is not always consistent, and seasonal oscillations in jet stream strength may limit tephra dispersal. For example, contemporary tephrochronology has identified that both Ksudach (1.71 ± 0.1 ka BP: van der Bilt et al. 2017; Mackay et al. 2016; Braitseva et al. 1996) and Okmok (2.026 ± 0.079 ka BP: Ponomareva et al. 2015a; Burgisser, 2005) exhibited multi-directional lobes of tephra dispersal, and ash from Novarupta (1912CE) appears limited to North America (Payne & Symeonakis, 2012) – dispersal trajectories seemingly independent from the polar jet. Recognizing this intricacy, hence, reduces confidence in attribution of NIED08-05 REE enrichments to concurrent eruptions in Alaska and Kamchatka.

The absence of a REE enrichment in concurrence with the Alaskan Mount Churchill (1.103 ± 0.001 ka BP) eruption is surprising, but also suggests karstic processes could significantly have affected tephra deposition and preservation. The AD860B isochron associated with this eruption, and the White River Ash eastern (*WRAe*) tephra unit (Jensen et al. 2014; Lerbekmo, 2008), is a key chronological marker in Europe - one of four key layers in the contemporary Polish tephrochronological record (alongside Askja-S, Askja1875 and Hässeldalen - Watson et al. 2017; Wulf et al. 2016). Tephra deposition over Poland from an eruption in Alaska would be sparse (Rose & Durant, 2009). Although the relative impact of karst hydrology on colloidal tephra transport and deposition remain to be constrained, the depth of stalagmite NIED08-05 below the surface combined with the dense forest and leaf litter above the cave may prevent the effective preservation of sparse ash deposits. Indeed, conditions at this temperate cave site are markedly different to those at low-latitude and/or more arid cave sites, where previous studies present encouraging evidence that speleothems can retain geochemical evidence of volcanism (Jamieson et al., 2015; Badertscher et al., 2014). Previous work suggests only exceptionally large eruptions produce sufficient ash to result in meaningful preservation >7000 km away (Lane et al. 2017), and this also reduces the likelihood for Southern Hemispheric eruption signals to manifest in the NIED08-05 geochemical record. Although the plumes of Mount Tambora (1815 CE), Krakatau (1883 CE) and Mount Samalas (1257 CE) exceeded 43km

altitude and reflect multi-directional axes of dispersal (Bouvet de Maisonneuve & Bergal-Kuvikas, 2020), the distance between Indonesia and Niedźwiedzia Cave is >10,000 km. Equally, Okataina (0.640 ± 0.012 ka BP), Taupo (3.410 ± 0.04 ka BP), Opala (1.340 ± 0.05 ka BP), Rabaul (1.267 ± 0.003 ka BP), Huayaputina (0.350 ka BP), Santa María (0.048 ka BP) and Ilopango (1.5 ± 0.03 ka BP) tephra remains unidentified in Europe, despite eruption magnitudes exceeding 6.0.

Evidently, only specific eruptive and atmospheric conditions facilitate widespread ash dispersal. Plume height (Prata et al. 2017; Bonadonna & Costa, 2013), mass eruption rate, aggregation (Brown et al. 2012), and atmospheric turbulence can all hinder effective preservation of tephra (Cashman & Rust, 2020), and thus attribution of geochemical excursions in stalagmite records to ephemeral eruption events. Contemporary research continues to evaluate the capacity for tephra fallout associated with Mediterranean (Jones et al. 2020; Vakhrameeva et al. 2019) and North American (Plunkett & Pilcher, 2018) volcanoes in Europe, however existing tephrochronological evidence is not yet strong enough to confidently link REE excursions in Niedźwiedzia Cave to large, distal Northern Hemispheric eruptions solely based on projections of ash dispersion.

5.3.3. Further Uncertainties

5.3.3.1. Chronological Error

Uncertainties within the NIED08-05 chronology may further confound detection of transient eruption events. The ^{14}C chronology used to date trace element enrichments in this study was developed assuming a constant rate of calcite accretion, however this does not account for growth rate variabilities in response to environmental change (Fairchild & Treble, 2009), which may manifest in the NIED08-05 record as distinct strata and/or Mg/Ca excursions (Lechleitner et al. 2016). For a temperate cave such as Niedźwiedzia, changes in stalagmite growth rate may occur due to oscillations in temperature and precipitation, linked to the dynamic atmospheric interactions controlling Central European climate. Resulting fluctuations in stalagmite growth could decrease the resolution of the age-depth model, and lead to over/under estimation of REE enrichment depth. This can be particularly problematic when attempting to detect geologically instantaneous events, such as volcanic eruptions, which can be dated to sub-decadal accuracy. Furthermore, uncertainties associated with dating of the NIED08-05 stalagmite increase with time, which in conjunction with reduced accuracy in dating of older eruptions, hinders accurate correlations between volcanism and trace element variability.

5.3.3.2. Environmental Factors

Local climate (Wassenburg et al. 2020; Day & Henderson, 2013; Huang & Fairchild, 2001) and seasonality (Stoll et al. 2012) can significantly affect trace element incorporation into calcite, making speleothem geochemical composition a key palaeoclimate indicator. The temperate climate at Niedźwiedzia cave and dense forest cover favour nutrient rich soils, however these likely affect preservation of tephra deposited in the region. Research conducted in provinces with low vegetation to ash deposit ratios, such as Iceland (Bonatotzky et al. 2019; Dugmore et al. 2018), the Patagonian steppe (Panebianco et al. 2017) and the Arctic (Cutler et al. 2016b) suggest tephra remobilization is directly proportional to wind strength, whereas dense vegetation matrices appear to intercept suspension of volcanic deposits (Dugmore et al. 2020; Cutler et al. 2018). Although greater vegetation abundance could be beneficial for incorporation of tephra into NIED08-05 by reducing solifluction, cryoturbation (Cutler et al. 2016a), and biological disturbances, it could also be detrimental. Remobilization of tephra by local winds is important for aeolian tephra transfer into the karst system, and this pathway is arguably the most direct and thus chronologically accurate (Badertscher et al. 2014). Dense vegetation in the Kleśnica Valley, typical of the temperate biome, could therefore hinder effective aeolian transfer of tephra into Niedźwiedzia Cave by preventing aeolian remobilization of deposits. However, airborne deposit concentration (Green et al. 2016) could also influence volcanic trace element incorporation into NIED08-05. Ash particle concentrations decrease as a function of distance from the source volcano (Bonadonna & Houghton, 2005), and wind turbulence, precipitation, and groundcover (Liu et al. 2014) can all increase the stochasticity of deposition. Lower particle concentrations may thus be more susceptible to loss through wind turbulence, resulting from surface reworking due to surface bioturbation, or mountainous terrain. Furthermore, the steep topography (> 30°) surrounding Niedźwiedzia cave is covered by rock debris (Kasprzak & Sobczyk, 2017), masking clear evidence for the size and locations of alternative cave entrances. This uncertainty, consequently, hinders our ability to quantify the influence of dry tephra deposition on the NIED08-05 geochemistry.

For tephra deposited at the surface, high rainfall would reduce the residence time of tephra in terrestrial soils (Jones, 2015), increasing the speed of surface-karst transfer. However, this may also cause greater particle spread, increased colloidal trace element flux through the cave hydrological network (Zhou et al. 2012), and reduced clarity of volcanic trace element deposits. Persistent infiltration of surface water into Niedźwiedzia Cave (albeit reduced by evapotranspiration in summer) and dense leaf litter appears to preclude unambiguous detection of transient volcanic episodes in Niedźwiedzia stalagmites. This is despite the presence of a pronounced Spring flush at Niedźwiedzia Cave, which is analogous to the flushing that occurs at low-latitude sites with the onset of the wet season. At these caves, tephra that has accumulated both at the surface and within the

cave during the dry season is flushed into the karst aquifer solely with the arrival of wet season rains. Therefore, successful tracing of volcanic-derived deposits in stalagmite records appear limited to low-latitude regions, characterised by pronounced seasonal variations in effective rainfall (Hartland et al. 2012) and thin overlying soil and vegetation cover.

Karst geology could further reduce the clarity of volcanic signals in NIED08-05, due to interactions between the bedrock and groundwater feeding the drip aquifer. Periods whereby water is in contact with bedrock for extended periods heightens the potential for congruent and incongruent dissolution (Rutlidge et al. 2014), resulting in mixing between seepage and dripwater (Stoll et al. 2012). The extent of hydrological mixing varies in relation to cave setting (Wong et al. 2011), and aquifer residence time (McDonald & Drysdale, 2007). Studies investigating the impact of these interactions on colloidal tephra transport appear limited to investigations of volcanic whole-rock weathering (Griffiths et al. 2010), intra-karst transport of Mg, Sr and Ba (Lead & Wilkinson, 2006) or sulphur signals (Frisia et al. 2008) rather than tephra deposits. Discriminating between REE signals originating from bedrock weathering and/or clastic components of the soil (Richter et al. 2004), and those originating from tephra deposition requires quantification of trace element partitioning during elevated and reduced water flux events (Fairchild et al. 2006). For Niedźwiedzia Cave this information is currently unavailable, so the extent to which intra-karstic processes affect the dissolution and transport of bedrock and soil trace elements into the NIED08-05 stalagmite is unclear.

5.3.3.3. Incomplete Eruption and Tephra Record

We have thus far discussed potential links between significant volcanic eruptions with reliable dates and trace element enrichments in the NIED08-05 chronology. However, there are notable absences of other exceptionally large Holocene eruption signals occurring since 3ka BP, but for whom l*ow* dating quality (Crosweller et al. 2012) caused their omission from the primary eruption list. Of 3130 volcanoes within the LaMEVE database, 85% are not associated with a known eruption (Brown et al. 2014) - reflecting the extended return intervals associated with explosive volcanism, and a global recording shortfall (Kiyosugi et al. 2015; Deligne et al. 2010) most prominent in regions such as Australasia, Indonesia, Alaska, South America and the Kuril Islands (Brown et al. 2014). The absence of high-quality dates for many large eruptions in these regions is arguably due to spatial dissimilarity in provision of evidence (Kiyosugi et al. 2015), limiting the application of high-resolution dating techniques. Furthermore, these regions reached the 100% global volcanic recording threshold considerably later (Newhall & Solidum, 2018; Rougier et al. 2016), limiting the number of studies conducted.

Tephra deposit preservation also influences eruption identification. For example, ejecta from eruptions such as Dakataua (0.998 ± 0.063 ka BP) and Ambrym (1.76 ± 0.135 ka BP) are scarcely documented, yet it is highly likely large quantities of fine ash were produced due to their exceptional magnitude. If primary tephra fallout occurred over ocean, detection becomes conditional on extraction and analysis of marine sediment cores – within which tephra horizons can become confounded by local remobilization, sea floor turbidity and bioturbation (Scudder et al. 2016; Schindlbeck et al. 2013). This could lead to misinterpretation and incorrect reconstruction of volcanic successions (Cassidy et al. 2014), causing a knock-on effect for identifying past eruptions in distal sequences. Terrestrial archives are also subject to similar uncertainty due to geographical variability in preservation of deposits. If primary fallout occurs proximal to the erupting volcano, erosion, degradation, and reworking can all reduce the clear stratification of discrete tephra layers (Kataoka & Nagahashi, 2019), and consequently cause difficulty establishing robust Holocene chronologies for individual volcanoes. This inevitably affects volcanic tracing in stalagmite chronologies. Links between trace element enrichment and volcanism are only robust if supported by evidence for a confirmed eruption, yet many prehistoric eruptions remain unknown (Watt et al. 2013).

Table 4: Eruptions exceeding M6.0 omitted from this study, due to low dating quality (grey shading) or a lack of ash fall evidence (white shading), since 3ka BP.

VOLCANO	REGION	DATE (KA BP)	MAGNITUDE
DAKATAUA	Australasia	0.998 ± 0.063	7.4
AMBRYM	Australasia	1.76 ± 0.135	6.8
QUILOTOA	South America	0.951 ± 0.322	6.4
APOYEQUE	Central America	2.0 ± 0.1	6.3
LONG ISLAND	Australasia	0.304 ± 0.012	6.3
OSHIMA-OSHIMA	Japan	0.709 ± 0.054	6.0
RAOUL ISLAND	New Zealand to Fiji	2.143 ± 0.328	6.0
FURNAS	Atlantic Ocean	1.3 ± 0.5	6.0
BILLY MITCHELL	Australasia	0.409 ± 0.134	6.0

The European tephrochronological record is also punctuated by layers unassigned to a source eruption. Key unidentified isochrons include GB4-182a, MOR-T4, Borge tephras 1-15 (Plunkett & Pilcher, 2018), and Glen Garry (GG) – the latter recently identified in north-east (Kinder et al. 2020) and western (Housley et al. 2014) Poland. GG shows geochemical similarity to deposits originating from Askja (Gudmundsdóttir et al. 2016), however intra-site geochemical variation (Barber et al. 2008), stochastic European distribution (Lawson et al. 2012), and a poorly constrained eruption date

confounds GG source confirmation. Further difficulties with assigning sources to unique tephra layers can result from missing eruptions, unique shard geochemistry, uncertainty over whether the ash represents a primary or secondary deposit, and/or spatial gaps in tephrochronological research. In this study, we define volcanic eruptions as those recorded by LaMEVE, however the presence of 'unknown' tephra layers suggests other, unrecorded discrete ash fall events may have occurred between 0-3ka BP. Thus, the eruption record used in this study represents a minimum ash fall event estimate, and the NIED08-05 trace element enrichments not corresponding to a known eruption could reflect these knowledge gaps.

6.0. DIM CAVE – *Results Chapter II*

6.1. *Site Description*

6.1.1. Regional Climate

The climate of Southern Turkey is characterised by persistently high temperatures which, on average, only drop below 10°C in January (Beck et al. 2018). However, the complex orography of the Taurus Mountains and complex meteorological interactions over Turkey (Unal et al. 2012; Deniz et al. 2010; Turkeş et al. 2008) generate high spatiotemporal precipitation variability (Tongal, 2019., Sensoy et al., 2008). Based on a 20-year Industrial Era dataset from the Global Historical Climatology Network (GHCN), precipitation ranges from 274.7 mm in December to 1.3 mm in July (**Figure 18B**), as depressions from the Atlantic travel east over Western Mediterranean basin and regenerate in prominent cyclogenesis centres around the southern Turkish coast (Turkeş et al. 2008). Climatic teleconnections such as the North Atlantic Oscillation (NAO: Dunzeli et al. 2018), the Arctic Oscillation (AO) Index and North Sea-Caspian Pattern (NSCP) (Türkeş & Erlat, 2018, 2005; Baltacı et al. 2017) all dictate intensities and trajectories of annual storm tracks, and thus the strength and quantity of winter precipitation.

6.1.2. Cave Monitoring

This study utilises a sample from stalagmite DIM-3, obtained from Dim (*Gavurini)* Cave (36°32'N, 32°06'E), approximately 6 km west of the Antalya coast, Turkey. Dim Cave is simple in morphology (**Figure 18C**), with a single main, horizontal passage ~360 m long and 10-15 m wide, terminating at a small subterranean lake on a bed of impermeable schist (Ünal-İmer et al. 2015). At 232m a.s.l. the cave is situated in the Southern Dim River Valley within the upper Alanya geological unit (Yumrudağ Nappe), which is constructed from Permian crystalline limestone (Bozkaya & Yalçın, 2004., Oktay & Ozgul, 1984). The cave was initially formed by phreatic speleogenesis, however tectonic uplift during the Plio-Pleistocene has rendered the hydrological system scarcely active, with the Dim River carved several hundred metres below the cave entrance. Aragonite speleothems grow in Dim Cave at present (Wickens et al. 2011; Gündalı et al. 1989), yet prior to 8 ka BP these speleothems show a primarily calcite composition (Rowe et al. 2020; Ünal-İmer et al. 2016, 2015). The solid rock epikarst is overlain by thin leptosol soils, characterised by poor nutrient density and water deficiency (Aksoy et al. 2010; Özden et al. 2001). Although ground vegetation cover is minimal (Rowe, 2020), a

coniferous *Pinus brutia* (Turkish Pine) woodland and shrub-dominated understory cover the valley (Kurt et al. 2015).

The cave possesses a mean annual temperature of 18-19°C with 90% humidity (Baykara, 2014), which is near identical to a recorded annual mean temperature of 18.8°C (1988-2018) at Antalya GHCN station (36°70'N, 30°73'E, 57 m a.s.l., 130km WNW). Drip data from six sites was collected over several months in 2009-2010 (Wickens, 2011), and pool water samples analysed by Ünal-İmer et al. (2015). Although the cave hitherto lacks a high-resolution drip-series, isotope composition of water samples suggests Eastern Mediterranean winter precipitation as the dominant source of moisture. Drip data shows close similarity to the Mediterranean Meteoric Water Line (Rowe, 2020), alongside consanguinity between December-February $\delta^{18}O$ and δD measurements for Dim Cave pool waters (-6.3, -6.2 and -29.0‰ VSMOW), and Antalya winter precipitation (-6.12 and -31.3‰ VSMOW) (Ünal-İmer et al. 2015). This water enters the karst via major fractures in the overlying limestone, feeding the drip aquifer by mechanisms of hydrological routing – a process common in crystalline, fractured limestone caves (Fairchild & Treble, 2009). Therefore, seepage flow is the primary mode of intra-karst moisture transfer (Rowe et al. 2020; Ünal-İmer et al. 2016, 2015; Baykara, 2014).

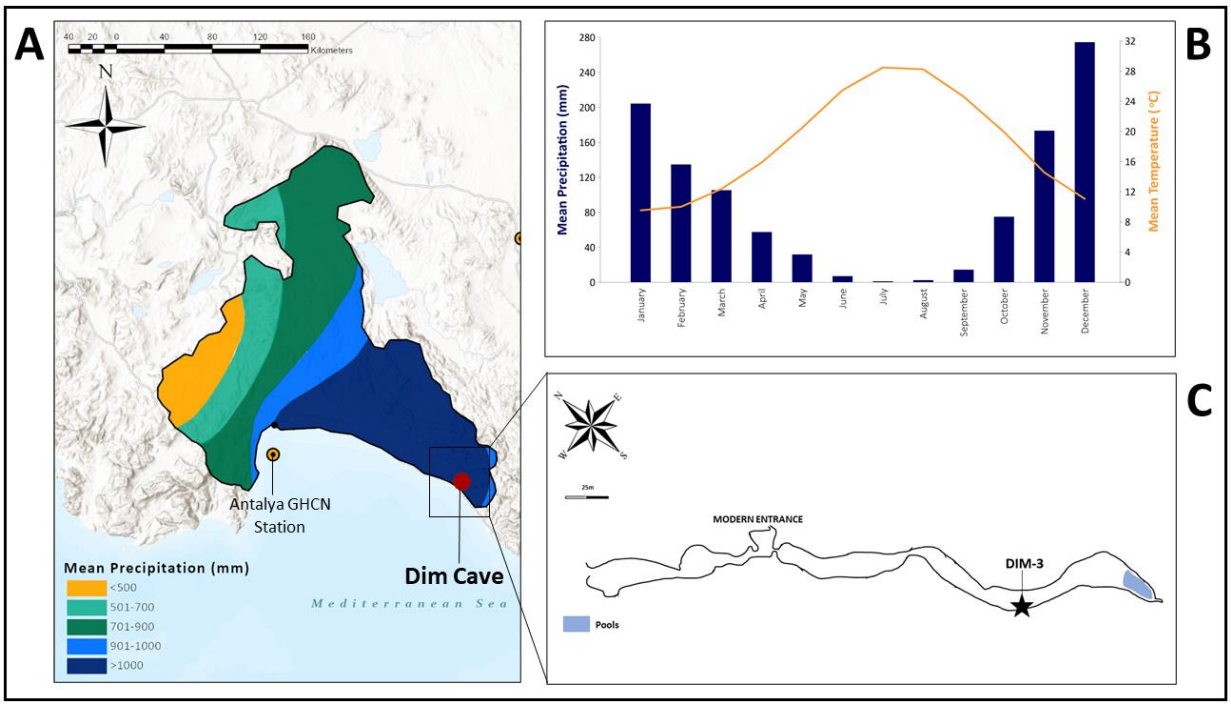

Figure 17: **A** - Map of mean annual precipitation in the Antalya Basin, adapted from Tongal (2019) and Irvem & Ozbuldu (2019); **B** - Mean monthly temperature and precipitation in Antalya during the period 1980-2010 (data sourced from KNMI Climate Explorer: https://climexp.knmi.nl) ; **C** - Plan-view diagram of Dim Cave, and the location at which stalagmite DIM-3 grew (adapted from Ünal-İmer et al. 2015)

6.1.3. Volcanic Signal Emplacement

The location and morphology of Dim Cave means preservation of volcanic signals within the DIM-3 sequence could occur by three mechanisms. The first is by pluvial entrainment of colloidal material, as thin soils and steep topography in the Dim River valley results in excess overland flow during heavy winter precipitation events associated with flash flooding (Koç & Thieken, 2018; Yilmaz, 2015) and soil erosion (Bryan, 2000). This may cause the mobilization and flushing (Zhou et al. 2012) of unconsolidated colloidal particles (including volcanic-derived material) into the drip aquifer during high flow events. The second is by cave ventilation. Dim Cave is shallow with a large entrance, so there is potential for deposition of atmospheric dust particulates originating from Central European (Újvári et al. 2010) and/or North African (Vaks et al. 2013; Prospero et al. 2002) dust storms (Ünal-İmer et al. 2016). The vesicular morphology of rhyolitic volcanic ash renders it highly aerodynamic (Stevenson et al. 2015) and similarly susceptible to distal transport by wind – meaning ash may become incorporated into the DIM-3 growth axis by impaction (directly falling onto the tip – Dredge et al. 2013; Petroff et al. 2008).

The third is by changes to karst hydrology and seepage rates. The Dim Cave aquifers are precipitation-fed and thus stalagmite records show responsivity to changes in external moisture variability (Rowe et al. 2020; Ünal-İmer et al. 2016), and modes of air flow in the East Mediterranean (Ünal-İmer et al. 2015) throughout the LGP. Evidence suggests the stratospheric conversion of erupted sulfur into sulphate aerosols (Robock, 2000) has the capacity to perturb atmospheric heat and moisture transfer; favouring cooler and drier conditions across broad geographical domains (e.g. Guillet et al. 2020; Jacobson et al. 2020; Pausata & Carmargo, 2019; Ridley et al. 2015; Stoffel et al. 2015; Sigl et al. 2015; Haywood et al. 2013). Thus, existing evidence suggests both modes of hydrological variability affecting Dim Cave may become susceptible to volcanic-induced perturbation, and so DIM-3 may capture signatures of volcanic-induced changes to Eastern Mediterranean hydrology.

6.2. *Methods*

6.2.1. DIM-3

Stalagmite DIM-3 was collected from Dim Cave in June 2012, approximately 125m from the modern cave entrance (**Figure 17C**). While predominantly calcite, the stalagmite also possesses clearly defined aragonite layers (Ünal-İmer et al. 2015). Micromorphological analysis suggests its growth

predominantly reflects water availability in Dim Cave, with open/elongated columnar fabric indicating fast water flow and high seepage rates (Ünal-İmer et al. 2016).

DIM-3 was micro-sampled along the growth axis along intervals of 2.5-36 mm (variable according to growth rate), and U-series dating performed on powder samples (50–100 mg) by Ünal-İmer et al. (2015) using Nu Plasma multi-collector ICP-MS (Zhou et al. 2011; full procedure detailed therein) at the University of Queensland (UQ). Generation of a linear chronology based on these discrete U-Th dated anchors reveals relatively consistent stalagmite growth between 89.7 ± 0.41 ka BP and 13 ± 0.31 ka BP. Three distinct periods of slow accumulation are defined, exhibiting fluctuations between 11.9 mm/kyr and 0.8 mm/kyr in response to external climate and aridity (Ünal-İmer et al. 2016). For this study, the COPRA (Breitenbach et al. 2012) chronology generated by SISAL (Comas-Bru et al. 2020) for DIM-3 was utilised for this study (**Figure 18A**). This chronology was chosen due to the variable growth rate and presence of aragonite layers identified in DIM-3 (Ünal-İmer et al. 2015), for which COPRA could account for and thus provide greater chronological precision; particularly important when considering transient environmental events with decadal-scale precision, as this study does. Using linear interpolation, COPRA outputs were used to construct a model best applicable to DIM-3-A.

The trace element profile utilised in this study was obtained from the lower 90 mm of the DIM-3 sample (320-230mm from the tip: **Figure 18B**), corresponding to a 20 kyr interval between 70 to 90 ka BP (herein referred to as DIM-3-A). This section was chosen due to the YTT event occurrence at ~74 ka BP, as tephrochronological evidence suggests the eruption plume was dispersed to the west of Sumatra toward Africa (Lane et al. 2013) and the Middle East (Schulz et al. 2002., Bühring & Sarnthein, 2000). Therefore, analysing the DIM-3 geochemical profile presents a good test of this archive's sensitivity to volcanism, and a unique opportunity for study of the eruption's impact in the Eastern Mediterranean. The slab was analysed at Goethe Universität, Germany, utilising a prototype RESO-lution M-50 excimer laser-ablation system (193nm), in conjunction with a two-volume laser-ablation cell. This cell was coupled to an Agilent 7500ce/cs quadrupole ICP-MS, and measurement of the speleothem profile was measured using a 140 x 10µm laser slit, a 10µm/s-1 scan speed and a 15 Hz repetition rate (90 mJ laser spot) (Müller et al. 2009). Calcium-43 was measured as an internal standard and the Iolite software package was used for data reduction, using NIST 612, 619 and MACS3 quantification standards (Paton et al. 2011).

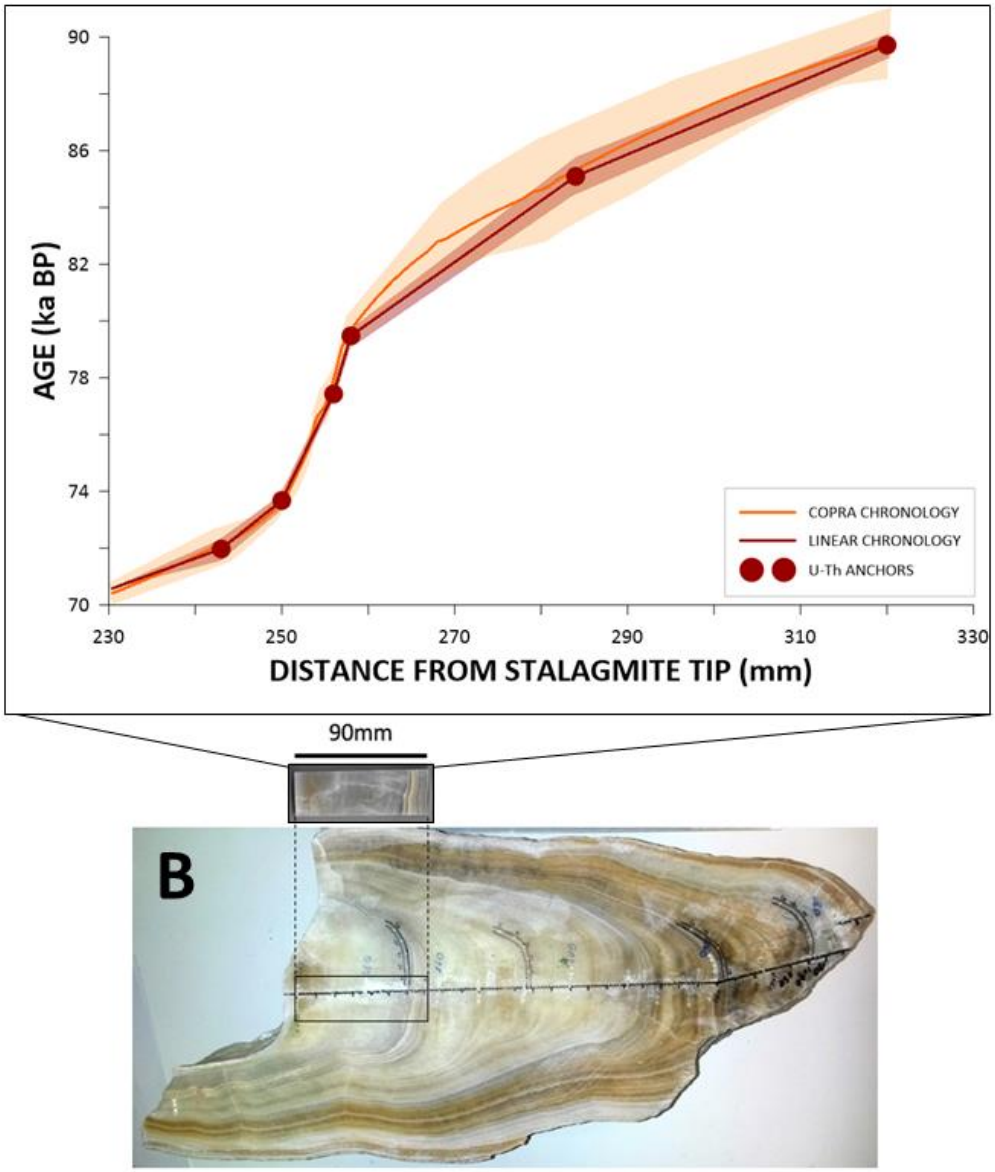

Figure 18A: A comparison of chronology outputs for DIM-3. Red circles mark U-Th dated anchors (Ünal-İmer et al. 2015; details therein). Red shading marks 95% confidence intervals for the LINEAR model age-depth trend (Ünal-İmer et al. 2015); orange shading marks 95% confidence intervals for the COPRA model age-depth trend (Comas-Bru et al. 2020); **B:** Diagram showing the petrographic location of the DIM-3-A slab analysed in this study (320-230mm from the sample base), equivalent to calculated ages from 70 to 90 ka BP.

6.2.2. PCA

Once trace element data had been checked for anomalies, PCA was conducted to identify any geochemical correlations and/or enrichments occurring across the 70-90 ka BP interval. Z-scores were calculated prior to analysis conduction to lessen analysis sensitivity to individual variables, and the MATLAB *pca* function (MathWorks, 2019) was used to extract coefficients, t-squared values, percentage-variance and principal component scores from the dataset. Scores were then plotted as

a time-series, using the COPRA chronology previously discussed (based on U-series chronology dates from Ünal-İmer et al. 2015).

6.2.3. Volcanic Eruptions

Eruption data (between 70 and 90 ka BP) was downloaded from the Large Magnitude Explosive Volcanic Eruptions (LaMEVE: Crosweller et al. 2012) database. To assess the presence of volcanic signals, exclusion criteria were applied to eliminate unsuitable eruptions and allow objective comparison. Dim Cave is not within 200 km of a Quaternary-active volcanic system. The closest volcano is Hasan Dağı ~240 km to the northeast (Aydar & Gourgaud, 1998), which has exhibited episodic explosive activity since the Miocene (6.316 ± 0.20 Ma ($^{40}Ar/^{39}Ar$ dating – Deniel et al. 1998). Other Mediterranean/Middle Eastern volcanic systems of West and East Turkey (Heineke et al. 2016; Aydar, 1998), Greece, and Italy with known activity all >500 km away. Therefore, aerial transmission is the mechanism by which fine-grained volcanic material is most likely to reach the cave site. Evidence suggests that ultra-distal stalagmites, within the same hemisphere, can also preserve climatological signals potentially attributed to high-magnitude volcanism (e.g. Du et al. 2019; Polyak et al. 2017; Carolin et al. 2013). Thus, the distance of Dim Cave from an active volcanic centre permits a test of the sensitivity of the DIM-3 record to not only ash fall directly associated with large eruption events, but also their large-scale repercussions.

The first criterion for eruption selection is dating uncertainty. This is particularly important - comparing volcanism to climate system perturbations significantly rely on objectivity and precision (Baldini et al. 2015) due to the transient nature of both events. For the Last Glacial Period, the number of eruptions with robust dates are notably low (Brown et al. 2014), however, to include a greater number of poorly dated eruptions would notably compromise any conclusions made. Therefore, eruptions with >5000-year dating uncertainties, an *Unknown* dating technique, and/or a *Poor* dating quality were removed. The aim to select eruptions as objectively as possible also influenced the decision to omit <M7.0 eruptions, as the uncertainty associated with magnitude estimates for these events is often greater due to: i) greater chance of evidence degradation and consequently underestimation, and ii) large differences in eruption style (e.g. a basaltic and a rhyolitic eruption measured at M4.0 may respectively emit very different ash/gas quantities). Larger eruptions also show a greater capacity for high ash yields and are more completely preserved in the geological record, as ultra-distal transport facilitates preservation of ash deposits in environments minimally affected by glaciation, eustatic change and rigorous terrestrial processes (Pyle et al. 2016). For this reason, these larger eruptions have hitherto attracted significant research interest.

For certain events, recent literature does not match the parameters given in LaMEVE, due to constantly evolving knowledge of these eruptions with refinement of new techniques and investigation of new sites/proxies. For example, in LaMEVE the LCY eruption of Atitlán is listed as 7.9, however new erupted mass estimates by Kutterolf et al. (2016) raise this estimate to 8.0. Therefore, independent literature checks were conducted on the dates, magnitudes, dating uncertainties, and dating techniques of eruptions remaining.

For this study, it was not deemed appropriate to use HYSPLIT modelling to quantify the potential for ash dispersion over Turkey. The extent to which the direction, and relative strength, of atmospheric circulatory systems differed compared to the Holocene is highly uncertain – reflected by the repeated occurrence of abrupt climate variabilities (such as D-O and Heinrich events) marking major scale reorganisations of the atmosphere (e.g. Rach et al. 2014., Menviel et al. 2014., Konecky et al. 2011). Therefore, conclusions are drawn using current knowledge of ash dispersion trajectories, based on tephrochronological evidence.

6.3. *Results & Discussion*

6.3.1. Volcanic Eruptions

Out of 63 known eruptions between 70 and 90 ka BP, only two satisfied all criteria for inclusion in this study (**Table 5**). Interestingly, these two eruptions are both located within the NH, and there are no comparably sized known eruptions in the Southern Hemisphere between 70 and 90 ka BP. This is potentially a function of natural coincidence (Papale, 2018), however, the incompleteness of the SH eruption record likely also influenced this discrepancy as greater ocean extent in the Southern Hemisphere (SH) means fewer continental volcanoes, and less land to suitably preserve erupted deposits. Unfavourable terrain and harsh climates in volcanically active southern regions (e.g. The Andes - Smith et al. 2019; Fontijn et al. 2016) also promote the removal/reworking of tephra deposits, erosion of geological evidence, and increased difficulty in fieldwork conduction (Fontijn et al 2014). As the accuracy of dating is contingent on the quality and quantity of sampled material (Baldini et al. 2015), these limitations have largely prevented constraint of SH eruption dates beyond multi-millennial uncertainties (Brown et al. 2014). The robustness of our study relied on chronological accuracy, so no SH eruptions were suitable. However, future work may allow for inclusion of more eruptions in such analyses as radiometric techniques become applicable to newly detected deposits.

Table 5: Table displaying the eruptions utilised in this study. Dates and uncertainty are sourced from LaMEVE and/or appropriate literature.

VOLCANO	REGION	UNIT	DATE (ka BP)	MAGNITUDE	DOMINANT BULK MAGMA COMPOSITION	REFERENCE(S)
Toba	Indonesia	*Youngest Toba Tuff*	73.88 ± 0.32	8.8	Dacite-Rhyolite	1, 2, 3
Atitlán	Mexico/Central America	*Los Chocoyos(H)*	84.0 ± 0.5	8.1	Dacite-Rhyolite	4, 5, 6

[1] Mark et al. (2017); [2] Storey et al. (2012); [3] Svensson et al. (2013); [4] Kutterolf et al. (2016); [5] Drexler et al. (1980); [6] Rose et al. (1999)

The YTT date utilised herein is that calculated by Storey et al. (2012). Relative to the AICC2012 chronology, NGRIP (Greenland) and EDML (Antarctica) ice core records suggest a radiometric date of 73.75 ka BP if interpreting 'NGRIP-T2' as the YTT: one of nine NGRIP, and four bipolar sulphate enrichments between 74-76 ka (Svensson et al. 2013). However, it is not clear which enrichment corresponds to Toba, and emplacement of different magma bodies over a protracted eruptive episode (Pearce et al. 2020) may have caused multiple Plinian phases. Toba's low-latitude location further lends to disadvantageous preservation of both aerosols (Rasmussen et al. 2014) and tephra (Abbott et al. 2012) in Greenland and Antarctic (Cole-Dai et al. 2009) ice sheet laminae, preventing complete establishment of the YTT's stratigraphic position (Costa et al. 2014). Nonetheless, the NGRIP eruption date defined by Svensson et al. (2013) is near indistinguishable from a recalculation of the YTT absolute eruption date to 73.7 ± 0.3/0.4 ka BP (Mark et al. 2017), based on novel applications of an $^{40}Ar/^{39}Ar$ optimisation model (Niespolo et al. 2016) to Indian Ocean marine core samples of YTT tephra. This date is 180 years younger than the astronomically calibrated age by Storey et al. (2012) (73.88 ± 0.32 ka BP), the latter representing the most precise date for the YTT currently proposed.

6.3.2. PCA

Principal Component Analysis reveals that 13% of trace element variability in DIM-3-A is explained by PC1, and this principal component is dominated by correlations between Sr, Ba and U (**Table 6**). Alkali earth elements are seemingly the primary mode of variation picked up by PC2, exhibiting an abrupt decrease with similar amplitude and timing as increases in Sr, Ba and U in PC1. This suggests the presence of aragonite layers – an interpretation supported by petrographic observations of clear, light-coloured layering ~70mm from the sample base (**Figure 19**).

Table 6: Table of descriptive statistics for 7849 measurements of 26 trace elements taken from DIM-3, and Principal Component 1 coefficients. Elements with positive coefficients are highlighted in grey.

Two common processes are linked to the occurrence of calcite-aragonite transitions in stalagmites (Fairchild & Treble, 2009). First is prior calcite precipitation (PCP), whereby low water availability and high evaporation increases the space within the karst aquifer occupied by gas, meaning water encounters a lower pCO_2 gas phase. This promotes CO_2 degassing, and elevation of the dripwater $CaCO_3$ saturation index (Sherwin & Baldini, 2011; Fairchild & McMillan, 2007; McDermott, 2004) in

Element	PC1	Max. (ppm)	Min. (ppm)	Median (ppm)	Standard Deviation (ppm)	Mean (ppm)
Magnesium (Mg)	-0.056	29888.91	42.51	7527.60	2517.3	8002.50
Aluminium (Al)	0.0089	13328	0.00	0.94	150.81	3.45
Phosphorus (P)	0.00	739.61	0.00	66.85	61.60	81.53
Sulfur (S)	0.00	1102.50	167.33	308.38	18.24	307.14
Titanium (Ti)	0.0090	42.26	0.00	0.38	0.83	0.43
Vanadium (V)	0.058	10.95	0.00	0.016	0.14	0.021
Manganese (Mn)	0.00	68.42	0.00	0.00	8.60	0.56
Cobalt (Co)	0.00	8.94	0.00	1.07	0.77	0.86
Copper (Cu)	0.00	427.07	0.00	1.08	4.89	1.33
Zinc (Zn)	0.21	52.38	0.00	2.0045	4.061	3.48
Bromine (Br)	0.00	13308	0.00	2768.90	3102.50	2695.60
Rubidium (Rb)	0.00	1.1735	0.00	0.026	0.039	0.028
Strontium (Sr)	0.43	849.11	15.60	40.37	87.90	57.54
Yttrium (Y)	0.00	4.22	0.00	0.007	0.15	0.041
Zirconium (Zr)	0.00	709.51	0.022	0.33	8.15	0.48
Cadmium (Cd)	0.00	20.81	0.00	0.00	0.26	0.022
Barium (Ba)	0.44	41.64	1.13	4.35	3.71	5.069
Lanthanum (La)	0.023	20.31	0.00	0.0018	0.24	0.013
Cerium (Ce)	0.023	6.20	0.00	0.00	0.092	0.0043
Neodymium (Nd)	0.069	5.20	0.00	0.00	0.080	0.0091
Ytterbium (Yb)	0.00	4.31	0.00	0.00	0.051	0.0046
Platinum (Pt)	0.0034	1.31	0.00	0.00	0.017	0.0014
Mercury (Hg)	0.00	15671	0.00	3274.32	4308.70	3015.70
Lead (Pb)	0.18	2.05	0.00	0.0276	0.072	0.043
Thorium (Th)	0.038	0.45	0.00	0.00	0.0087	0.007
Uranium (U)	0.42	32.78	0.016	0.24	3.0033	0.78

turn increasing the preferential removal of Ca^{2+} along the flow path. Second is incongruent calcite

dissolution (ICD), whereby prolonged interactions between the host rock and seepage waters elevate dissolution rates and release of trace elements (Wassenburg et al. 2020., McDonald et al. 2007; Fairchild et al. 2000). ICD and PCP instigate similar changes to dripwater geochemistry (Sinclair et al. 2012) and are detectable through observations of covariant change in Mg, Sr, U, and Ba concentrations (Wassenburg et al. 2012; Stoll et al. 2012**;** Wong et al. 2011; Baldini et al. 2006), as crystallographic differences between aragonite and calcite (Wassenburg et al. 2016) mean larger cations (e.g. Sr, Ba, and U) are preferentially incorporated into aragonite, whereas smaller cations such as Mg are preferentially incorporated into calcite (Swart, 2015). Such changes appear reflected in the DIM-3-A record, as aragonite layers are marked by abrupt elevation of Sr and Ba concentrations synchronous with sharp decreases in Mg.

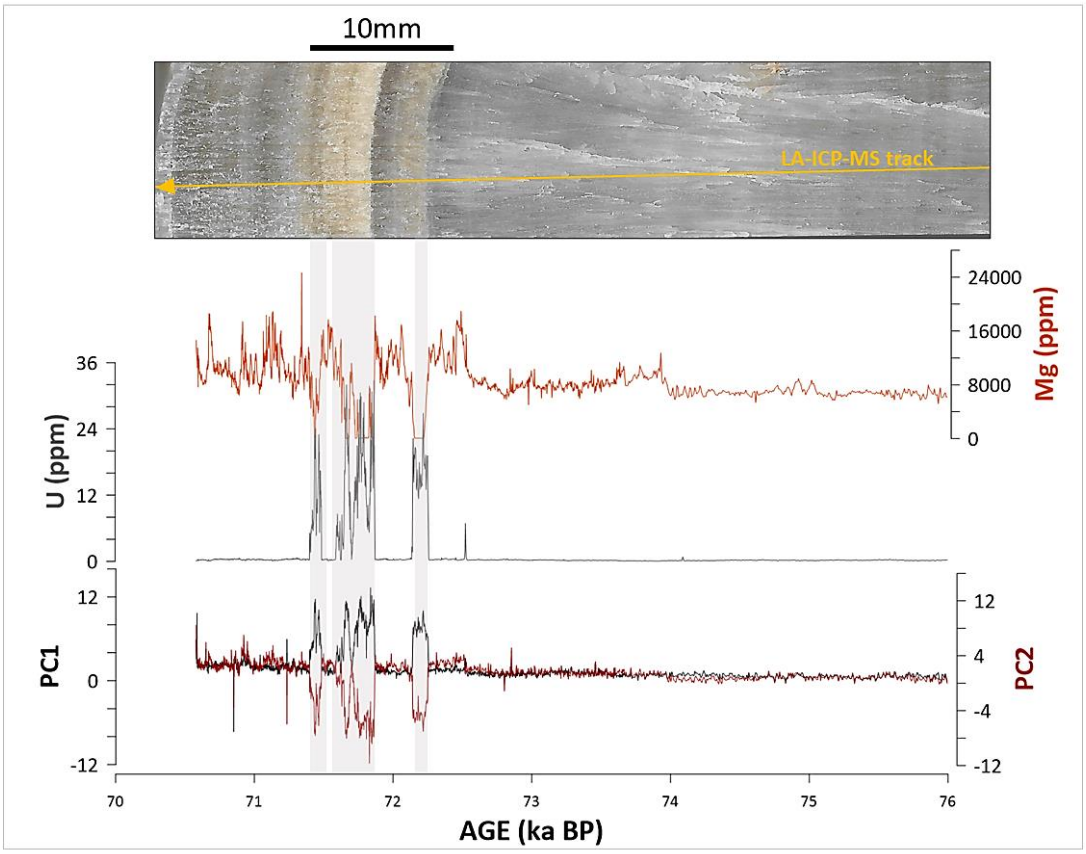

Figure 19: A comparison of the DIM-3-A petrography and geochemistry, focussing on aragonite layers at the top of the sample, alongside time-resolved PCA outputs. Grey shading highlights three aragonite layers, all ~0.2mm in length.

Correlations between trace elements involved in PCP, ICD, and formation of aragonite in DIM-3-A are interpreted here as signs of reduced moisture availability in Dim Cave. Prior studies have utilised aragonite formation (e.g. Martín-García et al. 2019; Domínguez-Villar et al. 2017; Wassenburg et al. 2012; Csoma et al. 2006**;** McMillan et al. 2005; Frisia et al. 2002), and related changes to trace elements such as U (e.g. Chen et al. 2020; Wassenburg et al. 2016; Jamieson et al. 2016; Chen et al.

2016; Bourdin et al. 2011) as proxies for paleo-aridity, on the basis that reduced effective precipitation (meteoric precipitation minus evapotranspiration) results in decreased water supply to dripwater aquifers, enhancing saturation with respect to $CaCO_3$ (Wassenburg et al. 2016). This interpretation is consistent with DIM-3-A geochemistry for multiple reasons. Firstly, Mg shows significant enrichment prior to aragonite formation (McMillan et al. 2005) suggesting dripwater became super-saturated, potentially due to increased seepage flow path length and/or greater aquifer residence times – both of which can link to arid external conditions. Less negative $\delta^{18}O$ and $\delta^{13}C$ from ~73.6 ka BP (**Figure 20**) also suggest reductions in surface vegetation and soil activity (Ünal-İmer et al. 2016), which have been interpreted as indicators of reduced ambient temperature and/or effective rainfall. In principle, such conditions would promote increased water-rock interactions and longer recharge, thus greater release of trace elements into dripwater supply. Therefore, the presence of aragonite layers within DIM-3-A suggest the stalagmite was subject to low moisture conditions during GI-19.2, and subsequently a drier external climate.

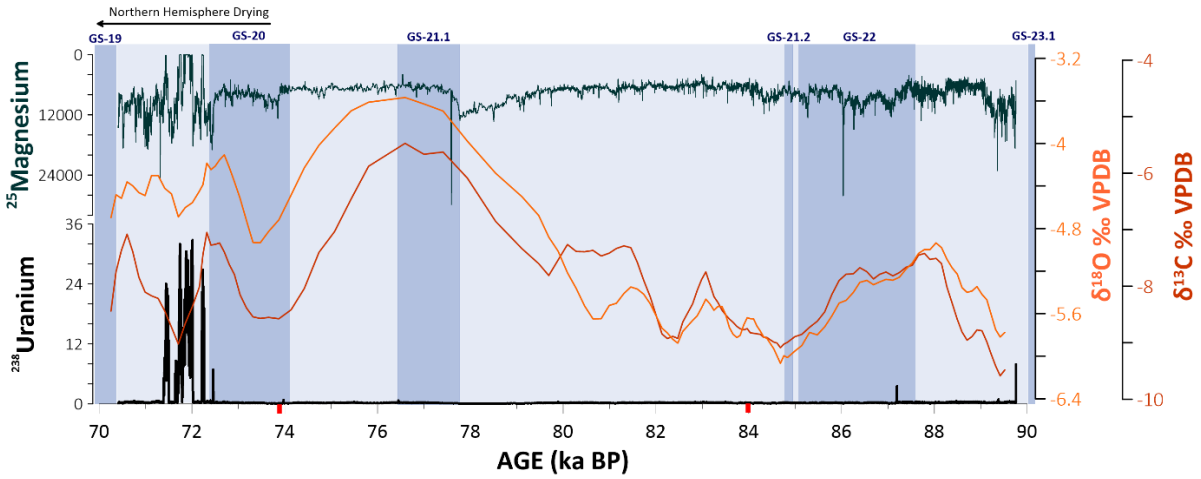

Figure 20: $\delta^{13}C$ and $\delta^{18}O$ values for DIM-3 (Ünal-İmer et al. 2015) plotted against ^{232}U and ^{25}Mg concentrations measured in DIM-3-A. Data is plotted in relation to the COPRA chronology generated for this study. Red squares on the x-axis mark the two major eruptions featured in this study: the Youngest Toba Tuff (~74 ka BP) and Los Chocoyos (~84 ka BP). A notable increase in Mg concentration is visible in concurrence with the YTT, and is followed by geochemical perturbations suggesting increasingly dry conditions.

PC1 also shows significant correlations between Zn and Pb**.** A small enrichment is visible at ~83 ka BP, however the highest concentrations are seen following ~74 ka BP (**Figure 21**). Both represent deviations from typical calcite composition; but their respective sources are unclear and could have resulted from either (1) enhanced bedrock weathering, or (2) increased atmospheric dust deposition.

For stalagmites fed by seepage flow, rates of (1) are enhanced by reduced water flux and relative leaching efficiency (Fairchild & Treble, 2009), both of which favour enhanced dissolution of bedrock constituents. Onset of Zn enrichment appears concurrent with an abrupt enrichment in Mg at ~73.5 ka BP, suggesting this trace element may derive from increased dissolution of the quartzofeldspathic bedrock forming Dim Cave (Bozkaya and Yalçın, 2004) by reductions in surface water infiltration. As these changes occur ~1.6 kyr prior to aragonite layers, Zn may mark the onset of dripwater saturation due to drier conditions, from which aragonite formation begun once a threshold had been surpassed (Wassenburg et al. 2012). This interpretation is supported by concurrent enrichment of $\delta^{18}O$, suggesting a northward shift of westerly wind trajectories over the Eastern Mediterranean (Ünal-İmer et al. 2015). Although such a track may result in lower humidity and decreases in total effective rainfall, interpretations linking isotope variability in DIM-3-A to changes in paleo-rainfall should be approached with caution. Karst moisture balance, drip rate, and rainfall quantity are often mutually exclusive (Fairchild & Treble, 2009) and thus rates of bedrock dissolution are not always directly proportional to surface rainfall. Changes in effective rainfall may not impact drip rate, and instead exert a dominant effect on stalagmite geochemistry by drip water saturation (by the mechanisms discussed above)**.** Moreover**,** the interpretation presented here contradicts prior evidence for 'wetter' stadials in the East Mediterranean (e.g. Rowe et al. 2020; Ünal-İmer et al. 2015; Frumkin et al. 2011; Sorin et al. 2010) resulting from southward westerly shifts due to increased polar ice volume, and increased surface elevation/pressure due to large ice sheets (Kwiecien et al. 2009) – emphasising the notable complexity associated with paleoenvironmental reconstruction in this region. The simultaneous onset of Zn, Mg, $\delta^{18}O$ enrichment in DIM-3-A does support the notion of abruptly reduced moisture availability in Dim Cave following ~74 ka BP, although it is unclear whether this directly reflects change in effective rainfall over Turkey.

Increased atmospheric dust deposition (2) can also influence the trace element geochemistry of stalagmites. Deposition of exotic elements (such as Pb) can occur by percolation in groundwater through the host rock or direct aeolian deposition onto the stalagmite growth tip (Vaks et al. 2013, 2010; Wassenberg et al. 2012; Goede et al. 1998), yet the relative influence of these processes will be contingent on cave morphology and location. Evidence suggesting Pb in DIM-3-A is dust-derived is seen by concurrence between spikes in Pb and ^{232}Th concentration. ^{232}Th (Rowland et al. 2017) and Pb (Jamieson et al. 2015) are both atypically incorporated into calcite, thus justifying their use as markers of transient deposition of particulates originating beyond the cave site. Furthermore, increased enrichment of these trace elements occur at the same time as other aridity indicators (e.g. aragonite). High atmospheric dust concentration is characteristic of arid conditions (Simonsen et al. 2019., Liu et al. 2013**.,** Újvári et al. 2010; Petit and Delmonte, 2009; Ruth et al. 2003), and for Dim

Cave these particulates would most likely originate from North Africa (Allen et al. 2020; Vaks et al. 2013; Prospero et al. 2002) or Central Europe (Újvári et al. 2010) – mobilized during a period of low atmospheric humidity and active westerly winds. It is unlikely Zn was also derived from atmospheric dust deposited at the surface. Zn enrichment occurs alongside increased $\delta^{13}C$ (Ünal-İmer et al. 2015) – interpreted to infer cooler temperatures and reduced CO_2 availability (Ahn & Brook, 2008), which favour thinner soils and lower vegetation abundance. Yet, research suggests colloidal Zn transport is associated with periods of high fluid flow into the karst, resulting in faster percolation of particles deposited at the surface through bedrock (e.g. Oster et al. 2020, 2017; Rutlidge et al. 2014; Hartland et al. 2012). This undermines the aridity inferred from variabilities in DIM-3-A Mg, $\delta^{18}O$, Sr, Ba, and U. Although the partitioning of Zn in stalagmites is poorly understood (Borsato et al. 2007; Reeder et al. 1996), evidence presented here suggests that Zn was not deposited into this record by soil-derived colloidal transport. However, this does not rule out the potential for Pb to be deposited in this manner.

Quantifying the magnitude and duration of climate change in the Mediterranean is challenging, as the defining features of a given perturbation vary depending on region (e.g. Dumitru et al. 2018; Mori et al. 2018; Carolin et al. 2016; Springer et al. 2014). For example, archives from the west Mediterranean document increases in effective precipitation during interstadial periods resulting from a strengthened hydrological cycle (e.g. Pérez-Mejías et al. 2019; Budsky et al. 2019; Denniston et al. 2018; Stoll et al. 2013; Vaks et al. 2010; Bar-Matthews et al. 2003). Whereas in the east Mediterranean, complex meteorological regimes lead to differing interpretations of $\delta^{18}O$ depletion/enrichment meaning rainfall amount is hard to quantify (e.g. Corrick et al. 2020; Ünal-İmer et al. 2015; Rowe et al. 2012; Bar-Matthews et al. 2003). The trace element geochemistry of DIM-3-A seems responsive to moisture availability, showing hydrochemical and trace element shifts indicative of reduced water provision to the stalagmite following ~74 ka BP. Enrichments of Zn and Pb suggest incorporation of extraneous material and, although these potentially derive from different sources, the positive correlation between them (PCA) suggests they both derive from a common process; suggested here to be aridity.

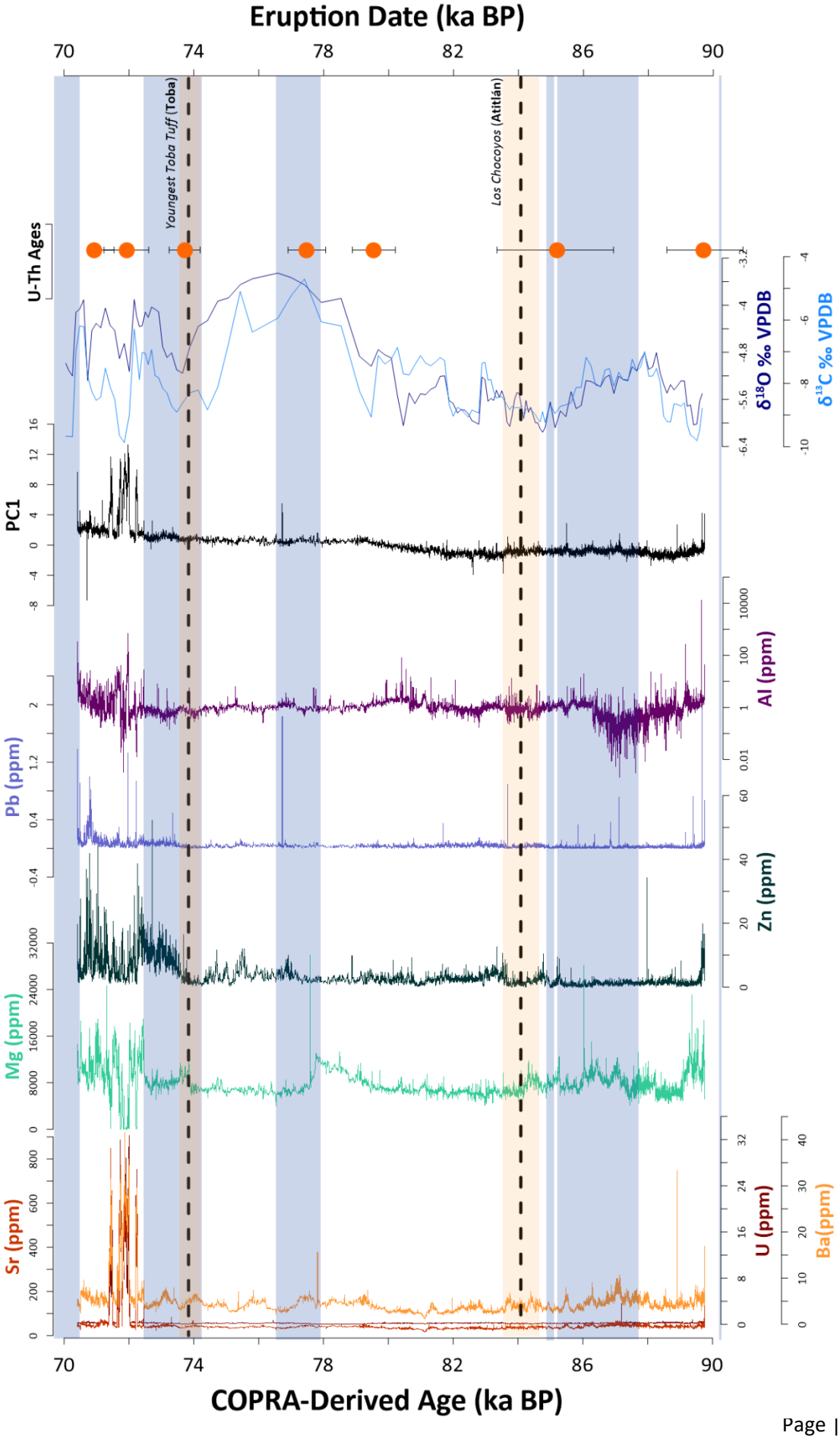
Eruption Date (ka BP)
70
74
78
82
86
90
Youngest Toba Tuff (Toba)
Los Chocoyos (Atitlán)
U-Th Ages
PC1
δ18O ‰ VPDB
δ13C ‰ VPDB
Pb (ppm)
Al (ppm)
Zn (ppm)
Mg (ppm)
Sr (ppm)
U (ppm)
Ba(ppm)
COPRA-Derived Age (ka BP)

Figure 21: A comparison of selected trace elements, isotope data (Ünal-İmer et al. 2015 – reported as per mil (‰) relative to the Vienna Peedee Belemnite (VPDB) standard), and PC1 scores for DIM-3-A. Uncertainties with the COPRA chronology for DIM-3 (SISAL: Comas-Bru et al. 2020) are marked as orange circles. The dates of the Youngest Toba Tuff (derived from $^{40}Ar/^{39}Ar$ – Storey et al. 2012) and Los Chocoyos (derived from oxygen isotope stratigraphy - Kutterolf et al. 2016) eruptions are marked as a dashed black line, with uncertainties highlighted in yellow. Blue highlight marks the timing and duration of Greenland Stadials, based on the INTIMATE stratigraphy (Rasmussen et al. 2014). The amplitude and frequency of trace element enrichments increase following the Youngest Toba Tuff, and Mg, Sr, and Ba denote the formation of aragonite layers during GI-19.2.

6.3.3. Volcanic Signals

6.3.3.1. Atitlán

The date of Los Chocoyos super-eruption of Atitlán, Guatemala has been constrained to 84 ± 0.5 ka BP based on oxygen-isotope anomalies in ocean-sediments (Drexler et al. 1980., Koch & McLean, 1975). Short-lived enrichment of Zn and Pb at ~83.8 ka BP occurs in DIM-3-A alongside a transient depletion of $\delta^{18}O$ (Ünal-İmer et al. 2015), ~200 years following the LCY eruption. However, this signal is extremely subtle, suggesting the LCY ash plume likely did not reach Turkey, nor did the eruption have a profound, long-term impact on Eastern Mediterranean climate.

The magnitude of the LCY event is exceptional, and the low-latitude location of Atitlán volcano renders a meridional spread of aerosols by Brewer-Dobson circulation more likely (Svensson et al. 2020., Baldini et al. 2015). Yet there are two factors which could explain a negligible impact of the eruption on NH climate: (1) baseline ice/climate conditions, and (2) exceptionally high volatile gas emission. The first factor (1) is influenced by eruption timing. A definitive ice core signal for the eruption is yet to be determined, as Zielinski et al. (1996) identify 5 SO_2^{-4} spikes in the GISP 2 record between 83-85ka BP. However, stratigraphic evidence suggests the LCY occurred during Greenland Interstadial (GI)-21.1 - one of the longest millennial-scale warm periods documented for the Quaternary (Zhang et al. 2020) during which atmospheric CO_2 and CH_4 (Griffiths et al. 2013) rose significantly (**Figure 22**), due to southward shift of the ITCZ and SH westerlies, and subsequent increases in Southern Ocean upwelling (Griffiths et al. 2013). Studies suggest intermediate ice volume associated with sea levels 68 – 71 m lower than present are those most likely to amplify the climatological impact of volcanism (Baldini et al. 2018, 2015), yet at ~84 ka BP atmospheric CO_2 was ~250ppm (Ahn & Brook, 2008) and sea level 20-50 m lower than present (Waelbroeck et al. 2002). This implies not only warmer surface temperatures and low ice volume conditions, but also a climate system more resilient to abrupt changes in temperature (Barker et al. 2019; Zhang et al. 2017, 2014) caused by the propagation of volcanic aerosols.

Greater climatic stability may have acted alongside (2): exceptionally high volatile gas emission, to further attenuate the climatological impact of LCY. Petrological estimates for LCY sulfur emission currently stand at 523 ± 94 Mt (Brenna et al. 2020), which is 10 times greater than estimates for other >M6.0 eruptions such as Tambora (53-58 Mt: Stenchikov et al. 2009; Self et al. 2004), Samalas (158 ± 12 Mt: Vidal et al. 2016), and Laacher See (~83Mt : Baldini et al. 2018). This evidence suggests LCY was exceptionally sulfur-rich, and modelling studies have suggested that timescales of radiative forcing induced by a sulfur-rich eruption may reduce if SO_2 concentrations exceed a 'maximum potency' threshold; by causing an enhanced greenhouse effect (Osipov et al. 2020) and rapid fallout of sulfate aerosols from the atmosphere (Timmreck et al. 2010). Less severe NH cooling, by extrapolation, may therefore have reduced the hemispheric temperature gradient and thus attenuated a millennial-scale climatic signal. Furthermore, if LCY generated a coignimbrite plume similar to the YTT (Costa et al. 2018; Matthews et al. 2012; Chesner & Rose, 1991), entrainment of water vapour by pyroclastic flows (Joshi & Jones, 2009) across the Caribbean and Eastern Pacific oceans surrounding Guatemala may have further attenuated the cooling associated with atmospheric injection of sulphate aerosol. However unlike (1), (2) possesses much less empirical support and existing studies are underpinned by analogue scaling – with uncertainties exacerbated by poorly constrained LCY eruptive parameters. For example, sulfur ejection estimates rely upon known ejecta volumes, which are continuously changing. Metzner et al. (2014) estimated a 686.59 Mt SO_2 yield, however recent expansion of known tephra limits (Kutterolf et al. 2016) incorporated into estimates by Brenna et al. (2020) prompted a reduction of 163 Mt; not accounting for uncertainties in aerosol conversion ratios, size and atmospheric lifetime, halogen content (Brenna et al. 2019., Klobas et al. 2017., Cadoux et al. 2015), altitude of volatile gas injection (Sheng et al. 2015., Shinohara et al. 2008., Scaillet et al. 2004), and scavenging of halogens by water in the eruption column (Brenna et al. 2019). Furthermore, magnitude is not directly proportional to sulfur emission (McCormick-Kilbride et al. 2016., Carn et al. 2016., Pyle, 2012) and magma degassing shows large geographical variability depending on tectonic setting (e.g. the CAVA - Schindlbeck et al. 2018., Bolge et al. 2009), and so analogue scaling increases the risk of over/underestimation of volatile yield, and the associated climatological implications.

The intricacy of mechanisms governing super-volcanism (e.g. Swallow et al. 2019; Andersen et al. 2019; Allan et al. 2017; de Silva & Gregg, 2014) causes great diversity in eruption petrology, and thus huge variance in gas ejection between events of a similar magnitude. This has significant implications for the climate response (Timmreck et al. 2012), and results in mixed model outputs for eruptions whereby parameters must be estimated (Timmreck et al. 2010; Robock et al. 2009; Jones et al. 2005) – such as those occurring prior to the Holocene. Due to the exceptional magnitude of

LCY, the cumulative effect of aerosol and tephra loading likely did disturb radiative forcing and diurnal cycles in the years following eruption (Brenna et al. 2020; Kutterolf et al. 2016; Metzner et al. 2014). However, evidence from DIM-3 and other speleothem records between 80 and 90ka BP (**Figure 22**) suggest the eruption's climatological impact was limited and did not cause widespread perturbation to Northern Hemispheric climate. This could result from interstadial conditions at the time of eruption, favouring climate system stability and less susceptibility to perturbation by volcanism. However, LCY is a notably understudied eruption, and so prevailing uncertainties in ejected tephra and gas volumes thwart the ability to make robust correlations between this exceptional eruption and NH climate during GI-21.1.

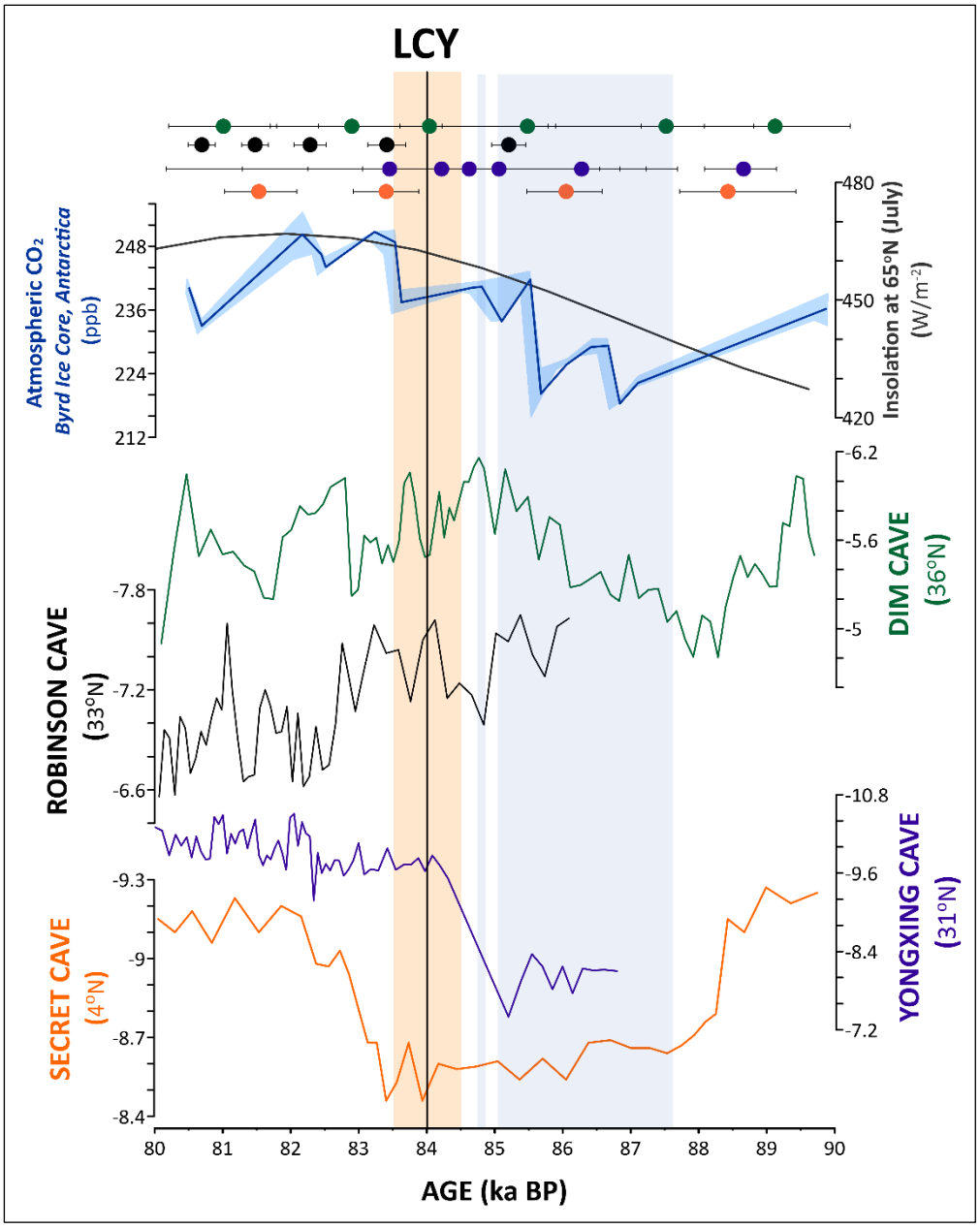

Figure 22: A stacked comparison of cave isotope records between 80 and 90 ka BP. Uncertainty in the Los Chocoyos (LCY) eruption date (based on Kutterolf et al. 2016) is marked by yellow highlight, and blue highlight marks stadial intervals as defined by Rasmussen et al. (2014). $\delta^{18}O$ data is reported as per mil (‰) relative to the Vienna Peedee Belemnite (VPDB) standard. Stalagmite isotope data was downloaded from SISAL (Comas-Bru et al. 2020), data sources include: *Dim Cave* – Ünal-İmer et al. (2015), *Secret Cave* – Carolin et al. (2013), *Robinson Cave* – Polyak et al. (2017), and *Yongxing Cave* - Chen et al. (2016). **Appendix Table 1** provides more information on all caves featured. Cave sites are presented in order of latitude, and circles with error bars mark chronological uncertainties associated with each stalagmite record. Atmospheric CO_2 data sourced from the Byrd Station, Antarctica (Ahn & Brook, 2008 – shading represents uncertainty in CO_2 estimates) and insolation data from (Berger & Loutre, 1991) are also presented.

6.3.3.2. Toba

With an estimated date of 73.88 ± 0.32 ka BP ($^{40}Ar/^{39}Ar$ derived - Storey et al. 2012), the Youngest Toba Tuff (YTT) eruption of Toba volcano, Indonesia, occurred within uncertainties of significant geochemical variability in DIM-3-A (shown in **Figure 21**). There are two ways these observed geochemical shifts could be linked to the YTT, yet three discrete interpretations: (1) simply no causal link (2) direct ash fall, or (3) forcing of climate resulting from aerosol loading by the YTT plume. These interpretations are discussed individually herein.

6.3.3.2.1. No Link

There is a chance that geochemical variability observed in DIM-3-A may not have been caused by the YTT at all, and instead reflect natural variabilities in karst conditions unrelated to volcanic-derived processes. For example, it is difficult to quantify 'background' input of volcanic trace elements into the soils resulting from intermittent, low-magnitude volcanic activity, due to disparities in eruption records between 70 and 90 ka BP. Deposits are often lost to erosion associated with recurrent glaciation, isostatic change, and progressive degradation (Baldini et al. 2015), and a lack of research can exacerbate this problem. Turkey is a key example of the latter, with a limited number of volcanological investigations (Bilim et al. 2018) despite the presence of several volcanic fields of Quaternary age in Anatolia (Aydar, 1998).

More research is also needed to better characterise the sensitivity and spatial diversity of climate regimes at ~74 ka BP before changes observed within DIM-3-A can be exclusively attributed to volcanism. Frameworks attempting to model the mechanisms underpinning atmospheric variability on stadial-interstadial timescales are notably limited in scope (Atwood et al. 2020), so disentangling the relative effects of volcanism and ice sheet growth on air mass trajectories and atmospheric teleconnections is complex; especially whereby the eruption in question occurs during a period of orbitally induced cooling, as the YTT does (Baldini et al. 2018, 2015; Berger & Loutre, 1999). Regional complexities associated with the Eastern Mediterranean climate system may have attenuated the

effects of, for example, volcanically forced ITCZ migration and thus variability of air mass trajectories recorded by the DIM-3 geochemical record. However, this is difficult to confirm while the respective long-term influence of eruption chemistry, intensity, and plume height on atmospheric circulation is ambiguous. Particularly for exceptionally large events such as the YTT; whereby all aforementioned parameters remain poorly constrained due to uncertainties in paleoenvironmental archive resolution (e.g. Du et al. 2019; Baldini et al. 2015), absolute eruption dates (e.g. Mark et al. 2017, 2014; Storey et al. 2012; Chesner, 1991), and eruption chronologies (Svensson et al. 2013).

6.3.3.2.2. Direct Ash Fall

Increased concentrations of Zn and Pb in DIM-3-A occur well within dating uncertainties of the YTT eruption, which could be interpreted as an indicator of volcanic ash deposition. If stratospheric injection of tephra is achieved during an eruption, deposition can occur >1000 kilometres from the eruptive centre (Lane et al. 2017; Matthews et al. 2012). Volcanic ash deposited in the soils overlying a karst system may subsequently be washed into a karst system by periods of high fluid flow and infiltration rates (Borsato et al. 2007). This would enable transport of surface colloids through the aquifer to the drip site (Hartland et al. 2012), which is a process upon which integration of Zn and Pb into stalagmites shows significant dependence. Based on tephrochronology it is unclear whether the YTT co-ignimbrite plume did reach the East Mediterranean, however modelling of the YTT plume dynamics suggest the eruption's exceptional (mass) eruption rate (1.75×10^{11}kg/s: Costa et al. 2018, 2014; Costa & Martí, 2016) likely resulted in rapid generation of a huge gravity current in the stratosphere. Generation of such a large current would facilitate a volumetric flow rate capable of dispersing ash over a huge area – which is supported by proxy evidence for YTT fallout in East/South Africa (Yost et al. 2018; Smith et al. 2018; Lane et al. 2013), India (Matthews et al. 2012), Malaysia (Smith et al. 2011), and the South China Sea (Liang et al. 2001; Song et al. 2000). YTT glasses also appear rich in Pb (e.g. Pearce et al. 2020) and elevated concentrations of this trace element have been previously interpreted as a volcanic indicator in stalagmites (Jamieson et al. 2015). Therefore, deposition of YTT ash over the East Mediterranean is not out of the question, under favourable atmospheric conditions.

However, it is unlikely the Zn and Pb excursions here result from fallout of coignimbrite generated by the YTT eruption, due to the duration of trace element enrichment (~2 kyr). Irrespective of eruption magnitude, the removal of tephra particles from the atmosphere typically occurs in <1 year (Costa et al. 2014; Lowe, 2011) and as a result discrete ash-fall events appear in stalagmites as spikes <50 years in duration (e.g. Jamieson et al. 2015; Badertscher et al. 2014; Frisia et al. 2008). The duration of volcanic-derived material deposition within a stalagmite (resulting from a single eruption) may be

prolonged if: (1) long-term changes to regional hydrology (favouring increased effective rainfall) caused remobilization of older deposits, and increased colloidal transport into the karst aquifer, (2) winds were persistently strong enough to disperse particulates across a large catchment, such as during stadial intervals (Simonsen et al. 2019), (3) the eruption exhibited multiple explosive/ash-producing phases. Scenarios (1) and (2) rely on accurate constraint of sedimentary processes occurring at the time of deposition, such as compaction, bioturbation, and eluviation (Cutler et al. 2020; Matthews et al. 2012) in order to discriminate between volcanic signals and biogeochemical cycling. However, insufficient temporal resolution of paleoenvironmental records from this period render the relative influence of these processes difficult to quantify. Identification of multiple sulfate peaks in Greenland ice-core records across the YTT boundary thus lends support to scenario (3), by suggesting that Toba could have exhibited multiple explosive phases across a single eruptive episode (Savarino et al. 2020; Svensson et al. 2013) and thus caused prolonged ash dispersion. Evidence for a multi-vent system (Costa et al. 2014) and tapping of petrologically-discrete magma reservoirs (Pearce et al. 2020) also backs this hypothesis. Yet, the four sulfate enrichments tentatively attributed to Toba are separated by <400 years, and the distance between Sumatra and Turkey raises the potential for attenuation of YTT signals by other, potentially unknown, more proximal eruptions. In either case, it would be near impossible to confidently differentiate YTT signals from other ash fall events within the DIM-3-A geochemical sequence.

6.3.3.2.2. Cooling/Aridity

The Zn and Pb enrichments observed here are interpreted as indicators of significant environmental change marking a transition to more arid conditions. This interpretation is supported by the presence of a distinct Mg enrichment at ~74 ka BP, which is indicative of reductions in karst moisture availability and thus increased dripwater saturation as due to increased bedrock-water interactions. Two observations also suggest the geochemical changes seen in DIM-3-A are not the product of 'typical' interstadial-stadial variability from the transition into GS-20 at 74.1 ± 0.06 ka BP (1σ). Trace elements showing mutually significant PCA coefficients (notably Zn and Pb) do not appear in such high concentrations during any other stadial periods between 70 and 90 ka BP, such as GS-21 (77.76 ± 0.1 ka BP (1σ)) or 22 (87.6 ± 0.04 ka BP (1σ)). Secondly, calcite-aragonite transitions are only observed during GI-19.2, and enrichment of trace elements such as Zn and Pb also continue during this interval. Interpreted here as indicators of low moisture availability, aragonite formation during GI-19.2 suggests this interstadial was significantly drier than those prior to 74 ka BP (**Figure 23**); such as GI-20 (76.44 ± 0.02 ka BP (1σ)) and GI-19.2 (72.34 ± 0.02 ka BP (1σ)). This suggests the presence of an additional forcing mechanism driving millennial-scale NH climate across the GS-20/GI-19.2 transition, for which the YTT seems a plausible candidate.

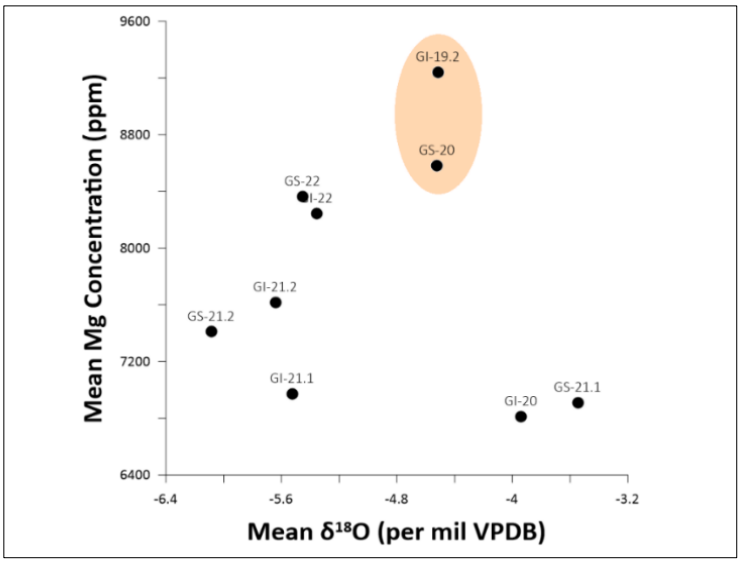

Figure 23: A scatterplot showing the relationship between $\delta^{18}O$ and Mg concentration in DIM-3-A, with mean values calculated for each Greenland stadial/interstadial event (based on the INTIMATE stratigraphy: Rasmussen et al. 2014). The stadial interval prior to which the YTT eruption occurred (GS-20), and first interstadial following the eruption (GI-19.2), are highlighted in orange, with both showing the highest average Mg concentration across the DIM-3-A interval. Due to the relationship between Mg and aridity, this could provide an indication that GS-20 and GI-19.2 were particularly dry in Turkey – resulting in supersaturation of dripwater feeding the stalagmite.

If DIM-3-A geochemical variability immediately after 74 ka BP are interpreted as indicators of aridity resulting from the YTT, the duration of their occurrence (>2 kyr) suggests they are not the result of direct, volcanic-induced radiative forcing effects. Historical observations show that mass stratospheric injection of volcanogenic material can reflect solar radiation back into space, and briefly cool the Earth's surface (e.g. Pinatubo – Diallo et al. 2017), however this effect appears short lived (Robock, 2000). Modelling studies have identified that, for a 'YTT-sized' eruption, radiative forcing would have returned to background levels in <10 years (Osipov et al. 2020; Timmreck et al. 2012; Robock et al. 2009). However, if aridity-driven variability in DIM-3-A's geochemistry was caused by the YTT, these findings would support a millennial-scale impact of the YTT on NH climate. Increasing evidence suggests that volcanism has the capacity to induce significant hemispheric asymmetry by preferentially cooling the eruption hemisphere and result in displacement of large-scale circulatory systems such as the ITCZ (Pausata et al. 2020; Baldini et al. 2015; Ridley et al. 2015). Following these observations, Baldini et al. (2015) suggest the same would occur following the YTT. Mass volcanogenic aerosol loading would invoke a southward ITCZ shift, resulting in elongation of the polar front (Schneider et al. 2014; Hudson et al. 2012) and a transition to cooler/more arid conditions in the NH (Baldini et al. 2015) – change amplified by ice/albedo and ocean circulation feedbacks manifesting as millennial-scale reductions in global mean surface temperature (Zanchettin et al. 2017; Boucher et al. 2013). Although the key processes driving inter-hemispheric responses to

volcanism are poorly understood (Zanchettin et al. 2014), it is plausible to assume the time taken for the NH climate system to return to a 'stable' state, either by natural regulation or an antagonistic forcing mechanism, would take hundreds-to-thousands of years. This is also supported by the DIM-3-A record, as the aforementioned indicators of aridity persist until ~71.5 ka BP.

Studying the climatological implications of the YTT eruption are nonetheless challenging, particularly in the EM. Not only are interpretations of isotope records across the region ambiguous (e.g. Corrick et al. 2020; Ünal-İmer et al. 2015; Rowe et al. 2012; Bar-Matthews et al. 2003), but significant uncertainties prevail concerning spatial and temporal differences in atmospheric composition and circulation so far back in time (Roberts et al. 2017). Both confound attempts to constrain the relative influence of volcanism on the DIM-3-A record, and consequently regional climate variability. For example, lesser $\delta^{18}O$ depletion of rainfall in SW Turkey (Ünal-İmer et al. 2015) is linked to increased influence from NW-SE European westerly tracks (Türkeş & Erlat, 2009), and northward migration of the ITCZ. Such depletion is seen in DIM-3-A following the YTT, however this is inconsistent with modelling studies (e.g. Pausata et al. 2020, 2015; Atwood et al. 2020; Pausata & Carmargo, 2019; McGee et al. 2014) suggesting that southward ITCZ migration would ensue following aerosol loading by a NH eruption. Initially, this suggests the YTT exerted a negligible effect on atmospheric circulation. However, modelling studies also suggest the direction and magnitude of ITCZ migration is longitudinally heterogenous (Atwood et al. 2020; McGee et al. 2014), and millennial-scale changes to the ITCZ's annual mean location (Roberts et al. 2017) is notably reduced compared to seasonal cyclicity (Donohoe et al. 2014). Moreover, the Mediterranean response to climate change differs from the averaged behaviour of regions at the same latitude (D'Agostino & Lionello, 2020) – thus the absence of a pronounced southward shift of the westerlies over SW Turkey may also result from a less pronounced ITCZ shift in this region. Despite this, a mean zonal southward shift across the entire NH, consequent elongation of the Polar Cell, and reductions in ambient temperature would likely still exert a significant cooling effect in regions north of the equator. Therefore, aridity induced by the YTT in SW Turkey may have been sustained by complex atmospheric feedbacks independent from air mass trajectories; with the latter exerting a dominant effect on rainfall composition rather than quantity. This mechanism would justify the hemisphere-wide aridity as observed not only in DIM-3-A's geochemistry, but across the NH (**Figure 24**). Robust assessment of whether the YTT did invoke climatological perturbation will greatly benefit from ongoing analyses of high-resolution, well-dated stalagmite sequences across a broad geographical domain - by attenuating regional variabilities in atmospheric circulation/composition, and defining the refined sequence of events and synchronicity of change occurring across the YTT interval.

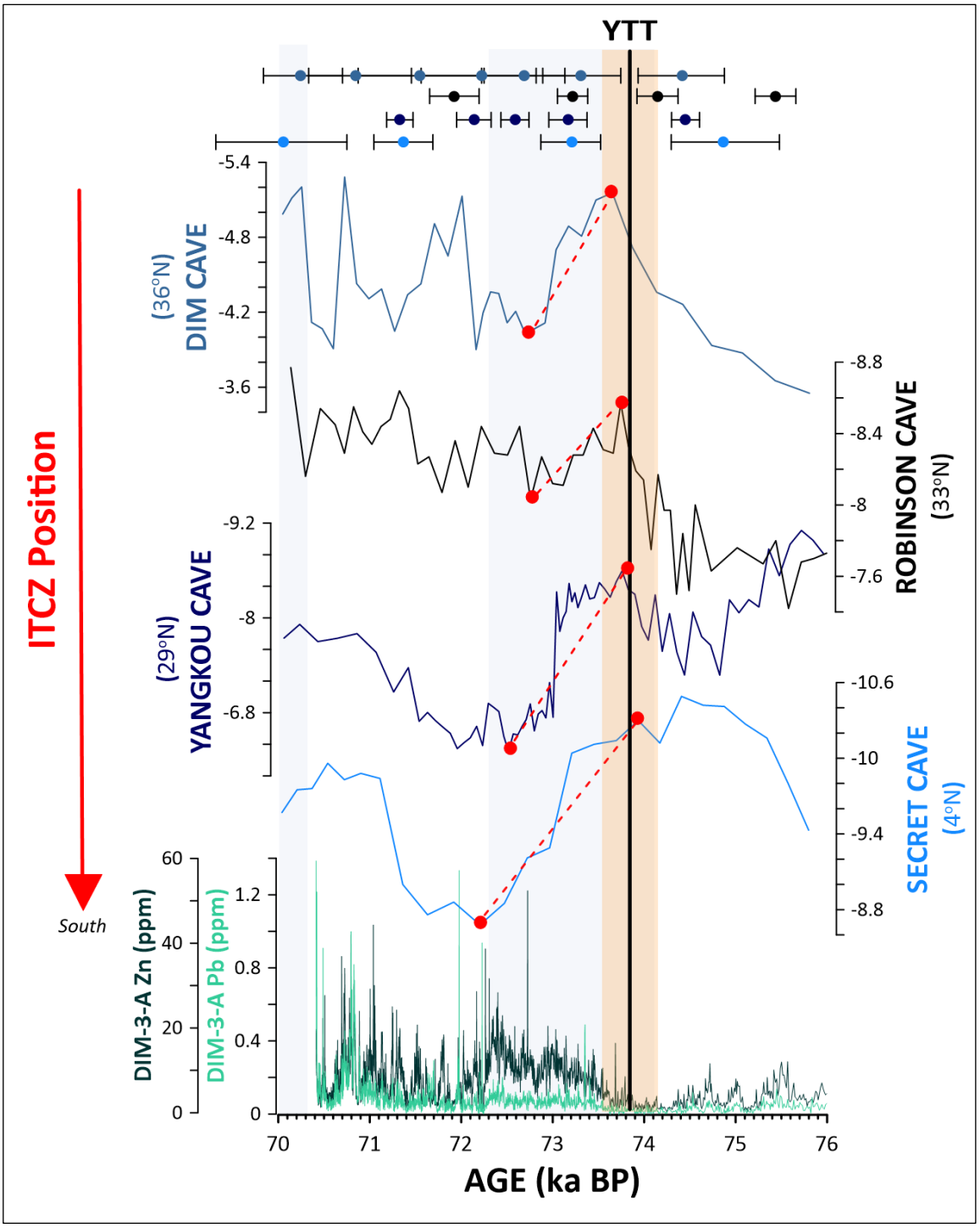

Figure 24: A stacked comparison of time-resolved Zn and Pb concentrations in DIM-3-A, $\delta^{18}O$ measured in DIM-3 by Ünal-İmer et al. (2015), and $\delta^{18}O$ records from other high-resolution, independently dated (U-series) Northern Hemisphere stalagmite archives (*Secret* – Carolin et al. 2013; *Yangkou* – Du et al. 2019., Zhang et al. 2017; *Robinson* – Polyak et al. 2017; *Dim* – Ünal-İmer et al. 2015. **Appendix Table 1** provides more information on all caves featured. $\delta^{18}O$ data is reported as per mil (‰) relative to the Vienna Peedee Belemnite (VPDB) standard. Circles with error bars at the top mark relative uncertainties for each stalagmite (colour coded according to record). YTT eruption timing (73.88 ± 0.32 ka BP) estimated by Storey et al. (2012), based on $^{40}Ar/^{39}Ar$ dating. Red circles mark reduced depletion in $\delta^{18}O$ observed following ~74 ka BP.

7.0. KEY IMPLICATIONS

This thesis aimed to explore the applicability of speleothem trace element datasets for detection of explosive volcanism. Stalagmites NIED08-05 and DIM-3 were independently assessed for the presence of volcanic-derived signals within their geochemical sequence resulting from either direct ash deposition or sustained climate perturbation, respectively, which presented raise three key considerations for future study.

Firstly, a comprehensive knowledge of karst structure and hydrology is required. Existing evidence from low-latitude records (e.g. Ünal-İmer et al. 2020; Jamieson et al. 2015; Badertscher et al. 2014; Frisia et al. 2008) combined with analyses presented here (**Chapter I**) suggest that shallow stalagmites grown in caves overlain by thin vegetation and soil cover, and modulated by a seasonally distinct hydrological cycle, may preserve volcanic ash fall signatures with greater success that those grown in temperate environments. However, it is unclear whether such findings are applicable at higher latitude sites, nor whether these hydrological characteristics would preserve longer-term impacts of volcanism with similar efficacy. Existing studies have also thus far focussed on characterisation of discrete ash fall events, rather than sustained perturbation of climate resulting from volcanic forcing. New evidence (**Chapter II**) tentatively suggests stalagmites grown under seepage flow regimes could retain evidence for millennial-scale, volcanic-induced climate change, yet robust assessment of these cause-effect relationships requires further evidence – sourced from annually resolved archives from a variety of latitudes, alongside well constrained eruption records. It seems not all stalagmites are suitable for paleo-volcanology, and environmental processes can attenuate the preservation of volcanic signatures within a stalagmite sequence. Continued research in this domain will ultimately allow for better constraint of karst systems yielding the most useful records for tephrochronological development.

Secondly, use of PCA to trace discrete eruption events appears ineffective for millennial-scale sequences. From a geochemical perspective, coefficient outputs were successful in identification of incorporated exotic material, by highlighting correlations between individual elements such as Zn, Pb (DIM-3-A), and REEs (NIED08-05). However, individual eruption events could not be identified using PC scores alone. For NIED08-05, a large number of known eruptions between 0 – 3 ka BP combined with Niedźwiedzia Cave's dynamic hydrological regime increased the 'noise' in the record. Subsequently, this increased the risk of volcanic signal attenuation by detrital particles, and so rendered distinguishing trace element enrichments caused by volcanic ash fall more challenging. Transient enrichments are also visible across the DIM-3-A time series, however, do not appear linked

to any known, well-dated volcanic eruptions. Research suggests stalagmites can record eruptions ≤M6.0 (Jamieson et al. 2015) so it is possible enrichments in DIM-3-A result from ash fall produced by unknown, smaller eruptions; however this is difficult to assess given the largely incomplete nature of the pre-Holocene volcanic record. PCA outputs were also dominated by variabilities resulting from calcite-aragonite transitions following ~74 ka BP, potentially muting the visibility of transient enrichments resulting from ash fall. Future studies should consider other dimension-reduction data analysis methods for detection of volcanic-derived geochemical variabilities in pre-Holocene sequences, because for these records eruption recording probability is < 100%, instrumental data is not available to confirm whether ash fall trajectories, and eruption dating uncertainties hinder robust attribution of these events to short-lived geochemical oscillations.

Thirdly, this research reinforces the need to address prevailing gaps in eruption records – which serve as limitations for both stalagmites analysed in this study. Most notably in pre-Holocene records such as DIM-3-A, for whom only two eruptions satisfied all filter criteria/possessed robust dates with < 500-year uncertainties. This is most likely an artefact of poor preservation of smaller events, however even known eruptions are subject to ambiguities. For example, the YTT is one of the most studied eruptions of the Quaternary, yet its absolute date, sulfur yield, and plume dynamics, remain enigmatic (e.g. Costa et al. 2018, 2014; Baldini et al. 2015; Chesner, 2012); further complicating our ability to attribute the eruption to observed climatological oscillations. Eruption record incompleteness also affects analysis of Holocene archives such as NIED08-05, whose growth interval precedes the historical era of volcanic observation by >2000 years. Parameters such as plume height, tephra chemistry, particle morphology, and eruption timing all exert a substantial, independent influence on tephra preservation, so robust detection of transient ash fall relies on volcanological knowledge of ash fall trajectories whereby instrumental/satellite data is unavailable, sourced from tephrochronology and modelling studies.

Despite the aforementioned limitations, there are evident benefits for utilising stalagmites in volcanology. Principally they can achieve similar chronological resolution to ice cores, and so provide a method for precisely constraining the timing and impacts of volcanic eruptions. By refining the techniques and analyses used to detect volcanic signals from complex geochemical datasets obtained from these records, we can gain distal evidence and thus key insights for undiscovered/lesser-known eruptions for which evidence may have degraded or become more difficult to find, and thus the volcano's eruptive history has been hitherto ambiguous (Cook et al. 2018). Such developments are also directly relevant to two other disciplines. The first is paleoclimatology. The high-chronological precision of stalagmite records means that, if volcanic signals are detected, these can act as time-stratigraphic markers for synchronization of marine and

terrestrial archives to better evaluate the environmental impact of volcanic forcing on decadal-to-millennial timescales. In turn, this could supplement our understanding of regional 'leads' and 'lags' in the Earth's climate system (e.g. Berben et al. 2020; Svensson et al. 2020; Timms et al. 2019; Lane et al. 2017), drivers of climate oscillations, global systems of atmospheric circulation and feedbacks, and synchronicity between climate events in the Northern and Southern hemispheres (Svensson et al. 2020, 2013; Sigl et al. 2015). The second discipline is natural hazard assessment. Diversifying the number of archives suitable for paleo-volcanic research will help to not only refine eruption chronologies, but also quantify patterns in volcanic system-specific eruptive tendencies and impacts – highlighting regions whereby volcanic hazards represent a poignant threat. Yet, these hazards are not strictly limited to direct eruption products (e.g. ash fall, gas emission), as climatological perturbation following exceptionally large eruptions may result in catastrophic alterations to ice extent (Zanchettin et al. 2014), sea level (Baldini et al. 2015), and biological cycles (Self & Blake, 2008). Such possibilities prompt consideration of the risk volcanism poses on an intercontinental scale. Continued interrogation of paleoenvironmental archives in contemporary Earth Science can help prepare for when, unescapably, quiescent volcanoes stir, and in turn improve the efficacy of natural hazard management in a rapidly-developing world.

Use of stalagmites in paleo volcanology is an evolving field, and the issues raised in this thesis mainly relate to knowledge gaps and chronological uncertainties – both of which have potential for improvement as new and existing stalagmite chronologies are refined. Future integration of studies investigating stalagmite geochemistry, regional climate, eruption records, and key environmental processes, will help to better deconvolute trace element enrichments caused by volcanic eruptions from karst-specific variabilities, and help to answer prevailing questions such as:

- *To what extent does tephra particle geochemistry influence their entrainment, deposition, and preservation within a karst system?*
- *What are the timescales of ash transfer from surface to stalagmite?*
- *How can we use stalagmites to define the causes of abrupt, volcanically-forced climate change?*

8.0. CONCLUSIONS

- Stalagmites can provide insights into the characteristics and consequences of explosive volcanic eruptions. Records from Belize (Jamieson et al. 2015), Turkey (Badertscher et al. 2014), and Italy (Frisia et al. 2008) present encouraging geochemical evidence for preservation of Holocene ash fall events, and millennial-scale records from Borneo (Carolin et al. 2013), China (Du et al. 2019),

New Mexico (Polyak et al. 2017), and Peru (Cheng et al. 2013) highlight potential for constraint of climatological perturbation resulting from high-magnitude volcanism of the Last Glacial Period.

- This study presents interpretations of two stalagmite trace element datasets grown under spatially and temporally discrete climate regimes, with the aim testing the sensitivity of the stalagmite volcanic archive and ultimately addressing the question: *can stalagmite trace element geochemistry preserve evidence of explosive volcanism?*
- Stalagmite NIED08-05 (Niedźwiedzia Cave, SW Poland) shows discrete REE enrichments with a potential volcanic source, however links between these enrichments and the Holocene eruption record are inconsistent. A constant supply of dripwater combined with a dense forest and soil/debris cover likely obfuscates signal preservation which, coupled with uncertainties relating to the presence of paleo-entrances to the cave, confounds any attempt to differentiate the influence of dry and/or wet volcanic ash deposition on the calcite sequence. For detection of transient ash fall events, shallow stalagmites modulated by seasonally pronounced rainfall may preserve volcanic signatures with greater success that those grown in temperate environments overlain by a thick organic debris horizon and dense vegetative cover.
- The DIM-3-A (Dim Cave, south Turkey) record shows enrichment of trace elements associated with increased bedrock dissolution (e.g. Zn), atmospheric dust flux (e.g. Pb, Th), supersaturation of dripwater (e.g. Mg), and formation of aragonite - evidence for a distinct reduction in karst moisture availability following ~74 ka BP. Indicative of paleo-aridity, the onset occurs in concurrence with the Youngest Toba Tuff super-eruption, Indonesia. It is possible that millennial-scale reorganization of major atmospheric systems in the NH resulting from volcanogenic aerosol injection promoted more arid conditions, explaining the abrupt and sustained (~2 kyr) changes seen in DIM-3-A. Chronological uncertainties coupled with incomplete knowledge of Eastern Mediterranean climate dynamics hinders confident attribution of these changes to volcanic-induced forcing by the YTT. However, the temporal coincidence between significant enrichments of extraneous, aridity-indicative trace elements in the DIM-3-A record, widespread records of drying following ~74 ka BP in the NH, and the largest known eruption of the Quaternary, is certainly worth further study. No geochemical variability is observed following the Los Chocoyos eruption, Guatemala, suggesting this event did not significantly impact East Mediterranean climate.
- Principal Component Analysis is a promising technique for analysis of multi-variate, high-resolution speleothem datasets. However, it appears best utilised as part of a 'forensic' approach – combining analyses of stalagmite geochemistry, regional climate, and key

environmental processes to successfully deconvolute trace element enrichments caused by volcanic eruptions from seasonal climate oscillations and/or local processes. In this study, PCA appears most valuable for identifying correlations between trace elements originating from outside the karst system.

- This study raises key considerations for future use of stalagmites in recording the direct and/or indirect effects of distal volcanism which include cave location, hydrology, chronological control, and constraint of eruption dates/parameters. Nonetheless, continuing to test the limits of discrete stalagmite archives in a volcanological context will ultimately allow construction of robust, low-latitude, and high-resolution tephrochronologies. Integrating these records into regional networks of sedimentary, lacustrine, marine, and archaeological archives, will not only help to improve eruption dating, but also constrain climatic transitions using volcanic events as time-stratigraphic markers.

Appendices

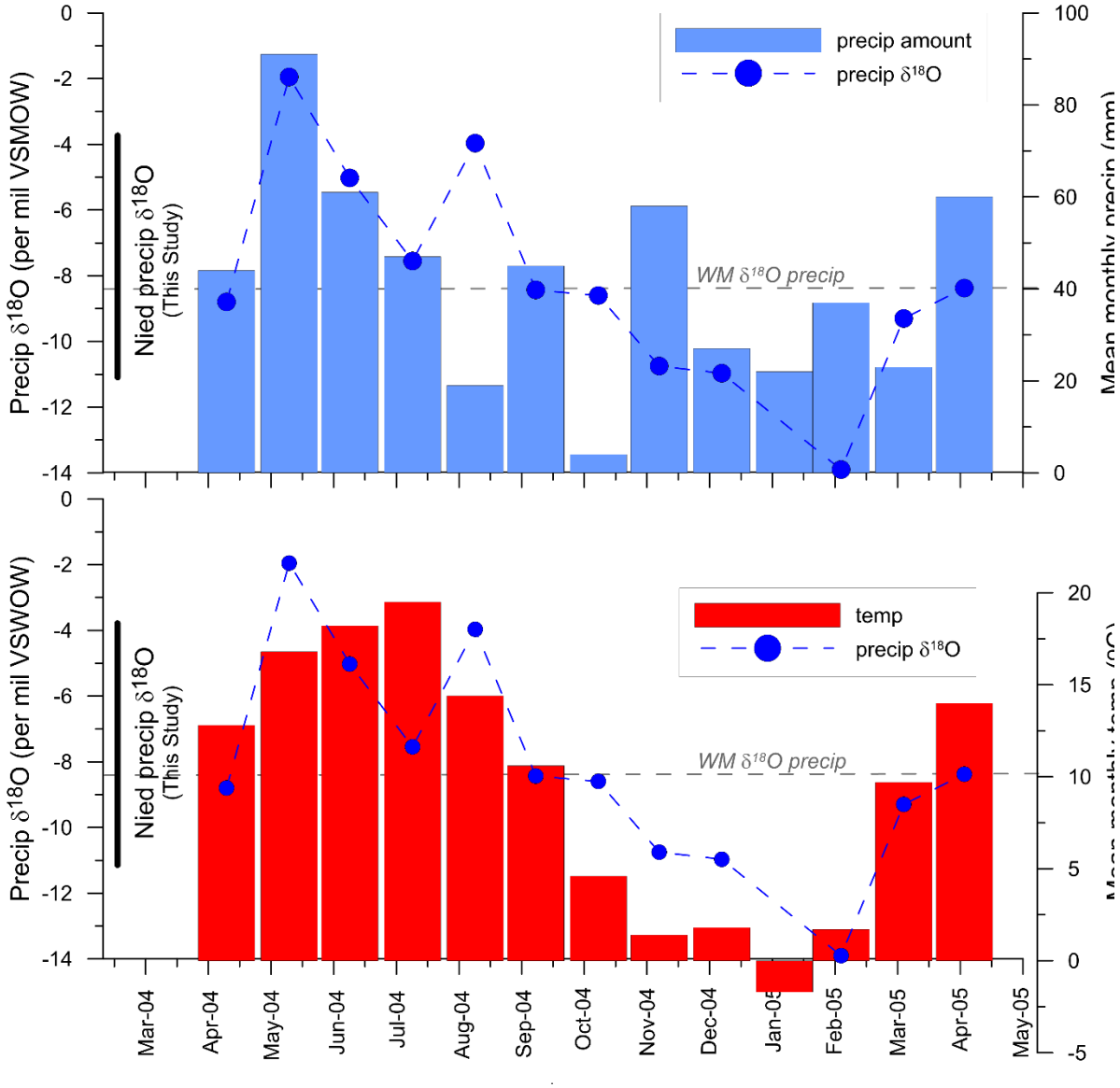

Figure S1: Wrocław mean monthly event precipitation $\delta^{18}O$ values from Gorka et al. (2008) ranged from -1.95 per mil VSMOW in June 2004 to -13.9 per mil VSMOW in March 2005. These data suggest a strong positive temperature effect on precipitation $\delta^{18}O$ in this region of SW Poland ($r^2 = 0.61$; $p < 0.01$) whilst the amount effect is not significant ($r^2 = 0.16$; $p = 0.2$). Precipitation samples collected at Niedźwiedzia cave for the present study ranged from -3.7 and -11.1 per mil VSMOW (black arrows).

Table S1: Further information on stalagmite records utilised in Chapter II, Figures **25** and **27**

CAVE	LOCATION	LATITUDE (N)	LONGITUDE (E)	DATING TECHNIQUE	CHRONOLOGY CALCULATION	REFERENCE
DIM	Turkey	36.3	32.06	U-series	COPRA	Ünal-İmer et al. (2015)
SANBAO	China	31.7	110.4	^{230}Th	COPRA	Wang et al. 2008)
YONGXING	China	31.6	111.2	^{230}Th	*Not stated*	Chen et al. (2016)
YANGKOU	China	29	107.2	U-Th	Oxcal	Du et al. (2019), Zhang et al. (2017)
SECRET	Borneo	4	115	U-Th	Linear interpolation	Carolin et al. (2013)
ROBINSON	USA (New Mexico)	33	-108	U-series	COPRA	Polyak et al. (2017)

References

Abbott, P.M., Griggs, A.J., Bourne, A.J., Davies, S.M., 2018. Tracing marine cryptotephras in the North Atlantic during the last glacial period: Protocols for identification, characterisation and evaluating depositional controls. *Marine Geology* **401**, 81–97. https://doi.org/10.1016/j.margeo.2018.04.008

Abbott, P.M., Davies, S.M., Steffensen, J.P., Pearce, N.J.G., Bigler, M., Johnsen, S.J., Seierstad, I.K., Svensson, A., Wastegård, S., 2012. A detailed framework of Marine Isotope Stages 4 and 5 volcanic events recorded in two Greenland ice-cores. *Quaternary Science Reviews* **36**, 59–77. https://doi.org/10.1016/j.quascirev.2011.05.001

Abdi, H., Williams, L.J., 2010. Principal component analysis. *Wiley Interdisciplinary Reviews: Computational Statistics* **2**, 433–459.

Abers, G. A., Plank, T., Hacker, B.R., 2003. The wet Nicaraguan slab. *Geophysical Research Letters* **30**, 1098.

Adams, N.K., de Silva, S., Self, S., Salas, G., Schubring, S., Permenter, J., Arbesman, K., 2001. The physical volcanology of the 1600 eruption of Huaynaputina, Southern Peru. *Bulletin of Volcanology* **62**, 493–518.

Adams, N.K., Houghton, B.F., Fagents, S.A., Hildreth, W., 2006. The transition from explosive to effusive eruptive regime: The example of the 1912 Novarupta eruption, Alaska. *GSA Bulletin* **118**, 620–634.

Agatemor, C., Beauchemin, D., 2011. Matrix effects in inductively coupled plasma mass spectrometry: A review. *Analytica Chimica Acta* **706**, 66–83.

Agenbroad, L.D., Fairbridge, R.W., 2018. Holocene Epoch.

Ahn, J., Brook, E.J., Buizert, C., 2014. Response of atmospheric CO2 to the abrupt cooling event 8200 years ago. *Geophysical Research Letters* **41**, 604–609.

Aiuppa, A., Burton, M., Caltabiano, T., Giudice, G., Guerrieri, S., Liuzzo, M., Muré, F., Salerno, G., 2010. Unusually large magmatic CO2 gas emissions prior to a basaltic paroxysm. *Geophysical Research Letters* **37**.

Aksoy, E., Panagos, P., Montanarella, L., Jones, A., 2010. Integration of the Soil Database of Turkey, Earth.

Allan, A. S., Morgan, D. J., Wilson, C. J., Millet, M.A., 2013. From mush to eruption in centuries: assembly of the super-sized Oruanui magma body. *Contributions to Minerology and Petrology* **166**, 1–22.

Allan, A. S., Wilson, C. J., Millet, M. A., Wysoczanski, R.J., 2012. The invisible hand: tectonic triggering and modulation of a rhyolitic supereruption. *Geology* **40**, 563–566.

Allan, A.S.R., Barker, S.J., Millet, M.A., Morgan, D.J., Rooyakkers, S.M., Schipper, C.I., Wilson, C.J.N., 2017. A cascade of magmatic events during the assembly and eruption of a super-sized magma body. *Contributions to Mineralogy and Petrology* **172**, 1–34. https://doi.org/10.1007/s00410-017-1367-8

Allen, J.R.M., Forrest, M., Hickler, T., Singarayer, J.S., Valdes, P.J., Huntley, B., 2020. Global vegetation patterns of the past 140,000 years. *Journal of Biogeography* 1–18. https://doi.org/10.1111/jbi.13930

Allen, J.R.M., Huntley, B., 2009. Last Interglacial palaeovegetation, palaeoenvironments and chronology: a new record from Lago Grande di Monticchio, southern Italy. *Quaternary Science Reviews* **28**, 1521–1538. https://doi.org/10.1016/j.quascirev.2009.02.013

Alley, R.B., 2000. Ice-core evidence of abrupt climate changes. *Proceedings of the National Academy of Sciences of the United States of America* **97**, 1331–1334. https://doi.org/10.1073/pnas.97.4.1331

Alley, R.B., Mayewski, P.A., Sowers, T., Stuiver, M., Taylor, K.C., Clark, P.U., 1997. Holocene climatic instability: a prominent, widespread event 8200 yr ago. *Geology* **25**, 483–486.

Alley, R.B., Ágústsdóttir, A.M., 2005. The 8k event: Cause and consequences of a major Holocene abrupt climate change. *Quaternary Science Reviews* **24**, 1123–1149. https://doi.org/10.1016/j.quascirev.2004.12.004

Alvarez-Solas, J., 2014. On the triggering mechanism of Heinrich events. *Proceedings of the National Academy of Sciences* **108**, E1359–E1360. https://doi.org/10.1073/pnas.1116575108

Alvarez-Solas, J., Montoya, M., Ritz, C., Ramstein, G., Charbit, S., Dumas, C., Nisancioglu, K., Dokken, T., Ganopolski, A., 2011. Heinrich event 1: an example of dynamical ice-sheet reaction to oceanic changes. *Climate of the Past* **7**, 1297–1306.

Álvarez-Solas, J., Ramstein, G., 2011. On the Triggering Mechanism of Heinrich Events. *Proceedings of the National Academy of Sciences USA* **108**, E1359–E1360.

Alvarez-Solas, J., Robinson, A., Montoya, M., Ritz, C., 2013. Iceberg discharges of the last glacial period driven by oceanic circulation changes. *Proceedings of the National Academy of Sciences* **110**, 16350–16354.

Ambrose, S.H., 1998. Late Pleistocene human population bottlenecks, volcanic winter, and differentiation of modern humans. *Journal of Human Evolution* **34**, 623–651.

Andersen, K.K., Azuma, N., Barnola, J.-M., Bigler, M., Biscaye, P., Caillon, N., Chappellaz, J., Clausen, N.B., Dahl-Jensen, D., Fischer, H., Fluckiger, J., Fritzsche, D., Fujii, Y., Goto-Azuma, K. Grønvold, K., Gundestrup, N. S., Hansson, M., Huber, C., A., , M. Leuenberger4, R. Lorrain11, V.M.-D., Miller7, H., Motoyama8, H., Narita12, H., Popp13, T., Rasmussen1, S.O., Raynaud3, D., , R. Rothlisberger4, U. Ruth7, D.S., , J. Schwander4, H.S., M.-L. Siggard-Andersen1, J. P. Steffensen1, T. Stocker4, A.E.S. ttir15, Svensson1, A., , M. Takata2, J.-L.T., Thorsteinsson16, T., Watanabe8, O., White13, F.W.& J.W.C., 2004. High-resolution record of Northern Hemisphere climate extending into the last interglacial period. *Nature* **431**, 147–151.

Andrews, B.J., Dufek, J., Ponomareva, V., 2018. Eruption dynamics and explosive-effusive transitions during the 1400 cal BP of Opala volcano Kamchatka, Russia. *Journal of Volcanology and Geothermal Research* **356**, 316–330.

Andrews, B.J., Gardner, J.E., Housh, T.B., 2008. Repeated recharge, assimilation, and hybridization in magmas erupted from El Chichón as recorded by plagioclase and amphibole phenocrysts. *Journal of Volcanology and Geothermal Research* **175**, 415–426.

Andrews, J.T., Voelker, A.H.L., 2018. "Heinrich events" (& sediments): A history of terminology and recommendations for future usage. *Quaternary Science Reviews* **187**, 31–40. https://doi.org/10.1016/j.quascirev.2018.03.017

Anselmetti, F.S., Hodell, D.A., Ariztegui, D., Brenner, M., Rosenmeier, M.F., 2007. Quantification of soil erosion rates related to ancient Maya deforestation. *Geology* **35**, 915–918.

Aragón, M., 2013. When day turned to night: The eruption of the Santa María volcano of 1902.

Armstrong, W.H., Anderson, R.S., Allen, J., Rajaram, H., 2016. Modeling the WorldView-derived seasonal velocity evolution of Kennicott Glacier, Alaska. *Journal of Glaciology* **62**, 763–777.

Arnalds, O., 2013. The influence of Volcanic Tephra (Ash) on ecosystems, in: Sparks, D. (Ed.), Advance in Agronomy. Elsevier, San Diego, pp. 331–380.

Asmerom, Y., Polyak, V.J., Burns, S.J., 2010. Variable winter moisture in the southwestern United States linked to rapid glacial climate shifts. *Nature Geoscience* **3**, 114–117. https://doi.org/10.1038/ngeo754

Aspinall, W., Woo, G., 2019. Counterfactual Analysis of Runaway Volcanic Explosions. *Frontiers in Earth Science* **7**, 1–15. https://doi.org/10.3389/feart.2019.00222

Atwood, A.R., Donohoe, A., Battisti, D.S., Liu, X., Pausata, F.S.R., 2020. Robust longitudinally-variable responses of the ITCZ to a myriad of climate forcings. *ESSOAR Preprint. Submitted to GRL.* 1–13. https://doi.org/https://doi.org/10.1002/essoar.10503115.1

Aydar, E., 1998. Early Miocene to Quaternary evolution of volcanism and the basin formation in western Anatolia: a review. *Journal of Volcanology and Geothermal Research* **85**, 69–82. https://doi.org/10.1016/S0377-0273(98)00050-X

Aydar, E., Gourgaud, A., 1998. The geology of Mount Hasan stratovolcano, central Anatolia, Turkey. *Journal of Volcanology and Geothermal Research* **85**, 129–152. https://doi.org/10.1016/S0377-0273(98)00053-5

Aydar, E., Schmitt, A.K., Çubukçu, H.E., Akin, L., Ersoy, O., Sen, E., Duncan, R.A., Atici, G., 2012. Correlation of ignimbrites in the central Anatolian volcanic province using zircon and plagioclase ages and zircon compositions. *Journal of Volcanology and Geothermal Research* **213**–**214**, 83–97. https://doi.org/10.1016/j.jvolgeores.2011.11.005

Baca, M., Mackiewicz, P., Stankovic, A., Popović, D., Stefaniak, K., Czarnogórska, K., Nadachowski, A., Gasiorowski, M., Hercman, H., Weglenski, P., 2014. Ancient DNA and dating of cave bear remains from Niedźwiedzia Cave suggest early appearance of Ursus ingressus in Sudetes. *Quaternary International* **339**–**340**, 217–223. https://doi.org/10.1016/j.quaint.2013.08.033

Bachmann, O., Bergantz, G.W., 2008. Rhyolites and their source mushes across tectonic settings. *Journal of Petrology* **49**, 2277–2285.

Bachmann, O., Huber, C., 2016. Silicic magma reservoirs in the Earth's crust. *American Mineralogist* **101**, 2377–2404.

Bacon, C.R., Lanphere, M.A., 2006. Eruptive history and geochronology of Mount Mazama and the Crater Lake region, Oregon. *Geological Society of America Bulletin* **118**, 1331–1359.

Badertscher, S., Borsato, A., Frisia, S., Cheng, H., Edwards, R.L., Tüysüz, O., Fleitmann, D., 2014. Speleothems as sensitive recorders of volcanic eruptions - the Bronze Age Minoan eruption recorded in a stalagmite from Turkey. *Earth and Planetary Science Letters* **392**, 58–66. https://doi.org/10.1016/j.epsl.2014.01.041

Badertscher, S., Borsato, A., Frisia, S., Cheng, H., Edwards, R.L., Tüysüz, O., Fleitmann, D., 2014. Speleothems as sensitive recorders of volcanic eruptions - the Bronze Age Minoan eruption recorded in a stalagmite from Turkey. *Earth and Planetary Science Letters* **392**, 58–66. https://doi.org/10.1016/j.epsl.2014.01.041

Baldini, J.U.L., 2010. Cave atmosphere controls on stalagmite growth rate and paleoclimate records. Geological Society of London Special Publication, London.

Baldini, J.U.L., 2010. Cave atmosphere controls on stalagmite growth rate and paleoclimate records, in: Pedley, H.M., Rgerson, M. (Ed.), Tufas and Speleothems: Unravelling the Microbial and Physical Controls. Geological Society of London Special Publication, London, London, pp. 282–294.

Baldini, J.U.L., Lechleitner, F. A., Breitenbach, S. F. M., van Hunen, J., Baldini, L. M., Wynn, P, M., Jamieson, R. A., Ridley, H. E., Baker, A. J., Walczak, I. W., Fohlmeister, J., *in press*. Detecting and quantifying palaeoseaonality in stalagmites using geochemical and modelling approaches. *Quaternary Science Reviews*

Baldini, J.U.L., McDermott, F., Fairchild, I.J., 2006. Spatial variability in cave dripwater hydrochemistry: implications for stalagmite paleoclimate records. *Chemical Geology* **235**, 290–304.

Baldini, J.U.L., Brown, R.J., Mawdsley, N., 2018. Evaluating the link between the sulfur-rich Laacher See volcanic eruption and the Younger Dryas climate anomaly. *Climate of the Past* **14**, 969–990. https://doi.org/10.5194/cp-14-969-2018

Baldini, J.U.L., Brown, R.J., McElwaine, J.N., 2015. Was millennial scale climate change during the Last Glacial triggered by explosive volcanism? *Scientific Reports* **5**, 1–9. https://doi.org/10.1038/srep17442

Baldini, L.M., Baldini, J.U.L., McDermott, F., Arias, P., Cueto, M., Fairchild, I.J., Hoffmann, D.L., Mattey, D.P., Müller, W., Nita, D.C., Ontañón, R., Garciá-Moncó, C., Richards, D.A., 2019. North Iberian temperature and rainfall seasonality over the Younger Dryas and Holocene. *Quaternary Science Reviews* **226**, 1–22.

Baldini, L.M., McDermott, F., Baldini, J.U.L., Arias, P., Cueto, M., Fairchild, I.J., Hoffman, D.L., Mattey, D.P., Müller, W., Nita, D.C., Ontañón, R., Garciá-Moncó, C., Richards, D.A., 2015. Regional temperature, atmospheric circulation, and sea-ice variability within the Younger Dryas Event constrained using a speleothem from northern Iberia. *Earth & Planetary Science Letters* **419**, 101–110.

Baldini, L.M., McDermott, F., Foley, A.M., Baldini, J.U.L., 2008. Spatial variability in the European winter precipitation d18O-NAO relationship: Implications for reconstructing NAO-mode climate variability in the Holocene. *Geophysical Research Letters* **35**, L04709.

Ballantyne, C.K., 2013. Paraglacial Geomorphology. *Encyclopedia of Quaternary Science: Second Edition* **21**, 553–565. https://doi.org/10.1016/B978-0-444-53643-3.00089-3

Baltacı, H., Akkoyunlu, B.O., Tayanç, M., 2017. Relationships between teleconnection patterns and Turkish climatic extremes. *Theoretical and Applied Climatology* **134**, 1365–1386. https://doi.org/10.1007/s00704-017-2350-z

Band, S., Yadava, M.G., Ahmad Lone, M., Shen, C.C., Sreee, L., Ramesh, R., 2018. High-resolution mid-Holocene Indian Summer Monsoon recorded in a stalagmite from the Kotumsar Cave, Central India. *Quaternary International* **479**, 19–24.

Barbante, C., Kehrwald, N.M., Marianelli, P., Vinther, B.M., Steffensen, J.P., Cozzi, G., Hammer, C.U., Clausen, H.B., Siggaard-Andersen, M.L., 2013. Greenland ice core evidence of the 79 AD Vesuvius eruption. *Climate of the Past* **9**, 1221–1232.

Barber, A.J., Crow, M.J., Milsom, J.S., 2005. Introduction and previous work, in: Barber, A.J., Crow, M.J., Milsom, J.S. (Ed.), Sumatra: Geology, Resources and Tectonic Evolution. Geological Society Memoirs, pp. 1–7.

Barber, K., Langdon, P., Blundell, A., 2008. Dating the Glen Garry tephra: a widespread late-Holocene marker horizon in the peatlands of northern Britain. *The Holocene* **18**, 31–43.

Barboni, M., Boehnke, P., Schmitt, A. K., Harrison, T. M., Shane, P., Bouvier, A.-S., Baumgartner, L., 2016. Warm storage for arc magmas. *Proceedings of the National Academy of Sciences USA* **113**, 13959–13964.

Barckhausen, U., Ranero, C. R., von Huene, R., Cande, S., & Roeser, H., 2001. Revised tectonic boundaries in the Cocos Plate off Costa Rica: Implications for the segmentation of the convergent margin and for plate tectonic models. *Journal of Geophysical Research* **106**, 207–220.

Barker, S. J., Wilson, C. J. N., Allan, A. S. R., Schipper, C.I., 2015. Fine-scale temporal recovery, reconstruction and evolution of a post-supereruption magmatic system. *Contributions to Mineralogy and Petrology* **170**, 1–40.

Barker, S.J., Van Eaton, A.R., Mastin, L.G., Wilson, C.J.N., Thompson, M.A., Wilson, T.M., Davis, C., Renwick, J.A., 2019. Modeling Ash Dispersal from Future Eruptions of Taupo Supervolcano. *Geochemistry, Geophysics, Geosystems* **20**, 3375–3401. https://doi.org/10.1029/2018GC008152

Barker, S., Chen, J., Gong, X., Jonkers, L., Knorr, G., Thronalley, D., 2015. Icebergs not the trigger for North Atlantic cold events. *Nature* **520**, 333–336. https://doi.org/10.1038/nature14330

Barker, S., Knorr, G., Conn, S., Lordsmith, S., Newman, D., Thornalley, D., 2019. Early Interglacial Legacy of Deglacial Climate Instability. *Paleoceanography and Paleoclimatology* **34**, 1455–1475. https://doi.org/10.1029/2019PA003661

Bar-Matthews, M., Ayalon, A., Gilmour, M., Matthews, A., Hawkesworth, C.J., 2003. Sea - land oxygen isotopic relationships from planktonic foraminifera and speleothems in the Eastern Mediterranean region and their implication for paleorainfall during interglacial intervals. *Geochimica et Cosmochimica Acta* **67**, 3181–3199. https://doi.org/10.1016/S0016-7037(02)01031-1

Barnes, E., Solomon, S., Polvani, L., 2016. Robust wind and precipitation responses to the Mount Pinatubo eruption, as simulated in the CMIP5 models. *Journal of Climate* **29**, 4763–4778.

Barr, I.D., Solomina, O., 2014. Pleistocene and Holocene glacier fluctuations upon the Kamchatka Peninsula. *Global and Planetary Change* **113**, 110–120.

Bartholomaus, T.C., Anderson, R.S., Anderson, S.P., 2008. Response of glacier basal motion to transient water storage. *Nature Geoscience* **1**, 33–37.

Bassis, J.N., Sierra, V., 2017. Heinrich events triggered by ocean forcing and modulated by isostatic adjustment. *Nature* **542**, 332–334. https://doi.org/10.1038/nature21069

Batchelor, C.L., Margold, M., Krapp, M., Murton, D.K., Dalton, A.S., Gibbard, P.L., Stokes, C.R., Murton, J.B., Manica, A., 2019. The configuration of Northern Hemisphere ice sheets through the Quaternary. *Nature Communications* **10**, 1–10. https://doi.org/10.1038/s41467-019-11601-2

Baykara, M.O., 2014. Güneybatı Anadolu'da mağara çökellerinin incelenmesi ve paleoiklimsel değerlendirmeleri. Pamukkale University.

Bazanova, L.I., Melekestev, I.V., Ponomareva, V.V., Dirksen, O.V., Dirksen, V.G., 2016. Late Pleistocene and Holocene Volcanic Catastrophes in Kamchatka and in the Kuril Islands. Part 1. Types and Classes of Catastrophic Eruptions as the Leading Components of Volcanic Catastrophism. *Journal of Volcanology and Seismology* **10**, 3–21.

Berben, S.M.P., Dokken, T.M., Abbott, P.M., Cook, E., Sadatzki, H., Simon, M.H., Jansen, E., 2020. Independent tephrochronological evidence for rapid and synchronous oceanic and atmospheric temperature rises over the Greenland stadial-interstadial transitions between ca. 32 and 40 ka b2k. *Quaternary Science Reviews* **236**, 106277. https://doi.org/10.1016/j.quascirev.2020.106277

Berger, A., Loutre, M.F., 1991. Insolation values for the climate of the last 10 million years. *Quaternary Science Reviews* **10**, 297–317. https://doi.org/10.1016/0277-3791(91)90033-Q

Berkelhammer, M., Sinha, A., Stott, L., Cheng, H., Pausata, F., Yoshimura, K., 2012. An abrupt shift in the Indian Monsoon 4,000 years ago, in: Giosan, L. (Ed.), Climates, Landscapes, and Civilizations: American Geophysical Union Geophysical Monograph. pp. 75–87.

Bertagnini, A., Landi, P., Rosi, M., Vigliargio, A., 1998. The Pomici di Base plinian eruption of Somma-Vesuvius. *Journal of Volcanology and Geothermal Research* **83**, 219–239.

Bieroński, J., Stefaniak, K., Hercman, H., Socha, P., Nadachowski, A., 2009. Palaeogeographic and palaeoecological analysis of sediments of the Niedźwiedzia Cave in Kletno, in: Stefaniak K., Tyc A., S.P. (Ed.), Karst of the Częstochowa Upland and of the Eastern. Studies of the Faculty of Earth Sciences University of Silesia, pp. 401–422.

Bigg, G.R., Levine, R.C., Clark, C.D., Greenwood, S.L., Haflidason, H., Hughes, A.L.C., Nygard, A., Sejrup, H.P., 2010. Last glacial ice-rafted debris off southwestern Europe: the role of the British-Irish Ice Sheet. *Journal of Quaternary Science* **25**, 689–699.

Biggs, J., Pritchard, M.E., 2017. Global volcano monitoring: What does it mean when volcanoes deform? *Elements* **13**, 17–22.

Bindeman, I. N., Eiler, J. M., Wing, B. A., Farquhar, J., 2007. Rare sulfur and triple oxygen isotope geochemistry of volcanogenic sulfate aerosols. *Geochimica et Cosmochimica Acta* **71**, 2326–2343.

Bini, M., Zanchetta, G., Perşoiu, A., Cartier, R., Català, A., Cacho, I., Dean, J.R., Di Rita, F., Drysdale, R.N., Finnè, M., Isola, I., Jalali, B., Lirer, F., Magri, D., Masi, A., Marks, L., Mercuri, A.M., Peyron, O., Sadori, L., Sicre, M.A., Welc, F., Zielhofer, C., Brisset, E., 2019. The 4.2 ka BP Event in the Mediterranean region: An overview. *Climate of the Past* **15**, 555–577. https://doi.org/10.5194/cp-15-555-2019

Bintanja, R., van de Wal, R.S.W., 2008. North American ice-sheet dynamics and the onset of 100,000-year glacial cycles. *Nature* **454**, 869–872.

Birtchnell, T., Büscher, M., 2011. Stranded: An Eruption of Disruption. *Mobilities* **6**, 1–9.

Blackford, J.J., Payne, R.J., Heggen, M.P., de la Riva Caballero, A., van der Plicht, J., 2014. Age and impacts of the caldera-forming Aniakchak II eruption in western Alaska. *Quaternary Research (United States)* **82**, 85–95. https://doi.org/10.1016/j.yqres.2014.04.013

Blockley, S.P.E., Bronk Ramsey, C., Pyle, D.M., 2008. Improved age modelling and high- precision age estimates of late Quaternary tephras, for accurate paleoclimate reconstruction. *Journal of Volcanology and Geothermal Research* **177**, 251–262.

Blockley, S.P.E., Lane, C.S., Hardiman, M., Rasmussen, S., Seierstad, I., Steffensen, J., Svensson, A., Lotter, A., Turney, C., Ramsey, C., 2012. Synchronisation of palaeoenvironmental records over the last 60,000 years, and an extended INTIMATE event stratigraphy to 48,000 b2k. *Quaternary Science Reviews* **36**, 2–10.

Bolge, L.L., Carr, M.J., Milidakis, K.I., Lindsay, F.N., Feigenson, M.D., 2009. Correlating geochemistry, tectonics, and volcanic volume along the Central American volcanic front. *Geochemistry, Geophysics, Geosystems* **10**. https://doi.org/10.1029/2009GC002704

Bonadonna, C., Costa, A., 2013. Plume height, volume, and classification of explosive volcanic eruptions based on the Weibull function. *Bulletin of Volcanology* **75**, 742.

Bonadonna, C., Costa, A., 2012. Estimating the volume of tephra deposits: a new simple strategy. *Geology* **40**, 415–418.

Bonadonna, C., Houghton, B.F., 2005. Total grain-size distribution and volume of tephra-fall deposits. *Bulletin of Volcanology* **67**, 441–456.

Bonatotzky, T., Ottner, F., Erlendsson, E., Gísladóttir, G., 2019. The weathering of volcanic tephra and how they impact histosol development. An example from South East Iceland. *Catena* **172**, 634–646. https://doi.org/10.1016/j.catena.2018.09.022

Bond, G., Showers, W., Cheseby, M., Lotti, R., Almasi, P., de Menocal, P., Priore, P., Cullen, H., Hajdas, I., Bonani, G., 1997. A pervasive millennial-scale cycle in the North Atlantic Holocene and glacial climates. *Science* **294**, 2130–2136.

Bond, G., Broecker, W., Johnsen, S., McManus, J., Labeyrie, L., Jouzel, J., Bonanl, G., 1993. Correlations between climate records from North Atlantic sediments and Greenland ice. *Nature* **365**, 143–147.

Borsato, A., Frisia, S., Fairchild, I.J., Somogyi, A., Susini, J., 2007. Trace element distribution in annual stalagmite laminae mapped by micrometer-resolution X-ray fluorescence: Implications for incorporation of environmentally significant species. *Geochimica et Cosmochimica Acta* **71**, 1494–1512. https://doi.org/10.1016/j.gca.2006.12.016

Bosmans, J.H.C., Drijfhout, S.S., Tuenter, E., Hilgen, F.J., Lourens, L.J., Rohling, E.J., 2015. Precession and obliquity forcing of the freshwater budget over the Mediterranean. *Quaternary Science Reviews* **123**, 16–30. https://doi.org/10.1016/j.quascirev.2015.06.008

Boucher, O., D. Randall, P. Artaxo, C. Bretherton, G., Feingold, P. Forster, V.-M. Kerminen, Y. Kondo, H. Liao, U., Lohmann, P. Rasch, S.K. Satheesh, S. Sherwood, B.S., Zhang, and X.Y., 2013. Clouds and Aerosols, in: Stocker, T.F., D. Qin, G.-K. Plattner, M. Tignor, S.K. Allen, J. Boschung, A., Nauels, Y. Xia, V.B. and P.M.M. (Eds.), Climate Change 2013: The Physical Science Basis. Contribution of Working Group I to the Fifth Assessment Report of the Intergovernmental Panel on Climate Change. Cambridge University Press, Cambridge.

Boulton, G. S., Dobbie, K. E., Zatsepin, S., 2001. Sediment deformation beneath glaciers and its coupling to the subglacial hydraulic system. *Quaternary International* **86**, 3–28.

Bourdin, C., Douville, E., Genty, D., 2011. Alkaline-earth metal and rare-earth element incorporation control by ionic radius and growth rate on a stalagmite from the Chauvet Cave, Southeastern France. *Chemical Geology* **290**, 1–11. https://doi.org/10.1016/j.chemgeo.2011.08.006

Bourne, A.J., Cook, E., Abbott, P.M., Seierstad, I.K., Steffensen, J.P., Svensson, A., Fischer, H., Schüpbach, S., Davies, S.M., 2015. A tephra lattice for Greenland and a reconstruction of volcanic events spanning 25 - 45 ka b2k. *Quaternary Science Reviews* **118**, 122–141. https://doi.org/10.1016/j.quascirev.2014.07.017

Bourne, A.J., Davies, S.M., Abbott, P.M., Rasmussen, S.O., Steffensen, J.P., Svensson, A., 2013. Revisiting the Faroe Marine Ash Zone III in two Greenland ice cores: implications for marine-ice correlations. *Journal of Quaternary Science* **28**, 641–646.

Bouvet de Maisonneuve, C., Bergal-Kuvikas, O., 2020. Timing, magnitude and geochemistry of major Southeast Asian volcanic eruptions: identifying tephrochronologic markers. *Journal of Quaternary Science* **35**, 272–287.

Bowles, F.A., Jack, R.N., Carmichael, I.S.E., 1973. Investigation of deep-sea volcanic ash layers from equatorial Pacific cores. *GSA Bulletin* **84**, 2371–2388.

Bozkaya, Ö., Yalçın, H., 2004. New mineralogic data and implications for the tectonometamorphic evolution of the Alanya Nappes, Central Tauride Belt, Turkey. *International Geology Review* **46**, 347–365.

Bradley, R.S., Bakke, J., 2019. Is there evidence for a 4.2 ka BP event in the northern North Atlantic region? *Climate of the Past* **15**, 1665–1676. https://doi.org/10.5194/cp-15-1665-2019

Braitseva, O.A., Melekestsev, I.V., Ponomareva, V.V., Kirianov, V.Y., 1996. The caldera-forming eruption of Ksudach volcano about cal. A.D. 240: The greatest explosive event of our era in Kamchatka, Russia. *Journal of Volcanology and Geothermal Research* **70**, 49–65.

Braitseva, O.A., Sulerzhitsky, L.D., Litasova, S.N., Melekestsev, I.V., Ponomareva, V.V., 1993. Radiocarbon dating and tephrochronology in Kamchatka. *Radiocarbon* **35**, 463–476.

Branney, M., Acocella, V., 2015. Calderas, in: Sigurdsson, H. (Ed.), Encyclopaedia of Volcanoes. Academic Press.

Brauer, A., Allen, J.R.M., Mingram, J., Dulski, P., Wulf, S., Huntley, B., 2007. Evidence for last interglacial chronology and environmental change from Southern Europe. *Proceedings of the National Academy of Sciences of the United States of America* **104**, 450–455. https://doi.org/10.1073/pnas.0603321104

Breitenbach, S.F.M., Rehfeld, K., Goswami, B., Baldini, J.U.L., Ridley, H.E., Kennett, D.J., Prufer, K.M., Aquino, V. V., Asmerom, Y., Polyak, V.J., Cheng, H., Kurths, J., Marwan, N., 2012. Constructing proxy records from age models (COPRA). *Climate of the Past* **8**, 1765–1779. https://doi.org/10.5194/cp-8-1765-2012

Brenna, H., Kutterolf, S., Krüger, K., 2019. Global ozone depletion and increase of UV radiation caused by pre-industrial tropical volcanic eruptions. *Scientific Reports* **9**, 1–14. https://doi.org/10.1038/s41598-019-45630-0

Brenna, H., Kutterolf, S., Mills, M.J., Krüger, K., 2020. The potential impacts of a sulfur- And halogen-rich supereruption such as Los Chocoyos on the atmosphere and climate. *Atmospheric Chemistry and Physics* **20**, 6521–6539. https://doi.org/10.5194/acp-20-6521-2020

Briffa, K.R., Jones, P.D., Osborn, T.J., 1998. Influence of volcanic eruptions on Northern Hemisphere summer temperature over the past 600 years. *Nature* **393**, 2–7.

Briffa, K.R., Osborn, T.J., Schweingruber, F.H., Harris, I.C., Jones, P.D., Shiyatov, S.G. and Vaganov, F.A., 2001. Low frequency temperature variations from a northern tree-ring density network. *Journal of Geophysical Research* **106D**, 2929–2941.

Broecker, W.S., 2004. The Role of the Ocean in Climate Yesterday, Today and Tomorrow. Eldigio Press, New York.

Broecker, W. S., Bond, G., Klas, M., Bonani, G., Wolfli, W., 1990. A salt oscillator in the glacial Atlantic? 1. The concept. *Paleoceanography* **5**, 469–477.

Broecker, W. S., Denton, G. H., Edwards, R. L., Cheng, H., A., R. B., Putnam, A.E., 2010. Putting the Younger Dryas cold event into context. *Quaternary Science Reviews* **29**, 1078–1081.

Broecker, W., Bond, G., McManus, J., 1994. Heinrich events: Triggers of ocean circulation change?, in: Peltier, W.R. (Ed.), Ice in the Climate System. Springer-Verlag, New York, pp. 161–166.

Bronk Ramsey, C., Albert, P.G., Blockley, S.P.E., Hardiman, M., Housley, R.A., Lane, C.S., Lee, S., Matthews, I.P., Smith, V.C., Lowe, J.J., 2015. Improved age estimates for key Late Quaternary European tephra horizons in the RESET lattice. *Quaternary Science Reviews* **118**, 18–32. https://doi.org/10.1016/j.quascirev.2014.11.007

Brown, R.J., Thordarson, T., Self, S., Blake, S., 2015. Disruption of tephra fall deposits caused by lava flows during basaltic eruptions. *Bulletin of Volcanology* **77**. https://doi.org/10.1007/s00445-015-0974-3

Brown, R.J., Andrews, G.D.M., 2015. Deposits of Pyroclastic Density Currents, in: Sigurdsson, H. (Ed.), Encyclopaedia of Volcanoes. Academic Press.

Brown, R.J., Bonadonna, C., Durant, A.J., 2012. A review of volcanic ash aggregation. *Physics & Chemistry of the Earth* **45**–**46**, 65–78.

Brown, S.K., Jenkins, S.F., Sparks, R.S.J., Odbert, H., Auker, M.R., 2017. Volcanic fatalities database: analysis of volcanic threat with distance and victim classification. *Journal of Applied Volcanology* **6**. https://doi.org/10.1186/s13617-017-0067-4

Brown, S.K., Crosweller, H.S., Sparks, R.S.J., Cottrell, E., Deligne, N.I., Guerrero, N.O., Hobbs, L., Kiyosugi, K., Loughlin, S.C., Siebert, L., Takarada, S., 2014. Characterisation of the Quaternary eruption record: Analysis of the Large Magnitude Explosive Volcanic Eruptions (LaMEVE) database. *Journal of Applied Volcanology* **3**, 1–22. https://doi.org/10.1186/2191-5040-3-5

Bryan, R.B., 2000. Soil erodibility and processes of water erosion on hillslope. *Geomorphology* **32**, 385–415.

Bryan, S.E., Peate, I.U., Peate, D.W., Self, S., Jerram, D.A., Mawby, M.R., Marsh, J.S.G., Miller, J.A., 2010. The largest volcanic eruptions on Earth. *Earth-Science Reviews* **102**, 207–229. https://doi.org/10.1016/j.earscirev.2010.07.001

Bryś, K., Bryś, T., 2010. Reconstruction of the 217-Year (1791 – 2007) Wrocław Air Temperature 121–171.

Buckland, H.M., Cashman, K. V., Engwell, S.L., Rust, A.C., 2020. Sources of uncertainty in the Mazama isopachs and the implications for interpreting distal tephra deposits from large magnitude eruptions. *Bulletin of Volcanology* **82**. https://doi.org/10.1007/s00445-020-1362-1

Buckley, M.W., Marshall, J., 2016. Observations, inferences, and mechanisms of the Atlantic Meridional Overturning Circulation: A review. *Reviews of Geophysics* **54**, 5–63. https://doi.org/10.1002/2015RG000493.Received

Budner, D., Cole-Dai, J., 2003. The number and magnitude of large explosive volcanic eruptions between 904 and 1865 A.D: Quantitative evidence from a new South Pole ice core. *Geophysical Monograph* **139**, 165–176.

Budsky, A., Wassenburg, J.A., Mertz-Kraus, R., Spötl, C., Jochum, K.P., Gibert, L., Scholz, D., 2019. Western Mediterranean Climate Response to Dansgaard/Oeschger Events: New Insights from Speleothem Records. *Geophysical Research Letters* **46**, 9042–9053. https://doi.org/10.1029/2019GL084009

Bühring, C., Sarnthein, M., 2000. Toba ash layers in the South China Sea: Evidence of contrasting wind directions during eruption ca. 74 ka. *Geology* **28**, 275–278.

Buizert, C., Adrian, B., Ahn, J., Albert, M., Alley, R.B., Baggenstos, D., Bauska, T.K., Bay, R.C., Bencivengo, B.B., Bentley, C.R., Brook, E.J., Chellman, N.J., Clow, G.D., Cole-Dai, J., Conway, H., Cravens, E., Cuffey, K.M., Dunbar, N.W., Edwards, J.S., Fegyveresi, J.M., Ferris, D.G., Fitzpatrick, J.J., Fudge, T.J., Gibson, C.J., Gkinis, V., Goetz, J.J., Gregory, S., Hargreaves, G.M., Iverson, N., Johnson, J.A., Jones, T.R., Kalk, M.L., Kippenhan, M.J., Koffman, B.G., Kreutz, K., Kuhl, T.W., Lebar, D.A., Lee, J.E., Marcott, S.A., Markle, B.R., Maselli, O.J., McConnell, J.R., McGwire, K.C., Mitchell, L.E., Mortensen, N.B., Neff, P.D., Nishiizumi, K., Nunn, R.M., Orsi, A.J., Pasteris, D.R., Pedro, J.B., Pettit, E.C., Price, P.B., Priscu, J.C., Rhodes, R.H., Rosen, J.L., Schauer, A.J., Schoenemann, S.W., Sendelbach, P.J., Severinghaus, J.P., Shturmakov, A.J., Sigl, M., Slawny, K.R., Souney, J.M., Sowers, T.A., Spencer, M.K., Steig, E.J., Taylor, K.C., Twickler, M.S., Vaughn, B.H., Voigt, D.E., Waddington, E.D., Welten, K.C., Wendricks, A.W., White, J.W.C., Winstrup, M., Wong, G.J., Woodruff, T.E., 2015. Precise interpolar phasing of abrupt climate change during the last ice age. *Nature* **520**, 661–665. https://doi.org/10.1038/nature14401

Büntgen, U., Myglan, V.S., Ljungqvist, F.C., McCormick, M., Cosmo, N. Di, Sigl, M., Jungclaus, J., Wagner, S., Krusic, P.J., Esper, J., Kaplan, J.O., Vaan, M.A.C. De, Luterbacher, J., Wacker, L., Tegel, W., 2016. Cooling and societal change during the Late Antique Little Ice Age from 536 to around 660 AD. *Nature Geoscience* **9**, 231–236. https://doi.org/10.1038/NGEO2652

Burden, R.E., Chen, L., Phillips, J.C., 2013. A statistical method for determining the volume of volcanic fall deposits. *Bulletin of Volcanology* **75**, 707.

Burgisser, A., 2005. Physical volcanology of the 2,050 BP caldera-forming eruption of Okmok volcano, Alaska. *Bulletin of Volcanology* **67**, 497–525.

Burns, S.J., Fleitmann, D., Matter, A., Kramers, J., Al-subbary, A.A., Burns, S.J., Fleitmann, D., Matter, A., Al-subbary, A.A., 2003. Indian Ocean Climate and an Absolute Chronology over Dansgaard / Oeschger Events 9 to Published by : American Association for the Advancement of Science Stable URL : http://www.jstor.com/stable/3835025 Linked references are available on JSTOR for this art **301**, 1365–1367.

Bursik, M.I., Kobs, S.E., Burns, A., Braitseva, O.A., Bazanova, L.I., Melekestsev, I. V., Kurbatov, A., Pieri, D.C., 2009. Volcanic plumes and wind: Jetstream interaction examples and implications for air traffic. *Journal of Volcanology and Geothermal Research* **186**, 60–67. https://doi.org/10.1016/j.jvolgeores.2009.01.021

Bursik, M.I., Woods, A.W., 1996. The dynamics and thermodynamics of large ash flows. *Bulletin of Volcanology* **58**, 175–193

Butchart, N, Butchart, Neal, 2014. The Brewer-Dobson circulation. *Reviews of Geophysics* **52**, 157–184. https://doi.org/10.1002/2013RG000448

Cadoux, A., Scaillet, B., Bekki, S., Oppenheimer, C., Druitt, T.H., 2015. Stratospheric Ozone destruction by the Bronze-Age Minoan eruption (Santorini Volcano, Greece). *Scientific Reports* **5**, 1–12. https://doi.org/10.1038/srep12243

Camuera, J., Jiménez-Moreno, G., Ramos-Román, M.J., García-Alix, A., Toney, J.L., Anderson, R.S., Jiménez-Espejo, F., Bright, J., Webster, C., Yanes, Y., Carrión, J.S., 2019. Vegetation and climate changes during the last two glacial-interglacial cycles in the western Mediterranean: A new long pollen record from Padul (southern Iberian Peninsula). *Quaternary Science Reviews* **205**, 86–105. https://doi.org/10.1016/j.quascirev.2018.12.013

Carey, R.J., Houghton, B.F., Thordarson, T., 2009. Tephra dispersal and eruption dynamics of wet and dry phases of the 1875 eruption of Askja Volcano, Iceland. *Bulletin of Volcanology* **72**, 259–278. https://doi.org/10.1007/s00445-009-0317-3

Carey, R.J., Houghton, B.F., Thordarson, T. dynamics, 2009. Abrupt shifts between wet and dry phases of the 1875 eruption of Askja volcano: microscopic evidence for macroscopic dynamics. *Journal of Volcanology and Geothermal Research* **184**, 256–270.

Carey, S., Sigurdsson, H., 1989. The intensity of Plinian eruptions. *Bulletin of Volcanology* **51**, 28–40.

Caricchi, L., Burlini, L., Ulmer, P., Gerya, T., Vassalli, M., Papale, P., 2007. Non-Newtonian rheology of crystal-bearing magmas and implications for magma ascent dynamics. *Earth & Planetary Science Letters* **264**, 402–419.

Caricchi, L., Simpson, G., Schaltegger, U., 2014. Zircons reveal magma fluxes in the Earth's crust. *Nature* **511**, 457–461.

Carlson, A. E., Clark, P.U., Haley, B.A., Klinkhammer, G.P., 2009. Routing of western Canadian Plains runoff during the 8.2 ka cold event. *Geophysical Research Letters* **36**, L14704.

Carlson, A.E., Clark, P.U., Haley, B.A., Klinkhammer, G.P., Simmons, K., Brook, E.J., Meissner, K.J., 2007. Geochemical proxies of North American freshwater routing during the Younger Dryas cold event. *Proceedings of the National Academy of Science* **104**, 6556–6561.

Carn, S.A., Clarisse, L., Prata, A.J., 2016. Multi-decadal satellite measurements of global volcanic degassing. *Journal of Volcanology and Geothermal Research* **311**, 99–134. https://doi.org/10.1016/j.jvolgeores.2016.01.002

Carolin, S.A., Cobb, K.M., Adkins, J.F., Clark, B., Conroy, J.L., Lejau, S., Malang, J., Tuen, A.A., 2013. Varied response of Western Pacific hydrology to climate forcings over the Last Glacial Period. *Science* **340**, 1564–1566.

Carolin, S.A., Cobb, K.M., Lynch-Stieglitz, J., Moerman, J.W., Partin, J.W., Lejau, S., Malang, J., Clark, B., Tuen, A.A., Adkins, J.F., 2016. Northern Borneo stalagmite records reveal West Pacific hydroclimate across MIS 5 and 6. *Earth and Planetary Science Letters* **439**, 182–193. https://doi.org/10.1016/j.epsl.2016.01.028

Carr, M. J., Patino, L.C., Feigenson, M.D., 2007. Petrology and geochemistry of lavas, in Central America, in: Buntschuh, J., Alvarado, G.E. (Ed.), Geology, Resources and Hazards. A.A.Balkema, Rotterdam, pp. 565–590.

Carr, M., Feigenson, M.D., Patino, L.C., Walker, J.A., 2003. Volcanism and geochemistry in Central America: Progress and problems, in: Eiler, J. (Ed.), Inside the Subduction Factory, Geophysical Monograph Series. American Geophysical Union, Washington DC, pp. 153–174.

Carr, M.J., 1984. Symmetrical and segmented variation of physical and geochemical characteristics of the Central American volcanic front. *Journal of Volcanology and Geothermal Research* **20**, 231–252. https://doi.org/10.1016/0377-0273(84)90041-6

Carrasco-Núñez, G., López-Martínez, M., Hernández, J., Vargas, V., 2017. Subsurface stratigraphy and its correlation with the surficial geology at Los Humeros geothermal field, eastern Trans-Mexican Volcanic Belt. *Geothermics* **67**, 1–17.

Carter, V. A., Shinker, J. J., Preece, J., 2018. Drought and vegetation change in the central Rocky Mountains and western Great Plains: potential climatic mechanisms associated with megadrought conditions at 4200 cal yr BP. *Climate of the Past* **14**, 1195–1212.

Cashman, K., Blundy, J., 2013. Petrological cannibalism: The chemical and textural consequences of incremental magma body growth. *Contributions to Mineralogy and Petrology* **166**, 703–729.

Cashman, K. V., Rust, A.C., 2020. Far-travelled ash in past and future eruptions: combining tephrochronology with volcanic studies. *Journal of Quaternary Science* **35**, 11–22. https://doi.org/10.1002/jqs.3159

Cashman, K. V., Sparks, R.S.J., Blundy, J.D., 2017. Vertically extensive and unstable magmatic systems: A unified view of igneous processes. *Science* **355**. https://doi.org/10.1126/science.aag3055

Cassidy, M., Watt, S.F.L., Palmer, M.R., Trofimovs, J., Symons, W., Maclachlan, S.E., Stinton, A.J., 2014. Construction of volcanic records from marine sediment cores: A review and case study (Montserrat, West Indies). *Earth-Science Reviews* **138**, 137–155. https://doi.org/10.1016/j.earscirev.2014.08.008

Catania, G. A., Neumann, T., Price, S.F., 2008. Characterizing englacial drainage in the ablation zone of the Greenland Ice Sheet. *Journal of Glaciology* **54**, 567–578.

Cavanagh, J.P., Lampkin, D.J., Moon, T., 2017. Seasonal variability in regional ice flow due to meltwater injection into the shear margins of Jakobshavn Isbræ. *Journal of Geophysical Research - Earth Surface* **122**, 2488–2505.

Chen, S., Wang, Y., Cheng, H., Edwards, R.L., Wang, X., Kong, X., Liu, D., 2016. Strong coupling of Asian Monsoon and Antarctic climates on sub-orbital timescales. *Scientific Reports* **6**, 1–7. https://doi.org/10.1038/srep32995

Chen, X.Y., Blockley, S.P., Tarasov, P.E., Xu, Y.G., McLean, D., Tomlinson, E.L., Albert, P.G., Liu, J.Q., Müller, S., Wagner, M., Menzies, M.A., 2017. Clarifying the distal to proximal tephrochronology of the Millennium (BeTm) eruption, Changbaishan Volcano, northeast China. *Quaternary Geochronology* **33**, 61–75.

Chen, X.Y., Blockley, S.P.E., Xu, Y.G., Menzies, M.A., 2020. Holocene tephrostratigraphic framework and monsoon evolution of East Asia: Key tephra beds for synchronising palaeoclimate records. *Quaternary Science Reviews* **242**, 106467. https://doi.org/10.1016/j.quascirev.2020.106467

Cheng, H., Lawrence Edwards, R., Shen, C., Polyak, V.J., Asmerom, Y., Woodhead, J., Hellstrom, J., Wang, Y., Kong, X., Spötl, C., Wang, X., Calvin Alexander, E., 2013. Improvements in ^{230}Th dating, ^{230}Th and ^{234}U half-life values, and U–Th isotopic measurements by multi-collector inductively coupled plasma mass spectrometry. *Earth & Planetary Science Letters* **371**–**372**, 82–91.

Cheng, H., Sinha, A., Cruz, F.W., Wang, X., Edwards, R.L., d'Horta, F.M., Ribas, C.C., Vuille, M., Stott, L.D., Auler, A.S., 2013. Climate change patterns in Amazonia and biodiversity. *Nature Communications* **4**, 1411.

Cheng, H., Edwards, R.L., Sinha, A., Spötl, C., Yi, L., Chen, S., Kelly, M., Kathayat, G., Wang, X., Li, X., Kong, X., Wang, Y., Ning, Y., Zhang, H., 2016. The Asian monsoon over the past 640,000 years and ice age terminations. *Nature* **534**, 640–646. https://doi.org/10.1038/nature18591

Cheng, H., Fleitmann, D., Edwards, R.L., Wang, X., Cruz, F.W., Auler, A.S., Mangini, A., Wang, Y., Kong, X., Burns, S.J., Matter, A., 2009. Timing and structure of the 8.2. kyr B.P. event inferred from δ^{18}O records of stalagmites from China, Oman, and Brazil. *Geology* **37**, 1007–1010. https://doi.org/10.1130/G30126A.1

Cheng, H., Zhang, H., Spötl, C., Baker, J., Sinha, A., Li, H., 2020. Timing and structure of the Younger Dryas event and its underlying climate dynamics. *Proceedings of the National Academy of Science* 1–10. https://doi.org/10.1073/pnas.2007869117

Cheng, H., Zhang, H., Zhao, J., Li, H., Ning, Y., Kathayat, G., 2019. Chinese stalagmite paleoclimate researches: A review and perspective. *Science China Earth Sciences* **62**, 1489–1513. https://doi.org/10.1007/s11430-019-9478-3

Chesner, C. A., Luhr, J.F., 2010. A melt inclusion study of the Toba Tuffs, Sumatra, Indonesia. *Journal of Volcanology and Geothermal Research* **197**, 259–278.

Chesner, C.A., Rose, W.I., Deino, A., Drake, R., Westgate, J.A., 1991. Eruptive history of earth's largest Quaternary caldera (Toba, Indonesia) clarified. *Geology* **19**, 200–203.

Chesner, C.A., 2012. The Toba Caldera Complex. *Quaternary International* **258**, 5–18. https://doi.org/10.1016/j.quaint.2011.09.025

Chesner, C.A., Luhr, J.F., 2010. A melt inclusion study of the Toba Tuffs, Sumatra, Indonesia. *Journal of Volcanology and Geothermal Research* **197**, 259–278. https://doi.org/10.1016/j.jvolgeores.2010.06.001

Chester, D.K., Duncan, A., Coutinho, R., Wallenstein, N., Branca, S., 2018. Communicating Information on Eruptions and Their Impacts from the Earliest Times Until the Late Twentieth Century, in: Observing the Volcano World, Advances in Volcanology. pp. 419–443.

Chester, D.K., 2005. Volcanoes, society, and culture, in: Volcanoes and the Environment. pp. 404–439.

Chew, D.M., Donelick, R.A., Donelick, M.B., Kamber, B.S., Stock, M.J., 2014. Apatite chlorine concentration measurements by LA-ICP-MS. *Geostandards and Geoanalytical Research* **38**, 23–35.

Chu, W., Schroeder, D.M., Seroussi, H., Creyts, T.T., Palmer, S.J., Bell, R.E., 2016. Extensive winter subglacial water storage beneath the Greenland Ice Sheet. *Geophysical Research Letters* **43**, 12484–12492.

Çiçek, İ., Duman, N., 2015. Seasonal and Annual Precipitation Trends in Turkey. *Carpathian Journal of Earth and Environmental Sciences* **10**, 77–84.

Cioni, R., Bertagnini, A., Santacroce, R., Andronico, D., 2008. Explosive activity and eruption scenarios at Somma-Vesuvius (Italy): towards a new classification scheme. *Journal of Volcanology and Geothermal Research* **178**, 331–346.

Clark, P.U., Hostetier, S.W., Pisias, N.G., Schmittner, A., Meissner, K.J., 2007. Mechanisms for an ~7-kyrs climate and sea-level oscillation during Marine Isotope Stage 3., in: Schmittner, A., Chiang, J.C.H., Hemming, S.R. (Ed.), Circulation: Mechanisms and Impacts? Past and Future Changes of Meridional Overturning. American Geophysical Union, Washington DC, p. 392.

Clark, P.U., Marshall, S.J., Clarke, G.K.C., Hostetler, S.W., Licciardi, J.M., Teller, J.T., 2001. Freshwater forcing of abrupt climate change during the last glaciation. *Science* **293**, 283–287.

Clark, P.U., Pisias, N.G., Stocker, T.F., Weaver, A.J., 2002. The role of the thermohaline circulation in abrupt climate change. *Nature* **415**, 863–869.

Clark, P.U., Dyke, A.S., Shakun, J.D., Carlson, A.E., Clark, J., Wohlfarth, B., Mitrovica, J.X., Hostetler, S.W., McCabe, A.M., 2009. The Last Glacial Maximum. *Science* **325**, 710–714. https://doi.org/10.1126/science.1172873

Clarke, G.K.C., 2005. Subglacial Processes. *Annual Review of Earth and Planetary Sciences* **33**, 247–276.

Clement, A.C., Peterson, L.C., 2008. MECHANISMS OF ABRUPT CLIMATE CHANGE OF THE LAST GLACIAL PERIOD. *Reviews of Geophysics* **46**, RG4002. https://doi.org/10.1029/2006RG000204.1.INTRODUCTION

Cole, J.W., Milner, D.M., Spinks, K.D., 2005. Calderas and caldera structures: A review. *Earth-Science Reviews* **69**, 1–26. https://doi.org/10.1016/j.earscirev.2004.06.004

Cole-Dai, J., Ferris, D., Lanciki, A., Savarino, J., Baroni, M., Thiemens, M.H., 2009. Cold decade (AD 1810-1819) caused by Tambora (1815) and another (1809) stratospheric volcanic eruption. *Geophysical Research Letters* **36**, 1–6. https://doi.org/10.1029/2009GL040882

Collins, M.R., Knutti, R., Arblaster, J., Dufresne, J-L., Fichefet, T., Friedlingstein, P., Gao, X., Gutowski, W., Johns, T., Krinner, G., Shongwe, M., Tebaldi, C., Weaver, A.J., Wehner, M., Joussaume, S., Mokssit, A., Taylor, K.E., Tett, S., 2013. Long-term climate change: Projections, commitments and irreversibility, in: Stocker, T.F., Qin, D., Plattner, G-K., Tignor, M., Allen, S.K., Boschung, J., Nauels, A., Xia, Y., Bex, V., Midgley, P.M. (Ed.), Climate Change 2013: The Physical Science Basis. Contribution of Working Group I to the Fifth Assessment Report of the Intergovernmental Panel on Climate Change. Cambridge University Press, Cambridge, pp. 1029–1136.

Collister, C., Mattey, D., 2008. Controls on water drop volume at speleothem drip sites: An experimental study. *Journal of Hydrology* **358**, 259–267.

Colose, C.M., LeGrande, A.N., Vuille, M., 2016. Hemispherically asymmetric volcanic forcing of tropical hydroclimate during the last millennium. *Earth System Dynamics* **7**, 681–696. https://doi.org/10.5194/esd-7-681-2016

Colucci, S., Palladino, D.M., Mulukutla, G.K., Proussevitch, A.A., 2013. 3-D Reconstruction of ash vesicularity: insights into the origin of ash-rich explosive eruptions. *Journal of Volcanology and Geothermal Research* **255**, 98–107.

Comas-Bru, L., Atsawawaranunt, K., Harrison, S., S.W.G.M., 2020. SISAL (Speleothem Isotopes Synthesis and AnaLysis Working Group) database version 2.0. *Database*.

Compton, K., Bennett, R.A., Hreinsdóttir, S., 2015. Climate driven vertical acceleration of Icelandic crust measure by CGPS geodesy. *Geophysical Research Letters* **42**, 743–750.

Connell, B., Gray-Jones, A., Redfern, R., Walker, D., 2012. A Bioarchaeological Study of Medieval Burials on the Site of St Mary Spital: Excavations at Spitalfields Market, London E1, 1991–2007. London.

Connor, C.B., McBirney, A.R., Furlan, C., 2006. What is the probability of explosive eruption at a long-dormant volcano?, in: Mader, H.M., Coles, S.G., Connor, C.B., Connor, L.J. (Ed.), Statistics in Volcanology. The Geological Society, London, pp. 39–48.

Cook, E., Portnyagin, M., Ponomareva, V., Bazanova, L., Svensson, A., Garbe-Schönberg, D., 2018. First identification of cryptotephra from the Kamchatka Peninsula in a Greenland ice core: Implications of a widespread marker deposit that links Greenland to the Pacific northwest. *Quaternary Science Reviews* **181**, 200–206. https://doi.org/10.1016/j.quascirev.2017.11.036

Cooper, C.J., Swindles, G.T., Savov, I.P., Schmidt, A., Bacon, K.L., 2018. Evaluating the relationship between climate change and volcanism. *Earth-Science Reviews* **177**, 238–247.

Cooper, C.L., Savov, I.P., Patton, H., Hubbard, A., Ivanovic, R.F., Carrivick, J.L., Swindles, G.T., 2020. Is there a Climatic Control on Icelandic Volcanism? *Quaternary Science Advances* 100004. https://doi.org/10.1016/j.qsa.2020.100004

Cooper, C.L., Savov, I.P., Swindles, G.T., 2019. Standard chemical-based tephra extraction methods significantly alter the geochemistry of volcanic glass shards. *Journal of Quaternary Science* **34**, 697–707. https://doi.org/10.1002/jqs.3169

Cooper, K. M., Kent, A.J.R., 2014. Rapid remobilization of magmatic crystals kept in cold storage. *Nature* **506**, 480–483.

Correa-Metrio, A., Bush, M.B., Cabrera, K.R., Sully, S., Brenner, M., Hodell, D.A., Escobar, J., Guilderson, T., 2012. Rapid climate change and no-analog vegetation in lowland Central America during the last 86,000 years. *Quaternary Science Reviews* **38**, 63–75. https://doi.org/10.1016/j.quascirev.2012.01.025

Corrick, E.C., Drysdale, R.N., Hellstrom, J.C., Capron, E., Rasmussen, S.O., Zhang, X., Fleitmann, D., Couchoud, I., Wolff, E., Monsoon, S.A., 2020. Synchronous timing of abrupt climate changes during the last glacial period. *Science* **969**, 963–969.

Costa, A., Caricchi, L., Bagdassarov, N., 2009. A model for the rheology of particle-bearing suspensions and partially molten rocks. *Geochemistry, Geophysics, Geosystems* **10**.

Costa, A., Martí, J., 2016. Stress field control during large caldera-forming eruptions. *Frontiers in Earth Science* **4**, 1–13. https://doi.org/10.3389/feart.2016.00092

Costa, A., Smith, V.C., Macedonio, G., Matthews, N.E., 2014. The magnitude and impact of the Youngest Toba Tuff super-eruption. *Frontiers in Earth Science* **2**, 1–8. https://doi.org/10.3389/feart.2014.00016

Costa, A., Suzuki, Y.J., Koyaguchi, T., 2018. Understanding the plume dynamics of explosive super-eruptions. *Nature Communications* **9**, 654. https://doi.org/10.1038/s41467-018-02901-0

Costa, F., Scaillet, B., Gourgaud, A., 2003. Massive atmospheric sulfur loading of the AD 1600 Huaynaputina eruption and implications for petrologic sulfur estimates. *Geophysical Research Letters* **30**, 1068.

Coulter, S.E., Pilcher, J.R., Plunkett, G., Baillie, M., Hall, V.A., Steffensen, J.P., Vinther, B.M., Clausen, H.B., Johnsen, S.J., 2012. Holocene tephras highlight complexity of volcanic signals in Greenland ice cores. *Journal of Geophysical Research Atmospheres* **117**, 1–11. https://doi.org/10.1029/2012JD017698

Crosweller, H.S., Arora, B., Brown, S.K., Cottrell, E., Deligne, N.I., Guerrero, N.O., Hobbs, L., Kiyosugi, K., Loughlin, S.C., Lowndes, J., Nayembil, M., Siebert, L., Sparks, R.S.J., Takarada, S., Venzke, E., 2012. Global database on large magnitude explosive volcanic eruptions (LaMEVE). *Journal of Applied Volcanology* **1**, 1–13. https://doi.org/10.1186/2191-5040-1-4

Crowley, T.J., 2000. Causes of Climate Change over the past 1000 Years. *Science* **289**, 270.

Cruz, F.W., Burns, S.J., Karmann, I., Sharp, W.D., Vuille, M., 2006. Reconstruction of regional atmospheric circulation features during the late Pleistocene in subtropical Brazil from oxygen isotope composition of speleothems. *Earth and Planetary Science Letters* **248**, 495–507. https://doi.org/10.1016/j.epsl.2006.06.019

Cruz, F.W., Burns, S.J., Karmann, I., Sharp, W.D., Vuille, M., Ferrari, J.A., 2006. A stalagmite record of changes in atmospheric circulation and soil processes in the Brazilian subtropics during the Late Pleistocene. *Quaternary Science Reviews* **25**, 2749–2761. https://doi.org/10.1016/j.quascirev.2006.02.019

Cruz, F.W., Vuille, M., Burns, S.J., Wang, X., Cheng, H., Werner, M., Lawrence Edwards, R., Karmann, I., Auler, A.S., Nguyen, H., 2009. Orbitally driven east-west antiphasing of South American precipitation. *Nature Geoscience* **2**, 210–214. https://doi.org/10.1038/ngeo444

Csoma, A.É., Goldstein, R.H., Pomar, L., 2006. Pleistocene speleothems of Mallorca: Implications for palaeoclimate and carbonate diagenesis in mixing zones. *Sedimentology* **53**, 213–236. https://doi.org/10.1111/j.1365-3091.2005.00759.x

Cutler, N. A., Bailey, R. M., Hickson, K. T., Streeter, R. T., Dugmore, A.J., 2016. Vegetation structure influences the retention of airfall tephra in a sub-Arctic landscape. *Progress in Physical Geography* **40**, 661–675.

Cutler, N.A., Streeter, R.T., Marple, J., Shotter, L.R., Yeoh, J.S., Dugmore, A.J., 2018. Tephra transformations: variable preservation of tephra layers from two well-studied eruptions. *Bulletin of Volcanology* **80**. https://doi.org/10.1007/s00445-018-1251-z

Cutler, N.A., Streeter, R.T., Engwell, S.L., Bolton, M.S., Jensen, B.J.L., Dugmore, A.J., 2020. How reliable are tephra layers as records of past eruptions? A calibration exercise. *Journal of Volcanology and Geothermal Research* 106883. https://doi.org/10.1016/j.jvolgeores.2020.106883

Cvijanovic, I., Chiang, J.C.H., 2013. Global energy budget changes to high latitude North Atlantic cooling and the tropical ITCZ response. *Climate Dynamics* **40**, 1435–1452. https://doi.org/10.1007/s00382-012-1482-1

D'Agostino, R., Lionello, P., 2020. The atmospheric moisture budget in the Mediterranean: Mechanisms for seasonal changes in the Last Glacial Maximum and future warming scenario. *Quaternary Science Reviews* **241**, 106392. https://doi.org/10.1016/j.quascirev.2020.106392

Dansgaard, A.W., Clausen, H.B., Gundestrup, N., Hammer, C.U., Johnsen, S.F., Reeh, N., 1982. A New Greenland Deep Ice Core. *Science* **218**, 1273–1277.

Davies, L. J., Jensen, B. J. L., Froese, D. G., Wallace, K.L., 2016. Late Pleistocene and Holocene tephrostratigraphy of interior Alaska and Yukon: Key beds and chronologies over the past 30,000 years. *Quaternary Science Reviews* **146**, 28–53.

Davies, S.M., Abbott, P.M., Pearce, N.J.G., Wastegård, S., Blockley, S.P.E., 2012. Integrating the INTIMATE records using tephrochronology: rising to the challenge. *Quaternary Science Reviews* **36**, 11–27.

Davies, S.M., Elmquist, M., Bergman, J., Wohlfarth, B., Hammarlund, D., 2007. Cryptotephra sedimentation processes within two lacustrine sequences from west central Sweden. *Holocene* **17**, 319–330.

Davies, S.M., 2015. Cryptotephras: The revolution in correlation and precision dating. *Journal of Quaternary Science* **30**, 114–130. https://doi.org/10.1002/jqs.2766

Davies, S.M., Larsen, G., Wastegård, S., Turney, C.S.M., Hall, V.A., Coyle, L., Thordarson, T., 2010. Widespread dispersal of Icelandic tephra: How does the Eyjafjöll eruption of 2010 compare to past Icelandic events? *Journal of Quaternary Science* **25**, 605–611. https://doi.org/10.1002/jqs.1421

de Silva, S., Lindsay, J.M., 2015. Primary Volcanic Landforms, in: Sigurdsson, H. (Ed.), Encyclopaedia of Volcanoes. Academic Press.

de Silva, S.L., Gregg, P.M., 2014. Thermomechanical feedbacks in magmatic systems: Implications for growth, longevity, and evolution of large caldera-forming magma reservoirs and their supereruptions. *Journal of Volcanology and Geothermal Research* **282**, 77–91. https://doi.org/10.1016/j.jvolgeores.2014.06.001

de Vernal, A., Hillaire-Marcel, C., Turon, J. L. & Matthiessen, J., 2000. Reconstruction of sea-surface temperature, salinity, and sea-ice cover in the northern North Atlantic during the Last Glacial Maximum based on dinocyst assemblages. *Canadian Journal of Earth Sciences* **37**, 725–750.

de Vernal, A., Eynaud, F., Henry, M., Hillaire-marcel, C., Londeix, L., Mangin, S., 2005. Reconstruction of sea-surface conditions at middle to high latitudes of the Northern Hemisphere during the Last Glacial Maximum (LGM) based on dinoflagellate cyst assemblages. *Quaternary Science Reviews* **24**, 897–924. https://doi.org/10.1016/j.quascirev.2004.06.014

De Vivo, B., Rolandi, G., Gans, P.B., Calvert, A., Bohrson, W.A., Spera, F.J., Belkin, H.E., 2001. New constraints on the pyroclastic eruptive history of the Campanian volcanic Plain (Italy). *Mineralogy and Petrology* **73**, 47–65.

Debret, M., Bout-Roumazeilles, V., Grousset, F., Desmet, M., McManus, J.F., Massei, N., Sebag, D., Petit, J.-R., Copard, Y., Trentesaux, A., 2007. The origin of the 1500-year climate cycles in Holocene North-Atlantic records. *Climate of the Past* **3**, 569–575.

Del Carlo, P., Di Roberto, A., D'Orazio, M., Petrelli, M., Angioletti, A., Zanchetta, G., Maggi, V., Daga, R., Nazzari, M., Rocchi, S., 2018. Late Glacial-Holocene tephra from southern Patagonia and Tierra del Fuego (Argentina, Chile): A complete textural and geochemical fingerprinting for distal correlations in the Southern Hemisphere. *Quaternary Science Reviews* **195**, 153–170. https://doi.org/10.1016/j.quascirev.2018.07.028

Deligne, N.I., Coles, S.G., Sparks, R.S.J., 2010. Recurrence rates of large explosive volcanic eruptions. *Journal of Geophysical Research* **115**, 1–16. https://doi.org/10.1029/2009JB006554

Deng, W., Liu, Y., Wei, G., Li, X., Tu, X., Xie, L., Zhang, H., Sun, W., 2010. High-precision analysis of Sr/Ca and Mg/Ca ratios in corals by laser ablation inductively coupled plasma optical emission spectrometry. *Journal of Analytical Atomic Spectrometry* **25**, 84–87. https://doi.org/10.1039/b912112a

Deniel, C., Aydar, E., Gourgaud, A., 1998. The Hasan Dagi stratovolcano (Central Anatolia, Turkey): Evolution from calc-alkaline to alkaline magmatism in a collision zone. *Journal of Volcanology and Geothermal Research* **87**, 275–302. https://doi.org/10.1016/S0377-0273(98)00097-3

Deniz, A., Toros, H., Incecik, S., 2011. Spatial variations of climate indices in Turkey. *International Journal of Climatology* **31**, 394–403. https://doi.org/10.1002/joc.2081

Denniston, R.F., Luetscher, M., 2017. Speleothems as high-resolution paleoflood archives. *Quaternary Science Reviews* **170**, 1–13.

Denniston, R.F., Houts, A.N., Asmerom, Y., Wanamaker, A.D., Haws, J.A., Polyak, V.J., Thatcher, D.L., Altan-Ochir, S., Borowske, A.C., Breitenbach, S.F.M., Ummenhofer, C.C., Regala, F.T., Benedetti, M.M., Bicho, N., 2018. A Stalagmite Test of North Atlantic SST and Iberian Hydroclimate Linkages over the Last Two Glacial Cycles. *Climate of the Past Discussions* 1–39. https://doi.org/10.5194/cp-2017-146

Desmarchelier, J.M., Hellstrom, J.C., McCulloch, M.T., 2006. Rapid trace element analysis of speleothems by ELA-ICP-MS. *Chemical Geology* **231**, 102–117. https://doi.org/10.1016/j.chemgeo.2006.01.002

Diallo, M., Ploeger, F., Konopka, P., Birner, T., Müller, R., Riese, M., Garny, H., Legras, B., Ray, E., Berthet, G., Jegou, F., 2017. Significant Contributions of Volcanic Aerosols to Decadal Changes in the Stratospheric Circulation. *Geophysical Research Letters* **44**, 10,780-10,791. https://doi.org/10.1002/2017GL074662

Ditlevsen, P. D., Andersen, K. K., Svensson, A., 2007. The DO-climate events are probably noise induced: statistical investigation of the claimed 1470 years cycle. *Climate of the Past* **3**, 129–134.

Dogan, A.U., Dogan, M., Kilinc, A., Locke, D., 2008. An isobaric - Isenthalpic magma mixing model for the Hasan Dagi volcano, Central Anatolia, Turkey. *Bulletin of Volcanology* **70**, 797–804. https://doi.org/10.1007/s00445-007-0167-9

Domínguez-Villar, D., Krklec, K., Pelicon, P., Fairchild, I.J., Cheng, H., Edwards, L.R., 2017. Geochemistry of speleothems affected by aragonite to calcite recrystallization – Potential inheritance from the precursor mineral. *Geochimica et Cosmochimica Acta* **200**, 310–329. https://doi.org/10.1016/j.gca.2016.11.040

Donnelly, T. W., Horne, G. S., Finch, R. C., López-Ramos, E., 1990. Northern Central America: The Maya and Chortis blocks, in: Case, J.E., Dengo, G. (Ed.), The Geology of North America: The Caribbean Region. The Geological Society of America, Boulder, pp. 37–76.

Donohoe, A., Marshall, J., Ferreira, D., Armour, K., McGee, D., 2014. The interannual variability of tropical precipitation and interhemispheric energy transport. *Journal of Climate* **27**, 3377–3392. https://doi.org/10.1175/JCLI-D-13-00499.1

Donovan, A., Oppenheimer, C., 2019. Volcanoes on borders: a scientific and (geo)political challenge. *Bulletin of Volcanology* **81**. https://doi.org/10.1007/s00445-019-1291-z

Draxler, R.R., Rolph, G.D., 2003. HYSPLIT (HYbrid Single-Particle Lagrangian Integrated Trajectory) model.

Drexler, J.W., Rose, W.I., Sparks, R.S.J., Ledbetter, M.T., 1980. The Los Chocoyos Ash, Guatemala: A Major Stratigraphic Marker in Middle America and in Three Ocean Basins. *Quaternary Research* **13**, 327–345.

Driscoll, S., Bozzo, A., Gray, L.J., Robock, A., S., G., 2012. Coupled model intercomparison project 5 (CMIP5) simulations of climate following volcanic eruptions. *Journal of Geophysical Research* **117**, D17105.

Druitt, T.H., McCoy, F.W., Vougioukalakis, G.E., 2019. The Late Bronze Age Eruption of Santorini Volcano and Its Impact on the Ancient Mediterranean World. *Elements* **15**, 185–190.

Drysdale, R., Zanchetta, G., Hellstrom, J., Maas, R., Fallick, A., Pickett, M., Cartwright, I., Piccini, L., 2006. Late Holocene drought responsible for the collapse of Old World civilizations is recorded in an Italian cave flowstone. *Geology* **34**, 101–104.

Du, W., Cheng, H., Xu, Y., Yang, X., Zhang, P., Sha, L., Li, H., Zhu, X., Zhang, M., Stríkis, N.M., Cruz, F.W., Edwards, R.L., Zhang, H., Ning, Y., 2019. Timing and structure of the weak Asian Monsoon event about 73,000 years ago. *Quaternary Geochronology* **53**, 101003. https://doi.org/10.1016/j.quageo.2019.05.002

Dubois, N., Kienast, M., Kienast, S., Normandeau, C., Calvert, S.E., Herbert, T.D., Mix, A., 2011. Millennial-scale variations in hydrography and biogeochemistry in the Eastern Equatorial Pacific over the last 100 kyr. *Quaternary Science Reviews* **30**, 210–223. https://doi.org/10.1016/j.quascirev.2010.10.012

Dugmore, A.J., Streeter, R., Cutler, N.A., 2018. The role of vegetation cover and slope angle in tephra layer preservation and implications for Quaternary tephrostratigraphy. *Palaeogeography, Palaeoclimatology, Palaeoecology* **489**, 105–116.

Dugmore, A.J., Thompson, P.I.J., Streeter, R.T., Cutler, N.A., Newton, A.J., Kirkbride, M.P., 2020. The interpretative value of transformed tephra sequences. *Journal of Quaternary Science* **35**, 23–38. https://doi.org/10.1002/jqs.3174

Dumitru, O.A., Onac, B.P., Polyak, V.J., Wynn, J.G., Asmerom, Y., Fornós, J.J., 2018. Climate variability in the western Mediterranean between 121 and 67 ka derived from a Mallorcan speleothem record. *Palaeogeography, Palaeoclimatology, Palaeoecology* **506**, 128–138. https://doi.org/10.1016/j.palaeo.2018.06.028

Duzenli, E., Tabari, H., Willems, P., Yilmaz, M.T., 2018. Decadal variability analysis of extreme precipitation in Turkey and its relationship with teleconnection patterns. *Hydrological Processes* **32**, 3513–3528. https://doi.org/10.1002/hyp.13275

Ebmeier, S.K., Andrews, B.J., Araya, M.C., Arnold, D.W.D., Biggs, J., Cooper, C., Cottrell, E., Furtney, M., Hickey, J., Jay, J., Lloyd, R., Parker, A.L., Pritchard, M.E., Robertson, E., Venzke, E., Williamson, J.L., 2018. Synthesis of global satellite observations of magmatic and volcanic deformation: implications for volcano monitoring & the lateral extent of magmatic domains. *Journal of Applied Volcanology* **7**, 1–26. https://doi.org/10.1186/s13617-018-0071-3

Economics, O., 2010. The Economic Impacts of Air Travel Restrictions Due to Volcanic Ash. Oxford.

Eddy, J.A., 1976. The Maunder Minimum. *Science* **192**, 1189–1202.

Eggins, S.M., Grün, R., McCulloch, M.T., Pike, A.W.G., Chappell, J., Kinsley, L., Mortimer, G., Shelley, M., Murray-Wallace, C. V., Spötl, C., Taylor, L., 2005. In situ U-series dating by laser-ablation multi-collector ICPMS: New prospects for Quaternary geochronology. *Quaternary Science Reviews* **24**, 2523–2538. https://doi.org/10.1016/j.quascirev.2005.07.006

El Hadri, H., Petersen, E.J., Winchester, M.R., 2016. Impact of and correction for instrument sensitivity drift on nanoparticle size measurements by single-particle ICP-MS. *Analytical and Bioanalytical Chemistry* **408**, 5099–5108.

Elíasson, J., 2014. Katla volcano in Iceland, potential hazards and risk assessment. *Natural Science* **6**, 99–107.

Elliot, M., Welsh, K., Chilcott, C., McCulloch, M., Chappell, J., Ayling, B., 2009. Profiles of trace elements and stable isotopes derived from giant long-lived Tridacna gigas bivalves: Potential applications in paleoclimate studies. *Palaeogeography, Palaeoclimatology, Palaeoecology* **280**, 132–142. https://doi.org/10.1016/j.palaeo.2009.06.007

Elming, S., 1998. A palaeomagnetic study and K–Ar age determinations of tertiary rocks in Nicaragua, Central America, in: Elming, S., Widenfalk, L., Rodriquez, D. (Ed.), Geoscientific Research in Nicaragua. Lulea University of Technology, Sweden, pp. 1–19.

Emile-Geay, J., Cane, M., Seager, R., Kaplan, A., Almasi, P., 2007. El Niño as a mediator of the solar influence on climate. *Paleoceanography* **22**, PA3210.

Emile-Geay, J.R., Seager, R., Cane, M.A., Cook, E.R., Haug, G.H., 2008. Volcanoes and ENSO over the past millennium. *Journal of Climate* **21**, 3134–3148.

English, J.M., Toon, O.B., Mills, M.J., 2013. Microphysical simulations of large volcanic eruptions: Pinatubo and Toba. *Journal of Geophysical Research: Atmospheres* **118**, 1880–1895. https://doi.org/10.1002/jgrd.50196

Engwell, S.L., Aspinall, W.P., Sparks, R.S.J., 2015. An objective method for the production of isopach maps and implications for the estimation of tephra deposit volumes and their uncertainties. *Bulletin of Volcanology* **77**. https://doi.org/10.1007/s00445-015-0942-y

Engwell, S.L., de' Michieli Vitturi, M., Esposti Ongaro, T., Neri, A., 2016. Insights into the formation and dynamics of coignimbrite plumes from one-dimensional models. *Journal of Geophysical Research: Solid Earth* **121**, 4211–4231. https://doi.org/10.1002/2016JB012793

Engwell, S.L., Sparks, R.S.J., Carey, S., 2014. Physical characteristics of tephra layers in the deep sea realm: The Campanian Ignimbrite eruption. *Geological Society Special Publication* **398**, 47–64. https://doi.org/10.1144/SP398.7

Erhardt, T., Capron, E., Olander Rasmussen, S., Schüpbach, S., Bigler, M., Adolphi, F., Fischer, H., 2019. Decadal-scale progression of the onset of Dansgaard-Oeschger warming events. *Climate of the Past* **15**, 811–825. https://doi.org/10.5194/cp-15-811-2019

Eriksson, A., Betti, L., Friend, A.D., Lycett, S.J., Singarayer, J.S., von Cramon-Taubadel, N., Valdes, P.J., Balloux, F., Manica, A., 2012. Late Pleistocene climate change and the global expansion of anatomically modern humans. *Proceedings of the National Academy of Science* **109**, 16089–16094.

Evans, D., Wade, B.S., Henehan, M., Erez, J., Müller, W., 2015. Revisiting carbonate chemistry controls on planktic foraminifera Mg / Ca: implications for sea surface temperature and hydrology shifts over the Paleocene–Eocene Thermal Maximum and Eocene–Oligocene Transition. *Climate of the Past Discussions* **11**, 3143–3185. https://doi.org/10.5194/cpd-11-3143-2015

Fairchild, I. J., Borsato, A., Tooth, A.F., Frisia, S., Hawkesworth, C.J., Huang, Y.M., McDermott, F., Spiro, B., 2000. Controls on trace element (Sr-Mg) compositions of carbonate cave waters: Implications for speleothem climatic records. *Chemical Geology* **166**, 255–269.

Fairchild, I.J., Treble, P.C., 2009. Trace elements in speleothems as recorders of environmental change. *Quaternary Science Reviews* **28**, 449–468. https://doi.org/10.1016/j.quascirev.2008.11.007

Fairchild, I.J., McMillan, E.A., 2007. Speleothems as indicators of wet and dry periods. *International Journal of Speleology* **36**, 69–74. https://doi.org/10.5038/1827-806X.36.2.2

Fearnley, C.J., Bird, D.K., Haynes, K., McGuire, W.J., Jolly, G., 2018. Advances in Volcanology: Observing the Volcano World. https://doi.org/ISSN 2364-3285

Feigenson, M. D., Carr, M.J., Maharaj, S.V., Juliano, S., Bolge, L.L., 2004. Lead isotope composition of Central American volcanoes: Influence of the Galapagos plume. *Geochemistry, Geophysics, Geosystems* **5**, Q06001.

Fensterer, C., Scholz, D., Hoffmann, D.L., Spötl, C., Schröder-Ritzrau, A., Horn, C., Pajón, J.M., Mangini, A., 2013. Millennial-scale climate variability during the last 12.5ka recorded in a Caribbean speleothem. *Earth and Planetary Science Letters* **361**, 143–151. https://doi.org/10.1016/j.epsl.2012.11.019

Fernandez-Cortes, A., Cuezva, A., Garcia-Anton, E., Garcia-Guinea, J., Sanchez-Moral, S., 2011. Rare Earth Elements in a Speleothem Analyzed by ICP-MS, EDS, and Spectra Cathodoluminescence. *Spectroscopy Letters* **44**, 474–479.

Fierstein, J.E., Nathenson, M., 1992. Another look at the calculation of tephra fallout volumes. *Bulletin of Volcanology* **54**, 156–167.

Fisher, R.V., Heiken, G., Hulen, J.B., 1997. Volcanoes: Crucibles of Change. Princeton University Press, Princeton.

Fleitmann, D., Cheng, H., Badertscher, S., Edwards, R.L., Mudelsee, M., Göktürk, O.M., Fankhauser, A., Pickering, R., Raible, C.C., Matter, A., Kramers, J., Tüysüz, O., 2009. Timing and climatic impact of Greenland interstadials recorded in stalagmites from northern Turkey. *Geophysical Research Letters* **36**, 1–5. https://doi.org/10.1029/2009GL040050

Fleitmann, D., Burns, S.J., Mudelsee, M., Neff, U., Kramers, J., Mangini, A., Matter, A., 2003. Holocene forcing of the Indian monsoon recorded in a stalagmite from Southern Oman. *Science* **300**, 1737–1739. https://doi.org/10.1126/science.1083130

Fleitmann, D., Burns, S.J., Pekala, M., Mangini, A., Al-Subbary, A., Al-Aowah, M., Kramers, J., Matter, A., 2011. Holocene and Pleistocene pluvial periods in Yemen, southern Arabia. *Quaternary Science Reviews* **30**, 783–787. https://doi.org/10.1016/j.quascirev.2011.01.004

Fohlmeister, J., Lechleitner, F.A., 2019. STAlagmite dating by radiocarbon (star): A software tool for reliable and fast age depth modelling. *Quaternary Geochronology* **51**, 120–129.

Fohlmeister, J., Schröder-Ritzrau, A., Scholz, D., Spötl, C., Riechelmann, D.F.C., Mudelsee, M., Wackerbarth, A., Gerdes, A., Riechelmann, S., Immenhauser, A., Richter, D.K., Mangini, A., 2012. Bunker Cave stalagmites: An archive for central European Holocene climate variability. *Climate of the Past* **8**, 1751–1764. https://doi.org/10.5194/cp-8-1751-2012

Fontijn, K., Lachowycz, S.M., Rawson, H., Pyle, D.M., Mather, T.A., Naranjo, J.A., Moreno-Roa, H., 2014. Late Quaternary tephrostratigraphy of southern Chile and Argentina. *Quaternary Science Reviews* **89**, 70–84. https://doi.org/10.1016/j.quascirev.2014.02.007

Fontijn, K., Rawson, H., Van Daele, M., Moernaut, J., Abarzúa, A.M., Heirman, K., Bertrand, S., Pyle, D.M., Mather, T.A., De Batist, M., Naranjo, J.A., Moreno, H., 2016. Synchronisation of sedimentary records using tephra: A postglacial tephrochronological model for the Chilean Lake District. *Quaternary Science Reviews* **137**, 234–254. https://doi.org/10.1016/j.quascirev.2016.02.015

Forni, F., Degrutyer, W., Bachmann, O., De Astis, G., Mollo, S., 2018. Long-term magmatic evolution reveals the beginning of a new caldera cycle at Campi Flegrei. *Science Advances* **4**, eeat9401.

Freundt, A., Halama, R., Suess, E., Volke, D., 2014. Introduction to the special issue on SFB 574 ‘‘Volatiles and fluids in subduction zones: Climate feedback and trigger mechanisms for natural disasters". *International Journal of Earth Sciences* **103**, 1729–1731.

Friedrich, W.L., Kromer, B., Friedrich, M., Heinemeier, J., Pfeiffer, T., Talamo, S., 2006. Santorini eruption radiocarbon dated to 1627–1600BC. *Science* **312**, 548.

Frisia S., B.A., 2010. Karst, in: Alonso-Zarza, A, M., Tanner, L.H. (Ed.), Carbonates in Continental Settings: Facies, Environments, and Processes. Elsevier, Amsterdam, pp. 269–318.

Frisia, S., Badertscher, S., Borsato, A., Susini, J., Göktürk, O.M., Cheng, H., Edwards, R.L., Kramers, R.L., Tüysüz, O., Fleitmann, D., 2008. The use of stalagmite geochemistry to detect past volcanic eruptions and their environmental impacts. *PAGES News* **16**, 25–26.

Frisia, S., Borsato, A., Fairchild, I.J., McDermott, F., Selmo, E.M., 2002. Aragonite-Calcite Relationships in Speleothems (Grotte De Clamouse, France): Environment, Fabrics, and Carbonate Geochemistry. *Journal of Sedimentary Research* **72**, 687–699.

Frumkin, A., Bar-Yosef, O., Schwarcz, H.P., 2011. Possible paleohydrologic and paleoclimatic effects on hominin migration and occupation of the Levantine Middle Paleolithic. *Journal of Human Evolution* **60**, 437–451. https://doi.org/10.1016/j.jhevol.2010.03.010

Furlan, C., 2010. Extreme value methods for modelling historical series of large volcanic magnitudes. *Statistical Modelling* **10**, 113-132#.

Gale, S.J., 2009. Event chronostratigraphy: a high-resolution tool for dating the recent past. *Quaternary Geochronology* **4**, 391–399.

Ganopolski, A., Rahmstorf, S., 2001. Rapid changes of glacial climate simulated in a coupled climate model. *Nature* **15**, 153–158.

Gansecki, C., Lee, R. L., Shea, T., Lundbland, S.P., Hon, K., Parcheta, C., 2019. The tangled tale of Kīlauea’s 2018 eruption as told by geochemical monitoring. *Science* **366**, 1212.

Ganti, V., Von Hagke, C., Scherler, D., Lamb, M.P., Fischer, W.W., Avouac, J.P., 2016. Time scale bias in erosion rates of glaciated landscapes. *Science Advances* **2**. https://doi.org/10.1126/sciadv.1600204

Gąsirowski, M., Hercman, H., Pruszczyńska, A., Błaszczyk, M., 2015. Drip rate and tritium activity in the Niedźwiedzia Cave system (Poland) as a tool for tracking water circulation paths and time in karstic systems. *Geochronometria* **42**, 210–216.

Gelman, S.E., Gutierrez, F.J., Bachmann, O., 2013. On the longevity of large upper crustal silicic magma reservoirs. *Geology* **41**, 759–762.

Genty, D., Blamart, D., Ouahdi, R., Gilmour, M., Baker, A., Jouzel, J., Van-Exter, S., 2003. Precise dating of Dansgaard-Oeschger climate oscillations in western Europe from stalagmite data. *Nature* **421**, 833–837. https://doi.org/10.1038/nature01391

Genty, D., Combourieu-Nebout, N., Peyron, O., Blamart, D., Wainer, K., Mansuri, F., Ghaleb, B., Isabello, L., Dormoy, I., von Grafenstein, U., Bonelli, S., Landais, A., Brauer, A., 2010. Isotopic characterization of rapid climatic events during OIS3 and OIS4 in Villars Cave stalagmites (SW-France) and correlation with Atlantic and Mediterranean pollen records. *Quaternary Science Reviews* **29**, 2799–2820. https://doi.org/10.1016/j.quascirev.2010.06.035

Geshi, N., Maeno, F., Nakagawa, S., Naruo, H., Kobayashi, T., 2017. Tsunami deposits associated with the 7.3 ka caldera-forming eruption of the Kikai Caldera, insights for tsunami generation during submarine caldera-forming eruptions. *Journal of Volcanology and Geothermal Research* **347**, 221–233.

Geyer, A., Martí, J., 2008. The new worldwide collapse caldera database (CCDB): A tool for studying and understanding caldera processes. *Journal of Volcanology and Geothermal Research* **175**, 334–354. https://doi.org/10.1016/j.jvolgeores.2008.03.017

Gibbard, P., van Kolfschoten, T., 2004. The Pleistocene and Holocene Epochs, in: Gradstein, F. M., Ogg, J. G., Smith, A.G. (Ed.), A Geologic Time Scale. Cambridge University Press, Cambridge.

Gibbard, P.L., Head, M, J., Walker, M.J.C., the S. on Q.S., 2010. Formal ratification of the Quaternary System/Period and the Pleistocene Series/Epoch with a base at 2.58 Ma. *Journal of Quaternary Science* **25**, 96–102.

Goede, A., McCulloch, M., McDermott, F., Hawkesworth, C., 1998. Aeolian contribution to strontium and strontium isotope variations in a Tasmanian speleothem. *Chemical Geology* **149**, 37–50. https://doi.org/10.1016/S0009-2541(98)00035-7

Górka, M., Jdrysek, M. -O., Strąpoć, D., 2008. Isotopic composition of sulphates from meteoric precipitation as an indicator of pollutant origin in Wroclaw (SW Poland). *Isotopes in Environmental and Health Studies* **44**, 177–188.

Gothmann, A.M., Stolarski, J., Adkins, J.F., Schoene, B., Dennis, K.J., Schrag, D.P., Mazur, M., Bender, M.L., 2015. Fossil corals as an archive of secular variations in seawater chemistry since the Mesozoic. *Geochimica et Cosmochimica Acta* **160**, 188–208. https://doi.org/10.1016/j.gca.2015.03.018

Gottschalk, J., Skinner, L.C., Misra, S., Waelbroeck, C., Menviel, L., Timmermann, A., 2015. Abrupt changes in the southern extent of North Atlantic Deep Water during Dansgaard-Oeschger events. *Nature Geoscience* **8**, 950–954. https://doi.org/10.1038/ngeo2558

Green, R.M., Bebbington, M.S., Jones, G., Cronin, S.J., Turner, M.B., 2016. Estimation of tephra volumes from sparse and incompletely observed deposit thicknesses. *Bulletin of Volcanology* **78**, 1–18. https://doi.org/10.1007/s00445-016-1016-5

Griffiths M. L., Drysdale R. N., Gagan M. K., Frisia S., Zhao J. X., Ayliffe L. K., Hantoro W. S., Hellstrom J. C., Fischer M. J., Feng Y. X., S.B.W., 2010. Evidence for Holocene changes in Australian-Indonesian monsoon rainfall from stalagmite trace element and stable isotope ratios. *Earth & Planetary Science Letters* **292**, 27–38.

Griffiths, M.L., Drysdale, R.N., Gagan, M.K., Hellstrom, J.C., Couchoud, I., Ayliffe, L.K., Vonhof, H.B., Hantoro, W.S., 2013. Australasian monsoon response to Dansgaard-Oeschger event 21 and teleconnections to higher latitudes. *Earth and Planetary Science Letters* **369**–**370**, 294–304. https://doi.org/10.1016/j.epsl.2013.03.030

Griffiths, N., Müller, W., Johnson, K.G., Aguilera, O.A., 2013. Evaluation of the effect of diagenetic cements on element/Ca ratios in aragonitic Early Miocene (~16Ma) Caribbean corals: Implications for “deep-time” palaeo-environmental reconstructions. *Palaeogeography, Palaeoclimatology, Palaeoecology* **369**, 185–200. https://doi.org/10.1016/j.palaeo.2012.10.018

Griggs, A.J., Davies, S.M., Abbott, P.M., Rasmussen, T.L., Palmer, A.P., 2014. Optimising the use of marine tephrochronology in the North Atlantic: A detailed investigation of the Faroe Marine Ash Zones II, III and IV. *Quaternary Science Reviews* **106**, 122–139. https://doi.org/10.1016/j.quascirev.2014.04.031

Grove, J., 2004. Little Ice Ages: Ancient and Modern. Routledge, New York.

Gualda, G.A., Ghiorso, M.S., 2013. The Bishop Tuff giant magma body: an alternative to the Standard Model. *Contributions to Mineralogy and Petrology* **166**, 755–775.

Gualda, G.A.R., Gravley, D.M., Deering, C.D., Ghiorso, M.S., 2019. Magma extraction pressures and the architecture of volcanic plumbing systems. *Earth and Planetary Science Letters* **522**, 118–124. https://doi.org/10.1016/j.epsl.2019.06.020

Gudmundsdóttir, E.R., Larsen, G., Björck, S., Ingólfsson, Ó., Striberger, J., 2016. A new high-resolution Holocene tephra stratigraphy in eastern Iceland: Improving the Icelandic and North Atlantic tephrochronology. *Quaternary Science Reviews* **150**, 234–249. https://doi.org/10.1016/j.quascirev.2016.08.011

Gudmundsson, G.H., 2013. Ice-shelf buttressing and the stability of marine ice sheets. *Cryosphere* **7**, 647–655. https://doi.org/10.5194/tc-7-647-2013

Guillet, S., Corona, C., Ludlow, F., Oppenheimer, C., Stoffel, M., 2020. Climatic and societal impacts of a "forgotten" cluster of volcanic eruptions in 1108-1110 CE. *Scientific Reports* **10**. https://doi.org/10.1038/s41598-020-63339-3

Guillet, S., Corona, C., Stoffel, M., Khodri, M., Lavigne, F., Ortega, P., Eckert, N., Sielenou, P.D., Daux, V., Churakova Sidorova, O. V., Davi, N., Edouard, J.L., Zhang, Y., Luckman, B.H., Myglan, V.S., Guiot, J., Beniston, M., Masson-Delmotte, V., Oppenheimer, C., 2017. Climate response to the Samalas volcanic eruption in 1257 revealed by proxy records. *Nature Geoscience* **10**, 123–128. https://doi.org/10.1038/ngeo2875

Gunawan, H., Surono., Budianto, A., Kristiano., Prambada, O., McCausland, W., Pallister, J., Iguchi, M., 2019. Overview of the eruptions of Sinabung Volcano, 2010 and 2013–present and details of the 2013 phreatomagmatic phase. *Journal of Volcanology and Geothermal Research* **382**, 103–119.

Gündalı, N., 1989. Dim Mağarası (Alanya) Araştırma Raporu, Mimari ve Elektrikasyon Uygulama Projeleri. General Directorate of Mineral Research and Exploration, Ankara, Turkey.

Günther, D., Hattendorf, B., 2005. Solid sample analysis using laser ablation inductively coupled plasma mass spectrometry. *Trends in Analytical Chemistry* **24**, 255–265.

Guo, S., Bluth, G. J.S., Rose, W.I., Watson, I.M., Prata, A.J., 2004. Re-evaluation of SO2 release of the 15 June 1991 Pinatubo eruption using ultraviolet and infrared satellite sensors. *Geochemistry, Geophysics, Geosystems* **5**, Q04001.

Gutjahr, M., Lippold, J., 2011. Early arrival of Southern Source Water in the deep North Atlantic prior to Heinrich event 2. *Paleoceanography* **26**, 1–9. https://doi.org/10.1029/2011PA002114

Hall, V.A., Pilcher, J.R., 2002. Late-Quaternary Icelandic tephras in Ireland and Great Britain: detection, characterization and usefulness. *The Holocene* **12**, 223–230.

Hare, D., Austin, C., Doble, P., 2012. Quantification strategies for elemental imaging of biological samples using laser ablation inductively coupled plasma-mass spectrometry. *Analyst* **137**, 1527.

Harning, D.J., Geirsdóttir, Á., Miller, G.H., 2018. Punctuated Holocene climate of Vestfirðir, Iceland, linked to internal/external variables and oceanographic conditions. *Quaternary Science Reviews* **189**, 31–42.

Hartland, A., Fairchild, I.J., Lead, J.R., Borsato, A., Baker, A., Frisia, S., Baalousha, M., 2012. From soil to cave: Transport of trace metals by natural organic matter in karst dripwaters. *Chemical Geology* **304**–**305**, 68–82. https://doi.org/10.1016/j.chemgeo.2012.01.032

Hartmann, A., Baker, A., 2017. Modelling karst vadose zone hydrology and its relevance for paleoclimate reconstruction. *Earth-Science Reviews* **172**, 178–192.

Haslam, M., Petraglia, M., 2010. Comment on "Environmental impact of the 73 ka Toba super-eruption in South Asia. *Paleogeography, Paleoclimatology, Paleoecology* **296**, 199–203.

Haywood, J. M., Jones, A., Bellouin, N., Stephenson, D., 2013. Asymmetric forcing from stratospheric aerosols impacts Sahelian rainfall. *Nature Climate Change* **3**, 660–665.

He, C., Liu, Z., Zhu, J., Zhang, J., Gu, S., Otto-Bliesner, B.L., Brady, E., Zhu, C., Jin, Y., Sun, J., 2020. North Atlantic subsurface temperature response controlled by effective freshwater input in "Heinrich" events. *Earth and Planetary Science Letters* **539**, 116247. https://doi.org/10.1016/j.epsl.2020.116247

Head, M.J., Gibbard, P.L., 2015. Formal subdivision of the Quaternary System/Period: Past, present, and future. *Quaternary International* **383**, 4–35.

Heineke, C., Niedermann, S., Hetzel, R., Akal, C., 2016. Surface exposure dating of Holocene basalt flows and cinder cones in the Kula volcanic field (Western Turkey) using cosmogenic 3He and 10Be. *Quaternary Geochronology* **34**, 81–91. https://doi.org/10.1016/j.quageo.2016.04.004

Heinrich, H., 1988. Origin and consequences of cyclic ice rafting in the Northeast Atlantic Ocean during the past 130,000 years. *Quaternary Research* **29**, 142–152. https://doi.org/10.1016/0033-5894(88)90057-9

Hemming, S.R., 2004. Heinrich events: Massive late Pleistocene detritus layers of the North Atlantic and their global climate imprint. *Reviews of Geophysics* **42**. https://doi.org/10.1029/2003RG000128

Henry, L.G., McManus, J. F., Curry, W.B., Roberts, N. L., Piotrowski, A.M., Keigwin, L.D., 2016. North Atlantic ocean circulation and abrupt climate change during the last glaciation. *Science* **353**, 470–474.

Hepworth, L.N., Daly, J.S., Gertisser, R., Johnson, C.G., Emeleus, H., O'Driscoll, B., 2020. Rapid crystallization of precious-metal-mineralized layers in mafic magmatic systems. *Nature Geoscience* **13**, 375–381.

Hernández, A., Martin-Puertas, C., Moffa-Sánchez, P., Moreno-Chamarro, E., Ortega, P., Blockley, S., Cobb, K., Comas-Bru, L., Giralt, S., Goosse, H., Luterbacher, J., Martrat, B., Muscheler, R., Parnell, A., Pla-Rabes, S., Sjolte, J., Scaife, A., Swingedouw, D., Wise, E., Xu, G., 2020. Modes of climate variability: Synthesis and review of proxy-based reconstructions through the Holocene. *Earth-Science Reviews* **209**, 103286. https://doi.org/10.1016/j.earscirev.2020.103286

Heydolph, K., Hoernle, K., Hauff, F., van den Bogaard, P., Portnyagin, M., Bindeman, I., Garbe-Schönberg, D., 2012. Along and across arc geochemical variations in NW Central America: Evidence for involvement of lithospheric pyroxenite. *Geochimica et Cosmochimica Acta* **84**, 459–491.

Hildreth, W., 1987. New perspectives on the eruption of 1912 in the Valley of Ten Thousand Smokes, Katmai National Park, Alaska. *Bulletin of Volcanology* **49**, 680–693.

Hildreth, W., 2004. Volcanological perspectives on Long Valley, Mammoth Mountain, and Mono Craters: several contiguous but discrete systems. *Journal of Volcanology and Geothermal Research* **136**, 169–198.

Hildreth, W., Fierstein, J., 2012. The Novarupta-Katmai eruption of 1912—largest eruption of the twentieth century; centennial perspectives. *U.S. Geological Survey Professional Paper* **1791**, 259.

Hildreth, W., Fierstein, J., 2000. Katmai volcanic cluster and the great eruption of 1912. *Geological Society of America Bulletin* **112**, 1594–1620.

Hodell, D.A., Anselmetti, F.S., Ariztegui, D., Brenner, M., Curtis, J.H., Gilli, A., Grzesik, D.A., Guilderson, T.J., Müller, A.D., Bush, M.B., Correa-Metrio, A., Escobar, J., Kutterolf, S., 2008. An 85-ka record of climate change in lowland Central America. *Quaternary Science Reviews* **27**, 1152–1165. https://doi.org/10.1016/j.quascirev.2008.02.008

Hoernle, K., Abt, D., Fischer, K., Nichols, H., Hauff, F., Abers, G., van den Bogaard, P., Heydolph, K., Alvarado, G.E., Protti, M., Strauch, W., 2008. Arc-parallel flow in the mantle wedge beneath Costa Rica and Nicaragua. *Nature* **451**, 1094–1097.

Hoernle, K., van den Bogaard, P., Werner, R., Lissinna, B., Alvarado, G.E., Garbe-Schonberg, C.-D., 2002. Missing history (16-71 Ma) of the Galapagos hotspot: Implications for the tectonic and biological evolution of the Americas. *Geology* **30**, 795–798.

Hoffman, J. S., Carlson, A.E., Winsor, K., Klinkhammer, G.P., LeGrande, A.N., Andrews, J.T., Strasser, J.C., 2012. Linking the 8.2 ka event and its freshwater forcing in the Labrador Sea. *Geophysical Research Letters* **39**, L18703.

Hoffmann, D.L., Rogerson, M., Spötl, C., Luetscher, M., Vance, D., Osborne, A.H., Fello, N.M., Moseley, G.E., 2016. Timing and causes of North African wet phases during the last glacial period and implications for modern human migration. *Scientific Reports* **6**, 1–7. https://doi.org/10.1038/srep36367

Holasek, R. E., Self, S., Woods, A.W., 1996. Satellite observations and interpretation of the 1991 Mount Pinatubo eruption plumes. *Journal of Geophysical Research* **101**, 27635–27655.

Holness, M.B., 2018. Melt segregation from silicic crystal mushes: a critical appraisal of possible mechanisms and their microstructural record. *Contributions to Mineralogy and Petrology* **173**, 1–17. https://doi.org/10.1007/s00410-018-1465-2

Holton, J. R., Haynes, P.H., McIntyre, M. E., Douglass, A. R., Rood, R. B., Pfister, L., 1995. Stratosphere-troposphere exchange. *Reviews of Geophysics* **33**, 403–439.

Houghton, B.F., Swanson, D.A., Rausch, J., Carey, R.J., Fagents, S.A., Orr, T.R., 2013. Pushing the volcanic explosivity index to its limit and beyond: Constraints from exceptionally weak explosive eruptions at Kilauea in 2008. *Geology* **41**, 627–630. https://doi.org/10.1130/G34146.1

Housley, R.A., MacLeod, A., Nalepka, D., Jurochnik, A., Masojć, M., Davies, L., Lincoln, P.C., Bronk Ramsey, C., Gamble, C.S., Lowe, J.J., 2014. Tephrostratigraphy of a Lateglacial lake sediment sequence at Węgliny, southwest Poland. *Quaternary Science Reviews* **77**, 4–18. https://doi.org/10.1016/j.quascirev.2013.07.014

Hu, Z. C., Liu, Y. S., Chen, L., Zhou, L., Li, M., Zong, K., Zhu, L., Gao, S., 2011. Contrasting matrix induced elemental fractionation in NIST SRM and rock glasses during laser ablation ICP-MS analysis at high spatial resolution. *Journal of Analytical Atomic Spectrometry* **26**, 425–430.

Huang Y. M., F.I.J., 2001. Partitioning of Sr2+ and Mg2+ into calcite under karst-analogue experimental conditions. *Geochimica et Cosmochimica Acta* **65**, 47–62.

Hudson, R.D., 2012. Measurements of the movement of the jet streams at mid-latitudes, in the Northern and Southern Hemispheres, 1979 to 2010. *Atmospheric Chemistry and Physics* **12**, 7797–7808.

Hulbe, C.L., 1997. An ice shelf mechanism for Heinrich layer production. *Paleoceanography* **12**, 711–717.

Hulbe, C.L., Macayeal, D.R., Denton, G.H., Kleman, J., Lowell, T. V, 2004. Catastrophic ice shelf breakup as the source of Heinrich event icebergs. *Paleoceanography* **19**, PA1004. https://doi.org/10.1029/2003PA000890

IPCC, 2014. Climate Change 2014: Synthesis Report, in: Pachauri, R.K., Meyer, L.A. (Ed.), Contribution of Working Groups I, II and III to the Fifth Assessment Report of the Intergovernmental Panel on Climate Change. IPCC, Switzerland, p. 151.

Irvem, A., Ozbuldu, M., 2019. Evaluation of Satellite and Reanalysis Precipitation Products Using GIS for All Basins in Turkey. *Advances in Meteorology* **2019**, 1–11. https://doi.org/10.1155/2019/4820136

Jackson, L.J., Stone, J.R., Cohen, A.S., Yost, C.L., 2015. High-resolution paleoecological records from Lake Malawi show no significant cooling associated with the Mount Toba supereruption at ca. 75 ka. *Geology* **43**, 823–826.

Jackson, M.D., Blundy, J., Sparks, R.S.J., 2018. Chemical differentiation, cold storage and remobilization of magma in the Earth's crust. *Nature* **564**, 405–409. https://doi.org/10.1038/s41586-018-0746-2

Jackson, S.E., Longerich, H.P., Horn, I. & Dunning, R., 1996. The application of laser ablation microprobe (LAM)-ICP-MS to in situ U-Pb zircon geochronology. *Journal of Conference Abstracts* **1**, 283.

Jacobson, T.W.P., Yang, W., Vecchi, G.A., Horowitz, L.W., 2020. Impact of volcanic aerosol hemispheric symmetry on Sahel rainfall. *Climate Dynamics* **55**, 1733–1758. https://doi.org/10.1007/s00382-020-05347-7

Jamieson, R. A., Baldini, J. U. L., Brett, M. J., Taylor, J., Ridley, H. E., Ottley, C. J., Prufer, K. M., Wassenburg, J. A., Scholz, D., Breitenbach, S.F.M., 2016. Intra- and inter-annual uranium concentration variability in a Belizean stalagmite controlled by prior aragonite precipitation: a new tool for reconstructing hydro-climate using aragonitic speleothems. *Geochimica et Cosmochimica Acta* **190**, 332–346.

Janebo, M.H., Thordarson, T., Houghton, B.F., Bonadonna, C., Larsen, G., Carey, R.J., 2016. Dispersal of key subplinian – Plinian tephras from Hekla volcano, Iceland : implications for eruption source parameters. *Bulletin of Volcanology* **78**, 66. https://doi.org/10.1007/s00445-016-1059-7

Jaxybulatov, K., Shapiro, N.M., Koulakov, I., Mordret, A., Landés, M., Sens-Schönfelder, C., 2014. A large magmatic sill complex beneath the Toba caldera. *Science* **346**, 617–619.

Jeffries, T.E., Jackson, S.E., Longerich, H.P., 1998. Application of a frequency quintupled Nd : YAG source (λ = 213 nm) for laser ablation inductively coupled plasma mass spectrometric analysis of minerals. *Journal of Analytical Atomic Spectrometry* **13**, 935–940.

Jensen, B.J.L., Pyne-O'Donnell, S., Plunkett, G., Froese, D.G., Hughes, P.D.M., Sigl, M., McConnell, J.R., Amesbury, M.J., Blackwell, P.G., van den Bogaard, C., Buck, C.E., Charman, D.J., Clague, J.J., Hall, V.A., Koch, J., Mackay, H., Mallon, G., McColl, L., Pilcher, J.R., 2014. Transatlantic distribution of the Alaskan White River Ash. *Geology* **42**, 875–878. https://doi.org/10.1130/G35945.1

Jessop, D.E., Gilchrist, J., Jellinek, A.M., Roche, O., 2016. Are eruptions from linear fissures and caldera ring dykes more likely to produce pyroclastic flows? *Earth and Planetary Science Letters* **454**, 142–153. https://doi.org/10.1016/j.epsl.2016.09.005

Jochum, K.P., Scholz, D., Stoll, B., Weis, U., Wilson, S.A., Yang, Q., Schwalb, A., Börner, N., Jacob, D.E., Andreae, M.O., 2012. Accurate trace element analysis of speleothems and biogenic calcium carbonates by LA-ICP-MS. *Chemical Geology* **318**–**319**, 31–44. https://doi.org/10.1016/j.chemgeo.2012.05.009

Johnson, H.L., Cessi, P., Marshall, D.P., Schloesser, F., Spall, M.A., 2019. Recent Contributions of Theory to Our Understanding of the Atlantic Meridional Overturning Circulation. *Journal of Geophysical Research: Oceans* **124**, 5376–5399. https://doi.org/10.1029/2019JC015330

Johnson, R.G., Lauritzen, S.-E., 1995. Hudson Bay-Hudson Strait jokulhlaups and Heinrich events: a hypothesis. *Paleogeography, Paleoclimatology, Paleoecology* **117**, 123–137.

Johnston, E.N., Sparks, R.S.J., Phillips, J.C., Carey, S., 2014. Revised estimates for the volume of the late bronze age Minoan eruption, Santorini, Greece. *Journal of the Geological Society* **171**, 583–590. https://doi.org/10.1144/jgs2013-113

Jones, G.S., Gregory, J.M., Stott, P.A., Tett, S.F.B., Thorpe, R.B., 2005. An AOGCM model of the climate response to a volcanic super-eruption. *Climate Dynamics* **25**, 725–738.

Jones, G., Davies, S.M., Staff, R.A., Loader, N.J., Davies, S.J., Walker, M.J.C., 2020. Traces of volcanic ash from the Mediterranean, Iceland and North America in a Holocene record from south Wales, UK. *Journal of Quaternary Science* **35**, 163–174. https://doi.org/10.1002/jqs.3141

Jones, M.T., Gislason, S.R., 2008. Rapid releases of metal salts and nutrients following the deposition of volcanic ash into aqueous environments. *Geochimica et Cosmochimica Acta* **72**, 3661–3680.

Jones, M.T., 2015. The environmental and climatic impacts of volcanic ash deposition. *Volcanism and Global Environmental Change* 260–274. https://doi.org/10.1007/9781107415683.018

Jordan, S.F., Murphy, B.T., O'Reilly, S.S., Doyle, K.P., Williams, M.D., Grey, A., Lee, S., McCaul, M.V., Kelleher, B.P., 2017. Mid-Holocene climate change and landscape formation in Ireland: evidence from a geochemical investigation of a coastal peat bog. *Organic Geochemistry* **109**, 67–76.

Joshi, M.M., Jones, G. s., 2009. The climatic effects of the direct injection of water vapour into the stratosphere by large volcanic eruptions. *Atmospheric Chemistry and Physics* **9**, 6109–6118. https://doi.org/10.5194/acp-9-6109-2009

Joughin, I., Das, S. B., King, M.A., Smith, B.E., Howat, I.M., Moon, T., 2008. Seasonal speedup along the Western margin of the Greenland ice sheet. *Science* **320**, 781–783.

Kageyama, M., Merkel, U., Otto-Bliesner, B., Prange, M., Abe-Ouchi, A., Lohmann, G., Ohgaito, R., Roche, D.M., Singarayer, J., Swingedouw, D., Zhang, X., 2013. Climatic impacts of fresh water hosing under Last Glacial Maximum conditions : a multi-model study. *Climate of the Past* **9**, 935–953. https://doi.org/10.5194/cp-9-935-2013

Kalliokoski, M., Guðmundsdóttir, E.R., Wastegård, S., 2020. Hekla 1947, 1845, 1510 and 1158 tephra in Finland : challenges of tracing tephra from moderate eruptions. *Journal of Quaternary Science* 1–14. https://doi.org/10.1002/jqs.3228

Kandlbauer, J., Sparks, R.S.J., 2014. New estimates of the 1815 Tambora eruption volume. *Journal of Volcanology and Geothermal Research* **286**, 93–100. https://doi.org/10.1016/j.jvolgeores.2014.08.020

Kanner, L.C., Burns, S.J., Cheng, H., Edwards, R.L., 2016. High-Latitude Forcing of the South American Summer Monsoon During the Last Glacial **328**, 1652–1656.

Karlstrom, L., Dufek, J., Manga, M., 2010. Magma chamber stability in arc and continental crust. *Journal of Volcanology and Geothermal Research* **190**, 249–270. https://doi.org/10.1016/j.jvolgeores.2009.10.003

Karmann, I., Cruz, F.W., Viana Jr., O., Burns, S.J., 2007. Climate influence on trace element geochemistry of waters from Santana–Pérolas cave system, Brazil. *Chemical Geology* **244**, 232–247.

Kasprzak, M., Sobczyk, A., 2015. Searching for the void: improving cave detection accuracy by multi-faceted geophysical survey reconciled with LiDAR DTM. *Zeitschrift für Geomorphologie* **59**, 227–245. https://doi.org/10.1127/zfg

Kataoka, K.S., Nagahashi, Y., 2019. From sink to volcanic source: Unravelling missing terrestrial eruption records by characterization and high-resolution chronology of lacustrine volcanic density flow deposits, Lake Inawashiro-ko, Fukushima, Japan. *Sedimentology* **66**, 2784–2827.

Kathayat, G., Cheng, H., Sinha, A., Spötl, C., Edwards, R.L., Zhang, H., Li, X., Yi, L., Ning, Y., Cai, Y., Lui, W.L., Breitenbach, S.F.M., 2016. Indian monsoon variability on millennial-orbital timescales. *Scientific Reports* **6**, 4–10. https://doi.org/10.1038/srep24374

Kaufman, A., Wasserburg, G.J., Porcelli, D., Bar-Matthews, M., Ayalon, A., Halicz, L., 1998. U-Th isotope systematics from the Soreq cave, Israel and climatic correlations. *Earth and Planetary Science Letters* **156**, 141–155. https://doi.org/10.1016/s0012-821x(98)00002-8

Kekonen, T., Moore, J., Perämäki, P., Martma, T., 2005. The Icelandic Lakí volcanic tephra layer in the Lomonosovfonna ice core, Svalbard. *Polar Research* **24**, 33–40.

Kennedy, B.M., Holohan, E.P., Gravley, D.M., Davidson, J.R.J., Cole, J.W., 2018. Magma plumbing beneath collapse caldera volcanic systems. *Earth-Science Reviews* **177**, 404–424.

Keskin, S., Kapur, S., 2001. SOIL GEOGRAPHICAL DATABASE OF TURKEY AT A SCALE 1 : 1,000.000 4th APPROXIMATION by General Directorate of Rural Services. *Anatolia* 1–16.

Kinder, M., Wulf, S., Appelt, O., Hardiman, M., Żarczyński, M., Tylmann, W., 2020. Late-Holocene ultra-distal cryptotephra discoveries in varved sediments of Lake Żabińskie, NE Poland. *Journal of Volcanology and Geothermal Research* **402**, 106988. https://doi.org/10.1016/j.jvolgeores.2020.106988

Kindler, P., Guillevic, M., Baumgartner, M., Schwander, J., Landais, A., Leuenberger, M., 2014. Temperature reconstruction from 10 to 120 kyr b2k from the NGRIP ice core. *Climate of the Past* **10**, 887–902. https://doi.org/10.5194/cp-10-887-2014

King, M.D., Howat, I.M., Candela, S.G., Noh, M.J., Jeong, S., Noël, B.P.Y., van den Broeke, M.R., Wouters, B., Negrete, A., 2020. Dynamic ice loss from the Greenland Ice Sheet driven by sustained glacier retreat. *Communications Earth & Environment* **1**, 1–7. https://doi.org/10.1038/s43247-020-0001-2

Kiyosugi, K., Connor, C., Sparks, R.S.J., Crosweller, H.S., Brown, S.K., Siebert, L., Wang, T., Takarada, S., 2015. How many explosive eruptions are missing from the geologic record? Analysis of the quaternary record of large magnitude explosive eruptions in Japan. *Journal of Applied Volcanology* **4**, 17.

Kleiven, H.K.F., Kissel, C., Laj, C., Ninnemann, U.S., Richter, T.O., Cortijo, E., 2008. Reduced North Atlantic deep water coeval with the glacial Lake Agassiz freshwater outburst. *Science* **319**, 60–64.

Kleppin, H., Jochum, M., Otto-Bliesner, B., Shields, A., Yeager, S., 2015. Stochastic Atmospheric Forcing as a Cause of Greenland Climate Transitions. *Journal of Climate* **28**, 7741–7763. https://doi.org/10.1175/JCLI-D-14-00728.1

Klobas, E.J., Wilmouth, D.M., Weisenstein, D.K., Anderson, J.G., Salawitch, R.J., 2017. Ozone depletion following future volcanic eruptions. *Geophysical Research Letters* **44**, 7490–7499. https://doi.org/10.1002/2017GL073972

Klockmann, M., Mikolajewicz, U., and Marotzke, J., 2018. Two AMOC States in Response to Decreasing Greenhouse Gas Concentrations in the Coupled Climate Model MPI-ESM. *Journal of Climate* **31**, 7969–7984.

Kobashi, T., Kawamura, K., Severinghaus, J.P., Barnola, J-M., Nakaegawa, T., Vinther, B.M., Johnsen, S.J., Box, J.E., 2011. High variability of Greenland surface temperature over the past 4000 years estimated from trapped air in an ice core. *Geophysical Research Letters* **38**, L21501.

Kobashi, T., Menviel, L., Jeltsch-Thömmes, A., Vinther, B.M., Box, J.E., Muscheler, R., Nakaegawa, T., Pfister, P.L., Döring, M., Leuenberger, M., Wanner, H., Ohmura, A., 2017. Volcanic influence on centennial to millennial Holocene Greenland temperature change. *Scientific Reports* **7**, 1–10. https://doi.org/10.1038/s41598-017-01451-7

Kobashi, T., Severinghaus, J.P., Brook, E.J., Barnola, J.M., Grachev, A.M., 2007. Precise timing and characterization of abrupt climate change 8200 years ago from air trapped in polar ice. *Quaternary Science Reviews* **26**, 1212–1222. https://doi.org/10.1016/j.quascirev.2007.01.009

Koç, G., Thieken, A.H., 2018. The relevance of flood hazards and impacts in Turkey: What can be learned from different disaster loss databases?, Natural Hazards. https://doi.org/10.1007/s11069-017-3134-6

Koch, A.J., McLean, H., 1975. Pleistocene Tephra and Ash-Flow Deposits in the Volcanic Highlands of Guatemala. *GSA Bulletin* **86**, 529–541.

Kohlstedt, D.L., Holtzman, B.K., 2009. Shearing Melt Out of the Earth: An Experimentalist's Perspective on the Influence of Deformation on Melt Extraction. *Annual Review of Earth and Planetary Sciences* **37**, 561–593. https://doi.org/10.1146/annurev.earth.031208.100104

Konecky, B.L., Russell, J.M., Johnson, T.C., Brown, E.T., Berke, M.A., Werne, J.P., Huang, Y., 2011. Atmospheric circulation patterns during late Pleistocene climate changes at Lake Malawi, Africa. *Earth and Planetary Science Letters* **312**, 318–326. https://doi.org/10.1016/j.epsl.2011.10.020

Kravitz, B., Robock, A., 2011. Climate effects of high-latitude volcanic eruptions: Role of the time of year. *Journal of Geophysical Research* **116**, D01105.

Kroslakova, I., Günther, D., 2007. Elemental fractionation in laser ablation-inductively coupled plasma-mass spectrometry: Evidence for mass load induced matrix effects in the ICP during ablation of a silicate glass. *Journal of Analytical Atomic Spectrometry* **22**, 51–62.

Kurt, L., Ketenoğlu, A.O., Akman, Y., Özdeniz, E., Şekerciler, F., Bölükbaşi, A., Özbey, B.G., 2015. Syntaxonomic analysis of the preforest and forest vegetation in the thermo-and eumediterranean zone around Antalya Gulf, Turkey. *Turkish Journal of Botany* **39**, 487–498.

Kutterolf, S., Freundt, A., Peréz, W., 2008. Pacific offshore record of plinian arc volcanism in Central America: 2. Tephra volumes and erupted masses. *Geochemistry, Geophysics, Geosystems* **9**, n/a-n/a. https://doi.org/10.1029/2007gc001791

Kutterolf, S., Freundt, A., Peréz, W., Mörz, T., Schacht, U., Wehrmann, H., Schmincke, H.-U., 2008. Pacific offshore record of plinian arc volcanism in Central America: 1. Along-arc correlations. *Geochemistry, Geophysics, Geosystems* **9**, n/a-n/a. https://doi.org/10.1029/2007gc001631

Kutterolf, S., Schindlbeck- Belo, J.C., Rohr, I., Rademacher, M., de León, A.C., Eisele, S., Freundt, A., Hernandez, W., Wang, K.L., 2020. The Arce Tephra: Two subsequent paroxysmal Plinian eruptions from Coatepeque Caldera (El Salvador). *Journal of Volcanology and Geothermal Research* **390**, 106673. https://doi.org/10.1016/j.jvolgeores.2019.106673

Kutterolf, S., Schindlbeck, J.C., Anselmetti, F.S., Ariztegui, D., Brenner, M., Curtis, J., Schmid, D., Hodell, D.A., Mueller, A., Pérez, L., Pérez, W., Schwalb, A., Frische, M., Wang, K.L., 2016. A 400-ka tephrochronological framework for Central America from Lake Petén Itzá (Guatemala) sediments. *Quaternary Science Reviews* **150**, 200–220. https://doi.org/10.1016/j.quascirev.2016.08.023

Kutterolf, S., Schindlbeck, J.C., Jegen, M., Freundt, A., Straub, S.M., 2019. Milankovitch frequencies in tephra records at volcanic arcs: The relation of kyr-scale cyclic variations in volcanism to global climate changes. *Quaternary Science Reviews* **204**, 1–16. https://doi.org/10.1016/j.quascirev.2018.11.004

Kwiecien, O., Arz, H.W., Lamy, F., Plessen, B., Bahr, A., Haug, G.H., 2009. North Atlantic control on precipitation pattern in the eastern Mediterranean/Black Sea region during the last glacial. *Quaternary Research* **71**, 375–384. https://doi.org/10.1016/j.yqres.2008.12.004

Kwon, K., Kim, P.H., 2019. Will the Dormant Volcano Erupt Again? Mt. Paektu and Contemporary Sino-Korean Relations. *The Asia-Pacific Journal* **17**, 5232.

Kyle, P.R., Ponomareva, V. V., Rourke Schluep, R., 2011. Geochemical characterization of marker tephra layers from major Holocene eruptions, Kamchatka Peninsula, Russia. *International Geology Review* **53**, 1059–1097. https://doi.org/10.1080/00206810903442162

Laepple, T., Huybers, P., 2014. Ocean surface temperature variability: large model–data differences at decadal and longer periods. *Proceedings of the National Academy of Science USA* **111**, 16682–16687.

Lane, C.S., Lowe, D.J., Blockley, S.P.E., Suzuki, T., Smith, V.C., 2017. Advancing tephrochronology as a global dating tool: Applications in volcanology, archaeology, and palaeoclimatic research. *Quaternary Geochronology* **40**, 1–7. https://doi.org/10.1016/j.quageo.2017.04.003

Lane, C.S., Blockley, S.P.E., Mangerud, J., Smith, V.C., Lohne, Ø.S., Tomlinson, E.L., 2012. Was the 12.1 ka Icelandic Vedde Ash one of a kind? *Quaternary Science Reviews* **33**, 87–99.

Lane, C.S., Cullen, V.L., White, D., Bramham-Law, C.W.F., Smith, V.C., 2014. Cryptotephra as a dating and correlation tool in archaeology. *Journal of Archaeological Science* **42**, 42–50.

Lane, C.S., Chorn, B.T., Johnson, T.C., 2013. Ash from the Toba supereruption in Lake Malawi shows no volcanic winter in East Africa at 75 ka. *Proceedings of the National Academy of Sciences* **110**. https://doi.org/10.1073/pnas.1301474110

Larsen, G., 2000. Holocene eruptions within the Katla volcanic system, south Iceland: characteristics and environmental impact. *Jökull* **49**, 1–28.

Larsen, G., 2010. Katla: tephrochronology and eruption history. *Developments in Quaternary Science* **13**, 23–49.

Laumonier, M., Karakas, O., Bachmann, O., Gaillard, F., Lukács, R., Seghedi, I., Menand, T., Harangi, S., 2019. Evidence for a persistent magma reservoir with large melt content beneath an apparently extinct volcano. *Earth and Planetary Science Letters* **521**, 70–90.

Lavigne, F., Degeai, J.P., Komorowski, J.C., Guillet, S., Robert, V., Lahitte, P., Oppenheimer, C., Stoffel, M., Vidal, C.M., Suronoh, Pratomo, I., Wassmer, P., Hajdas, I., Hadmoko, D.S., De Belizal, E., 2013. Source of the great A.D. 1257 mystery eruption unveiled, Samalas volcano, Rinjani Volcanic Complex, Indonesia. *Proceedings of the National Academy of Sciences of the United States of America* **110**, 16742–16747. https://doi.org/10.1073/pnas.1307520110

Lawson, I.T., Swindles, G.T., Plunkett, G., Greenberg, D., 2012. The spatial distribution of Holocene cryptotephras in north-west Europe since 7 ka: Implications for understanding ash fall events from Icelandic eruptions. *Quaternary Science Reviews* **41**, 57–66. https://doi.org/10.1016/j.quascirev.2012.02.018

Lay, T., Kanamori, H., Ammon, C.J., Nettles, M., Ward, S.N., Aster, R., Beck, S.L., Bilek, S.L., Brudzinski, M.R., Butler, R., DeShon, H.R., Ekström, G., Satake, K., Sipkin, S., 2005. The Great Sumatra-Andaman Earthquake of 26 December 2004. *Science* **308**, 1127–1133.

Lead, J.R., Wilkinson, K.J., 2006. Aquatic colloids and nanoparticles: current knowledge and future trends. *Environmental Chemistry* **3**, 159–171.

Lechleitner, F.A., Fohlmeister, J., McIntyre, C., Baldini, L.M., Jamieson, R.A., Hercman, H., Gasiorowski, M., Pawlak, J., Stefaniak, K., Socha, P., Eglinton, T.I., Baldini, J.U.L., 2016. A novel approach for construction of radiocarbon-based chronologies for speleothems. *Quaternary Geochronology* **35**, 54–66. https://doi.org/10.1016/j.quageo.2016.05.006

Ledbetter, M.T., 1985. Tephrochronology of marine tephra adjacent to Central America. *GSA Bulletin* **96**, 77–82.

LeGrande, A.N., Schmidt, G.A., 2008. Ensemble, water isotope-enabled, coupled general circulation modelling insights into the 8.2 ka event. *Paleoceanography* **23**.

Lemos, A., Shepherd, A., McMillan, M., Hogg, A. E., Hatton, E., & Joughin, I., 2018. Ice velocity of Jakobshavn Isbræ, Petermann glacier, Nioghalvfjerdsfjorden, and Zachariæ Isstrøm, 2015–2017, from sentinel 1-a/b SAR imagery. *The Cryosphere* **12**, 2087–2097.

Lenton, T.M., Held, H., Kriegler, E., Hall, J.W., Lucht, W., Rahmstorf, S., Schellnhuber, H.J., 2008. Tipping elements in the Earth's climate system. *Proceedings of the National Academy of Sciences of the United States of America* **105**, 1786–1793. https://doi.org/10.1073/pnas.0705414105

Lerbekmo, J.F., 2008. The White River Ash: largest Holocene Plinian tephra. *Canadian Journal of Earth Sciences* **45**, 693–700.

Leydet, D. J., Carlson, A. E., Teller, J. T., Breckenridge, A., B., A. M., Ullman, D. J., Sinclair, G., Milne, G. A., Cuzzone, J.K., and Caffee, M.W., 2018. Opening of glacial Lake Agassiz's eastern outlets by the start of the Younger Dryas cold period. *Geology* **46**, 155–158.

Li, C., Battisti, D.S., Schrag, D.P., Tziperman, E., 2005. Abrupt climate shifts in Greenland due to displacements of the sea ice edge. *Geophysical Research Letters* **32**, L19702.

Li, Q., Parrish, R.R., Horstwood, M.S.A., McArthur, J.M., 2014. U-Pb dating of cements in Mesozoic ammonites. *Chemical Geology* **376**, 76–83. https://doi.org/10.1016/j.chemgeo.2014.03.020

Liang, X.R., Wei, G.J., Shao, L., Li, X.H., Wang, R.C., 2001. Records of Toba eruptions in the South China Sea - Chemical characteristics of the glass shards from ODP 1143A. *Science in China Series D – Earth Sciences* **44**, 871–878.

Lilja, C., Lind, E.M., Morén, B., Wastegård, S., 2013. A Lateglacial-early Holocene tephrochronology for SW Sweden. *Boreas* **42**, 544–554.

Limbeck, A., Galler, P., Bonta, M., Bauer, G., Nischkauer, W., V., 2015. Recent advances in quantitative LA-ICP-MS analysis: challenges and solutions in the life sciences and environmental chemistry. *Analytical and Bioanalytical Chemistry* **407**, 6593–6617.

Lin, J., Liu, Y., Yang, Y., Hu, Z., 2016. Calibration and correction of LA-ICP-MS and LA-MC-ICP-MS analyses for element contents and isotopic ratios. *Solid Earth Sciences* **1**, 5–27.

Liu, E.J., Cashman, K.V., Beckett, F.M., Witham, C.S., Leadbetter, S.J., Hort, M.C., Guðmundsson, S., 2014. Ash mists and brown snow: Remobilization of volcanic ash from recent Icelandic eruptions. *Journal of Geophysical Research: Atmospheres* **119**, 9463–9480.

Liu, F.G., Feng, Z.D., 2012. A dramatic climatic transition at ~4000 cal. yr BP and its cultural responses in Chinese cultural domains. *Holocene* **22**, 1181–1197.

Liu, W., Xie, S.P., Liu, Z., Zhu, J., 2017. Overlooked possibility of a collapsed Atlantic Meridional Overturning Circulation in warming climate. *Science Advances* **3**, e1601666.

Liu, Y., Shi, G., Xie, Y., 2013. Impact of dust aerosol on glacial-interglacial climate. *Advances in Atmospheric Sciences* **30**, 1725–1731. https://doi.org/10.1007/s00376-013-2289-7

Liu, Z., Colin, C., Trentesaux, A., 2006. Major element geochemistry of glass shards and minerals of the Youngest Toba Tephra in the southwestern South China Sea. *Journal of Asian Earth Sciences* **27**, 99–107. https://doi.org/10.1016/j.jseaes.2005.02.003

Lohmann, J., Ditlevsen, P.D., 2019. Objective extraction and analysis of statistical features of Dansgaard – Oeschger events. *Climate of the Past* **15**, 1771–1792.

Lohse, J.C., Hamilton, W.D., Brenner, M., Curtis, J., Inomata, T., Morgan, M., Cardona, K., Aoyama, K., Yonenobu, H., 2018. Late Holocene volcanic activity and environmental change in Highland Guatemala. *Quaternary Science Reviews* **191**, 378–392. https://doi.org/10.1016/j.quascirev.2018.05.014

Lolis, C.J., Türkeş, M., 2016. Atmospheric circulation characteristics favouring extreme precipitation in Turkey. *Climate Research* **71**, 139–153. https://doi.org/10.3354/cr01433

Loosmore, G.A., Cederwall, R.T., 2004. Precipitation scavenging of atmospheric aerosols for emergency response applications: testing an updated model with new real-time data. *Atmospheric Environment* **38**, 993–1003.

Lowe, D.J., Shane, P.A.R., Alloway, B.V., Newnham, R.M., 2008. Fingerprints and age models for widespread New Zealand tephra marker beds erupted since 30,000 years ago: a framework for NZ-INTIMATE. *Quaternary Science Reviews* **27**, 95–126.

Lowe, D.J., Pearce, N.J.G., Jorgensen, M.A., Kuehn, S.C., Tryon, C.A., Hayward, C.L., 2017. Correlating tephras and cryptotephras using glass compositional analyses and numerical and statistical methods: Review and evaluation. *Quaternary Science Reviews* **175**, 1–44. https://doi.org/10.1016/j.quascirev.2017.08.003

Lowe, J. J., Walker, M., 1997. Reconstructing Quaternary Environments, 2nd Editio. ed. Routledge, New York.

Lucci, F., Carrasco-Núñez, G., Rossetti, F., Theye, T., Charles White, J., Urbani, S., Azizi, H., Asahara, Y., Giordano, G., 2020. Anatomy of the magmatic plumbing system of Los Humeros Caldera (Mexico): Implications for geothermal systems. *Solid Earth* **11**, 125–159. https://doi.org/10.5194/se-11-125-2020

Lund, K. A., Benediktsson, K., 2011. Inhabiting a risky earth: The Eyjafjallajökull eruption in 2010 and its impacts. *Anthropology Today* **27**, 6–9.

Lynch-Stieglitz, J., 2017. The Atlantic Meridional Overturning Circulation and Abrupt Climate Change. *Annual Review of Marine Science* **9**, 83–104. https://doi.org/10.1146/annurev-marine-010816-060415

MacAyeal, D.R., 1993. Binge/purge oscillations of the Laurentide Ice Sheet as a cause of the North Atlantic's Heinrich events. *Paleoceanography* **8**, 775–784.

MacDonald, J.M., Faithfull, J.W., Roberts, N.M.W., Davies, A.J., Holdsworth, C.M., Newton, M., Williamson, S., Boyce, A., John, C.M., 2019. Clumped-isotope palaeothermometry and LA-ICP-MS U–Pb dating of lava-pile hydrothermal calcite veins. *Contributions to Mineralogy and Petrology* **174**, 1–15. https://doi.org/10.1007/s00410-019-1599-x

Macedonio, G., Costa, A., Folch, A., 2008. Ash fallout scenarios at Vesuvius: Numerical simulations and implications for hazard assessment. *Journal of Volcanology and Geothermal Research* **178**, 366–377.

Mackay, H., Hughes, P.D.M., Jensen, B.J.L., Langdon, P.G., Pyne-O'Donnell, S.D.F., Plunkett, G., Froese, D.G., Coulter, S., Gardner, J.E., 2016. A mid to late Holocene cryptotephra framework from eastern North America. *Quaternary Science Reviews* **132**, 101–113. https://doi.org/10.1016/j.quascirev.2015.11.011

Maeno, F., Taniguchi, H., 2007. Spatiotemporal evolution of a marine caldera-forming eruption, generating a low-aspect ratio pyroclastic flow, 7.3 ka, Kikai caldera, Japan: Implication from near-vent eruptive deposits. *Journal of Volcanology and Geothermal Research* **167**, 212–238.

Maher, N., McGregor, S., England, M., Sen Gupta, A., 2015. Effects of volcanism on tropical variability. *Geophysical Research Letters* **42**, 6024–6033.

Manatsa, D., Chingombe, W., Matarira, C.H., 2008. The impact of the positive Indian Ocean dipole on Zimbabwe droughts Tropical climate is understood to be dominated by. *International Journal of Climatology* **2029**, 2011–2029. https://doi.org/10.1002/joc

Mangini, A., Verdes, P., Spötl, C., Scholz, D., Vollweiler, N., Kromer, B., 2007. Persistent influence of the North Atlantic hydrography on central European winter temperature during the last 9000 years. *Geophysical Research Letters* **34**, L02704.

Mann, M. E., Zhang, Z., Hughes, M.K., Bradley, R.S., Miller, S.K., Rutherford, S., Ni, F., 2008. Proxy-based reconstructions of hemispheric and global surface temperature variations over the past two millennia. *Proceedings of the National Academy of Sciences USA* **105**, 13252–13257.

Mann, M.E., Zhang, Z., Rutherford, S., Bradley, R.S., Hughes, M.K., Shindell, D., Ammann, C., Faluvegi, G., Ni, F., 2009. Global signatures and dynamical origins of the little ice age and medieval climate anomaly. *Science* **326**, 1256–1260. https://doi.org/10.1126/science.1177303

Marcantonio, F., Hostak, R., Hertzberg, J.E., Schmidt, M.W., 2020. Deep Equatorial Pacific Ocean Oxygenation and Atmospheric CO2 over the Last Ice Age. *Scientific Reports* **10**, 1–10. https://doi.org/10.1038/s41598-020-63628-x

Marcott, S.A., Clark, P.U., Padman, L., Klinkhammer, G.P., Springer, S.R., Liu, Z., Otto-bliesner, B.L., Carlson, A.E., Padman, J., He, F., Cheng, J., Schmittner, A., 2011. Ice-shelf collapse from subsurface warming as a trigger for Heinrich events. *Proceedings of the National Academy of Sciences of the United States of America* **108**, 13415–13419. https://doi.org/10.1073/pnas.

Mark, D.F., Petraglia, M., Smith, V.C., Morgan, L.E., Barfod, D.N., Ellis, B.S., Pearce, N.J., Pal, J.N., Korisettar, R., 2014. A high-precision 40 Ar / 39 Ar age for the Young Toba Tuff and dating of ultra-distal tephra : Forcing of Quaternary climate and implications for hominin occupation of India. *Quaternary Geochronology* **21**, 90–103. https://doi.org/10.1016/j.quageo.2012.12.004

Mark, D.F., Renne, P.R., Dymock, R.C., Smith, V.C., Simon, J.I., Morgan, L.E., Staff, R.A., Ellis, B.S., Pearce, N.J.G., 2017. High-precision $^{40}Ar/^{39}Ar$ dating of Pleistocene tuffs and temporal anchoring of the Matuyama-Brunhes boundary. *Quaternary Geochronology* **39**, 1–23. https://doi.org/10.1016/j.quageo.2017.01.002

Markle, B.R., Steig, E.J., Buizert, C., Schoenemann, S.W., Bitz, C.M., Fudge, T.J., Pedro, J.B., Ding, Q., Jones, T.R., White, J.W.C., Sowers, T., 2017. Global atmospheric teleconnections during Dansgaard–Oeschger events. *Nature Geoscience* **10**, 36–40. https://doi.org/10.1038/NGEO2848

Martin, C., Ménot, G., Thouveny, N., Davtian, N., Andrieu-Ponel, V., Reille, M., Bard, E., 2019. Impact of human activities and vegetation changes on the tetraether sources in Lake St Front (Massif Central, France). *Organic Geochemistry* **135**, 38–52.

Martin, R.S., Watt, S.F.L., Pyle, D.M., Mather, T.A., Matthews, N.E., Georg, R.B., Day, J.A., Fairhead, T., Witt, M.L.I., Quayle, B.M., 2009. Environmental effects of ashfall in Argentina from the 2008 Chaitén volcanic eruption. *Journal of Volcanology and Geothermal Research* **184**, 462–472. https://doi.org/10.1016/j.jvolgeores.2009.04.010

Martín-García, R., Alonso-Zarza, A.M., Frisia, S., Rodríguez-Berriguete, Á., Drysdale, R., Hellstrom, J., 2019. Effect of aragonite to calcite transformation on the geochemistry and dating accuracy of speleothems. An example from Castañar Cave, Spain. *Sedimentary Geology* **383**, 41–54. https://doi.org/10.1016/j.sedgeo.2019.01.014

Martin-Jones, C.M., Lane, C.S., Pearce, N.J.G., Smith, V.C., Lamb, H.F., Oppenheimer, C., Asrat, A., Schaebitz, F., 2017. Glass compositions and tempo of post-17 ka eruptions from the Afar Triangle recorded in sediments from lakes Ashenge and Hayk, Ethiopia. *Quaternary Geochronology* **37**, 15–31. https://doi.org/10.1016/j.quageo.2016.10.001

Martin-Puertas, C., Brauer, A., Wulf, S., Ott, F., Lauterbach, S., Dulski, P., 2014. Annual proxy data from lago grande di monticchio (southern Italy) between 76 and 112 ka: New chronological constraints and insights on abrupt climatic oscillations. *Climate of the Past* **10**, 2099–2114. https://doi.org/10.5194/cp-10-2099-2014

Mason, B.G., Pyle, D.M., Oppenheimer, C., 2004. The size and frequency of the largest explosive eruptions on Earth. *Bulletin of Volcanology* **66**, 735–748. https://doi.org/10.1007/s00445-004-0355-9

Mastin, L.G., Van Eaton, A.R., Lowenstern, J.B., 2014. Modelling ash fall distribution from a Yellowstone supereruption. *Geochemistry, Geophysics, Geosystems* **15**, 3459–3475.

Mather, T.A., Pyle, D.M., Oppenheimer, C., 2003. Tropospheric volcanic aerosol, in: Volcanism and the Earth's Atmosphere. American Geophysical Union, Washington DC, pp. 189–212.

MathWorks, 2019. MATLAB and Statistics Toolbox Release 2019b.

Matthews, J. A., Briffa, K.R., 2005. 'The "Little Ice Age": Re-evaluation of an evolving concept. *Geografiska Annaler: Series A: Physical Geography* **87**, 17–36.

Matthews, N.E., Smith, V.C., Costa, A., Durant, A.J., Pyle, D.M., Pearce, N.J.G., 2012. Ultra-distal tephra deposits from super-eruptions: Examples from Toba, Indonesia and Taupo Volcanic Zone, New Zealand. *Quaternary International* **258**, 54–79. https://doi.org/10.1016/j.quaint.2011.07.010

Mattsson, L.G., Jenelius, E., 2015. Vulnerability and resilience of transport systems–a discussion of recent research. *Transportation Research Part A: Policy Practice* **81**, 16–34.

Mayewski, P. A., Meeker, L.D., Twickler, M.S., Whitlow, S., Yang, Q., Lyons, W.B., Prentice, M., 1997. Major features and forcing of high-latitude northern hemisphere atmospheric circulation using a 110,000-year-long glaciochemical series. *Journal of Geophysical Research - Oceans* **102**, 26345–26366.

Mayewski, P.A., Rohling, E.E., Stager, J.C., Karlén, W., Maasch, K.A., Meeker, L.D., Meyerson, E.A., Gasse, F., van Kreveld, S., Holmgren, K., Lee-Thorp, J., Rosqvist, G., Rack, F., Staubwasser, M., Schneider, R.R., Steig,

E.J., 2004. Holocene climate variability. *Quaternary Research* **62**, 243–255. https://doi.org/10.1016/j.yqres.2004.07.001

McBirney, A.R., 1969. Compositional variations in Cenozoic calcalkaline suites of Central America. *Proceedings of the Andesite Conference, Oregon Department of Geology and Minerology Research Bulletin* 185–189.

McConnell, J.R., Burke, A., Dunbar, N.W., Köhler, P., Thomas, J.L., Arienzo, M.M., Chellman, N.J., Maselli, O.J., Sigl, M., Adkins, J.F., Baggenstos, D., Burkhart, J.F., Brook, E.J., Buizert, C., Cole-Dai, J., Fudge, T.J., Knorr, G., Graf, H.F., Grieman, M.M., Iverson, N., McGwire, K.C., Mulvaney, R., Paris, G., Rhodes, R.H., Saltzman, E.S., Severinghaus, J.P., Steffensen, J.P., Taylor, K.C., Winckler, G., 2017. Synchronous volcanic eruptions and abrupt climate change ~17.7 ka plausibly linked by stratospheric ozone depletion. *Proceedings of the National Academy of Sciences of the United States of America* **114**, 10035–10040. https://doi.org/10.1073/pnas.1705595114

McConnell, J.R., Sigl, M., Plunkett, G., Burke, A., Kim, W.M., Raible, C.C., Wilson, A.I., Manning, J.G., Ludlow, F., Chellman, N.J., Innes, H.M., Yang, Z., Larsen, J.F., Schaefer, J.R., Kipfstuhl, S., Mojtabavi, S., Wilhelms, F., Opel, T., Meyer, H., Steffensen, J.P., 2020. Extreme climate after massive eruption of Alaska's Okmok volcano in 43 BCE and effects on the late Roman Republic and Ptolemaic Kingdom. *Proceedings of the National Academy of Sciences of the United States of America* **117**, 15443–15449. https://doi.org/10.1073/pnas.2002722117

McCormick Kilbride, B., Edmonds, M., Biggs, J., 2016. Observing eruptions of gas-rich compressible magmas from space. *Nature Communications* **7**, 1–8. https://doi.org/10.1038/ncomms13744

McDermott, F., 2004. Palaeo-climate reconstruction from stable isotope variations in speleothems: A review. *Quaternary Science Reviews* **23**, 901–918. https://doi.org/10.1016/j.quascirev.2003.06.021

McDonald, J., Drysdale, R., 2007. Hydrology of cave drip waters at varying bedrock depths from a karst system in southeastern Australia. *Hydrological Processes* **21**, 1737–1748.

McDonald, J., Drysdale, R., Hill, D., Chisari, R., Wong, H., 2007. The hydrochemical response of cave drip waters to sub-annual and inter-annual climate variability, Wombeyan Caves, SE Australia. *Chemical Geology* **244**, 605–623. https://doi.org/10.1016/j.chemgeo.2007.07.007

McGann, J.J., Weller, B., 1992. The complete poetical works. Claredon Press, Oxford.

McGee, D., Donohoe, A., Marshall, J., Ferreira, D., 2014. Changes in ITCZ location and cross-equatorial heat transport at the Last Glacial Maximum, Heinrich Stadial 1, and the mid-Holocene. *Earth and Planetary Science Letters* **390**, 69–79. https://doi.org/10.1016/j.epsl.2013.12.043

McKee, C.O., Baillie, M.G., Reimer, P.J., 2015. A revised age of AD 667-699 for the latest major eruption at Rabaul. *Bulletin of Volcanology* **77**, 65.

McLean, D., Albert, P.G., Nakagawa, T., Staff, R.A., Suzuki, T., Smith, V.C., 2016. Identification of the Changbaishan 'Millennium' (B-Tm) eruption deposit in the Lake Suigetsu (SG06) sedimentary archive, Japan: synchronisation of hemispheric wide paleoclimate archives. *Quaternary Science Reviews* **150**, 301–307.

McMillan, E.A., Fairchild, I.J., Frisia, S., Borsato, A., McDermott, F., 2005. Annual trace element cycles in calcite-aragonite speleothems: Evidence of drought in the western Mediterranean 1200-1100 yr BP. *Journal of Quaternary Science* **20**, 423–433. https://doi.org/10.1002/jqs.943

Mead, S., Magill, C., 2014. Determining change points in data completeness for the Holocene eruption record. *Bulletin of Volcanology* **76**, 874.

Medhaug, I., Langehaug, H.R., Eldevik, T., Firevik, T., Bentsen, M., 2012. Mechanisms for decadal scale variability in a simulated Atlantic meridional overturning circulation. *Climate Dynamics* **39**, 77–93.

Mehterian, S., Pourmand, A., Sharifi, A., Lahijani, H.A.K., Naderi, M., Swart, P.K., 2017. Speleothem records of glacial/interglacial climate from Iran forewarn of future Water Availability in the interior of the Middle East. *Quaternary Science Reviews* **164**, 187–198. https://doi.org/10.1016/j.quascirev.2017.03.028

Members, E.C., 2006. One-to-one coupling of glacial climate variability in Greenland and Antarctica. *Nature* **444**, 195–198.

Menounos, B., Clague, J.J., Osborn, G., Luckman, B.H., Lakeman, T.R., Minkus, R., 2008. Western Canadian glaciers advance in concert with climate change circa 4.2 ka. *Geophysical Research Letters* **35**, L07501.

Menviel, L., Timmermann, A., Friedrich, T., England, M.H., 2014. Hindcasting the continuum of Dansgaard-Oeschger variability: Mechanisms, patterns and timing. *Climate of the Past* **10**, 63–77. https://doi.org/10.5194/cp-10-63-2014

Mertz-Kraus, R., Brachert, T.C., Jochum, K.P., Reuter, M., Stoll, B., 2009. LA-ICP-MS analyses on coral growth increments reveal heavy winter rain in the Eastern Mediterranean at 9 Ma. *Palaeogeography, Palaeoclimatology, Palaeoecology* **273**, 25–40. https://doi.org/10.1016/j.palaeo.2008.11.015

Merz, N., Raible, C.C., Woollings, T., 2015. North Atlantic eddy-driven jet in interglacial and glacial winter climates. *Journal of Climate* **28**, 3977–3997. https://doi.org/10.1175/JCLI-D-14-00525.1

Metzner, D., Kutterolf, S., Toohey, M., Timmreck, C., Niemeier, U., Freundt, A., Krüger, K., 2014. Radiative forcing and climate impact resulting from SO2 injections based on a 200,000-year record of Plinian eruptions along the Central American Volcanic Arc. *International Journal of Earth Sciences* **103**, 2063–2079. https://doi.org/10.1007/s00531-012-0814-z

Meyer, C.R., Robel, A.A., Rempel, A.W., 2019. Frozen fringe explains sediment freeze-on during Heinrich events. *Earth and Planetary Science Letters* **524**, 115725. https://doi.org/10.1016/j.epsl.2019.115725

Miller, C. F., Wark, D.A., 2008. Supervolcanoes and their explosive supereruptions. *Elements* **4**, 11–16.

Miller, G.H., Geirsdóttir, Á., Zhong, Y., Larsen, D.J., Otto-Bliesner, B.L., Holland, M.M., Bailey, D.A., Refsnider, K.A., Lehman, S.J., Southon, J.R., Anderson, C., Björnsson, H., Thordarson, T., 2012. Abrupt onset of the Little Ice Age triggered by volcanism and sustained by sea-ice/ocean feedbacks. *Geophysical Research Letters* **39**, 1–5. https://doi.org/10.1029/2011GL050168

Mix, A., Bard, E., Schneider, R., 2001. Environmental processes of the ice age: land, oceans, and glaciers. *Quaternary Science Reviews* **20**, 627–657.

Moles, J.D., McGarvie, D., Stevenson, J.A., Sherlock, S.C., Abbott, P.M., Jenner, F.E., Halton, A.M., 2019. Widespread tephra dispersal and ignimbrite emplacement from a subglacial volcano (Torfajökull, Iceland). *Geology* **47**, 577–580.

Monticelli, D., Di Iorio, A., Ciceri, E., Castelletti, A., Dossi, C., 2009. Tree ring microanalysis by LA-ICP-MS for environmental monitoring: Validation or refutation? Two case histories. *Microchimica Acta* **164**, 139–148. https://doi.org/10.1007/s00604-008-0049-7

Moreno, A., Stoll, H., Jiménez-Sánchez, M., Cacho, I., Valero-Garcés, B., Ito, E., Edwards, R.L., 2010. A speleothem record of glacial (25-11.6 kyr BP) rapid climatic changes from northern Iberian Peninsula. *Global and Planetary Change* **71**, 218–231. https://doi.org/10.1016/j.gloplacha.2009.10.002

Mori, T., Kashiwagi, K., Amekawa, S., Kato, H., Okumura, T., Takashima, C., Wu, C.C., Shen, C.C., Quade, J., Kano, A., 2018. Temperature and seawater isotopic controls on two stalagmite records since 83 ka from maritime Japan. *Quaternary Science Reviews* **192**, 47–58. https://doi.org/10.1016/j.quascirev.2018.05.024

Mucek, A.E., Danis, M., Silva, S.L. De, Schmitt, A.K., Pratomo, I., Coble, M.A., 2017. Post-supereruption recovery at Toba Caldera. *Nature Communications* **8**, 15248. https://doi.org/10.1038/ncomms15248

Mueller, A.D., Anselmetti, F.S., Ariztegui, D., Brenner, M., Hodell, D.A., Curtis, J.H., Escobar, J., Gilli, A., Grzesik, D.A., Guilderson, T.P., Kutterolf, S., Plötze, M., 2010. Late Quaternary palaeoenvironment of northern Guatemala: Evidence from deep drill cores and seismic stratigraphy of Lake Petén Itzá. *Sedimentology* **57**, 1220–1245. https://doi.org/10.1111/j.1365-3091.2009.01144.x

Müller, W., Fietzke, J., 2016. The Role of LA–ICP–MS in Palaeoclimate Research. *Elements* **12**, 329–334.

Müller, W., Shelley, M., Miller, P., Broude, S., 2009. Initial performance metrics of a new custom-designed ArF excimer LA-ICPMS system coupled to a two-volume laser-ablation cell. *Journal of Analytical Atomic Spectrometry* **24**, 209.

Muthers, S., Anet, J.G., Raible, C.C., Brönnimann, S., Rozanov, E., Arfeuille, F., Peter, T., Shapiro, A.I., Beer, J., Steinhilber, F., Brugnara, Y., Schmutz, W., 2014. Northern hemispheric winter warming pattern after tropical volcanic eruptions: Sensitivity to the ozone climatology. *Journal of Geophysical Research: Atmospheres* **119**, 1340–1355.

Myers, M.L., Wallace, P.J., Wilson, C.J.N., Morter, B.K., Swallow, E.J., 2016. Prolonged ascent and episodic venting of discrete magma batches at the onset of the Huckleberry Ridge supereruption, Yellowstone. *Earth and Planetary Science Letters* **451**, 285–297.

Nanayama, F., Maeno, F., 2018. Evidence on the Koseda coast of Yakushima Island of a tsunami during the 7.3 ka Kikai caldera eruption. *Wiley Island Arc* **28**, 12291.

Newhall, C., Solidum, R.U., 2018. Volcanic Hazard Communication at Pinatubo from 1991 to 2015, in: Observing the Volcano World, Advances in Volcanology. pp. 189–203.

Newhall, C.G., 2018. Cultural Differences and the Importance of Trust Between Volcanologists and Partners in Volcanic Risk Mitigation, in: Fearnley, C., Bird, D.K., Haynes, K., McGuire, W.J., Jolly, G. (Ed.), Observing the Volcano World, Advances in Volcanology. pp. 515–527.

Newhall, C.G., Daag, A.S., Delfin, F.G., Hoblitt, R.P., McGeehin, J., Pallister, J.S., Regalado, T.M., Rubin, M., Tubianosa, B.S., Tamayo, R.A., Umbal, J.V., 1996. Eruptive History of Mount Pinatubo. Fire and Mud: Eruptions and Lahars of Mount Pinatubo, Philippines. Philippine Institute of Volcanology and Seismology, Quezon City.

Newhall, C.G., 1987. Geology of the Lake Atitlán Region, Western Guatemala. *Journal of Volcanology and Geothermal Research* **33**, 23–55. https://doi.org/10.1016/0377-0273(87)90053-9

Niespolo, E.M., Rutte, D., Deino, A.L., Renne, P.R., 2017. Intercalibration and Age of the Alder Creek Sanidine $^{40}Ar/^{39}Ar$ Standard. *Quaternary Geochronology* **39**, 205–213.

Ninkovich, D., 1979. Distribution, age and chemical composition of tephra layers in deep-sea sediments off western Indonesia. *Journal of Volcanology and Geothermal Research* **5**, 67–86. https://doi.org/10.1016/0377-0273(79)90033-7

Noack, C.W., Dzombak, D.A., Karamalidis, A.K., 2014. Rare Earth Element Distributions and Trends in Natural Waters with a Focus on Groundwater. *Environmental Science and Technology* **48**, 4317–4326.

Nomikou, P., Druitt, T.H., Hübscher, C., Mather, T.A., Paulatto, M., Kalnins, L.M., Kelfoun, K., Papanikolaou, D., Bejelou, K., Lampridou, D., Pyle, D.M., Carey, S., Watts, A.B., Weiß, B., Parks, M.M., 2016. Post-eruptive flooding of Santorini caldera and implications for tsunami generation. *Nature Communications* **7**.

Oktay Akkoyunlu, B., Baltaci, H., Tayanc, M., 2019. Atmospheric conditions of extreme precipitation events in western Turkey for the period 2006-2015. *Natural Hazards and Earth System Sciences* **19**, 107–119. https://doi.org/10.5194/nhess-19-107-2019

Óladóttir, B.A., Sigmarsson, O., Larsen, G., Thordarson, T., 2008. Katla volcano, Iceland: Magma composition, dynamics and eruption frequency as recorded by Holocene tephra layers. *Bulletin of Volcanology* **70**, 475–493. https://doi.org/10.1007/s00445-007-0150-5

Olichwer, T., Otrębski, A., 2016. Groundwater renewable resources in karst areas, the case of the Kleśnica River basin (Sudety Mountains, Poland). *Geoscience Records* **2**, 17–23. https://doi.org/10.1515/georec-2016-0003

Olsen, J., Anderson, N.J., Knudsen, M.F., 2012. Variability of the North Atlantic Oscillation over the past 5,200 years. *Nature Geoscience* **5**, 808–812.

Oman, L., Robock, A., Stenchikov, G.L., Thordarson, T., Koch, D., Shindell, D.T., Gao, C., 2006. Modeling the distribution of the volcanic aerosol cloud from the 1783-1784 Laki eruption. *Journal of Geophysical Research Atmospheres* **111**, 1–15. https://doi.org/10.1029/2005JD006899

Oppenheimer, C., 2011. Eruptions that shook the world. Cambridge University Press, Cambridge.

Oppenheimer, C., 2002. Limited global change due to the largest known Quaternary eruption, Toba ~74 kyr BP ? *Quaternary Science Reviews* **21**, 1593–1609.

Oppenheimer, C., 2003. Climatic, environmental and human consequences of the largest known historic eruption: Tambora volcano (Indonesia) 1815. *Progress in Physical Geography* **27**, 230–259. https://doi.org/10.1191/0309133303pp379ra

Oppenheimer, C., 2003. Ice core and palaeoclimatic evidence for the timing and nature of the great mid-13th century volcanic eruption. *International Journal of Climatology* **23**, 417–426.

Oppenheimer, C., Donovan, A., 2015. On the nature and consequences of super-eruptions. *Volcanism and Global Environmental Change* 16–29. https://doi.org/10.1007/9781107415683.003

Oppenheimer, C., Scaillet, B., Woods, A., Sutton, A.J., Elias, T., Moussallam, Y., 2018. Influence of eruptive style on volcanic gas emission chemistry and temperature. *Nature Geoscience* **11**, 678–681. https://doi.org/10.1038/s41561-018-0194-5

Oppenheimer, C., Wacker, L., Xu, J., Galván, J.D., Stoffel, M., Guillet, S., Corona, C., Sigl, M., Di Cosmo, N., Hajdas, I., Pan, B., Breuker, R., Schneider, L., Esper, J., Fei, J., Hammond, J.O.S., Büntgen, U., 2017. Multi-proxy dating the 'Millennium Eruption' of Changbaishan to late 946 CE. *Quaternary Science Reviews* **158**, 164–171. https://doi.org/10.1016/j.quascirev.2016.12.024

Oppo, D. W., McManus, J. F., Cullen, J.L., 2003. Deepwater variability in the Holocene epoch. *Nature* **422**, 277–278.

Orland, I.J., Burstyn, Y., Bar-Matthews, M., Kozdon, R., Ayalon, A., Matthews, A., Valley, J.W., 2014. Seasonal climate signals (1990-2008) in a modern Soreq Cave stalagmite as revealed by high-resolution geochemical analysis. *Chemical Geology* **363**, 322–333. https://doi.org/10.1016/j.chemgeo.2013.11.011

Ortega, P., Guilyardi, E., Swingedouw, D., Mignot, J., Nguyen, S., 2017. Reconstructing extreme AMOC events through nudging of the ocean surface: a perfect model approach. *Climate Dynamics* **49**, 3425–3441. https://doi.org/10.1007/s00382-017-3521-4

Osborn, T.J., Briffa, K.R., 2006. The spatial extent of 20th-century warmth in the context of the past 1200 years. *Science* **311**, 841–844.

Osipov, S., Stenchikov, G., Tsigaridis, K., LeGrande, A.N., Bauer, S.E., 2020. The Role of the SO 2 Radiative Effect in Sustaining the Volcanic Winter and Soothing the Toba Impact on Climate. *Journal of Geophysical Research: Atmospheres* **125**. https://doi.org/10.1029/2019JD031726

Oster, J.L., Sharp, W.D., Covey, A.K., Gibson, J., Rogers, B., Mix, H., 2017. Climate response to the 8.2 ka event in coastal California. *Scientific Reports* **7**, 1–9. https://doi.org/10.1038/s41598-017-04215-5

Oster, J.L., Weisman, I.E., Sharp, W.D., 2020. Multi-proxy stalagmite records from northern California reveal dynamic patterns of regional hydroclimate over the last glacial cycle. *Quaternary Science Reviews* **241**, 106411. https://doi.org/10.1016/j.quascirev.2020.106411

Özden, D.M., Dinç, U., Kapur, S., 2001. SOIL GEOGRAPHICAL DATABASE OF TURKEY AT A SCALE 1:1.000.000 [WWW Document]. URL http://www.wossac.com/downloads/19811_turkeysoilmap.pdf (accessed 5.20.20).

Palacios, D., Stokes, C.R., Phillips, F.M., Clague, J.J., Alcalá-Reygosa, J., Andrés, N., Angel, I., Blard, P.H., Briner, J.P., Hall, B.L., Dahms, D., Hein, A.S., Jomelli, V., Mark, B.G., Martini, M.A., Moreno, P., Riedel, J., Sagredo, E., Stansell, N.D., Vázquez-Selem, L., Vuille, M., Ward, D.J., 2020. The deglaciation of the Americas during the Last Glacial Termination. *Earth-Science Reviews* **203**, 103113. https://doi.org/10.1016/j.earscirev.2020.103113

Palais, J.M., Taylor, K., Mayewski, P.A., Grootes, P., 1991. Volcanic ash from the 1362 A.D. Öræfajökull eruption (Iceland) in the Greenland ice sheet. *Geophysical Research Letters* **18**, 1241–1244.

Pallister, J.S., Schneider, D.J., Griswold, J.P., Keeler, R.H., Burton, W.C., Noyles, C., Newhall, C.G., Ratdomopurbo, A., 2013. Merapi 2010 eruption - Chronology and extrusion rates monitored with satellite radar and used in eruption forecasting. *Journal of Volcanology and Geothermal Research* **261**, 144–152.

Panebianco, J.E., Mendez, M.J., Buschiazzo, D.E., Bran, D., Gaitán, J.J., 2017. Dynamics of volcanic ash remobilisation by wind through the Patagonian steppe after the eruption of Cordón Caulle, 2011. *Scientific Reports* **7**, 45529.

Papale, P., 2018. Global time-size distribution of volcanic eruptions on Earth. *Scientific Reports* **8**, 1–11. https://doi.org/10.1038/s41598-018-25286-y

Parker, C.F., 2015. Complex negative events and the diffusion of crisis: Lessons from the 2010 and 2011 Icelandic volcanic ash cloud events. *Geografiska Annaler: Series A: Physical Geography* **97**, 97–108.

Partin, J.W., Cobb, K.M., Adkins, J.F., Clark, B., Fernandez, D.P., 2007. Millennial-scale trends in west Pacific warm pool hydrology since the Last Glacial Maximum. *Nature* **449**, 452–455. https://doi.org/10.1038/nature06164

Pashchenko, A., Dublyansky, Y., Andreichuk, V., 1993. Aerosol study in the Kungur Ice Cave (Urals, Russia)., in: Proceedings of the XI International Congress of Speleology, Beijing.

Patino, L. C., Carr, M., Feigenson, M.D., 2000. Local and regional variations in Central American arc lavas controlled by variations in subducted sediment input. *Contributions to Mineralogy and Petrology* **138**, 256–283.

Paton, C., Hellstrom, J., Paul, B., Woodhead, J., Hergt, J., 2011. Iolite: freeware for the visualisation and processing of mass spectrometric data. *Journal of Analytical Atomic Spectrometry* **26**, 2508.

Pausata, F.S.R., Battisti, D.S., Nisancioglu, K.H., Bitz, C.M., 2011. Chinese stalagmite $\delta^{18}O$ controlled by changes in the Indian monsoon during a simulated Heinrich Event. *Nature Geoscience* **4**, 474–480. https://doi.org/10.1038/ngeo1169

Pausata, F.S.R., Camargo, S.J., 2019. Tropical cyclone activity affected by volcanically induced ITCZ shifts. *Proceedings of the National Academy of Sciences of the United States of America* **116**, 7732–7737. https://doi.org/10.1073/pnas.1900777116

Pausata, F.S.R., Chafik, L., Caballero, R., Battisti, D.S., 2015. Impacts of high-latitude volcanic eruptions on ENSO and AMOC. *Proceedings of the National Academy of Sciences of the United States of America* **112**, 13784–13788. https://doi.org/10.1073/pnas.1509153112

Pausata, F.S.R., Karamperidou, C., Caballero, R., Battisti, D.S., 2016. ENSO response to high-latitude volcanic eruptions in the Northern Hemisphere: The role of the initial conditions. *Geophysical Research Letters* **43**, 8694–8702. https://doi.org/10.1002/2016GL069575

Pausata, F.S.R., Zanchettin, D., Karamperidou, C., Caballero, R., Battisti, D.S., Battisti, D.S., 2020. ITCZ shift and extratropical teleconnections drive ENSO response to volcanic eruptions. *Science Advances* **6**, 1–12. https://doi.org/10.1126/sciadv.aaz5006

Payne, R., Blackford, J., van der Plicht, J., 2008. Using cryptotephras to extend regional tephrochronologies: An example from southeast Alaska and implications for hazard assessment. *Quaternary Research* **69**, 42–55.

Payne, R.J., Symeonakis, E., 2012. The spatial extent of tephra deposition and environmental impacts from the 1912 Novarupta eruption. *Bulletin of Volcanology* **74**, 2449–2458. https://doi.org/10.1007/s00445-012-0674-1

Payne, R., Gehrels, M., 2010. The formation of tephra layers in peatlands: An experimental approach. *Catena* **81**, 12–23. https://doi.org/10.1016/j.catena.2009.12.001

Pearce, N.J.G., Perkins, W.T., Westgate, J.A., Wade, S.C., 2011. Trace-element microanalysis by LA-ICP-MS: the quest for comprehensive chemical characterisation of single, sub-10 µm volcanic glass. *Quaternary International* **246**, 57–81.

Pearce, N.J.G., Westgate, J.A., Gatti, E., Pattan, J.N., Parthiban, G., Achyuthan, H., 2014. Individual glass shard trace element analyses confirm that all known Toba tephra reported from India is from the c. 75-ka Youngest Toba eruption. *Journal of Quaternary Science* **29**, 729–734.

Pearce, N.J.G., Westgate, J.A., Gualda, G.A.R., Gatti, E., Muhammad, R.O.S.F., 2020. Tephra glass chemistry provides storage and discharge details of five magma reservoirs which fed the 75 ka Youngest Toba Tuff eruption, northern Sumatra. *Journal of Quaternary Science* **35**, 256–271. https://doi.org/10.1002/jqs.3149

Pearson, C.L., Dale, D.S., Brewer, P.W., Kuniholm, P.I., Lipton, J., Manning, S.W., 2009. Dendrochemical analysis of a tree-ring growth anomaly associated with the Late Bronze Age eruption of Thera. *Journal of Archaeological Science* **36**, 1206–1214.

Peckover, E.N., Andrews, J.E., Leeder, M.R., Rowe, P.J., Marca, A., Sahy, D., Noble, S., Gawthorpe, R., 2019. Coupled stalagmite – Alluvial fan response to the 8.2 ka event and early Holocene palaeoclimate change in Greece. *Paleogeography, Paleoclimatology, Paleoecology* **532**, 109252.

Pedrazzi, D., Sunye-Puchol, I., Aguirre-Díaz, G., Costa, A., Smith, V.C., Poret, M., Dávila-Harris, P., Miggins, D.P., Hernández, W., Gutiérrez, E., 2019. The Ilopango Tierra Blanca Joven (TBJ) eruption, El Salvador: Volcano-stratigraphy and physical characterization of the major Holocene event of Central America. *Journal of Volcanology and Geothermal Research* **377**, 81–102.

Pedro, J.B., Jochum, M., Buizert, C., He, F., Barker, S., Rasmussen, S.O., 2018. Beyond the bipolar seesaw: Toward a process understanding of interhemispheric coupling. *Quaternary Science Reviews* **192**, 27–46. https://doi.org/10.1016/j.quascirev.2018.05.005

Pérez-Mejías, C., Moreno, A., Sancho, C., Martín-García, R., Spötl, C., Cacho, I., Cheng, H., Edwards, R.L., 2019. Orbital-to-millennial scale climate variability during Marine Isotope Stages 5 to 3 in northeast Iberia. *Quaternary Science Reviews* **224**. https://doi.org/10.1016/j.quascirev.2019.105946

Petersen, S. V, Schrag, D.P., Clark, P.U., 2013. A new mechanism for Dansgaard-Oeschger cycles. *Paleoceanography* **28**, 24–30. https://doi.org/10.1029/2012PA002364

Petit, J.R., Delmonte, B., 2009. A model for large glacial–interglacial climate-induced changes in dust and sea salt concentrations in deep ice cores (central Antarctica): palaeoclimatic implications and prospects for refining ice core chronologies. *Tellus B* **61**. https://doi.org/10.3402/tellusb.v61i5.16880

Petraglia, M., Korisettar, R., Boivin, N., Clarkson, C., Ditchfield, P., Jones, S., Koshy, J., Lahr, M. M., Oppenheimer, C., Pyle, D., Roberts, R., Schwenniger, J.-C., Arnold, L., White, K., 2007. Middle Pleistocene assemblages from the Indian subcontinent before and after the Toba super-eruption. *Science* **317**, 114–116.

Petrelli, M., Laeger, K., Perugini, D., 2016. High spatial resolution trace element determination of geological samples by laser ablation quadrupole plasma mass spectrometry: implications for glass analysis in volcanic products. [WWW Document]. URL https://arxiv.org/ftp/arxiv/papers/1706/1706.10120.pdf (accessed 11.18.19).

Petroff, A., Mailliat, A., Amielh, M., Anselmet, F., 2008. Aerosol dry deposition on vegetative canopies. Part I: review of present knowledge. *Atmospheric Environment* **42**, 3625–3653.

Pilcher, J., Bradley, R.S., Francus, P., Anderson, L., 2005. A Holocene tephra record from the Lofoten Islands, Arctic Norway. *Boreas* **34**, 136–156.

Piotrowski, A.M., Goldstein, S.L., Hemming, S.R., Fairbanks, G., Foster, A., Levin, B., Zool, J., 2005. Temporal Relationships of Carbon Cycling and Ocean Circulation at Glacial Boundaries Published by : American Association for the Advancement of Science Linked references are available on JSTOR for this article : Temporal Relationships of Carbon Cycling an **307**, 1933–1938.

Plag, H., Stein, S., Brocklebank, S., Jules-plag, S., Campus, P., 2014. Extreme Geohazards : Reducing Disaster Risk and Increasing Resilience, EGU General Assembly 2014.

Plunkett, G.M., 1999. Environmental Change in the Late Bronze Age in Ireland (1200–600 cal. BC). Queen's University Belfast.

Plunkett, G., Pilcher, J.R., 2018. Defining the potential source region of volcanic ash in northwest Europe during the Mid- to Late Holocene. *Earth-Science Reviews* **179**, 20–37. https://doi.org/10.1016/j.earscirev.2018.02.006

Polyak, V.J., Asmerom, Y., Lachniet, M.S., 2017. Rapid speleothem δ13C change in southwestern North America coincident with Greenland stadial 20 and the Toba (Indonesia) supereruption. *Geology* **45**, 843–846. https://doi.org/10.1130/G39149.1

Ponomareva, V. V., Kyle, P.R., Melekestsev, I. V., Rinkleff, P.G., Dirksen, O. V., Sulerzhitsky, L.D., Zaretskaia, N.E., Rourke, R., 2004. The 7600 (^{14}C) year BP Kurile Lake caldera-forming eruption, Kamchatka, Russia: Stratigraphy and field relationships. *Journal of Volcanology and Geothermal Research* **136**, 199–222. https://doi.org/10.1016/j.jvolgeores.2004.05.013

Ponomareva, V., Portnyagin, M., Pevzner, M., Blaauw, M., Kyle, P., Derkachev, A., 2015. Tephra from andesitic Shiveluch volcano, Kamchatka, NW Pacific: chronology of explosive eruptions and geochemical fingerprinting of volcanic glass. *International Journal of Earth Sciences* **104**, 1459–1482.

Ponomareva, V.V., Melekestsev, I., Braitseva, O., Churikova, T., Pevzner, M., and Sulerzhitsky, L., 2007. Late Pleistocene-Holocene volcanism on the Kamchatka Peninsula, northwest Pacific region, in: Eichelberger, J., Gordeev, E., Kasahara, M., Izbekov, P., and Lees, J. (Ed.), Volcanism and Subduction: The Kamchatka Region. Geophysical Monograph Series: American Geophysical Union, Washington DC, pp. 263–282.

Ponomareva, V., Portnyagin, M., Davies, S.M., 2015. Tephra without borders: Far-reaching clues into past explosive eruptions. *Frontiers in Earth Sciences* **3**, 1–16. https://doi.org/10.3389/feart.2015.00083

Porinchu, D.F., MacDonald, G.M., Moser, K.A., Rolland, N., Kremenetski, K., Seppä, H., Rühland, K.M., 2019. Evidence of abrupt climate change at 9.3 ka and 8.2 ka in the central Canadian Arctic: Connection to the North Atlantic and Atlantic Meridional Overturning Circulation. *Quaternary Science Reviews* **219**, 204–217. https://doi.org/10.1016/j.quascirev.2019.07.024

Post, J.D., 1977. The last great subsistence crisis in the Western World. The Johns Hopkins University Press, Baltimore MD.

Pouget, S., Bursik, M., Cortés, J.A., Hayward, C., 2014. Use of principal component analysis for identification of Rockland and Trego hot springs tephras in the Hat Creek Graben, northeastern California, USA. *Quaternary Research* **81**, 125–137.

Pouget, S., Bursik, M., Rogova, G., 2014. Tephra redeposition and mixing in a Late-glacial hillside basin determined by fusion of clustering analyses of glass-shard geochemistry. *Journal of Quaternary Science* **29**, 789–802.

Prata, F., Robock, A., Hamblyn, R., 2018. The sky in Edvard Munch's 'The Scream.' *Bulletin of the American Meteorological Society* **99**, 1377–1390.

Prata, F., Woodhouse, M., Huppert, H. E., Prata, A., Thordarson, T., Carn, S., 2017. Atmospheric processes affecting the separation of volcanic ash and SO_2 in volcanic eruptions: Inferences from the May 2011 Grímsvötn eruption. *Atmospheric Chemistry and Physics* **17**, 10709–10732.

Prival, J.M., Thouret, J.C., Japura, S., Gurioli, L., Bonadonna, C., Mariño, J., Cueva, K., 2020. New insights into eruption source parameters of the 1600 CE Huaynaputina Plinian eruption, Peru. *Bulletin of Volcanology* **82**. https://doi.org/10.1007/s00445-019-1340-7

Global Volcanism Program., 2020. Report on Reykjanes (Iceland): Weekly Volcanic Activity Report, 11 March-17 March 2020.

Prospero, J.M., Ginoux, P., Torres, O., Nicholson, S.E., Gill, T.E., 2002. Environmental characterization of global sources of atmospheric soil dust identified with the Nimbus 7 Total Ozone Mapping Spectrometer (TOMS) absorbing aerosol product. *Reviews of Geophysics* **40**, 2-1-2–31. https://doi.org/10.1029/2000RG000095

Pyle, D.M., Barclay, J., 2020. Historical records of volcanic eruptions deserve more attention. *Nature Reviews Earth & Environment* **1**, 183–184.

Pyle, D.M., 2018. What Can We Learn from Records of Past Eruptions to Better Prepare for the Future?, in: Observing the Volcano World, Advances in Volcanology. pp. 445–462.

Pyle, D.M., 2016. Field observations of tephra fallout deposits, in: Cashman, K., Ricketts, H., Rust, A., Watson, M., Mackie, S. (Ed.), Volcanic Ash: Hazard Observation. Elsevier, pp. 25–37.

Pyle, D.M., 1995. Mass and energy budgets of explosive volcanic eruptions. *Geophysical Research Letters* **22**, 563–566.

Pyle, D.M., 2015. Sizes of Volcanic Eruptions, in: Sigurdsson, H. (Ed.), Encyclopaedia of Volcanoes. Academic Press.

Pyne O'Donnell, S.D.F., Jensen, B.J.L., 2020. Glacier Peak and mid - Lateglacial Katla cryptotephras in Scotland : potential new intercontinental and marine - terrestrial correlations GP-G GP-B. *Journal of Quaternary Science* **35**, 155–162. https://doi.org/10.1002/jqs.3171

Pyne-O'Donnell, S.D.F., Hughes, P.D.M., Froese, D.G., Jensen, B.J.L., Kuehn, S.C., Mallon, G., Amesbury, M.J., Charman, D.J., Daley, T.J., Loader, N.J., Mauquoy, D., Street-Perrott, F.A., Woodman-Ralph, J., 2012. High-precision ultra-distal Holocene tephrochronology in North America. *Quaternary Science Reviews* **52**, 6–11. https://doi.org/10.1016/j.quascirev.2012.07.024

Rach, O., Brauer, A., Wilkes, H., Sachse, D., 2014. Delayed hydrological response to Greenland cooling at the onset of the Younger Dryas in western Europe. *Nature Geoscience* **7**, 109–112. https://doi.org/10.1038/ngeo2053

Rahmstorf, S., 2002. Ocean circulation and climate during the past 120,000 years. *Nature* **419**, 207–214.

Railsback, L.B., Liang, F., Brook, G.A., Voarintsoa, N.R.G., Sletten, H.R., Marais, E., Hardt, B., Cheng, H., Edwards, R.L., 2018. The timing, two-pulsed nature, and variable climatic expression of the 4.2 ka event: A review and new high-resolution stalagmite data from Namibia. *Quaternary Science Reviews* **186**, 78–90. https://doi.org/10.1016/j.quascirev.2018.02.015

Ramos, S.J., Dinali, G.S., Oliveira, C., Martins, G.C., Moreira, C.G., Siqueira, J.O, Guilherme, L.R.G., 2016. Rare Earth Elements in the Soil Environment. *Current Pollution Reports* **2**, 28–50.

Rampino, M. R., Self, S., 1992. Volcanic winter and accelerated glaciation following the Toba super-eruption. *Nature* **359**, 50–53.

Rampino, M. R., Self, S., 1993. Climate-volcanism feedback and the Toba eruption of ~74,000 years ago. *Quaternary Research* **40**, 269–280.

Rampino, M.R., Ambrose, S.H., 2000. Volcanic winter in the Garden of Eden: the Toba supereruption and the late Pleistocene human population crash, in: McCoy, F.W., Heiken, G. (Ed.), Volcanic Hazards and Disasters in Human Antiquity. Geological Society of America Special Paper 345. Geological Society of America, pp. 71–82.

Rampino, M.R., 1991. Volcanism, Climatic Change, and the Geologic Record, in: Fisher, R.V., Smith, G.A. (Ed.), Sedimentation in Volcanic Settings. SEPM Society for Sedimentary Geology 45.

Ran, M., Chen, L., 2019. The 4.2 ka BP climatic event and its cultural responses. *Quaternary International* **521**, 158–167. https://doi.org/10.1016/j.quaint.2019.05.030

Rasmussen, S.O., Bigler, M., Blockley, S.P., Blunier, T., Buchardt, S.L., Clausen, H.B., Cvijanovic, I., Dahl-Jensen, D., Johnsen, S.J., Fischer, H., Gkinis, V., Guillevic, M., Hoek, W.Z., Lowe, J.J., Pedro, J.B., Popp, T., Seierstad, I.K., Steffensen, J.P., Svensson, A.M., Vallelonga, P., Vinther, B.M., Walker, M.J.C., Wheatley, J.J., Winstrup, M., 2014. A stratigraphic framework for abrupt climatic changes during the Last Glacial period based on three synchronized Greenland ice-core records: Refining and extending the INTIMATE event stratigraphy. *Quaternary Science Reviews* **106**, 14–28. https://doi.org/10.1016/j.quascirev.2014.09.007

Rawson, H., Naranjo, J. A., Smith, V., Fontijn, K., Pyle, D. M., Mather, T. A., Moreno, H., 2015. The frequency and magnitude of post-glacial explosive eruptions at Volcán Mocho-Choshuenco, southern Chile. *Journal of Volcanology and Geothermal Research* **299**, 103–129.

Rawson, H., Pyle, D.M., Mather, T.A., Smith, V.C., Fontijn, K., Lachowycz, S.M., Naranjo, J.A., 2016. The magmatic and eruptive response of arc volcanoes to deglaciation: insights from southern Chile. *Geology* **44**, 251–254.

Reeder, R.J., Nugent, M., Lamble, G.M., Tait, C.D., Morris, D.E., 2000. Uranyl incorporation into calcite and aragonite: XAFS and luminescence studies. *Environmental Science and Technology* **34**, 638–644.

Regattieri, E., Zanchetta, G., Isola, I., Bajo, P., Perchiazzi, N., Drysdale, R.N., Boschi, C., Hellstrom, J.C., Francke, A., Wagner, B., 2018. A MIS 9/MIS 8 speleothem record of hydrological variability from Macedonia (F.Y.R.O.M.). *Global and Planetary Change* **162**, 39–52. https://doi.org/10.1016/j.gloplacha.2018.01.003

Rehfeld, K., Münch, T., Ho, S.L., Laepple, T., 2018. Global patterns of declining temperature variability from the Last Glacial Maximum to the Holocene. *Nature* **554**, 356–359. https://doi.org/10.1038/nature25454

Reichardt, U., Gudmundur, F.U., Pétursdóttir, G., 2018. Volcanic ash and aviation: Recommendations to improve preparedness for extreme events. *Transportation Research Part A* **113**, 101–113.

Reid, M.R., 2008. How Long Does It Take to Supersize an Eruption? *Elements* **4**, 23–29.

Renssen, H., Seppä, H., Crosta, X., Goosse, H., Roche, D.M., 2012. Global characterization of the Holocene Thermal Maximum. *Quaternary Science Reviews* **48**, 7–19. https://doi.org/10.1016/j.quascirev.2012.05.022

Renssen, H., Goosse, H., Fichefet, T., 2007. Simulation of Holocene cooling events in a coupled climate model. *Quaternary Science Reviews* **26**, 2019–2029. https://doi.org/10.1016/j.quascirev.2007.07.011

Ridley, H.E., Asmerom, Y., Baldini, J.U.L., Breitenbach, S.F.M., Aquino, V. V., Prufer, K.M., Culleton, B.J., Polyak, V., Lechleitner, F.A., Kennett, D.J., Zhang, M., Marwan, N., Macpherson, C.G., Baldini, L.M., Xiao, T., Peterkin, J.L., Awe, J., Haug, G.H., 2015. Aerosol forcing of the position of the intertropical convergence zone since ad 1550. *Nature Geoscience* **8**, 195–200. https://doi.org/10.1038/ngeo2353

Roberts, N., 2014. The Holocene: An environmental history, 3rd Editio. ed. Wiley-Blackwell, Hoboken, NJ.

Roberts, N., Brayshaw, D., Kuzucuoglu, C., Perez, R., Sadori, L., 2011. The mid-Holocene climatic transition in the Mediterranean causes and consequences. *Holocene* **21**, 3–13.

Roberts, R.G., Storey, M., Haslam, M., 2013. Toba supereruption: Age and impact on East African ecosystems. *Proceedings of the National Academy of Sciences* **110**, E3047.

Roberts, W.H.G., Valdes, P.J., Singarayer, J.S., 2017. Can energy fluxes be used to interpret glacial/interglacial precipitation changes in the tropics? *Geophysical Research Letters* **44**, 6373–6382. https://doi.org/10.1002/2017GL073103

Roberts, W.H.G., Payne, A.J., Valdes, P.J., 2016. The role of basal hydrology in the surging of the Laurentide Ice Sheet. *Climate of the Past* **12**, 1601–1617. https://doi.org/10.5194/cp-12-1601-2016

Robock, A., Ammann, C.M., Oman, L., Shindell, D. Levis, S., Stenchikov, G., 2009. Did the Toba Volcanic Eruption of ~74k BP Produce Widespread Glaciation? *Journal of Geophysical Research* **114**, D10107.

Robock, A., 2000. Volcanic Eruptions and Climate. *Reviews of Geophysics* **38**, 191–219.

Robock, A., Ammann, C.M., Oman, L., Shindell, D., Levis, S., Stenchikov, G., 2009. Did the Toba volcanic eruption of ∼74 ka B.P. produce widespread glaciation? *Journal of Geophysical Research Atmospheres* **114**, 1–9. https://doi.org/10.1029/2008JD011652

Rogers, N., 2015. The Composition and Origin of Magmas, in: Sigurdsson, H. (Ed.), Encyclopaedia of Volcanoes. Academic Press.

Rohling, E.J., Pälike, H., 2005. Centennial-scale climate cooling with a sudden cold event around 8,200 years ago. *Nature* **434**, 975–979.

Roland, T.P., 2012. Was there a 4.2 kyr event in Great Britain and Ireland? Evidence from the peatland record. University of Exeter.

Roland, T.P., Caseldine, C.J., Charman, D.J., Turney, C.S.M., Amesbury, M.J., 2014. Was there a "4.2ka event" in Great Britain and Ireland? Evidence from the peatland record. *Quaternary Science Reviews* **83**, 11–27.

Rolandi, G., 1998. The eruptive history of Somma-Vesuvius, in: Cortini, M., de Vivo, B. (Ed.), Volcanism and Archaeology in Mediterranean Area. Research Signpost Pandalai, India., pp. 77–88.

Rolandi, G., Barrella, A.M., Borrelli, A., 1993. The 1631 eruption of Vesuvius. *Journal of Volcanology and Geothermal Research* **58**, 183–201.

Rolandi, G., Munno, R., Postiglione, I., 2004. The A.D. 472 eruption of the Somma volcano. *Journal of Volcanology and Geothermal Research* **129**, 291–319.

Rolandi, G., Paone, A., Di Lascio, M., Stefani, G., 2007. The 79 AD eruption of Somma: The relationship between the date of the eruption and the Southeast Tephra dispersion. *Journal of Volcanology and Geothermal Research* **169**, 87–98. https://doi.org/10.1016/j.jvolgeores.2007.08.020

Rose, W, I., Grant, N.K., Easter, J., 1979. Geochemistry of the Los Chocoyos Ash, Guatemala, in: Elston, W., Chapin, C. (Ed.),. Geological Society of America Special Paper, pp. 87–99.

Rose, W.I., Chesner, C.A., 1987. Dispersal of ash in the great Toba eruption, 75 ka. *Geology* **15**, 913–917.

Rose, W.I., Durant, A.J., 2009. Fine ash content of explosive eruptions. *Journal of Volcanology and Geothermal Research* **186**, 32–39. https://doi.org/10.1016/j.jvolgeores.2009.01.010

Rose, W.I., Conway, F.M., Pullinger, C.R., Deino, A., McIntosh, W.C., 1999. An improved age framework for late Quaternary silicic eruptions in northern Central America. *Bulletin of Volcanology* **61**, 106–120. https://doi.org/10.1007/s004450050266

Rosenberg, C.L., Handy, M.R., 2005. Experimental deformation of partially melted granite revisited: implications for the continental crust. *Journal of Metamorphic Geology* **23**, 19–28.

Rosenheim, B.E., Thorrold, S.R., Roberts, M.L., 2008. Accelerator mass spectrometry 14C determination in CO2 produced from laser decomposition of aragonite. *Rapid Communications in Mass Spectrometry* **22**, 3443–3449.

Rougier, J., Sparks, R.S.J., Cashman, K.V., 2018. Regional and global under-recording of large explosive eruptions in the past 1000 years. *Journal of Applied Volcanology* **7**, 1.

Rougier, J., Sparks, R.S.J., Cashman, K.V., 2016. Global recording rates for large eruptions. *Journal of Applied Volcanology* **5**, 11.

Rougier, J., Sparks, R.S.J., Cashman, K. V., Brown, S.K., 2018. The global magnitude–frequency relationship for large explosive volcanic eruptions. *Earth and Planetary Science Letters* **482**, 621–629. https://doi.org/10.1016/j.epsl.2017.11.015

Rowe, P.J., Mason, J.E., Andrews, J.E., Marca, A.D., Thomas, L., Van Calsteren, P., Jex, C.N., Vonhof, H.B., Al-Omari, S., 2012. Speleothem isotopic evidence of winter rainfall variability in northeast Turkey between 77 and 6 ka. *Quaternary Science Reviews* **45**, 60–72. https://doi.org/10.1016/j.quascirev.2012.04.013

Rowe, P.J., Wickens, L.B., Sahy, D., Marca, A.D., Peckover, E., Noble, S., Özkul, M., Baykara, M.O., Millar, I.L., Andrews, J.E., 2020. Multi-proxy speleothem record of climate instability during the early last interglacial in southern Turkey. *Palaeogeography, Palaeoclimatology, Palaeoecology* **538**. https://doi.org/10.1016/j.palaeo.2019.109422

Rowland, G.H., Ng, H.C., Robinson, L.F., McManus, J.F., Mohamed, K.J., McGee, D., 2017. Investigating the use of 232Th/230Th as a dust proxy using co-located seawater and sediment samples from the low-latitude North Atlantic. *Geochimica et Cosmochimica Acta* **214**, 143–156. https://doi.org/10.1016/j.gca.2017.07.033

Rowland, J.V., Wilson, C.J.N., Gravley, D.M., 2010. Spatial and temporal variations in magma-assisted rifting, Taupo Volcanic Zone, New Zealand. *Journal of Volcanology and Geothermal Research* **190**, 89–108.

Rubin, A. E., Cooper, K.M., Till, C.B., Kent, A.J.R., Costa, F., Bose, M., Gravely, D., Deering, C., Cole, J., 2017. Rapid cooling and cold storage in a silicic magma reservoir recorded in individual crystals. *Science* **356**, 1154–1156.

Russell, J. M., Johnson, T.C., 2005. Late Holocene climate change in the North Atlantic and equatorial Africa: Millennial-scale ITCZ migration. *Geophysical Research Letters* **32**, L17705.

Russo, R.E., Mao, X., Gonzalez, J.J., Mao, S.S., 2002. Femtosecond laser ablation ICP-MS. *Journal of Analytical Atomic Spectrometry* **17**, 1072–1075.

Ruth, U., Wagenbach, D., Steffensen, J.P., Bigler, M., 2003. Continuous record of microparticle concentration and size distribution in the central Greenland NGRIP ice core during the last glacial period. *Journal of Geophysical Research: Atmospheres* **108**, 1–12. https://doi.org/10.1029/2002jd002376

Rutlidge, H., Baker, A., Marjo, C.E., Andersen, M.S., Graham, P.W., Cuthbert, M.O., Rau, G.C., Roshan, H., Markowska, M., Mariethoz, G., Jex, C.N., 2014. Dripwater organic matter and trace element geochemistry in a semi-arid karst environment: Implications for speleothem paleoclimatology. *Geochimica et Cosmochimica Acta* **135**, 217–230. https://doi.org/10.1016/j.gca.2014.03.036

Sadatzki, H., Dokken, T.M., Berben, S.M.P., Muschitiello, F., Stein, R., Fahl, K., Menviel, L., Timmermann, A., Jansen, E., 2019. Sea ice variability in the southern Norwegian Sea during glacial Dansgaard-Oeschger climate cycles. *Science Advances* **25**, 1–10.

Sáenz, F., Durán-Quesada, A.M., 2015. A climatology of low level wind regimes over Central America using a weather type classification approach. *Frontiers in Earth Science* **3**, 1–18. https://doi.org/10.3389/feart.2015.00015

Sahetapy-Engel, S., Self, S., Carey, R.J., Nairn, I.A., 2014. Deposition and generation of multiple widespread fall units from the c. AD 1314 Kaharoa rhyolitic eruption, Tarawera, New Zealand. *Bulletin of Volcanology* **76**, 836.

Sánchez Goñi, M.F., Bard, E., Landais, A., Rossignol, L., D'errico, F., 2013. Air-sea temperature decoupling in western Europe during the last interglacial-glacial transition. *Nature Geoscience* **6**, 837–841. https://doi.org/10.1038/ngeo1924

Santacroce, R., Cioni, R., Marianelli, P., Sbrana, A., Sulpizio, R., Zanchetta, G., Donahue, D.J., Joron, J.L., 2008. Age and whole rock-glass compositions of proximal pyroclastics from the major explosive eruptions of Somma-Vesuvius: A review as a tool for distal tephrostratigraphy. *Journal of Volcanology and Geothermal Research* **177**, 1–18. https://doi.org/10.1016/j.jvolgeores.2008.06.009

Sarikaya, M.A., Çiner, A., 2015. Late pleistocene glaciations and paleoclimate of Turkey. *Bulletin of the Mineral Research and Exploration* **2015**, 111–132. https://doi.org/10.19111/bmre.35245

Sarnthein, M., Karl Stattegger, D.D., Erlenkeuser, H., Schulz, M., Seidov, D., Simstich, J., Van Kreveld, S., 2001. Fundamental Modes and Abrupt Changes in North Atlantic Circulation and Climate over the last 60 ky, in: Schäfer P., Ritzrau W., Schlüter M., T.J. (Ed.), The Northern North Atlantic: A Changing Environment. Springer, Berlin, pp. 365–410.

Savarino, J., Gautier, E., Caillon, N., Albalat, E., Albarède, F., Hattori, S., Petit, J.-R., A., Lipenkov, V., n.d. Where is the Toba eruption in the Vostok ice core? Clues from tephra, O and S isotopes. *EGU General Assembly 2020*. https://doi.org/https://doi.org/10.5194/egusphere-egu2020-4

Scaillet, B., Clemente, B., Evans, B.W., Pichavant, M., 1998. Redox control of sulfur degassing in silicic magmas. *Journal of Geophysical Research: Solid Earth* **103**, 23937–23949. https://doi.org/10.1029/98jb02301

Scaillet, B., Luhr, J.F., Carroll, M.R., 2003. Petrological and volcanological constraints on volcanic sulfur emissions to the atmosphere. *Geophysical Monograph Series* **139**, 11–40. https://doi.org/10.1029/139GM02

Scandone, R., Giacomelli, L., Gasparini, P., 1993. Mount Vesuvius: 2000 yrs of volcanological observations. *Journal of Volcanology and Geothermal Research* **58**, 263–271.

Schacht, U., Wallmann, K., Kutterolf, S., Schmidt, M., 2008. Volcanogenic sediment–seawater interactions and the geochemistry of pore waters. *Chemical Geology* **249**, 321–338.

Schaen, A.J., Cottle, J.M., Singer, B.S., Keller, C.B., Garibaldi, N., Schoene, B., 2017. Complementary crystal accumulation and rhyolite melt segregation in a late Miocene Andean pluton. *Geology* **45**, 835–838.

Schindlbeck, J.C., Kutterolf, S., Freundt, A., Alvarado, G.E., Wang, K.L., Straub, S.M., Hemming, S.R., Frische, M., Woodhead, J.D., 2016. Late Cenozoic tephrostratigraphy offshore the southern Central American Volcanic Arc: 1. Tephra ages and provenance. *Geochemistry, Geophysics, Geosystems* **17**, 4641–4668. https://doi.org/10.1002/2016GC006503

Schindlbeck, J.C., Kutterolf, S., Freundt, A., Scudder, R.P., Pickering, K.T., Murray, R.W., 2013. Emplacement processes of submarine volcaniclastic deposits (IODP Site C0011, Nankai Trough). *Marine Geology* **343**, 115–124.

Schindlbeck, J.C., Kutterolf, S., Freundt, A., Alvarado, G.E., Wang, K.L., Straub, S.M., Hemming, S.R., Frische, M., Woodhead, J.D., 2016. Late Cenozoic tephrostratigraphy offshore the southern Central American Volcanic Arc: 1. Tephra ages and provenance. *Geochemistry, Geophysics, Geosystems* **17**, 4641–4668. https://doi.org/10.1002/2016GC006503

Schmidt, A., Thordarson, T., Oman, L.D., Robock, A., Self, S., 2012. Climatic impact of the long-lasting 1783 Laki eruption: Inapplicability of mass-independent sulfur isotopic composition measurements. *Journal of Geophysical Research Atmospheres* **117**, 1–10. https://doi.org/10.1029/2012JD018414

Schmidt, G. A., Jungclaus, J.H., Ammann, C.M., Bard, E., Braconnot, P., Crowley, T.J., Delaygue, G., Joos, F., Krivova, N.A., Muscheler, R., Otto-Bliesner, B.L., Pongratz, J., Shindell, D.T., Solanki, S.K., Steinhilber, F., Vieira, L.E.A., 2011. Climate forcing reconstructions for use in PMIP simulations of the last millennium (v1.0). *Geoscientific Model Development* **4**, 33–45.

Schmith, J., Höskuldsson, Á., Holm, P.M., Larsen, G., 2018. Large explosive basaltic eruptions at Katla volcano, Iceland: Fragmentation, grain size and eruption dynamics. *Journal of Volcanology and Geothermal Research* **354**, 140–152. https://doi.org/10.1016/j.jvolgeores.2018.01.024

Schmitt, A.K., Danišík, M., Aydar, E., Şen, E., Ulusoy, I., Lovera, O.M., 2014. Identifying the volcanic eruption depicted in a Neolithic painting at Çatalhöyük, Central Anatolia, Turkey. *PLoS ONE* **9**. https://doi.org/10.1371/journal.pone.0084711

Schneider, T., Bischoff, T., Haug, G.H., 2014. Migrations and dynamics of the intertropical convergence zone. *Nature* **513**, 45–53. https://doi.org/10.1038/nature13636

Schoene, B., Schaltegger, U., Brack, P., Latkoczy, C., Stracke, A., Günther, D., 2012. Rates of magma differentiation and emplacement in a ballooning pluton recorded by U-Pb TIMS-TEA, Adamello batholith, Italy. *Earth and Planetary Science Letters* **355**–**356**, 162–173.

Schulz, M., 2002. The tempo of climate change during Dansgaard-Oeschger interstadials and its potential to affect the manifestation of the 1470-year climate cycle. *Geophysical Research Letters* **29**, 2001GL013277.

Schumann, U., Weinzierl, B., Reitebuch, O., Schlager, H., Minikin, A., Forster, C., Baumann, R., Sailer, T., Graf, K., Mannstein, H., Voigt, C., Rahm, S., Simmet, R., Scheibe, M., Lichtenstern, M., Stock, P., Rüba, H., Schauble, D., Tafferner, A., Rautenh, K., 2011. Airborne observations of the Eyjafjalla volcano ash cloud over Europe during air space closure in April and May 2010. *Atmospheric Chemistry and Physics* **11**, 2245–2279.

Scudder, R.P., Murray, R.W., Schindlbeck, J.C., Kutterolf, S., Hauff, F., Underwood, M.B., Gwizd, S., Lauzon, R., McKinley, C.C., 2016. Geochemical approaches to the quantification of dispersed volcanic ash in marine sediment, Progress in Earth and Planetary Science. Progress in Earth and Planetary Science. https://doi.org/10.1186/s40645-015-0077-y

Selbekk, R.S., Trønnes, R.G., 2006. The 1362 AD Öræfajökull eruption, Iceland: Petrology and geochemistry of large-volume homogeneous rhyolite. *Journal of Volcanology and Geothermal Research* **160**, 42–58.

Self, S., 1991. Krakatau Revisited: The Course of Events and Interpretation of the 1883 Eruption. *Geojournal* **28**, 109–121.

Self, S., Blake, S., 2008. Consequences of explosive supereruptions. *Elements* **4**, 41–46.

Self, S., Gertisser, R., 2015. Tying down eruption risk. *Nature Geoscience* **8**, 248–250.

Self, S., Gertisser, R., Thordarson, T., Rampino, M.R., Wolff, J.A., 2004. Magma volume, volatile emissions, and stratospheric aerosols from the 1815 eruption of Tambora. *Geophysical Research Letters* **31**, L20608.

Sensoy, S., Demircan, M., Ulupinar, U., Balta, I., 2008. Climate of Turkey [WWW Document]. URL http://www.dmi.gov.tr/iklim/iklim.aspx (accessed 5.20.20).

Shakun, J.D., Burns, S.J., Fleitmann, D., Kramers, J., Matter, A., Al-Subary, A., 2007. A high-resolution, absolute-dated deglacial speleothem record of Indian Ocean climate from Socotra Island, Yemen. *Earth and Planetary Science Letters* **259**, 442–456. https://doi.org/10.1016/j.epsl.2007.05.004

Sharma, K., Self, S., Blake, S., Thordarson, T., Larsen, G., 2008. The AD 1362 Öræfajökull eruption, S.E. Iceland: Physical volcanology and volatile release. *Journal of Volcanology and Geothermal Research* **178**, 719–739. https://doi.org/10.1016/j.jvolgeores.2008.08.003

Sheldrake, T., Caricchi, L., 2017. Regional variability in the frequency and magnitude of large explosive volcanic eruptions. *Geology* **45**, 111–114. https://doi.org/10.1130/G38372.1

Sheng, J.X., Weisenstein, D.K., Luo, B.P., Rozanov, E., Arfeuille, F., Peter, T., 2015. A perturbed parameter model ensemble to investigate Mt. Pinatubo's 1991 initial sulfur mass emission. *Atmospheric Chemistry and Physics* **15**, 11501–11512. https://doi.org/10.5194/acp-15-11501-2015

Shinohara, H., 2008. Excess degassing from volcanoes and its role on eruptive and intrusive activity. *Reviews of Geophysics* **46**, 1–31. https://doi.org/10.1029/2007RG000244

Siebert, L., Cottrell, E., Venzke, E., Andrews, B., 2015. Earth's Volcanoes and their Eruptions: An Overview, in: Sigurdsson, H. (Ed.), Encyclopaedia of Volcanoes. Academic Press.

Siebert, L., Simkin, T., Kimberly, P., 2010. Volcanoes of the World, 3rd Editio. ed. University of California Press, Berkeley.

Sigl, M., Winstrup, M., McConnell, J.R., Welten, K.C., Plunkett, G., Ludlow, F., Büntgen, U., Caffee, M., Chellman, N., Dahl-Jensen, D., Fischer, H., Kipfstuhl, S., Kostick, C., Maselli, O.J., Mekhaldi, F., Mulvaney, R., Muscheler, R., Pasteris, D.R., Pilcher, J.R., Salzer, M., Schüpbach, S., Steffensen, J.P., Vinther, B.M., Woodruff, T.E., 2015. Timing and climate forcing of volcanic eruptions for the past 2,500 years. *Nature* **523**, 543–549. https://doi.org/10.1038/nature14565

Sigmarsson, O., Vlastelic, I., Andreasen, R., Bindemann, I., Devidal, J.L., Moune, S., Keiding, J.K., Höskuldsson, A., Thordarason, T., 2011. Remobilization of silicic intrusion by mafic magmas during the 2010 Eyjafjallajökull eruption. *Solid Earth* **2**, 271–281.

Sigurdsson, H., Carey, S., Alexandri, M., Vougioukalakis, G., Croff, K., Roman, C., Sakellariou, D., Anagnostou, C., Rousakis, G., Ioakim, C., Goguo, A., Ballas, D., Misaridis, T., Nomikou, P., 2006. Marine investigations of Greece's Santorini volcanic field. *EOS Transactions, American Geophysical Union* **87**, 337–348.

Siklósy, Z., Demény, A., Vennemann, T.W., Pilet, S., Kramers, J., Leél-Őssy, S., Bondár, M., Shen, C-C., Hegner, E., 2009. Bronze Age volcanic event recorded in stalagmites by combined isotope and trace element studies. *Rapid Communications in Mass Spectrometry* **23**, 801–808. https://doi.org/10.1002/rcm

Silver, E., Day, S., Ward, S., Hoffmann, G., Llanes, P., Driscoll, N., Appelgate, B., Saunders, S., 2009. Volcano collapse and tsunami generation in the Bismarck Volcanic Arc, Papua New Guinea. *Journal of Volcanology and Geothermal Research* **186**, 210–222.

Simonsen, M.F., Baccolo, G., Blunier, T., Borunda, A., Delmonte, B., Frei, R., Goldstein, S., Grinsted, A., Kjær, H.A., Sowers, T., Svensson, A., Vinther, B., Vladimirova, D., Winckler, G., Winstrup, M., Vallelonga, P., 2019. East Greenland ice core dust record reveals timing of Greenland ice sheet advance and retreat. *Nature Communications* **10**. https://doi.org/10.1038/s41467-019-12546-2

Sinclair, D.J., Banner, J.L., Taylor, F.W., Partin, J., Jenson, J., Mylroie, J., Goddard, E., Quinn, T., Jocson, J., Miklavič, B., 2012. Magnesium and strontium systematics in tropical speleothems from the Western Pacific. *Chemical Geology* **294–295**, 1–17. https://doi.org/10.1016/j.chemgeo.2011.10.008

Sinclair, D.J., Kinsley, L.P.J., McCulloch, M.T., 1998. High resolution analysis of trace elements in corals by laser ablation ICP-MS. *Geochimica et Cosmochimica Acta* **62**, 1889–1901. https://doi.org/10.1016/S0016-7037(98)00112-4

Sinha, A., Cannariato, K.G., Stott, L.D., Li, H.C., You, C.F., Cheng, H., Edwards, R.L., Singh, I.B., 2005. Variability of Southwest Indian summer monsoon precipitation during the Bølling-Ållerød. *Geology* **33**, 813–816. https://doi.org/10.1130/G21498.1

Smith, E.I., Jacobs, Z., Johnsen, R., Ren, M., Fisher, E.C., Oestmo, S., Wilkins, J., Harris, J.A., Karkanas, P., Fitch, S., Ciravolo, A., Keenan, D., Cleghorn, N., Lane, C.S., 2018. Humans thrived in South Africa through the Toba eruption about 74,000 years ago. *Nature* **555**, 511–515. https://doi.org/10.1038/nature25967

Smith, R.E., Smith, V.C., Fontijn, K., Gebhardt, A.C., Wastegård, S., Zolitschka, B., Ohlendorf, C., Stern, C., Mayr, C., 2019. Refining the Late Quaternary tephrochronology for southern South America using the Laguna Potrok Aike sedimentary record. *Quaternary Science Reviews* **218**, 137–156. https://doi.org/10.1016/j.quascirev.2019.06.001

Smith, V.C., Isaia, R., Pearce, N.J.G., 2011. Tephrostratigraphy and glass compositions of post-15 kyr Campi Flegrei eruptions: implications for eruption history and chronostratigraphic markers. *Quaternary Science Reviews* **30**, 3638–3660.

Smith, V.C., Pearce, N.J.G., Matthews, N.E., Westgate, J.A., Petraglia, M.D., Haslam, M., Lane, C.S., Korisettar, R., Pal, J.N., 2011. Geochemical fingerprinting of the widespread Toba tephra using biotite compositions. *Quaternary International* **246**, 97–104. https://doi.org/10.1016/j.quaint.2011.05.012

Sneed, S.B., Mayewski, P.A., Sayre, W.G., Handley, M.J., Kurbatov, A. V., Taylor, K.C., Bohleber, P., Wagenbach, D., Erhardt, T., Spaulding, N.E., 2015. New LA-ICP-MS cryocell and calibration technique for sub-millimeter analysis of ice cores. *Journal of Glaciology* **61**, 233–242. https://doi.org/10.3189/2015JoG14J139

Sobczyk, A., Kasprzak, M., Marciszak, A., Stefaniak, K., 2016. Karst phenomena in metamorphic rocks of the Śnieżnik Massif (East Sudetes): state-of-the-art and significance for tracing a Late-Cenozoic evolution of the Sudetes. *Przeglad Geologiczny* **64**, 710–718.

Solano, J. M. S., Jackson, M. D., Sparks, R. S. J., Blundy, J.D., 2014. Evolution of major and trace element composition during melt migration through crystalline mush: implications for chemical differentiation in the crust. *American Journal of Science* **314**, 895–939.

Solano, J.M.S., Jackson, M.D., Sparks, R.S.J., Blundy, J.D., Annen, C., 2012. Segregation in deep crustal hot zones: a mechanism for chemical differentiation, crustal assimilation and the formation of evolved magmas. *Journal of Petrology* **53**, 1999–2026.

Song, S.R., Chen, C.H., Lee, M.Y., Yang, T.F., Iizuka, Y., Wei, K.Y., 2000. Newly discovered eastern dispersal of the youngest Toba Tuff. *Marine Geology* **167**, 303–312. https://doi.org/10.1016/S0025-3227(00)00034-7

Sonnek, K.M., Mårtensson, T., Veibäck, E., Tunved, P., Grahn, H., von Schoenberg, P., Brännström, N., Bucht, A., 2017. The impacts of a Laki-like eruption on the present Swedish society. *Natural Hazards* **88**, 1565–1590.

Sorin, L., Anton, V., Miryam, B.M., Roi, P., Amos, F., 2010. Late Pleistocene palaeoclimatic and palaeoenvironmental reconstruction of the Dead Sea area (Israel), based on speleothems and cave

stromatolites. *Quaternary Science Reviews* **29**, 1201–1211. https://doi.org/10.1016/j.quascirev.2010.01.018

Spanos, S., Maheras, P., Karacostas, T., Pennas, P., 2003. Objective climatology of 500-hPa cyclones in central and East Mediterranean region during warm-dry period of the year. *Theoretical and Applied Climatology* **75**, 167–178. https://doi.org/10.1007/s00704-003-0726-8

Sparks, R.S.J., Annen, C., Blundy, J.D., Cashman, K. V., Rust, A.C., Jackson, M.D., 2019. Formation and dynamics of magma reservoirs. *Philosophical Transactions of the Royal Society A: Mathematical, Physical and Engineering Sciences* **377**. https://doi.org/10.1098/rsta.2018.0019

Sparks, R.S.J., Folkes, C.B., Humphreys, M.C.S., Barfod, D.N., Clavero, J., Sunagua, M.C., McNutt, S.R., Pritchard, M.E., 2008. Uturuncu volcano, Bolivia: Volcanic unrest due to mid-crustal magma intrusion. *American Journal of Science* **308**, 727–769. https://doi.org/10.2475/06.2008.01

Sparks, R.S.J., Bursik, M.I., Carey, S., Gilbert, J.S., Glaze, L.S., Sigurdsson, H., Woods, A.W., 1997. Volcanic plumes. Wiley, New York.

Sparks, R.S.J., Cashman, K., 2017. Dynamic magma systems: Implications for forecasting volcanic activity. *Elements* **13**, 35–40.

Sparks, R.S.J., Self, S., Grattan, J.P., Oppenheimer, C., Pyle, D.M., Rymer, H., 2005. Supereruptions: global effects and future threats. London.

Sparks, R.S.J., Wilson, L., Sigurdsson, H., 1981. The pyroclastic deposits of the 1875 eruption of Askja, Iceland. *Philosophical Transactions of the Royal Society London* **299**, 241–273.

Springer, G.S., Rowe, H.D., Hardt, B., Cheng, H., Edwards, R.L., 2014. Geophysical Research Letters. *Geophysical Research Letters* **41**, 3233–3237. https://doi.org/10.1002/2014GL061184.Received

Stefaniak, K., 2015. Neogene and Quaternary Cervidae from Poland. Institute of Systematics and Evolution of Animals Polish Academy of Sciences, Kraków.

Steffensen, Jørgen. Peder., Andersen, Katrine. K., Bigler, Matthias., Clausen, Henrik. B., Dahl-Jensen, Dorthe., Fischer, Hubertus., Goto-Azuma, Kumiko., Johnsen, Sigfús. J., Jouzel, Jean., Masson-Delmotte, Valérie., Popp, Trevor., Rasmussen, Sune. O., Rö, J.W.C., 2008. High-Resolution Greenland Ice Core Data Show Abrupt Climate Change Happens in Few Years. *Science* **321**, 680–684.

Stein, A.F., Draxler, R.R, Rolph, G.D., Stunder, B.J.B., Cohen, M.D., Ngan, F., 2015. NOAA's HYSPLIT atmospheric transport and dispersion modelling system. *Bulletin of the American Meteorological Society* **96**, 2059–2077.

Stenchikov, G., Delworth, T.L., Ramaswamy, V., Stouffer, R.J., Wittenberg, A., Zeng, F., 2009. Volcanic signals in oceans. *Journal of Geophysical Research Atmospheres* **114**, 1–13. https://doi.org/10.1029/2008JD011673

Stevens, L.A., Behn, M.D., McGuire, J.J., Das, S.B., Joughin, I., Herring, T., Shean, D.E., King, M.A., 2015. Hydrologically Induced Basal Slip Triggers Greenland Supraglacial Lake Drainages. *Nature* **522**, 73–76.

Stevenson, J.A., Millington, S.C., Beckett, F.M., Swindles, G.T., Thordarson, T., 2015. Big grains go far: Understanding the discrepancy between tephrochronology and satellite infrared measurements of volcanic ash. *Atmospheric Measurement Techniques* **8**, 2069–2091. https://doi.org/10.5194/amt-8-2069-2015

Stivrins, N., Wulf, S., Wastegård, S., Lind, E.M., Alliksaar, T., Gałka, M., Andersen, T.J., Heinsali, A., Seppä, H., Veski, S., 2016. Detection of the Askja AD 1875 cryptotephra in Latvia, Eastern Europe. *Journal of Quaternary Science* **31**, 437–441.

Stocker, T. F., Johnsen, S.J., 2003. A minimum thermodynamic model for the bipolar seesaw. *Paleoceanography* **18**, 1087.

Stoffel, M., Khodri, M., Corona, C., Guillet, S., Poulain, V., Bekki, S., Guiot, J., Luckman, B.H., Oppenheimer, C., Lebas, N., Beniston, M., Masson-Delmotte, V., 2015. Estimates of volcanic-induced cooling in the Northern Hemisphere over the past 1,500 years. *Nature Geoscience* **8**, 784–788. https://doi.org/10.1038/ngeo2526

Stokes, C., Clark, C., Darby, D., Hodgson, D., 2005. Late Pleistocene ice export events into the Arctic Ocean from the M'Clure Strait Ice Stream, Canadian Arctic Archipelago. *Global and Planetary Change* **49**, 139–162.

Stoll, H.M., Moreno, A., Mendez-Vicente, A., Gonzalez-Lemos, S., Jimenez-Sanchez, M., Dominguez-Cuesta, M.J., Edwards, R.L., Cheng, H., Wang, X., 2013. Paleoclimate and growth rates of speleothems in the northwestern Iberian Peninsula over the last two glacial cycles. *Quaternary Research (United States)* **80**, 284–290. https://doi.org/10.1016/j.yqres.2013.05.002

Stoll, H.M., Müller, W., Prieto, M., 2012. I-STAL, a model for interpretation of Mg/Ca, Sr/Ca and Ba/Ca variations in speleothems and its forward and inverse application on seasonal to millennial scales. *Geochemistry, Geophysics, Geosystems* **13**, 1–27. https://doi.org/10.1029/2012GC004183

Storey, M., Roberts, R.G., Saidin, M., 2012. Astronomically calibrated 40 Ar / 39 Ar age for the Toba supereruption and global synchronization of late Quaternary records. *Proceedings of the National Academy of Science* **109**, 18684–18688. https://doi.org/10.1073/pnas.1208178109/-/DCSupplemental.www.pnas.org/cgi/doi/10.1073/pnas.1208178109

Stothers, R.B., 2000. Climatic and demographic consequences of the massive eruption of 1258. *Climate Change* **45**, 361–374.

Strikis, N.M., Cruz, F.W., Cheng, H., Karmann, I., Edwards, R.L., Vuille, M., Wang, X.F., de Paula , M.S., Novello, V.F., Auler, A.S., 2011. Abrupt variations in South American monsoon rainfall during the Holocene based on a speleothem record from central-eastern Brazil. *Geology* **39**, 1075–1078.

Stríkis, N.M., Cruz, F.W., Barreto, E.A.S., Naughton, F., Vuille, M., Cheng, H., Voelker, A.H.L., Zhang, H., Karmann, I., Lawrence Edwards, R., Auler, A.S., Santos, R.V., Sales, H.R., 2018. South American monsoon response to iceberg discharge in the North Atlantic. *Proceedings of the National Academy of Sciences of the United States of America* **115**, 3788–3793. https://doi.org/10.1073/pnas.1717784115

Stroński Park Aktywności, n.d. Jaskinia Niedźwiedzia: Description of the Cave [WWW Document]. URL http://jaskinianiedzwiedzia.pl/index/opis-jaskini.html (accessed 1.16.20).

Sun, C., Plunkett, G., Liu, J., Zhao, H., Sigl, M., McConnell, J.R., Pilcher, J.R., Vinther, B., Steffensen, J.P., Hall, V., 2014. Ash from Changbaishan Millennium eruption recorded in Greenland ice: implications for determining the eruptions timing and impact. *Geophysical Research Letters* **41**, 694–701.

Sun, C., Liu, J., You, H., Nemeth, K., 2017. Tephrostratigraphy of Changbaishan volcano, northeast China, since the mid-Holocene. *Quaternary Science Reviews* **177**, 104–119. https://doi.org/10.1016/j.quascirev.2017.10.021

Svensson, A., Bigler, M., Blunier, T., Clausen, H.B., Dahl-Jensen, D., Fischer, H., Fujita, S., Goto-Azuma, K., Johnsen, S.J., Kawamura, K., Kipfstuhl, S., Kohno, M., Parrenin, F., Popp, T., Rasmussen, S.O., Schwander,

J., Seierstad, I., Severi, M., Steffensen, J.P., Udisti, R., Uemura, R., Vallelonga, P., Vinther, B.M., Wegner, A., Wilhelms, F., Winstrup, M., 2013. Direct linking of Greenland and Antarctic ice cores at the Toba eruption (74 ka BP). *Climate of the Past* **9**, 749–766. https://doi.org/10.5194/cp-9-749-2013

Svensson, A., Dahl-Jensen, D., Steffensen, J.P., Blunier, T., Rasmussen, S.O., Vinther, B.M., Vallelonga, P., Capron, E., Gkinis, V., Cook, E., Kjær, H.A., Muscheler, R., Kipfstuhl, S., Wilhelms, F., Stocker, T.F., Fischer, H., Adolphi, F., Erhardt, T., Sigl, M., Landais, A., Parrenin, F., Buizert, C., McConnell, J.R., Severi, M., Mulvaney, R., Bigler, M., 2020. Bipolar volcanic synchronization of abrupt climate change in Greenland and Antarctic ice cores during the last glacial period. *Climate of the Past* **16**, 1565–1580. https://doi.org/10.5194/cp-16-1565-2020

Swallow, E.J., Wilson, C.J., Myers, M.L., Wallace, P.J., Collins, K.S., Smith, E.G.C., 2018. Evacuation of multiple magma bodies and the onset of caldera collapse in a supereruption, captured in glass and mineral compositions. *Contributions to Mineralogy and Petrology* **173**, 33.

Swallow, E.J., Wilson, C.J.N., Charlier, B.L.A., Gamble, J.A., 2019. The Huckleberry Ridge Tuff, Yellowstone: Evacuation of multiple magmatic systems in a complex episodic eruption. *Journal of Petrology* **60**, 1371–1426. https://doi.org/10.1093/petrology/egz034

Swart, P.K., 2015. The geochemistry of carbonate diagenesis: The past, present and future. *Sedimentology* **62**, 1233–1304. https://doi.org/10.1111/sed.12205

Swindles, G. T., Watson, E. J., Savov, I. P., Lawson, I. T., Schmidt, A., Hooper, A., Cooper, C. L., Connor, C.B., Gloor, M., Carrivick, J.L., 2018. Climatic control on Icelandic volcanic activity during the mid-Holocene. *Geology* **46**, 47–50.

Swindles, G.T., Galloway, J., Outram, Z., Turner, K., Schofield, J.E., Newton, A.J., Dugmore, A.J., Church, M.J., Watson, E.J., Batt, C., Bond, J., Edwards, K.J., Turner, V., Bashford, D., 2013. Re-deposited cryptotephra layers in Holocene peats linked to anthropogenic activity. *Holocene* **23**, 1493–1501.

Swindles, G.T., Lawson, I.T., Savov, I.P., Connor, C.B., Plunkett, G., 2011. A 7000 yr perspective on volcanic ash clouds affecting northern Europe. *Geology* **39**, 887–890.

Swindles, G.T., Watson, E.J., Savov, I.P., Cooper, C.L., Lawson, I.T., Schmidt, A., Carrivick, J.L., 2017. Holocene volcanic ash database for Northern Europe. *Database*. https://doi.org/10.13140/RG.2.2.11395.60966.

Sylvester, P.J., Jackson, S.E., 2016. A Brief History of Laser Ablation Inductively Coupled Plasma Mass Spectrometry (LA–ICP–MS). *Elements* **12**, 307–310.

Symons, G.J., n.d. The Eruption of Krakatoa, and Subsequent Phenomena. Trübner, London.

Syracuse, E. M., & Abers, G.A., 2006. Global compilation of variations in slab depth beneath arc volcanoes and implications. *Geochemistry, Geophysics, Geosystems* **7**, Q05017.

Szwed, M., 2019. Variability of precipitation in Poland under climate change. *Theoretical and Applied Climatology* **135**, 1003–1015. https://doi.org/10.1007/s00704-018-2408-6

Szymanowski, D., Wotzclaw, J.-F., Ellis, B.S., Bachmann, O., Guillong, M., von Quadt, A., 2017. Protracted near-solidus storage and pre-eruptive rejuvenation of large magma reservoirs. *Nature Geoscience* **10**, 777–782.

Tatsumi, Y., Suzuki-Kamata, K., Matsuno, T., Ichihara, H., Seama, N., Kiyosugi, K., Nakaoka, R., Nakahigashi, K., Takizawa, H., Hayashi, K., Chiba, T., Shimizu, S., Sano, M., Iawmaru, H., Morozumi, H., Sugioka, H., Yamamoto, Y., 2018. Giant rhyolite lava dome formation after 7.3 ka supereruption at Kikai caldera, SW Japan. *Scientific Reports* **8**, 2753.

Tavazzani, L., Peres, S., Sinigoi, S., Demarchi, G., Economos, R.C., Quick, J.E., 2020. Timescales and Mechanisms of Crystal-mush Rejuvenation and Melt Extraction Recorded in Permian Plutonic and Volcanic Rocks of the Sesia Magmatic System (Southern Alps, Italy). *Journal of Petrology* **egga049**.

Teller, J.T., 1995. The impact of large ice sheets on continental paleohydrology, in: Gregory, K., Baker, V., Starkel, L. (Ed.), Global Continental Paleohydrology. pp. 109–129.

Teller, J.T., Leverington, D.W., Mann, J.D., 2002. Freshwater outbursts to the oceans from glacial Lake Agassiz and their role in climate change during the last deglaciation. *Quaternary Science Reviews* **21**, 879–887.

Thomas, E.R., Wolff, E.W., Mulvaney, R., Johnsen, S.J., Steffensen, J.P., Arrowsmith, C., 2009. Anatomy of a Dansgaard-Oeschger warming transition : High-resolution analysis of the North Greenland Ice Core Project ice core. *Journal of Geophysical Research* **114**, 1–9. https://doi.org/10.1029/2008JD011215

Thompson, D.P., Menounos, B., Osborn, G., 2009. Holocene and latest Pleistocene alpine glacier fluctuations: a global perspective. *Quaternary Science Reviews* **28**, 2021–2033.

Thorarinsdottir, E. F., Arnalds, O., 2012. Wind erosion of volcanic materials in the Hekla area, South Iceland. *Aeolian Research* **4**, 39–50.

Thordarson, T., Rampino, M., Keszthelyi, L., Self, S., 2009. Effects of megascale eruptions on Earth and Mars, in: Chapman, M.G., Keszthelyi, L.P. (Ed.), Preservation of Random Megascale Events on Mars and Earth: Influence on Geologic History. Geological Society of America Special Paper, pp. 37–55.

Thordarson, T., Self, S., 2003. Atmospheric and environmental effects of the 1783-1784 Lakí eruption: a review and reassessment. *Journal of Geophysical Research* **108**, D1.

Thordarson, T., Self, S., 1993. The Laki (Skaftár Fires) and Grímsvötn eruptions in 1783–1785. *Bulletin of Volcanology* **55**, 233–263.

Thordarson, T., Self, S., Óskarsson, N., Hulsebosch, T., 1996. Sulfur, chlorine, and fluorine degassing and atmospheric loading by the 1783–1784 AD Laki (Skaftár fires) eruption in Iceland. *Bulletin of Volcanology* **58**, 205–225.

Thordarson, T., Larsen, G., 2007. Volcanism in Iceland in historical time: Volcano types, eruption styles and eruptive history. *Journal of Geodynamics* **43**, 118–152. https://doi.org/10.1016/j.jog.2006.09.005

Thordarson, T., Hoskuldsson, A., 2008. Postglacial volcanism in Iceland. *Jokull* **58**, 197–228.

Thouret, J-C., Juvigné, E., Marino, J., Moscol, M., Loutsch, I., Davila, J., Legeley-Padovani, A., Lamadon, S., Rivera, M., 2002. Late Pleistocene and Holocene tephrostratigraphy and chronology in Southern Peru. *Boletín Sociedad geológica del Perú* **93**, 45–61.

Tierz, P., Loughlin, S.C., Calder, E.S., 2019. VOLCANS: an objective, structured and reproducible method for identifying sets of analogue volcanoes. *Bulletin of Volcanology* **81**. https://doi.org/10.1007/s00445-019-1336-3

Till, C. B., Vazquez, J. A., Boyce, J.W., 2015. Months between rejuvenation and volcanic eruption at Yellowstone caldera, Wyoming. *Geology* **43**, 695–698.

Timmreck, C., 2012. Modelling the climatic effects of large explosive volcanic eruptions. *Wiley Interdisciplinary Reviews: Climate Change* **3**, 545–564. https://doi.org/10.1002/wcc.192

Timmreck, C., Graf, H.F., Zanchettin, D., Hagemann, S., Kleinen, T., Krüger, K., 2012. Climate response to the Toba super-eruption: regional changes. *Quaternary International* **258**, 30–44.

Timmreck, C., Graf, H.F., Lorenz, S.J., Niemeier, U., Zanchettin, D., Matei, D., Jungclaus, J.H., Crowley, T.J., 2010. Aerosol size confines climate response to volcanic super - eruptions. *Geophysical Research Letters* **37**, 1–5. https://doi.org/10.1029/2010GL045464

Timms, R.G.O., Matthews, I.P., Lowe, J.J., Palmer, A.P., Weston, D.J., MacLeod, A., Blockley, S.P.E., 2019. Establishing tephrostratigraphic frameworks to aid the study of abrupt climatic and glacial transitions: a case study of the Last Glacial-Interglacial Transition in the British Isles (c. 16-8 ka BP). *Earth-Science Reviews* **192**, 34–64. https://doi.org/10.1016/j.earscirev.2019.01.003

Tomlinson, E.L., Smith, V.C., Albert, P.G., Aydar, E., Civetta, L., Cioni, R., Çubukçu, E., Gertisser, R., Isaia, R., Menzies, M.A., Orsi, G., Rosi, M., Zanchetta, G., 2015. The major and trace element glass compositions of the productive Mediterranean volcanic sources: tools for correlating distal tephra layers in and around Europe. *Quaternary Science Reviews* **118**, 48–66.

Tomlinson, E.L., Smith, V.C., Albert, P.G., Aydar, E., Civetta, L., Cioni, R., Çubukçu, E., Gertisser, R., Isaia, R., Menzies, M.A., Orsi, G., Rosi, M., Zanchetta, G., 2015. The major and trace element glass compositions of the productive Mediterranean volcanic sources: Tools for correlating distal tephra layers in and around Europe. *Quaternary Science Reviews* **118**, 48–66. https://doi.org/10.1016/j.quascirev.2014.10.028

Tongal, H., 2019. Spatiotemporal analysis of precipitation and extreme indices in the Antalya Basin, Turkey. *Theoretical and Applied Climatology* **138**, 1735–1754. https://doi.org/10.1007/s00704-019-02927-4

Toohey, M., Krüger, K., Niemeier, U., Timmreck, C., 2011. The influence of eruption season on the global aerosol evolution and radiative impact of tropical volcanic eruptions. *Atmospheric Chemistry and Physics* **11**, 12351–12367. https://doi.org/10.5194/acp-11-12351-2011

Toohey, M., Krüger, K., Schmidt, H., Timmreck, C., Sigl, M., Stoffel, M., Wilson, R., 2019. Disproportionately strong climate forcing from extratropical explosive volcanic eruptions. *Nature Geoscience* **12**, 100–107. https://doi.org/10.1038/s41561-018-0286-2

Toohey, M., Krüger, K., Sigl, M., Stordal, F., Svensen, H., 2016. Climatic and societal impacts of a volcanic double event at the dawn of the Middle Ages. *Climatic Change* **136**, 401–412. https://doi.org/10.1007/s10584-016-1648-7

Törnqvist, T. E., Hijma, M.P., 2012. Links between early Holocene ice-sheet decay, sea-level rise and abrupt climate change. *Nature Geoscience* **5**, 601–606.

Townsend, M., Huber, C., Degruyter, W., Bachmann, O., 2019. Magma Chamber Growth During Intercaldera Periods: Insights From Thermo-Mechanical Modeling With Applications to Laguna del Maule, Campi Flegrei, Santorini, and Aso. *Geochemistry, Geophysics, Geosystems* **20**, 1574–1591. https://doi.org/10.1029/2018GC008103

Tramontano, S., Gualda, G.A., Ghiorso, M.S., 2017. Internal triggering of volcanic eruptions: tracking overpressure regimes for giant magma bodies. *Earth and Planetary Science Letters* **472**, 142–151.

Treble, P., Shelley, J.M.G., Chappell, J., 2003. Comparison of high-resolution sub-annual records of trace elements in a modern (1911–1992) speleothem with instrumental climate data from southwest Australia. *Earth and Planetary Science Letters* **216**, 141–153.

Trouet, V., Esper, J., Graham, N.E., Baker, A., Scourse, J.D., Frank, D.C., 2009. Persistent positive north atlantic oscillation mode dominated the medieval climate anomaly. *Science* **324**, 78–80. https://doi.org/10.1126/science.1166349

Tupper, A., Oswalt, J. S., Rosenfeld, D., 2005. Satellite and radar analysis of the volcanic - cumulonimbi at Mount Pinatubo, Philippines, 1991. *Journal of Geophysical Research: Atmospheres* **110**, D09204.

Türkeş, M., Erlat, E., 2005. Climatological responses of winter precipitation in Turkey to variability of the North Atlantic Oscillation. *Theoretical Applications in Climatology* **81**, 45–69.

Türkeş, M., Koç, T., Sariş, F., 2008. Spatiotemporal variability of precipitation total series over Turkey. *International Journal of Climatology* **29**, 1056–1074.

Türkeş, M., Erlat, E., 2009. Winter mean temperature variability in Turkey associated with the North Atlantic Oscillation. *Meteorology and Atmospheric Physics* **105**, 211–225. https://doi.org/10.1007/s00703-009-0046-3

Türkeş, M., Erlat, E., 2018. Variability and trends in record air temperature events of Turkey and their associations with atmospheric oscillations and anomalous circulation patterns. *International Journal of Climatology* **38**, 5182–5204. https://doi.org/10.1002/joc.5720

Tzedakis, P.C., Channell, J.E.T., Hodell, D.A., Kleiven, H.F., Skinner, L.C., 2012. Determining the natural length of the current interglacial. *Nature Geoscience* **5**, 138–142. https://doi.org/10.1038/ngeo1358

Ubide, T., McKenna, C.A., Chew, D.M., Kamber, B.S., 2015. High-resolution LA-ICP-MS trace element mapping of igneous minerals: In search of magma histories. *Chemical Geology* **409**, 157–168.

Uerlings, R., Matusch, A., Weiskirchen, R., 2016. Standardization and Normalization of Data from Laser Ablation Inductively Coupled Plasma Mass Spectrometry., in: Yong, D. (Ed.), Applications of Laser Ablation - Thin Film Deposition, Nanomaterial Synthesis and Surface Modification. https://doi.org/http://dx.doi.org/10.5772/64769

Újvári, G., Kovács, J., Varga, G., Raucsik, B., Marković, S.B., 2010. Dust flux estimates for the Last Glacial Period in East Central Europe based on terrestrial records of loess deposits: A review. *Quaternary Science Reviews* **29**, 3157–3166. https://doi.org/10.1016/j.quascirev.2010.07.005

Unal, Y.S., Deniz, A., Toros, H., Incecik, S., 2012. Temporal and spatial patterns of precipitation variability for annual, wet, and dry seasons in Turkey. *International Journal of Climatology* **32**, 392–405. https://doi.org/10.1002/joc.2274

Ünal-Imer, E., Shulmeister, J., Zhao, J.X., Tonguç Uysal, I., Feng, Y.X., Duc Nguyen, A., Yüce, G., 2015. An 80 kyr-long continuous speleothem record from Dim Cave, SW Turkey with paleoclimatic implications for the Eastern Mediterranean. *Scientific Reports* **5**, 1–11. https://doi.org/10.1038/srep13560

Ünal-Imer, E., Shulmeister, J., Zhao, J.X., Uysal, I.T., Feng, Y.X., 2016. High-resolution trace element and stable/radiogenic isotope profiles of late Pleistocene to Holocene speleothems from Dim Cave, SW Turkey. *Palaeogeography, Palaeoclimatology, Palaeoecology* **452**, 68–79. https://doi.org/10.1016/j.palaeo.2016.04.015

Unglert, K., Radić, V., Jellinek, A.M., 2016. Principal component analysis vs. self-organizing maps combined with hierarchical clustering for pattern recognition in volcanic seismic spectra. *Journal of Volcanology and Geothermal Research* **320**, 58–74.

Vakhrameeva, P., Wulf, S., Koutsodendris, A., Tjallingii, R., Fletcher, W.J., Appelt, O., Ludwig, T., Knipping, M., Trieloff, M., Pross, J., 2019. Eastern Mediterranean volcanism during Marine Isotope Stages 9 to 7e (335–235 ka): Insights based on cryptotephra layers at Tenaghi Philippon, Greece. *Journal of Volcanology and Geothermal Research* **380**, 31–47.

Vaks, A., Bar-Matthews, M., Matthews, A., Ayalon, A., Frumkin, A., 2010. Middle-Late Quaternary paleoclimate of northern margins of the Saharan-Arabian Desert: Reconstruction from speleothems of Negev Desert, Israel. *Quaternary Science Reviews* **29**, 2647–2662. https://doi.org/10.1016/j.quascirev.2010.06.014

van Breukelen, M.R., Vonhof, H.B., Hellstrom, J.C., Wester, W.C.G., Kroon, D., 2008. Fossil dripwater in stalagmites reveals Holocene temperature and rainfall variation in Amazonia. *Earth and Planetary Science Letters* **275**, 54–60. https://doi.org/10.1016/j.epsl.2008.07.060

Van de Wal, R.S.W., Boot, W., Van den Broeke, M.R., Smeets, C.J.P.P., Reijmer, C.H., Donker, J.J. A., Oerlemans, J., 2008. Large and rapid melt-induced velocity changes in the ablation zone of the Greenland ice sheet. *Science* **321**, 111–113.

van der Bilt, W.G.M., Lane, C.S., Bakke, J., 2017. Ultra-distal Kamchatkan ash on Arctic Svalbard: Towards hemispheric cryptotephra correlation. *Quaternary Science Reviews* **164**, 230–235. https://doi.org/10.1016/j.quascirev.2017.04.007

Vandergoes, M. J., Hogg, A.G., Lowe, D.J., Newnham, R.M., Denton, G.H., Southon, J., Barrell, D.J.A., Wilson, C.J.N., McGlone, M.S., Allan, A.S.R., Almond, P.C., Petchy, F., Dabell, K., Dieffenbacher-Krall, A.C., Blaauw, M., 2013. A revised age for the Kawakawa/Oruanui tephra, a key marker for the last Glacial Maximum in New Zealand. *Quaternary Science Reviews* **74**, 195–201.

Venzke, E., 2013. Global Volcanism Programme, Volcanoes of the World, v. 4.8.5.

Verbitsky, M., Saltzman, B., 1995. A diagnostic analysis of Heinrich glacial surge events. *Paleoceanography* **10**, 59–65.

Viau, A. E., Gajewski, K., Sawada, M. C., Fines, P., 2006. Millennial-scale temperature variations in North America during the Holocene. *Journal of Geophysical Research* **111**.

Vidal, C.M., Komorowski, J.C., Métrich, N., Pratomo, I., Kartadinata, N., Prambada, O., Michel, A., Carazzo, G., Lavigne, F., Rodysill, J., Fontijn, K., Surono, 2015. Dynamics of the major plinian eruption of Samalas in 1257 A.D. (Lombok, Indonesia). *Bulletin of Volcanology* **77**. https://doi.org/10.1007/s00445-015-0960-9

Vidal, C.M., Métrich, N., Komorowski, J.C., Pratomo, I., Michel, A., Kartadinata, N., Robert, V., Lavigne, F., 2016. The 1257 Samalas eruption (Lombok, Indonesia): The single greatest stratospheric gas release of the Common Era. *Scientific Reports* **6**, 1–13. https://doi.org/10.1038/srep34868

Vigier, N., Rollion-Bard, C., Levenson, Y., Erez, J., 2015. Lithium isotopes in foraminifera shells as a novel proxy for the ocean dissolved inorganic carbon (DIC). *Comptes Rendus Geoscience* **347**, 43–51.

Vinther, B.M., Clausen, H.B., Johnsen, S.J., Rasmussen, S.O., Andersen, K.K., Buchardt, S.L., Dahl-Jensen, D., Seierstad, I.K., Siggaard-Andersen, M.L., Steffensen, J.P., Svensson, A., Olsen, J., Heinemeier, J., 2006. A synchronized dating of three Greenland ice cores throughout the Holocene. *Journal of Geophysical Research Atmospheres* **111**, 1–11. https://doi.org/10.1029/2005JD006921

Vitousek, P.M., Sanford, R.L., 1986. Nutrient cycling in moist tropical forest. *Annual Review of Ecology and Systematics* **17**, 137–167.

Voelker, A.H.L., 2002. Global distribution of centennial-scale records for Marine Isotope Stage (MIS) 3: a database. *Quaternary Science Reviews* **21**, 1185–1212.

Vogel, T.A., Patino, L.C., Eaton, J.K., Valley, J.W., Rose, W.I., Alvarado, G.E., Viray, E.L., 2006. Origin of silicic magmas along the Central American volcanic front: Genetic relationship to mafic melts. *Journal of Volcanology and Geothermal Research* **156**, 217–228. https://doi.org/10.1016/j.jvolgeores.2006.03.002

Wadge, G., Scheuchl, B., Cabey, L., Palmer, M.D., Riley, C., Smith, A., Stevens, N.F., 1999. Operational use of InSAR for volcano observatories: experience from Montserrat, in: Proceedings of the FRINGE99 Symposium. p. 8.

Wadsworth, F.B., Witcher, T., Vasseur, J., Dingwell, D.B., Scheu, B., 2017. When Does Magma Break?, in: Gottsman, J., Neuberg, J., Scheu, B. (Ed.), Volcanic Unrest: From Science to Society. pp. 171–184.

Waelbroeck, C., Labeyrie, L., Michel, E., Duplessy, J.C., McManus, J.F., Lambeck, K., Balbon, E., Labracherie, M., 2002. Sea-level and deep water temperature changes derived from benthic foraminifera isotopic records. *Quaternary Science Reviews* **21**, 295–305. https://doi.org/10.1016/S0277-3791(01)00101-9

Wagner, A.J., Morrill, C., Otto-Bliesner, B.L., Rosenbloom, N., Watkins, K.R., 2013. Model support for forcing of the 8.2 ka event by meltwater from the Hudson Bay ice dome. *Climate Dynamics* **41**, 2855–2873.

Wagner, J.D.M., Cole, J.E., Beck, J.W., Patchett, P.J., Henderson, G.M., Barnett, H.R., 2010. Moisture variability in the southwestern United States linked to abrupt glacial climate change. *Nature Geoscience* **3**, 110–113. https://doi.org/10.1038/ngeo707

Wang, T., Bebbington, M.S., 2012. Estimating the likelihood of an eruption from a volcano with missing onsets in its record. *Journal of Volcanology and Geothermal Research* **243–244**, 14–23.

Wang, T., Schofield, M., Bebbington, M., Kiyosugi, K., 2019. Bayesian modelling of marked point processes with incomplete records: volcanic eruptions. *Applied Statistics* **69**, 109–130.

Wang, W., 2004. Discussion on the large-scale cultural changes at ∼2000 BC in China. *Archaeology* **1**, 67–77.

Wang, X., Auler, A.S., Edwards, R.L., Cheng, H., Ito, E., Solheid, M., 2006. Interhemispheric anti-phasing of rainfall during the last glacial period. *Quaternary Science Reviews* **25**, 3391–3403. https://doi.org/10.1016/j.quascirev.2006.02.009

Wang, Y., Cheng, H., Edwards, R.L., He, Y., Kong, X., An, Z., Wu, J., Kelly, M. J., Dykoski, C. A., Li, X., 2005. The Holocene Asian monsoon: Links to solar changes and North Atlantic climate. *Science* **308**, 854–857.

Wang, Y.J., Cheng, H., Edwards, R.L., An, Z.S., Wu, J.Y., Shen, C.-C., Dorale, J.A., 2001. A high-resolution absolute-dated Late Pleistocene monsoon record from Hulu Cave, China. *Science* **294**, 2345–2348.

Wang, Y., Cheng, H., Edwards, R.L., Kong, X., Shao, X., Chen, S., Wu, J., Jiang, X., Wang, X., An, Z., 2008. Millennial- and orbital-scale changes in the East Asian monsoon over the past 224,000 years. *Nature* **451**, 1090–1093. https://doi.org/10.1038/nature06692

Wanner, H., Beer, J., Bütikofer, J., Crowley, T.J., Cubasch, U., Flückiger, J., Goosse, H., Grosjean, M., Joos, F., Kaplan, J.O., Küttel, M., Müller, S.A., Prentice, I.C., Solomina, O., Stocker, T.F., Tarasov, P., Wagner, M., Widmann, M., 2008. Mid- to Late Holocene climate change: an overview. *Quaternary Science Reviews* **27**, 1791–1828. https://doi.org/10.1016/j.quascirev.2008.06.013

Wanner, H., Bütikofer, J., 2008. Holocene bond cycles: Real or imaginary? *Geografie-Sbornik* **113**, 338–350.

Wanner, H., Solomina, O., Grosjean, M., Ritz, S.P., Jetel, M., 2011. Structure and origin of Holocene cold events. *Quaternary Science Reviews* **30**, 3109–3123. https://doi.org/10.1016/j.quascirev.2011.07.010

Ward, K. M., Zandt, G., Beck, S. L., Christensen, D. H., McFarlin, H., 2014. Seismic imaging of the magmatic underpinnings beneath the Altiplano-Puna volcanic complex from the joint inversion of surface wave dispersion and receiver functions. *Earth and Planetary Science Letters* **404**, 43–53.

Wassenburg, J.A., Scholz, D., Jochum, K.P., Cheng, H., Oster, J., Immenhauser, A., Richter, D.K., Häger, T., Jamieson, R.A., Baldini, J.U.L., Hoffmann, D., Breitenbach, S.F.M., 2016. Determination of aragonite trace element distribution coefficients from speleothem calcite–aragonite transitions. *Geochimica et Cosmochimica Acta* **190**, 347–367. https://doi.org/10.1016/j.gca.2016.06.036

Wassenburg, J.A., Riechelmann, S., Schröder-Ritzrau, A., Riechelmann, D.F.C., Richter, D.K., Immenhauser, A., Terente, M., Constantin, S., Hachenberg, A., Hansen, M., Scholz, D., 2020. Calcite Mg and Sr partition coefficients in cave environments: Implications for interpreting prior calcite precipitation in speleothems. *Geochimica et Cosmochimica Acta* **269**, 581–596. https://doi.org/10.1016/j.gca.2019.11.011

Watanabe, M., Iwasaka, Y., Shibata, T., Hayashi, M., Fujiwara, M., Neuber, R., 2004. The evolution of Pinatubo aerosols in the Arctic stratosphere during 1994-2000. *Atmospheric Research* **69**, 199–215. https://doi.org/10.1016/j.atmosres.2003.09.006

Watanabe, O., Jouzel, J., Johnsen, S., Parrenin, F., Shoji, H., Yoshida, N., 2003. Homogeneous climate variability across East Antarctica over the past three glacial cycles. *Nature* **422**, 509–512. https://doi.org/10.1038/nature01525

Watson, E.J., Kołaczek, P., Słowiński, M., Swindles, G.T., Marcisz, K., Gałka, M., Lamentowicz, M., 2017. First discovery of Holocene Alaskan and Icelandic tephra in Polish peatlands. *Journal of Quaternary Science* **32**, 457–462. https://doi.org/10.1002/jqs.2945

Watson, E.J., Swindles, G.T., Lawson, I.T., Savov, I.P., 2016. Do peatlands or lakes provide the most comprehensive distal tephra records? *Quaternary Science Reviews* **139**, 110–128. https://doi.org/10.1016/j.quascirev.2016.03.011

Watson, E.J., Swindles, G.T., Lawson, I.T., Savov, I.P., 2015. Spatial variability of tephra and carbon accumulation in a Holocene peatland. *Quaternary Science Reviews* **124**, 248–264. https://doi.org/10.1016/j.quascirev.2015.07.025

Watson, E.J., Swindles, G.T., Savov, I.P., Lawson, I.T., Connor, C.B., Wilson, J.A., 2017. Estimating the frequency of volcanic ash clouds over Northern Europe. *Earth & Planetary Science Letters* **460**, 41–49.

Watson, E.J., Swindles, G.T., Savov, I.P., Bacon, K.L., 2015. First discovery of Holocene cryptotephra in Amazonia. *Scientific Reports* **5**, 1–9. https://doi.org/10.1038/srep15579

Watt, S.F.L., Pyle, D.M., Mather, T.A., 2013. The volcanic response to deglaciation: Evidence from glaciated arcs and a reassessment of global eruption records. *Earth-Science Reviews* **122**, 77–102. https://doi.org/10.1016/j.earscirev.2013.03.007

Waythomas, C.F., 2015. Geomorphic consequences of volcanic eruptions in Alaska: A review. *Geomorphology* **246**, 123–145.

Weber, S.L., Crowley, T.J., van der Schrier, G., 2004. Solar irradiance forcing of centennial climate variability: linear and nonlinear responses in a coupled model. *Climate Dynamics* **22**, 539–553.

Wei, H., Liu, G., Gill, J., 2013. Review of eruptive activity at Tianchi volcano, Changbaishan, northeast China: implications for possible future eruptions. *Bulletin of Volcanology* **75**, 706.

Weijer, W., Cheng, W., Drijfhout, S.S., Fedorov, A. V., Hu, A., Jackson, L.C., Liu, W., McDonagh, E.L., Mecking, J. V., Zhang, J., 2019. Stability of the Atlantic Meridional Overturning Circulation: A Review and Synthesis. *Journal of Geophysical Research: Oceans* **124**, 5336–5375. https://doi.org/10.1029/2019JC015083

Weiss, H., 2017. 4.2 ka BP megadrought and the Akkadian collapse, in: Weiss, H. (Ed.), Megadrought and Collapse: From Early Agriculture to Angkor. Oxford University Press, Oxford, pp. 93–160.

Weiss, H., 2016. Global megadrought, societal collapse and resilience at 4.2–3.9 ka BP across the Mediterranean and west Asia. *PAGES* **24**, 62–63.

Whelley, P.L., Newhall, C.G., Bradley, K.E., 2015. The frequency of explosive volcanic eruptions in Southeast Asia. *Bulletin of Volcanology* **77**. https://doi.org/10.1007/s00445-014-0893-8

Wickens, L., Rowe, P., Marca, A., Noble, S. R., Millar, I. L., Chilvers, G., Dennis, P., Leze, B., Özkul, M., Baykara, O., Andrews, J., 2011. The Last Interglacial and Holocene in SW Turkey: evidence from calcite-aragonite speleothems. American Geophysical Union, Fall Meeting, pp. PP21D-02.

Wickens, L.B., 2013. Geochemistry and Petrography of Speleothems From Turkey and Iran: Palaeoclimate and Diagenesis 280.

Wilcock, J., Goff, F., Minarik, W. G., Stix, J., 2013. Magmatic recharge during the formation and resurgence of the Valles caldera, New Mexico, USA: evidence from quartz compositional zoning and geothermometry. *Journal of Petrology* **54**, 635–664.

Williams, H., 1960. Volcanic history of the Guatemalan Highlands. *Geological Science* **38**, 1–87.

Williams, M., 2012. The ~73 ka Toba super-eruption and its impact: History of a debate. *Quaternary International* **258**, 19–29.

Williams, M., Ambrose, S.H., van der Kaars, S., Ruehlemann, C., Chattopadhyaya, U., Pal, J., Chauhan, P.R., 2009. Environmental impact of the 73 ka Toba super-eruption in South Asia. *Palaeogeography, Palaeoclimatology, Palaeoecology* **284**, 295–314.

Williams, M.A.J., Ambrose, S.H., van der Kaars, S., Ruehlemann, C., Chattopadhyaya, U., Pal, J., Chauhan, P., 2009. Reply to the comment on 'Environmental impact of the 73 ka Toba super-eruption in South Asia' by Martin A. J. Williams, M.A.J., Ambrose, S.H., van der Kaars, S., Ruehlemann, C., Chattopadhyaya, U., Pal, J., Chauhan, P.R. *Palaeogeography, Palaeoclimatology, Palaeoecology* **296**, 204–211.

Williams, S.N., Self, S., 1983. The October 1902 Plinian Eruption of Santa Maria volcano, Guatemala. *Journal of Volcanology and Geothermal Research* **16**, 33–56.

Wilson, C.J.N., 2008. Supereruptions and Supervolcanoes: Processes and Products. *Elements* **4**, 29–34.

Wilson, C.J.N., Gravley, D.M., Leonard, G.S., Rowland, J.V., 2009. Volcanism in the central Taupo Volcanic Zone, New Zealand: Tempo, styles and controls, in: Thordarson, T., Self, S., Larsen, G., Rowland, S.K., Hoskuldsson, A. (Ed.), Studies in Volcanology: The Legacy of George Walker. Special Publications of IAVCEI (Geological Society), London, pp. 225–247.

Winchester, S., 2003. Krakatoa: The Day the World Exploded. Penguin Books, London.

Witham, C. S., Oppenheimer, C., 2004. Mortality in England during the 1783-4 Lakí Craters eruption. *Bulletin of Volcanology* **67**, 15–26.

Witt, M.L.I., Mather, T.A., Pyle, D.M., Aiuppa, A., Bagnato, E., Tsanev, V.I., 2008. Mercury and halogen emissions from Masaya and Telica volcanoes, Nicaragua. *Journal of Geophysical Research - Solid Earth* **113**, B06203.

Wohletz, K.H., 2000. Were the dark ages triggered by volcano-related climate changes in the 6th century? *Eos Transactions American Geophysical Union* **48**, F1305.

Wolff-Boernish, D., Gislason, S.R., Oelkers, E., Putnis, C.V., 2004. The dissolution rates of natural glasses as a function of their composition at pH4 and 10.6, and temperatures from 25 to 74oC. *Geochemica et Cosmochimica Acta* **68**, 4843–4858.

Wong, C. I., Banner, J.L., Musgrove, M., 2011. Seasonal dripwater Mg/Ca and Sr/Ca variations driven by cave ventilation: Implications for and modelling of speleothem paleoclimate records. *Geochimica et Cosmochimica Acta* **75**, 3514–3529.

Woods, A.W., Wohletz, K., 1991. Dimensions and dynamics of co-ignimbrite eruption columns. *Nature* **350**, 225–227.

Wotzlaw, J.-F., Bindeman, I.N., Stern, R.A., D'Abzac, F.-X., Schaltegger, U., 2015. Rapid heterogeneous assembly of multiple magma reservoirs prior to Yellowstone supereruptions. *Scientific Reports* **5**, 14026.

Wulf, S., Dräger, N., Ott, F., Serb, J., Appelt, O., Gudmundsdóttir, E., van den Bogaard, C., Słowiński, M., Błaszkiewicz, M., Brauer, A., 2016. Holocene tephrostratigraphy of varved sediment records from Lakes Tiefer See (NE Germany) and Czechowskie (N Poland). *Quaternary Science Reviews* **132**, 1–14. https://doi.org/10.1016/j.quascirev.2015.11.007

Wynn, P.M., Fairchild, I.J., Borsato, A., Baker, A., Frisia, S., 2013. Biogeochemical cycling of sulphur in the speleothem record. *Biogeochemistry* **114**, 255–267.

Yilmaz, A.G., 2015. The effects of climate change on historical and future extreme rainfall in Antalya, Turkey. *Hydrological Sciences Journal* **60**, 2148–2162. https://doi.org/10.1080/02626667.2014.945455

Yost, C.L., Jackson, L.J., Stone, J.R., Cohen, A.S., 2018. Subdecadal phytolith and charcoal records from Lake Malawi , East Africa imply minimal effects on human evolution from the ~ 74 ka Toba supereruption. *Journal of Human Evolution* **116**, 75–94. https://doi.org/10.1016/j.jhevol.2017.11.005

Young, S.R., 1990. Physical volcanology of Holocene airfall deposits from Mt Mazama, Crater Lake, Oregon. University of Lancaster.

Yu, Z., Campbell, I. D., Campbell, C., Vitt, D. H., Bond, G. C., Apps, M.J., 2003. Carbon sequestration in western Canadian wet-dry climate cycles at millennial scales. *The Holocene* **13**, 801–808.

Zanchetta, G., Sulpizio, R., Roberts, N., Cioni, R., Eastwood, W.J., Siani, G., Caron, B., Paterne, M., Santacroce, R., 2011. Tephrostratigraphy, chronology and climatic events of the Mediterranean basin during the Holocene: An overview. *Holocene* **21**, 33–52. https://doi.org/10.1177/0959683610377531

Zanchettin D,. Bothe, O., Graf, H.F., Lorenz, S.J., Luterbacher, J., Timmreck, C., Jungclaus, J.H., 2013. Background conditions influence the decadal climate response to strong volcanic eruptions. *Journal of Geophysical Research - Atmospheres* **118**, 4090–4106.

Zanchettin, D., Bothe, O., Timmreck, C., Bader, J., Beitsch, A., Graf, H.F., Notz, D., Jungclaus, J.H., 2014. Inter-hemispheric asymmetry in the sea-ice response to volcanic forcing simulated by MPI-ESM (COSMOS-Mill). *Earth System Dynamics* **5**, 223–242. https://doi.org/10.5194/esd-5-223-2014

Zhang, X., Lohmann, G., Knorr, G., Purcell, C., 2014. Abrupt glacial climate shifts controlled by ice sheet changes. *Nature* **512**, 290–294.

Zhang, X., Xiao, H., Chou, Y.C., Cai, B., Lone, M.A., Shen, C.C., Jiang, X., 2020. A detailed East Asian monsoon history of Greenland Interstadial 21 in southeastern China. *Palaeogeography, Palaeoclimatology, Palaeoecology* **552**, 109752. https://doi.org/10.1016/j.palaeo.2020.109752

Zhang, X., Knorr, G., Lohmann, G., Barker, S., 2017. Abrupt North Atlantic circulation changes in climate state. *Nature Geoscience* **10**. https://doi.org/10.1038/NGEO2974

Zhang, X., Lohmann, G., Knorr, G., Purcell, C., 2014. Abrupt glacial climate shifts controlled by ice sheet changes. *Nature* **512**, 290–294. https://doi.org/10.1038/nature13592

Zhang, Y., Renssen, H. Heikki, S., 2015. Effects of melting ice sheets and orbital forcing on the early Holocene warming in the extratropical Northern Hemisphere. *Climate of the Past* **12**, 1119–1135.

Zhong, Y., Miller, G. H., Otto-Bliesner, B. L., Holland, M. M., Bailey, D. A., Schneider, D. P., Geirsdottir, A., 2011. Centennial scale climate change from decadally-paced explosive volcanism: a coupled sea ice-ocean mechanism. *Climate Dynamics* **37**, 2373–2387.

Zhou, H., Wang, Q., Zhao, J., Zheng, L., Guan, H., Feng, Y., Greig, A., 2008. Rare earth elements and yttrium in a stalagmite from Central China and potential paleoclimatic implications. *Palaeogeography Palaeoclimatology Palaeoecology* **207**, 128–138.

Zhou, H.Y., Chi, B.Q., Lawrence, M., Zhao, J.X., Yan, J., Greig, A., Feng, Y.X., 2008. High resolution and precisely dated record of weathering and hydrological dynamics recorded by manganese and rare earth elements in a stalagmite from central China. *Quaternary Research* **68**, 438–446.

Zhou, H., Zhao, J., Feng, Y., Gagan, M.K., Zhou, G., Yan, J., 2008. Distinct climate change synchronous with Heinrich event one, recorded by stable oxygen and carbon isotopic compositions in stalagmites from China. *Quaternary Research* **69**, 306–315. https://doi.org/10.1016/j.yqres.2007.11.001

Zhu, L., Liu, Y., Hu, Z., Hu, Q., Tong, X., Zong, K., Chen, H., Gao, S., 2013. Simultaneous analysis of major and trace elements in fused volcanic rock powders by using a hermetic vessel heater and LA-ICP-MS. *Geostandards and Geoanalytical Research* **37**, 207–229.

Zielinski, G. A., Mayewski, P. A., Meeker, L. D., Whitlow, S., Twickler, M. S., Taylor, K., 1996. Potential atmospheric impact of the Toba Mega Eruption ~71,000 years ago. *Geophysical Research Letters* **23**, 837–840.

Zielinski, G.A., Mayewski, P.A., Meeker, L.D., Whitlow, S., Twickler, M.S., 1996. A 110,000-Yr Record of Explosive Volcanism from the GISP2 (Greenland) Ice Core. *Quaternary Research* **45**, 109–118. https://doi.org/10.1006/qres.1996.0013

Ziemen, F.A., Kapsch, M., Klockmann, M., Mikolajewicz, U., 2018. Heinrich events show two-stage climate response in transient glacial simulations. *Climate of the Past Discussions* 1–22.

Zwally, H. J., Abdalati, W., Herring, T., Larson, K.M., Saba, J., Steffen, K., 2002. Surface melt-induced acceleration of Greenland Ice-Sheet flow. *Science* **297**, 218–222.